



FLUID INCLUSION AND OXYGEN ISOTOPE STUDIES OF  
THE NABARLEK URANIUM DEPOSIT, N.T., AUSTRALIA

by

Kazuo Fuzikawa

Submitted at the University of Adelaide  
as requirement for the Degree of Doctor  
of Philosophy (Ph.D.) in 1982.

This thesis contains no material which has been accepted for the award of any other degree or diploma in any University nor, to the best of my knowledge and belief, does it contain any material previously published or written by another person except where due reference is made in the text.

✓ K. Fuzikawa /

To Leiko and our children:

Alberto, Priscila, Agnes, and Cíntia

TABLE OF CONTENTS

i.

	<u>Page</u>
<u>INTRODUCTION</u>	1
<u>CHAPTER I - GEOLOGY AND MINERALOGY</u>	4
I.1 Regional geology	4
I.2 Geology of the Nabarlek Area	9
I.3 The Mineral Paragenesis	13
<u>CHAPTER II - FLUID INCLUSION STUDY</u>	19
II.1 Methods and Principles	19
II.1.1 Non-destructive Methods	19
II.1.1.1 Petrographic microscopy	20
II.1.1.2 Microthermometry	20
II.1.1.3 Equipment and calibration	33
II.1.1.4 Other non-destructive methods	37
II.1.2 Destructive methods	37
II.1.2.1 The crushing stage	39
II.1.2.2 Crushing under pressure	42
II.1.2.3 Scanning electron microscope (SEM)	43
II.2 Samples Studied	46
II.2.1 Uraniferous samples	47
Sample A-495-172	47
a) Introduction	47
b) Quartz crystal A-495-172A	47
c) Quartz crystal A-495-172B	51
d) Quartz crystal A-495-172D	57
e) Quartz crystal A-495-172F	58
f) Crushing tests	62
g) Scanning electron microscopy	63
h) General conclusions for sample A-495-172	63
Sample A-495-168	64
Sample A-495-171	69
Sample A-495-162	70
Pitchblende samples	73
II.2.2 Non-uraniferous samples	75



TABLE OF CONTENTS (cont'd)

	<u>Page</u>
III.1.4.4 Mass spectrometry and standards	126
III.2 Samples Studied	128
III.2.1 Previous Oxygen Isotope Works on Hydrothermal Uranium Deposits	128
III.2.2 Analytical Results and Discussion	129
III.2.2.1 Quartz from D.H.Na77	129
III.2.2.2 Metamorphic quartz	133
III.2.2.3 Other quartz (Table 3)	134
III.2.2.4 Calcite	136
III.2.2.5 Calculation of $\delta^{18}\text{O}$ of parent solutions	138
III.2.2.6 Dolerite	144
III.2.2.7 Quartz-actinolite-schist	145
III.2.2.8 Granitic rocks	146
III.2.2.9 Pitchblende	148
III.2.2.10 Temperatures and isotopic equilibrium	149
III.3 Summary and Conclusions	153
<u>CHAPTER IV - DISCUSSIONS AND CONCLUSIONS</u>	155
IV.1 Introduction	155
IV.2 The Common Characteristics of Unconformity-related Uranium Deposits	155
IV.3 Data of the Present Work and the Conditions of Uranium Mineralization	157
a) Mixing of very saline and dilute solutions	157
b) Chemical composition of the concentrated and dilute $\text{CO}_2$ or $\text{CH}_4$ -rich solutions	158
c) Origin of fluids	159
d) Formation of highly saline solutions	160
e) Temperature and pressure	161
IV.4 Genetic Models	161
<u>APPENDICES</u>	167
APPENDIX 1 - List of studied samples from Nabarlek uranium deposit with $\delta^{18}\text{O}$ values	168
APPENDIX 2 - Fluid inclusion study of samples from Nabarlek uranium deposit	173
APPENDIX 3 - Autoradiographic studies	177
APPENDIX 4 - Chemical composition of some samples from Nabarlek area	181
APPENDIX 5 - Fluid inclusion study of samples from Jabiluka uranium deposit	184

TABLE OF CONTENTS (cont'd)

	<u>Page</u>
Sample A-495-1	184
Sample A-495-3	187
Sample A-495-5	190
Sample A-495-11	191
a) Cluster A	194
b) Cluster B	196
c) Cluster C	203
d) Cluster D	204
e) Cluster E	205
f) Cluster F	207
g) Cluster G	207
Conclusions for sample A-495-11	212
General conclusions	213

REFERENCES

215

PLATES I to XVIII

(follow references)

Name : KAZUO FUZIKAWA .. Course : .....

I give consent to this copy of my thesis, when deposited in the University Library, being available for loan and photocopying.

Date : Sept. 23rd, 1982 .....



LIST OF FIGURES AND TABLES

Figures	<u>Page</u>
23 - Sample A-495-172. Homogenization temperature ( $T_H$ ) frequency histogrammes of fluid inclusions in the same four quartz crystals of figure 22.	54
24 - Phase changes during the microthermometry of inclusion No. 1 from sample A-495-172B.	55
25 - Typical phase changes during the microthermometry of one inclusion from quartz crystal A-495-172F.	61
26 - Sample A-495-168. Type (a) (liquid-rich) and type (b) (vapour-rich) inclusion from zone of growth of a quartz crystal.	66
27 - Frequency histogrammes of microthermometry of fluid inclusions in quartz from samples A-495-168 (late-stage), A-495-171 (early-stage), and A-495-178 (late-stage).	68
28 - Sample A-495-162. $T_F$ and $T_H$ frequency histogrammes of fluid inclusions in hydrothermal quartz.	72
29 - Solubility in kerosene of gas bubbles released by pitchblende during the crushing test.	76
30 - Sample A-495-176. $T_F$ frequency histogrammes of fluid inclusions in three different early-stage quartz.	78
31 - Sample A-495-176. $T_H$ frequency histogrammes of fluid inclusions in the same quartz samples of figure 30.	79
32 - Frequency histogramme of microthermometry of fluid inclusions in early-stage (A-495-176D) and late-stage (A-495-176E and F) quartz.	84
33 - Sample A-495-176. Solubility in kerosene of gas bubbles released upon crushing quartz grain with type (b) inclusions.	87
34 - Sample A-495-176. Compressibility curves of three gas bubbles released upon crushing a quartz grain with type (b) inclusions.	90
35 - Sample A-495-174. $T_H$ frequency histogrammes of fluid inclusions in late-stage (A-495-174A) and early-stage quartz (A-495-174B and C).	92
36 - Types of fluid inclusions present in quartz (metamorphogenic) from sample A-495-179.	94
37 - Sample A-495-179. $T_F$ and $T_H$ frequency histogrammes of fluid inclusions in metamorphogenic quartz.	97
38 - Sample A-495-157. $T_F$ and $T_H$ frequency histogrammes of fluid inclusions in quartz and the relation $T_F/T_H$ .	100
39 - Sample A-495-113. $T_F$ and $T_H$ frequency histogrammes of fluid inclusions in quartz and the relation $T_F/T_H$ .	102
40 - Frequency histogrammes of microthermometry of fluid inclusions in quartz from sample A-495-113B and in quartz from sample A-495-156.	104
41 - Sample A-495-113. Solubility in kerosene of gas bubbles released upon crushing quartz.	106

## Figures

Page

- 42 - Compressibility of two gas bubbles released upon crushing a quartz grain from sample A-495-113. 108
- 43 - Frequency histogrammes of microthermometry of fluid inclusions in quartz from samples A-495-191, A-495-144, and A-495-164 (late-stage). 109
- 44 - Sample A-495-144.  $T_F$  and  $T_H$  frequency histogrammes of fluid inclusions in calcite. 113
- 45 - Sample A-495-220.  $T_F$  and  $T_H$  frequency histogrammes of fluid inclusions in calcite and the relation  $T_F/T_H$ . 114

CHAPTER III

- 46 - Correlation curve between the results from mass spectrometry (NAA) unit from the Institute of Nuclear Science, Lower Hutt, N.Z. ( $\delta R_{46}$ ) and the SMOW scale when  $BrF_5$  method is used. 127
- 47 - Calculated  $\delta^{18}O$  values of solutions in equilibrium with quartz and calcite of the Nabarlek uranium deposit. 139
- 48 - Water (liq.) - water (vap.) solution effects at  $25^\circ C$ . 140
- 49 - Isotopic effects of  $NH_4Cl$ ,  $KCl$ ,  $CaCl_2$  solutions (liq.) - water (liq.) between  $25^\circ C$  and  $275^\circ C$ . 141
- 50 - Isotopic effects of  $NaCl$  and  $MgCl_2$  solutions (liq.) - water (liq.) between  $25^\circ C$  and  $275^\circ C$ . 142
- 51 - Diagram indicative of the control of  $\delta^{18}O$  of altered dolerites by the % opaques/% sericites ratio. 147

CHAPTER IV

- 52 - Schematic presentation of the environment of U deposition at Nabarlek. 164

APPENDICES

- 53 - Sample A-495-162. Autoradiography of pitchblende inclusion in quartz. 179
- 54 - Sample A-495-1 (Jabiluka).  $T_F$  frequency histogramme of fluid inclusion in quartz. 186
- 55 - Sample A-495-3 (Jabiluka).  $T_F$  and  $T_H$  frequency histogrammes of fluid inclusions in quartz. 188
- 56 - Sample A-495-11 (Jabiluka). Multiphase inclusions in quartz. 193
- 57 - Sample A-495-11 (Jabiluka).  $T_F$  frequency histogrammes of four clusters of fluid inclusions (A, B, C, and D) in quartz. 197
- 58 - Sample A-495-11 (Jabiluka). Unusual phase changes in inclusion no. 2, cluster B, during the freezing tests. 198



ILLUSTRATIONSPageCHAPTER I

## Figures

1 - Locality map	2
2 - Regional geology of the Alligator River uranium province	5
3 - Geological map of the Nabarlek uranium deposit	8
4 - Schematic cross-section from Gabor to Nabarlek uranium deposit	11
5 - Borehold section A-A' (from figure 3)	12
6 - Longitudinal section through the Mine area	14
7 - Longitudinal section through the Mine area indicating the location of samples.	16
8 - Paragenetic sequence of quartz, pitchblende, and calcite from the Nabarlek uranium deposit.	18

CHAPTER II

9 - Phase diagrams of the systems NaCl-H <sub>2</sub> O and KCl-H <sub>2</sub> O	22
10 - Phase diagram of the system CaCl <sub>2</sub> -NaCl-H <sub>2</sub> O	24
11 - Temperature-composition model of the system CaCl <sub>2</sub> -NaCl-H <sub>2</sub> O	25
12 - Phase diagram of the system CaCl <sub>2</sub> -H <sub>2</sub> O below 200 <sup>o</sup> C based mainly on data from Yanatieva (1946).	26
13 - Phase diagram of the system MgCl <sub>2</sub> -H <sub>2</sub> O below 200 <sup>o</sup> C based mainly on data from Yanatieva (1946).	27
14 - Phase diagram of the system FeCl <sub>2</sub> -H <sub>2</sub> O below 120 <sup>o</sup> C	28
15 - Phase diagram of the system AlCl <sub>3</sub> -H <sub>2</sub> O below 100 <sup>o</sup> C	29
16 - Phase diagram of the system CO <sub>2</sub> -CH <sub>4</sub> at low pressures and temperatures.	32
17 - Phase diagram of CO <sub>2</sub> hydrate near 0 <sup>o</sup> C and the influence of NaCl content on the melting temperature of the hydrate.	34
18 - Temperature correlation diagram for freezing temperature measurements made with 25x and 10x objective lenses.	36
19 - Temperature calibration curve determined for the Chaix-Meca stage No. 10CRPG using a thin silica window with Reichert cat. 40/0.52, 250/1,5 Qu objective.	38
20 - Comparative chart for gases released during crushing test at a magnification of 35x.	40
21 - Sample A-495-172. Inclusions of 3 different generations in quartz crystal.	48
22 - Sample A-495-172. Freezing temperature (T <sub>F</sub> ) frequency histogrammes of fluid inclusions from four late-stage quartz crystals.	52

ABSTRACT

The Nabarlek uranium deposit is the smallest of four major deposits from the East Alligator Rivers area in the Northern Territory of Australia, but also contains the highest grades.

The genesis of the mineralization was studied by fluid inclusion and oxygen isotope methods, which methods were amplified by chemical analysis, X-ray fluorescence, atomic absorption and scanning electron microscopy and autoradiography.

The most prominent aspect of the E. Alligator River uranium deposits is their proximity to the unconformity between retrograde metamorphic chlorite-rich schist of the Pine Creek Geosyncline and the undeformed Carpentarian Kombolgie Sandstone.

The fluid inclusion studies - microthermometry, scanning electron microscopy, crushing, and thermobarometric crushing - indicated the presence of several fluids, the mixing of which produced a wide range of salinities: 0.4 to 37 wt.%  $\text{CaCl}_2$  equivalent. (Because  $\text{CaCl}_2$  appeared to be present in amounts far larger than  $\text{NaCl}$ , all salinities have been presented in wt.% equivalence of  $\text{CaCl}_2$ ). These high  $\text{CaCl}_2$  salinities and some unusual phase changes: like partial freezing for instance, have not been recorded before in fluid inclusion studies. Homogenization temperatures ( $T_H$ ) pointed to values around  $150^\circ\text{C}$  as the higher limit and around  $70^\circ\text{C}$  as the lower range. High pressure gas-rich inclusions with salinities in the same range as those of liquid-rich inclusions are probably due to the exsolution of gas during a fluid mixing process rather than through boiling of a homogeneous fluid. This idea is supported by the low  $T_H$  of inclusions with highly saline solutions which would have been incapable of dissolution of the amounts of gasses observed. Hydrocarbons are a dominant constituent of the gas phase occasionally exceeding  $\text{CO}_2$ .

The contribution of meteoric waters during the hydrothermal process has been well established by oxygen isotope study. Coexisting chlorite-sericite from local alteration indicated a temperature of  $150^\circ\text{C}$ , which figure is

similar to those of the fluid inclusion data.

The data are compatible with a model in which the unconformity also represents the confluence of two hydrothermal domains, a very saline brine one and a more dilute CO<sub>2</sub>-rich solution.

The location of the Nabarlek deposit is spatially closely related to the interface of these hydrothermal domains, as indicated by numerous salinity reversals. It is suggested that the salinity of the brines interfered with the stability of uranyl carbonate complexes, which became reduced by hydrocarbons.

Several spot checks on fluid inclusions from the Jabiluka deposit seems to indicate a similar genesis as Nabarlek.

## ACKNOWLEDGEMENTS

The assistance of Professor P.J.M. Ypma who has been my supervisor throughout the research work is deeply acknowledged. He has not only introduced me to the fluid inclusion study techniques but has helped with useful discussions as well. The constructive criticisms regarding the draft versions of this study were of inestimable value.

The permission to spend many years doing this graduation work and the necessary financial support are owed to Empresas Nucleares Brasileiras S.A. - NUCLEBRÁS. I am profoundly grateful to Drs. J.M.A. Forman, Director; C.H.C. Azuaga, Assistant to the Director; J.H. Javaroni, Superintendent; and J.N. Villaca, Manager of the Belo Horizonte office, for their continuous support and encouragement.

I acknowledge Dr. R.A. Both's orientation and suggestions which were of great value during the research work.

I also wish to thank Drs. K. Bartusek for his support during the scanning electron microscopy, K. Turnbull for useful suggestions and discussions in the field of chemistry; J. Stanley for X-ray fluorescence determinations and R. Oliver for his help in the petrographic studies.

I am greatly indebted to Dr. P. Blattner from the Institute of Nuclear Sciences, D.S.I.R., New Zealand, for his introduction to the oxygen isotope analysis technique and useful suggestions during the interpretation of the data.

The assistance of the Pancontinental Mining Ltd., the Queensland Mines Ltd., and the Commonwealth Scientific and Industrial Research Organization (CSIRO) in allowing access to drill cores is gratefully acknowledged. To Dr. J. Ferguson who<sup>o</sup>I owe ~~retrograde~~ <sup>useless</sup> helpful information and ~~useful~~ discussions.

To Miss E. Hogg for her patient and tireless help during the correction of part of the English manuscript, my special thanks.

I wish to extend my thanks to Mr. W. Mussared, who prepared the fluid inclusion thick sections, polished sections, and petrographic thin sections; Mr. P. McDuire who prepared the samples for X-ray fluorescence analysis; Mr. E. Bleys, who helped with the production of photographic plates and autoradiographic emulsion processings, Mrs. S. Proferes, Miss C.G. Guimarães, and Miss A.G. Mansur for drafting the figures, Mrs. J. Brumby and Mrs. M.L.S. Mello for typing the thesis, and Mrs. H. Malby for helping in many ways during my stay at the Department.

Finally, I would like to acknowledge everyone who, although not explicitly mentioned, has directly or indirectly aided in the achievement of this study.



## INTRODUCTION

The Nabarlek uranium deposit is the smallest of four major uranium deposits (\*) at the East Alligator River Uranium Field. The deposit is situated in Arnhem Land, at the eastern boundary of the Pine Creek Geosyncline, at approximately 12°18'S, 133°20'E. Darwin, the capital city of the Northern Territory, is situated 270 km to the west (Figure 1).

Access to Nabarlek from Darwin is by sealed road: the Arnhem Highway to Jabiru. A dirt road connects Jabiru with the Oenpelli Mission. Nabarlek is linked to Oenpelli Mission by 40 km of unimproved road. Nabarlek can also be reached by air. The climate is a summer monsoonal one with an average annual rainfall of 1100 mm mainly during the wet season (December to April), which causes the main river system (Magela Plain) to flood.

The most prominent topographic feature in the area is a coarse sandstone escarpment which forms the edge of the Arnhem Land Plateau. The Plateau is dissected by deep joints and faults which control the hydrography. The radioactive anomalies have been detected where the sandstone cover was eroded and underlying metamorphics were exposed. Nabarlek is located in one of these areas which was formed by erosional action of the Cooper Creek. In fact, all deposits and radiometric anomalies are situated close to the unconformity between the sandstone (Kombolgie Formation) and the metamorphic schists (Cahill Formation).

The present work was initiated by Professor P. Ypma of the Department of Economic Geology at the University of Adelaide. The study was later integrated into a comprehensive regional study of East Alligator River Uranium Field, which was coordinated by a Committee representing the Bureau of Mineral Resources, the Commonwealth Scientific Industrial Research Organization and private industry working in the area.

It was originally our intention to study all relevant aspects of mineral genesis at Nabarlek, and to include petrography, chemistry and mineralogy of ore and host rock. However the Coordinating Committee decided that petrology

---

(\*) The other deposits are Koongarra, Ranger, and Jabiluka.

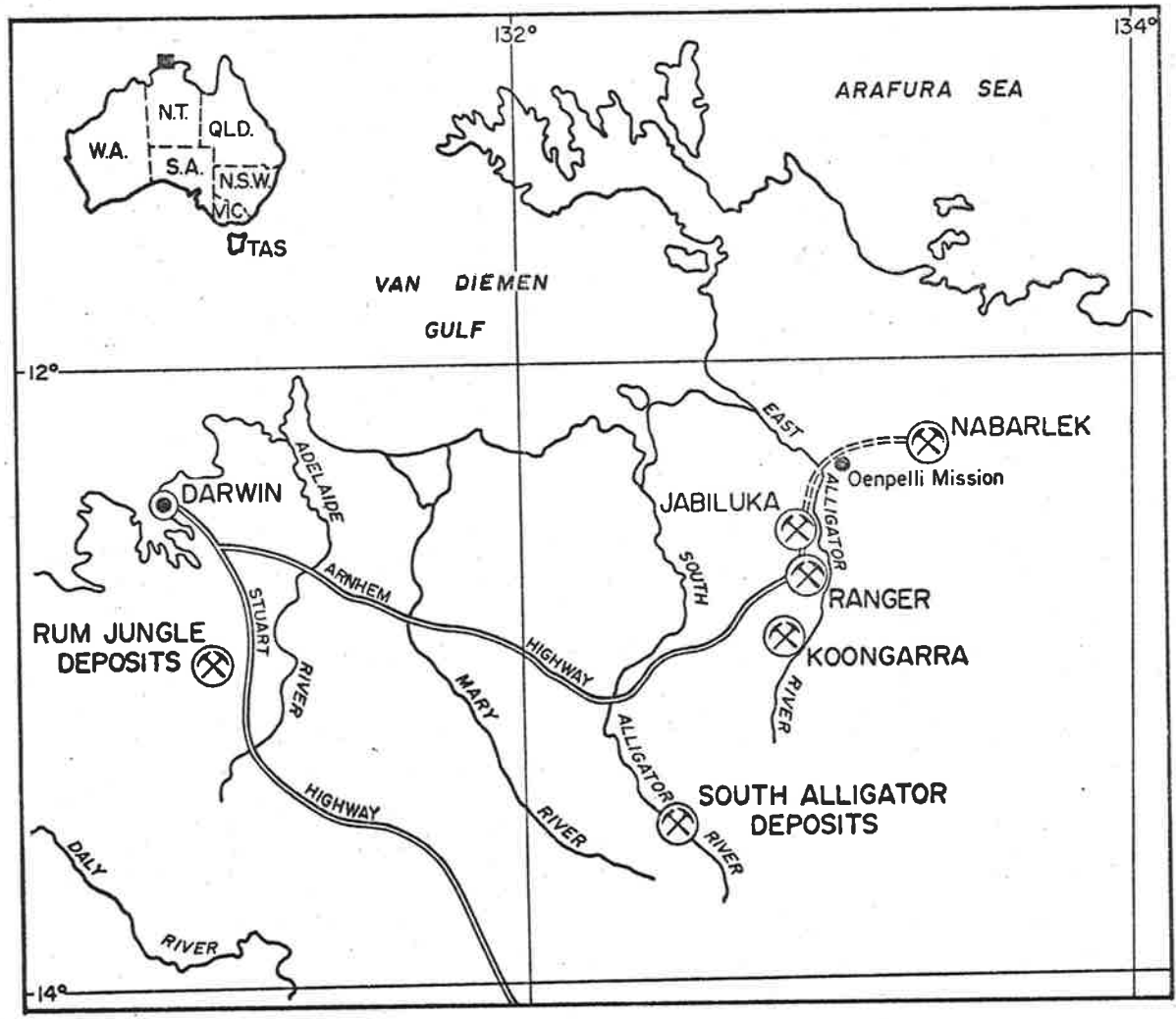


Figure 1: Locality Map

mineralogy and petrochemistry were best left to other research institutions and that this study should be confined to fluid inclusions and oxygen isotopes. Unfortunately a detailed study of Nabarlek's petrology and mineralogy has never eventuated, and never will be in the future as the orebody was ~~CRAP~~ mined out in 1979, which demonstrates that the scope of a scientific endeavour is best left to the individual and not to a committee.

The main goal of the fluid inclusion study was the investigation of the geochemistry of the mineralizing solutions. In order to do this on transparent gangue minerals (quartz, calcite), a paragenetic relationship between gangue and ore minerals had to be first established. A search was made for evidence which could link fluid inclusions of gangue and uranium minerals. Autoradiography was used for this purpose.

For the study of fluid and solid phases in the inclusions, the following techniques were applied: transmitted and incident light microscopy, microthermometry, crushing tests, and scanning electron microscopy (SEM) in connection with energy dispersive analysis by X-ray (EDAX).

The oxygen isotope analysis was carried out as an attempt to determine the origin of the solutions involved in the uranium mineralization and eventually to cross-check the temperatures and other information obtained from fluid inclusion microthermometry. Oxygen isotope determinations were made mainly for silicate gangue minerals and whole rock samples. The bromine pentafluoride method was used for oxygen extraction.

Sampling was oriented towards specimens containing transparent minerals associated with uranium mineralization. By far the most common gangue mineral is quartz.

All studied samples were from diamond drill-cores because no outcrops with primary mineralization were present on the surface in the Nabarlek area at the time of study.

## CHAPTER I

### GEOLOGY AND MINERALOGY



#### I.1 Regional Geology

The Lower Proterozoic strata of the Pine Creek Geosyncline was recognized as host rocks of a most significant series of uranium deposits of the Northern Territory. Consequently, extensive and detailed geological and geophysical studies have been carried out in the area.

The first extensive general description of the geology and economic geology, dealing mainly with the western and southern parts of the geosyncline was published by Walpole et al. in 1968. This work was based on information obtained by geologists of the Bureau of Mineral Resources during a regional geological study over the period 1953 to 1958.

Renewed exploration efforts in the late 1960s and early 1970s led to the discovery of some of the world's largest uranium deposits in the E. Alligator River area. These discoveries were followed by detailed mapping (1:100,000) and airborne magnetic and radiometric surveys (1:250,000) of the northeastern part of the geosyncline (Smart et al., 1976). Needham and Stuart-Smith (1976 and 1979) presented comprehensive regional geological studies of the area (Figure 2). This area is now known as the E. Alligator River Uranium Province world-wide. The western area of the Province is dominated by a structure known as Nanambu Complex which is a mantled gneiss dome of Archaean age. This dome is overlain by Lower Proterozoic metasediments of the Kakadu Group and Cahill Formation. The latter Formation conformably overlies the former Group and, in turn, is overlain by the Nourlangie Schist. To the northeast of the Province, according to Needham and Stuart-Smith (1976), "... the metasediments grade into a large migmatite complex (the Nimbuwah Complex) of late Lower Proterozoic age, (1800 m.y. according to Page and Needham, in prep.). The Lower Proterozoic rocks are intruded by pre- and post-deformation basic igneous rocks which are known as: the Zamu Complex (numerous basic sills later folded by an event contemporaneous with the Nimbuwah Complex),

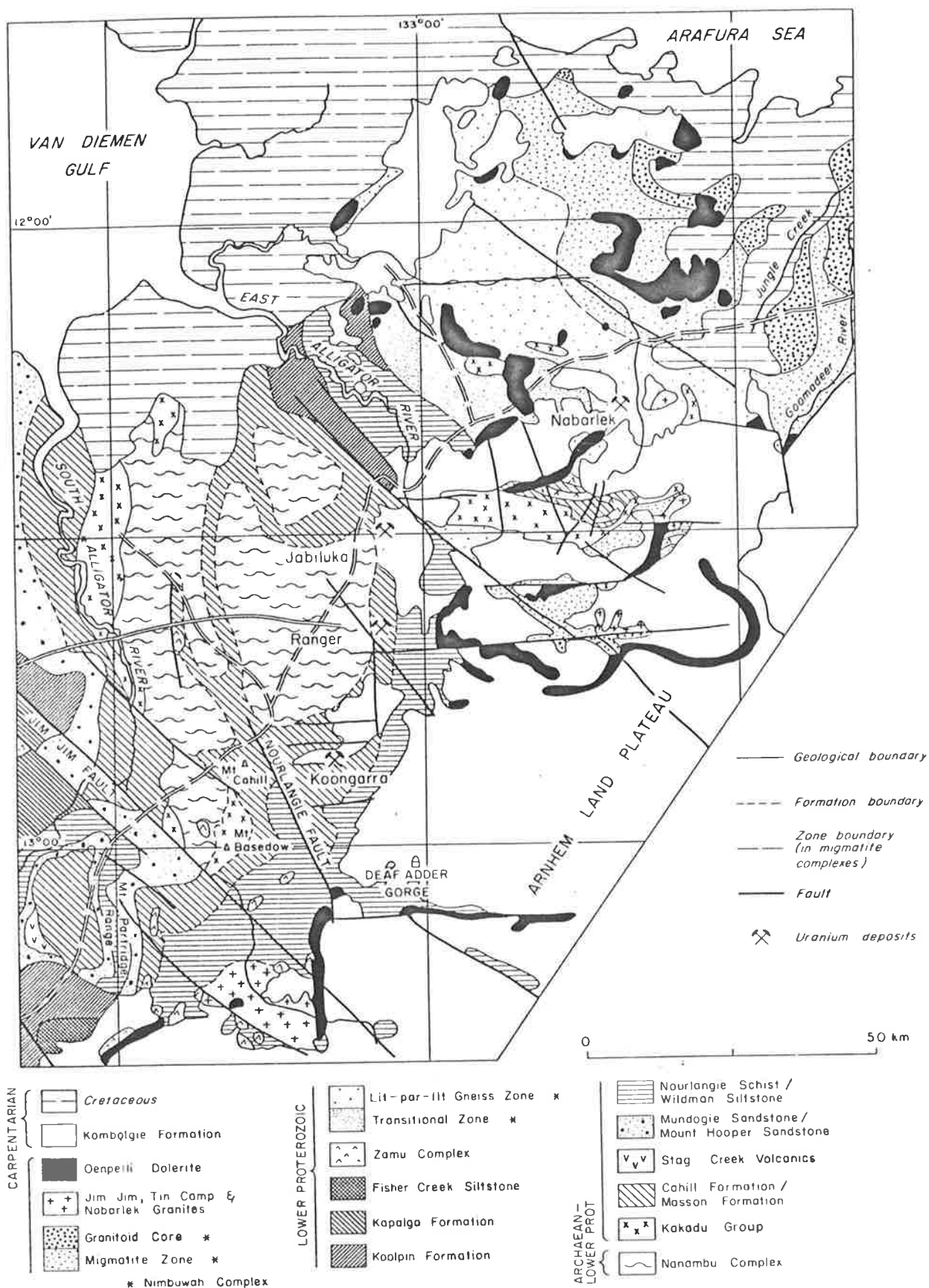


Figure 2: Regional Geology of the Alligator River Uranium Province. (After Needham and Stuart-Smith, 1979).

and the Oenpelli Dolerite (an extensive series of lopolith-like basins and attendant dykes). The Nimbuwah migmatic event culminated with the intrusion of early Carpentarian anatectic granites (the Jim-Jim, Tin Camp, and Nabarlek Granites). All these rocks are overlain with marked unconformity in the east and southeast of the uranium field by an extensive Carpentarian plateau sandstone with interbedded volcanics (the Kombolgie Formation)".

Recent geochronological determinations of these rock units by Pate et al. (1979) indicated the following ages:

- The granite in the centre of the Nanambu Complex is probably not older than 2500 m.y.
- The granitoid development of the Nimbuwah Complex took place at 1870 m.y.
- The regional metamorphism ended at 1800 m.y. ago, and the Jim-Jim, Tin Camp, and Nabarlek Granites yielded ages between 1760 and 1780 m.y.
- The Pine Creek Geosyncline metasediments have an estimated stratigraphic age bracket of between 2,400 and 1,800 m.y.
- The emplacement of the Oenpelli Dolerite has been determined at 1688 m.y. This age set a maximum age for the Kombolgie Formation.
- The retrograde chloritization affecting the host metasediments of uranium deposits has a suggested age of 1600 m.y. This alteration was a rather localized low-temperature metasomatism.
- At Nabarlek, radiometric analyses of the ore zone points to a low temperature alteration event between 850 and 1000 m.y. This range is not in great disagreement with the ages determined by Hills and Richard (1976) in pitchblende and uranite. The alteration process represents the last recorded remobilization of uranium ore and growth of secondary sericite and chlorite in the deposit. These alteration products are the equivalent of the "replacive chlorites" of Anthony (1976), the immediate host of uranium ore mineralization.
- Finally, ages between 1200 and 1370 m.y. were determined for the late-Carpentarian, post-Kombolgie dykes. These ages combined with

the age of Oenpelli Dolerite limit the deposition of the Kombolgie Formation between 1688 and 1370 m.y.

The unit of major interest within this geological sequence is the Cahill Formation, host of uranium deposits. This Formation extends around the Nanambu Complex and grades towards the NE into a migmatite terrain of the Nimbuwah Complex (Figure 2). Needham and Stuart-Smith (1979) informally subdivided the Cahill Formation into lower and upper members. "The lower member, which contains the major uranium deposits of the area, is a sequence of interbanded pyritic carbonaceous mica schist, chloritized feldspathic quartzite and quartz schist, para-amphibolite, calc-silicate rocks, and lenses of massive dolomite up to 250m thick. The lower member ranges in thickness from 300 to 600m..." "Carbonaceous rocks have the highest U, Th, Zn, Ni and S values. The upper member is composed of 2500m of interlayered feldspathic quartz schist, feldspathic schist, feldspathic quartzite and minor mica schist, and quartzo-feldspathic gneiss".

Ferguson (1979) has demonstrated the occurrence of two metamorphic provinces in the Lower Proterozoic metasediments of the Pine Creek Geosyncline: a low-grade metamorphic province to the west of South Alligator Hinge Zone - which approximately follows the South Alligator River - and a medium- to high-grade metamorphic province to the east of the same Hinge Zone. These are the host rocks of the uranium deposits. The metapelites of the Cahill Formation contain the mineral paragenesis of almandine + kyanite/sillimanite + biotite + muscovite + staurolite + plagioclase + K-feldspar.

Chloritization of ferro-magnesian minerals and sericitization of feldspars are considered products of retrograde metamorphism. Hematitization is common and associated with chlorite alteration and in some places with uranium mineralization. Microstructures indicate at least four phases of deformation, which are supposed to be related to the 1800 m.y. metamorphic event (Needham and Stuart-Smith, 1976).

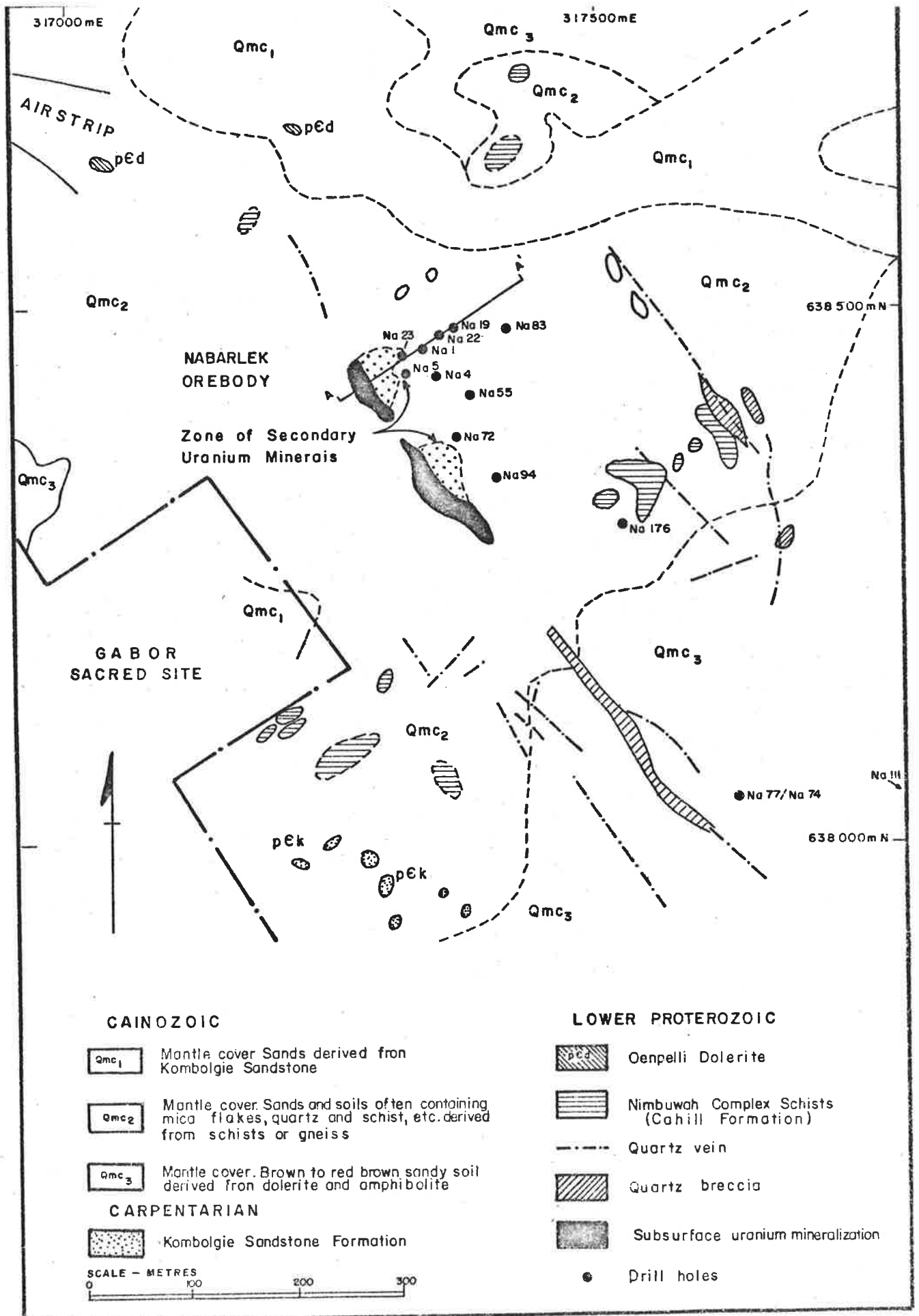


Figure 3: Geological map of the Nabarlek uranium deposit.  
(Modified from Queensland Mines Ltd.).



## I.2 Geology of the Nabarlek Area

Outcrops of the Lower Proterozoic metasediments in the Nabarlek area are rare. The present day surface is probably close to the unconformity between the metasediments and the Kombolgie Sandstone. One kilometer to the southwest of the deposit, the Kombolgie Formation crops out at the Green Ant Hill; in the same direction, at approximately 300m from the deposit, huge blocks of sandstone remain on the surface (Figures 3 and 4).

The uranium mineralization is concentrated in a deformation zone within a structure which appears to be the controlling factor. Heavy chloritization (850 to 1000 m.y., Page et al., 1979), is present along this zone. The structure is a shear zone which can be followed on the surface for nearly 600m. It strikes about  $330^{\circ}$  and dips  $30^{\circ}$  to  $45^{\circ}$  to the east. A 250m thick dolerite sill (Oenpelli Dolerite) appears to truncate this structure at the depth (Anthony, 1976). The orebody itself has an irregularly outlined tabular shape which approximately follows the shear zone. A cross-section of the deposit shows the orebody wedging out at the depth of 50m against the Oenpelli Dolerite (Figure 5). The orebody has an extension of 250m and a thickness in the range 0 to 20m (average of 10m). The deepest ore outlined by drill holes was at -85m, but most of the orebody is above -45m from the ground level.

Hopwood (1971) reports at least three deformation events in the Nabarlek area. The fold styles are tight isoclinal overturned to recumbent and assymetricl such as normally associated with thrust folding. These deformation events produced assymetrical successively: folding, faulting, shearing and brecciation in the Cahill metasediments.

The lithology of these metasediments is somewhat different from the description given by Needham and Stuart-Smith (1979) and also from the rock types found at Jabiluka, Ranger and Koongarra. Carbonaceous schists and massive dolomites which are present with or adjacent to uranium mineralization have not been intersected in drill cores, but were found later during the mining operation. No!

Schists and gneisses with variable amounts of micaceous and siliceous minerals form the main rock types. Anthony (1976) described five different types from the bottom to the top of the deposit (Figure 6):

- Siliceous chlorite schist - predominantly chlorite with some quartz and feldspar.
- Chlorite schist - essentially chlorite with some sericite. It is the most common rock unit in the Mine area.
- Micaceous chlorite schist - essentially chlorite and 25 percent white mica. This unit intertongues with the chlorite schist and the chlorite mica schist.
- Chlorite mica schist - chlorite and more than 50 percent white mica. This unit also includes mica schists which contain more than 90 percent white mica.
- Quartz mica schist and quartz schist - the quartz and mica contents are highly variable. Quartz ranges from 25 to 90 percent.

All stock types are present in the Mine area. However, to the south the chlorite mica schist disappears rapidly while the micaceous chlorite schist diminishes progressively; the siliceous chlorite schist becomes more conspicuous. Apart from these five rock types, a unit formed by actinolite schist is present between the dolerite sill and the siliceous chlorite schist in the southern area. This actinolite schist is considered a metadolerite.

Distinct from these units there are two intrusive igneous rocks. One is the above-mentioned dolerite sill which is deeply altered at the top part. Alteration reaches as deep as 40m from the top (Figure 5). Mafic minerals are chloritized and feldspars are sericitized to different degrees. Generally, the dolerite texture is still preserved but in a few cases, the intensity of alteration had obliterated completely the texture of the rock. Quartz may be locally present in vugs and veins. Apparently there were two stages of alteration. The first stage was probably related to the retrogressive metamorphism (1600 m.y.). It was observed not only in the ore zone but also in outcrops approximately 1 km northwest of the orebody as well. The second was

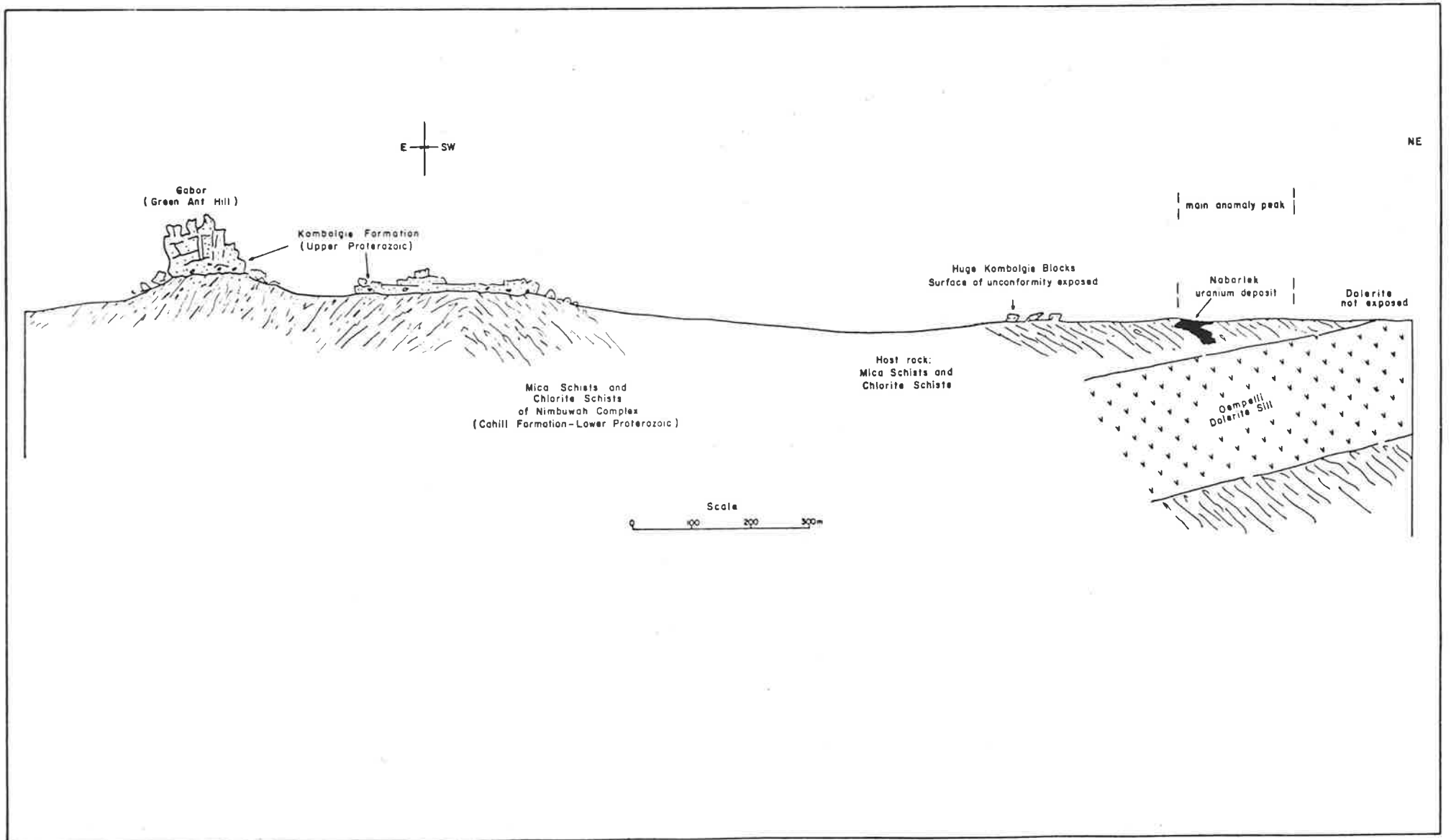


Figure 4: Sketch cross-section from Gabor to Nabarlek uranium deposit. (Modified from Queensland Mines Ltd.).

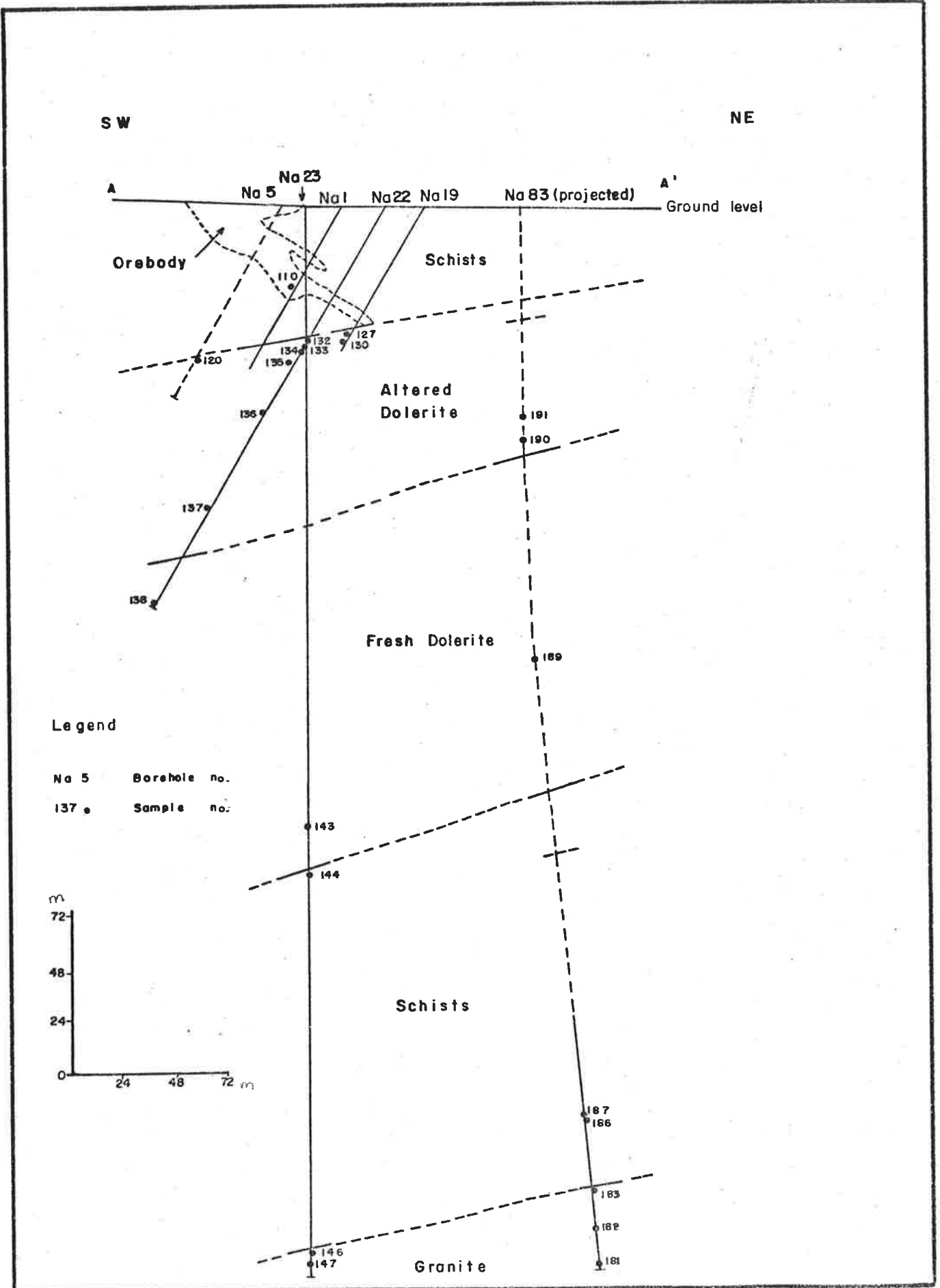


Figure 5: Borehole Section A-A' (from Figure 3).  
 (Data from Queensland Mines Ltd.).

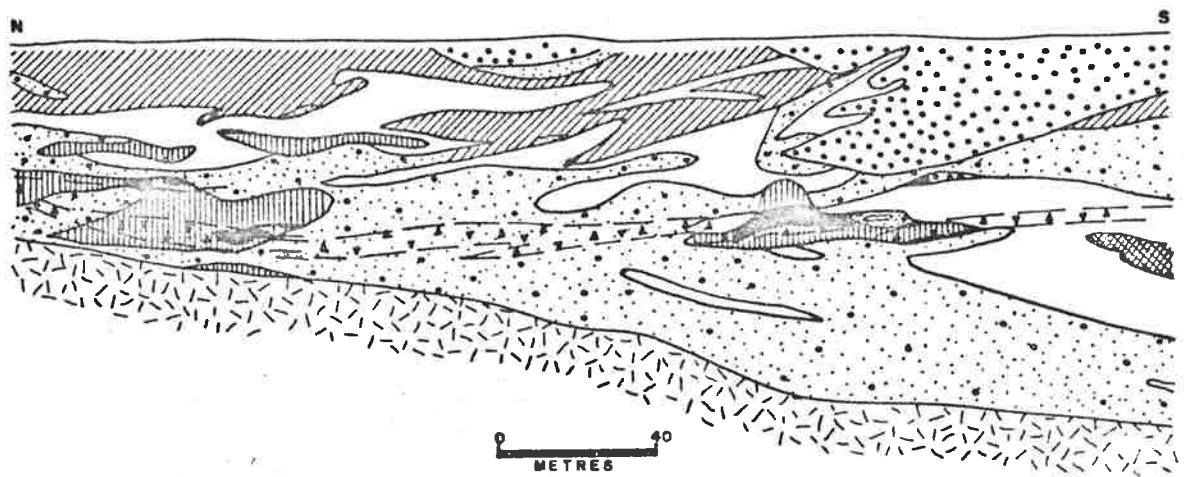
probably related to the hydrothermal alteration of the ore zone and seems to have been superimposed on the previous alterations. Actually, the distinction between both stages in dolerite samples from under the ore zone is difficult to make. The other intrusive igneous rock is a medium to coarse-grained, pink to greenish, non-foliated granite. It appears at 400m below the surface intruding the metasediments below the dolerite sill. Feldspars from this granite are also sericitized to different degrees. The outline of these two igneous bodies were detected mainly by two vertical boreholes: D.H. Na23 and D.H. Na83 (figure 5). A granite outcropping 7 km east of Nabarlek is probably part of the same stock.

At Nabarlek, the uranium mineralization is associated with a massive chlorite unit which is distinct from the chlorite schist. The rock is fine-grained, dark green and possibly shows flow textures and chlorite in radial aggregates. No signs of schistosity were observed in these rocks. Their textures are cutting across with regard to the schistosity indicating emplacement of the mineralization after the regional metamorphic event. This has been confirmed by radiometric dates by Page et al. (1979). Pitchblende is intimately associated with chlorite (precipitated between the chlorite flakes). Locally the pitchblende forms massive concentrations as in samples A-495-110 (Plate IV, photo 1) and A-495-116. Oxidation makes these types of samples become reddish to mottled with massive limonite (goethite?) and coarse pitchblende blebs.

A short description of each sample is given in the Appendix 1.

### I.3 The Mineral Paragenesis

The major limitation for the fluid inclusion study on samples from Nabarlek was the scarcity of suitable material in drill cores from the orebody. The oxygen isotope study was also hampered by limitation in mineral selection. Chlorite was almost always contaminated either by sericite or by opaque minerals and sericite was contaminated by chlorite. Crushing tests could be performed only on three massive pitchblende samples from the ore zone. The other selected samples were from holes drilled at the southeastern extension of the orebody cutting the shear zone. Among these holes Na77 presented the



L E G E N D










	QUARTZ MICA SCHIST- QUARTZ SCHIST		DOLERITE
	CHLORITE MICA SCHIST		CHLORITE ROCK
	MICACEOUS CHLORITE SCHIST		ORE
	CHLORITE SCHIST		CRUSH ZONE
	SILICEOUS CHLORITE SCHIST		

Figure 6: Geological longitudinal section through the Mine area.  
(After Anthony, 1976).

best sequence of samples with quartz, some of them being associated with uranium mineralization (Figure 3 and 7).

Apart from quartz, no other minerals were present in veins and cavities in amounts significant enough to permit the establishment of a paragenetic sequence. Pitchblende is present in different types of quartz. Calcite has been detected in only three samples. Sulphides were observed mostly in microscopic amounts.

#### Quartz

Quartz in metasediments from Nabarlek samples could be distinguished from quartz from hydrothermal origin. Metamorphogenic quartz (always from retrogressed schists) has variable grain sizes. In some places it appears as small lenses parallel to the schistosity (A-495-179), while in others quartz occurs as part of the sedimentary sequence: quartzites (A-495-172). Both are characterized by effects of metamorphism like undulose extinction, recrystallization and irregular contours of the grains. Furthermore, the quartz layers are always parallel to the schistosity.

Quartz originating from hydrothermal solutions is always found on the walls of cavities, veins, as open-spaces fillings, or in breccias. The best example is from sample A-495-176 (Plate V, photos 3 and 4). They are well crystallized into late-stage idiomorphic crystals. In the quartz crystallized at an earlier stage (closer to the wall rock) - even when disrupted by numerous fractures - still the original zones of growth of the mineral could be observed and no metamorphic effects are present. Although no detailed paragenetical sequence of all vein quartz could yet be determined, a distinction between the quartz crystallized at an early-stage and those crystallized at a late-stage could be made. Obviously no exact time correlation was expected for all quartz of each stage from different samples. But the studies performed indicated that these two types of quartz contain inclusions with different homogenization temperatures and present different oxygen isotope composition.

Concluding, quartz from samples collected at the Nabarlek uranium deposit area could be separated into three different categories:

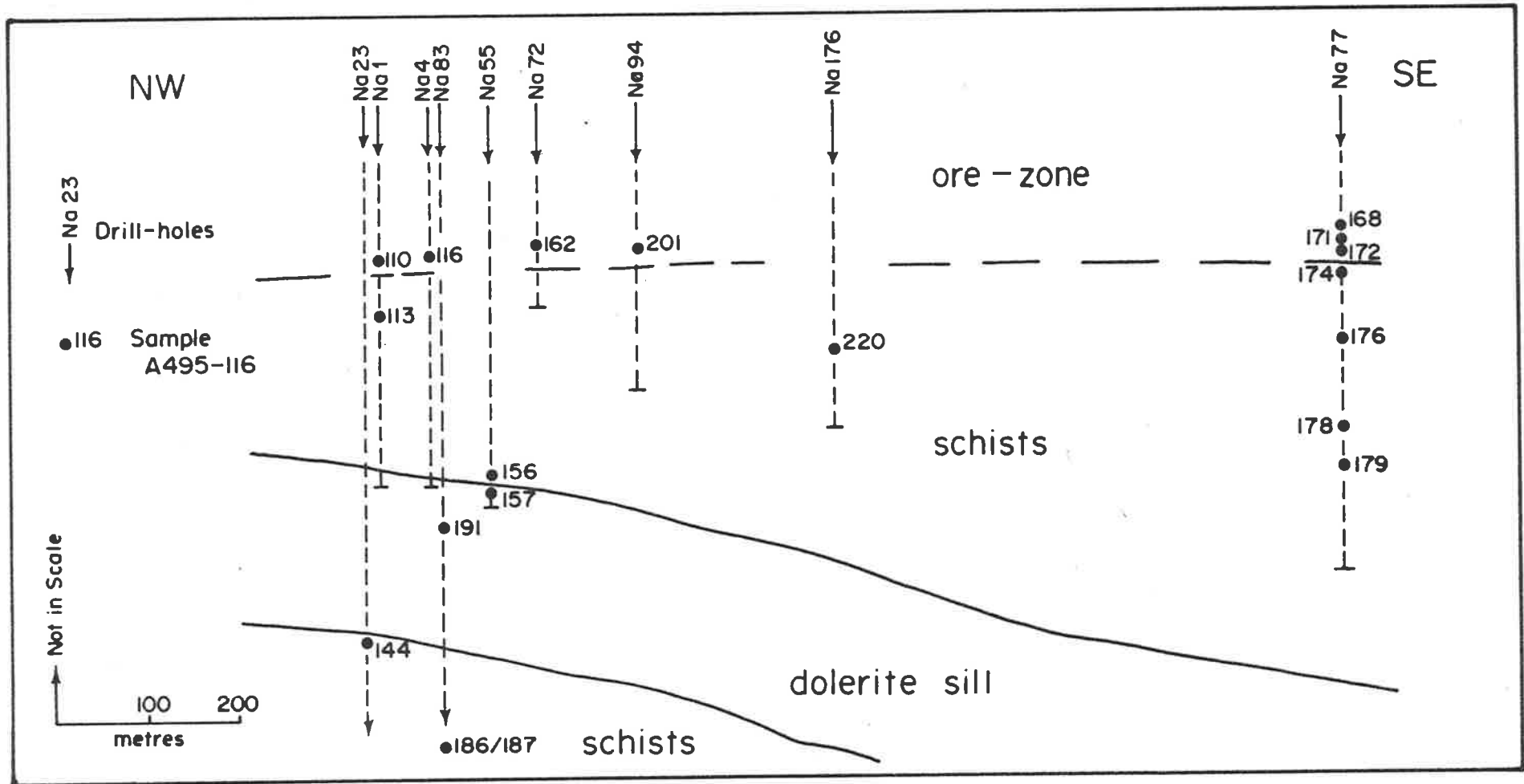


Figure 7: Longitudinal section through the Mine area indicating the location of samples.



Phase I	- metamorphogenic and original sedimentary	
Phase II	- early-stage	)
		) hydrothermal origin
Phase III	- late-stage	)

#### Pitchblende

The successive remobilization and concentration of uranium, up to the present stage of formation of the Alligator River deposits, has been suggested in several papers: Anthony, 1976; Needham and Stuart-Smith, 1976; Hegge, 1977. At Nabarlek some pitchblende has been observed in metamorphogenic quartz while most of it precipitated before, during and after the crystallization of late-stage quartz (e.g. samples A-495-168, A-495-172). There appears to be more or less a continuous remobilization and redeposition of pitchblende. The last phase of pitchblende formation in these samples (A-495-168 and A-495-172) forms the last phase in pitchblende paragenesis (Phase IV) (Plate I, photo 2; Plate II, photos 3 and 4; Plate III, photo 2; and Plate IV, photo 2), which is also the major one.

The massive pitchblende of the ore zone is not commonly associated with hydrothermal quartz. However, this pitchblende phase is intimately associated with the chlorite of the massive chlorite rock, which is also considered to be a product of hydrothermal activity. The closest hydrothermal quartz associated with this massive chlorite-rock was observed in sample A-495-113 located immediately below the orebody. Therefore, the assumption that the pitchblende from the orebody and the pitchblende associated with hydrothermal quartz studied in samples from drill hole Na77 are, at least partially, contemporaneous appears justified. By inference it also seems reasonable to assume that at least part of the orebody was formed during the phase IV. This assumption is also in agreement with the findings of Page et al. (1979) for the 850 to 1000 m.y. alteration episode as the last recorded period of re-deposition of uranium ore at Nabarlek.

#### Calcite

Calcite was detected in only three samples, always as veinlets. In sample A-495-220 a calcite veinlet cuts across an altered feldspar actinolite

schist while in sample A-495-144 it forms on hydrothermal quartz. In the third sample (A-495-110; Plate IV, photo 1), fibrous calcite cuts across massive pitchblende. Considering the paragenetic relation of calcite pitchblende and quartz in sample A-495-144 and with the alteration effects of samples A-495-220 and A-495-110, calcite appears to be youngest of the three minerals (Phase V). The calcites from A-495-144 and A-495-220 may have been formed during phase IV.

In conclusion, the following mineral paragenetic sequence will be suggested:

	Phase I	Phase II	Phase III	Phase IV	Phase V
Metamorphogenic quartz	_____				
Hydrothermal quartz: early-stage		_____			
Hydrothermal quartz: late-stage			_____		
Pitchblende	_____	_____	_____	_____	
Calcite				_____ ?	_____

Figure 8. Paragenetic sequence of quartz, pitchblende, and calcite from the Nabarlek uranium deposit.

## CHAPTER II

FLUID INCLUSION STUDYII.1 Methods and Principles

A great variety of methods have been used in the study of the composition of fluid inclusions, and many new techniques have been applied during recent years. These techniques can be classified into non-destructive and destructive methods. (Roedder, 1967 and 1972).

II.1.1 Non-destructive methods

Among the range of non-destructive techniques only a few are generally applicable. The major limiting factors are the transparency of the host minerals and the size of the inclusions.

Although non-destructive methods can only produce qualitative and, at the best, semi-quantitative results, the main advantage of these techniques is that it is possible to repeat the same test or to apply different tests on the same specimen. However, repetition of analysis is precluded in the following cases:

- a) when leakage occurs because of a fracture of the host mineral caused by expansion of the fluid phase either during freezing or during heating tests;
- b) when metastable conditions are present. Phase changes under these conditions are rate dependent and may produce different end results (e.g. sample A-495-172 F);
- c) when irreversible pH or Eh changes take place due to imperceptible loss of volatiles from the inclusions during thermal cycles (see heating test of sample A-495-172 B).

A second advantage of non-destructive methods is that they can be performed on very small samples. Some samples studied (e.g. A-495-220) were tiny calcite crystals of less than 0.5 mm.

Although tiny crystals or pieces of transparent mineral may be used, the usual type of sample is a thick section of mineral or rock. The thickness

varies according to the transparency of the host minerals and the size of the inclusions present in them. Because of these limitations, Ermakov (1965, p.92) recommends sections of 0.2 to 0.1 mm thick for semi-transparent minerals, and Roedder (1972) states that thickness exceeding 0.5 to 5 mm range would seldom be necessary. Leroy (1971) and Schwartzkopff et al. (1974) recommend a thickness of 0.1 to 0.25 mm. In the present work sections ~0.2 mm thick or less were used in samples with minerals of poor transparency because very few inclusions exceeded 0.1 mm in diameter. The sections were normally polished on both sides to minimize the effects of total reflection on fluid inclusion boundaries and scattering of light.

The main non-destructive methods are:

#### II.1.1.1 Petrographic microscopy

The main non-destructive tool is still the ordinary petrographic microscope. Morphology of inclusions and the solid phases present in them, number of phases present, different phase-ratios, viscosity of liquid phases, colour of liquid and solid phases, wetting characteristics, index of refractions, and birefringence, are all properties which can be studied satisfactorily with a petrographic microscope and its usual accessories.

In addition to the investigation of the normal thick doubly polished sections, the use of small transparent chips has been shown to be a quick and useful method for a preliminary study of fluid inclusions. This method is not very useful for strained or intensely fractured minerals. Such host minerals tend to lose their fluids by leakage when fractured.

#### II.1.1.2 Microthermometry

Special stages, which fit onto the petrographical microscope, are used for cooling or heating of fluid inclusions. The heating stage enables phase changes to be observed for microscopic specimens. The phase changes during heating or cooling give information about the chemical composition of the fluid inclusions.

Descriptions of the different microthermometric techniques used are found in the following papers: Roedder, 1962; Ypma, 1965; Bazarov, 1966;

Hayakawa et al., 1969; Kelly and Goddard, 1969; Proceedings of COFFI, 1969, p. 4-7; Khetagurov, 1971; Leroy, 1971; Kharlamov, 1973; Kalyuzhni, 1973; Smith, 1973; Gallup et al., 1975; Poty et al., 1976.

During cooling, a depression of the melting point of the fluid phase will allow the determination of salinity of solutions. A problem occurs when the fluids contain compounds that form gas clathrates. The formation of clathrates will increase the salinity of the remaining solution. If the last ice melts before the clathrates, the temperature will indicate a salinity which is, as that temperature, higher than the actual salinity of the fluid. When this is the case, salinity determinations as proposed by some authors need to be corrected by the amount of water tied to the gas clathrates (e.g. Hollister & Burruss, 1976; Weisbrod et al., 1976).

When daughter minerals are present, the temperatures of their dissolution upon heating gives the indication of the salinity. In both cases the determination is made using the phase equilibria of the salt - H<sub>2</sub>O system. The salinity is usually given in equivalence of NaCl weight percent using the NaCl-H<sub>2</sub>O system (Figure 9). However, even when NaCl daughter minerals are present, the salinity indicated by the temperature of dissolution of the salt may be misleading if it is not interpreted in conjunction with the results of freezing tests. This is easily understood if one examines the temperature-composition diagram of the system CaCl<sub>2</sub>-NaCl-H<sub>2</sub>O (Figures 10 and 11). Solutions containing 31 wt.% CaCl<sub>2</sub> and only 3 wt.% NaCl will nucleate only a NaCl daughter mineral. On cooling to 20°C, such solutions have been interpreted as NaCl - saturated solutions which salinities have been calculated from the temperature of dissolution of NaCl. The presence of CaCl<sub>2</sub> could easily have been missed. The results in this case will therefore be qualitative and quantitatively misleading. A low initial melting temperature of ice will be the only indication alerting the observer of the presence of CaCl<sub>2</sub> or MgCl<sub>2</sub>. Destructive methods are needed to interpret the significance of NaCl daughter minerals. A test for the presence of CaCl<sub>2</sub> or MgCl<sub>2</sub> should be carried out when the last ice melts at a temperature well below the eutectic point of the

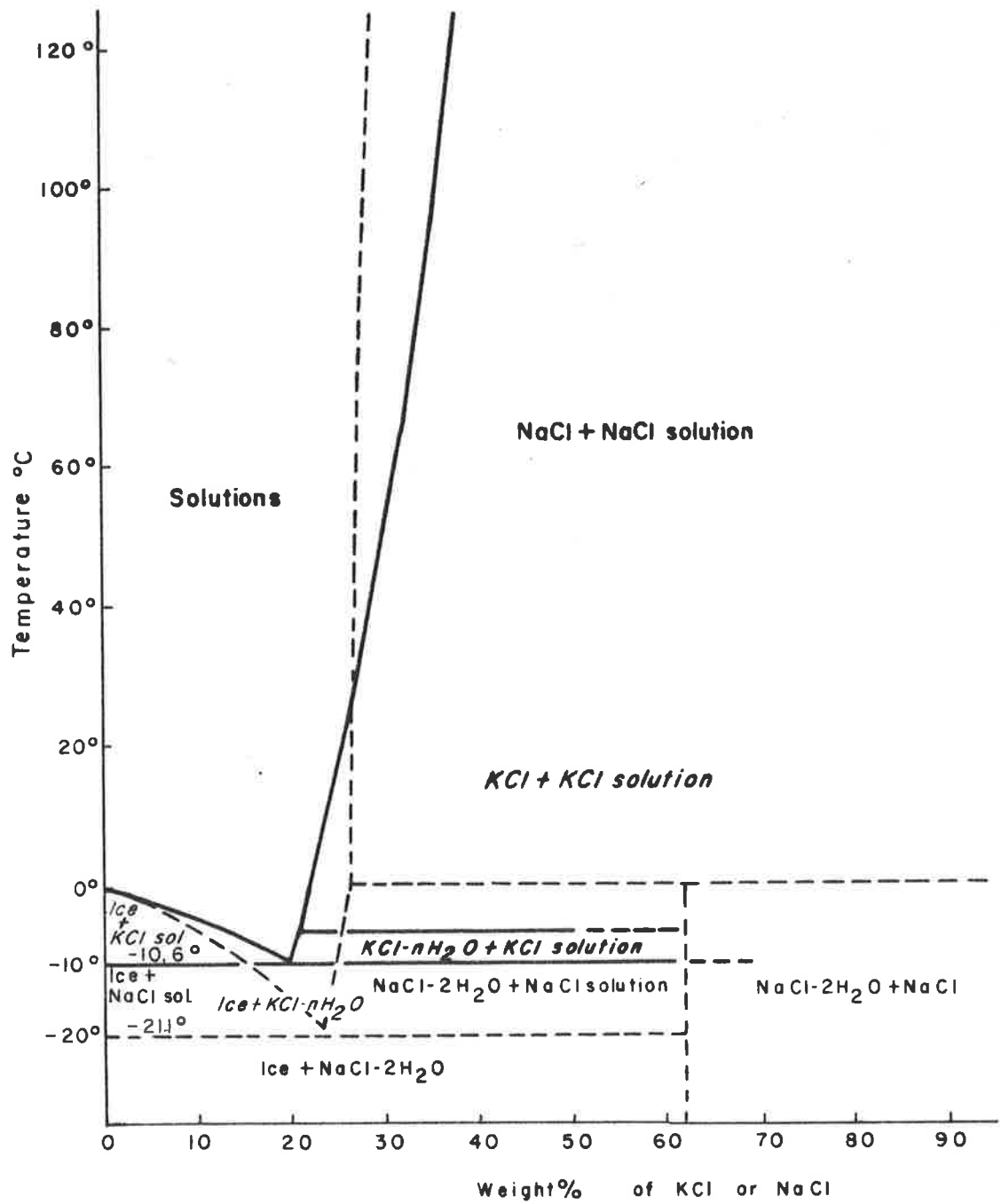


Figure 9: Phase diagram of the systems NaCl-H<sub>2</sub>O (dashed line) and KCl-H<sub>2</sub>O (heavy line).

(Data from Linke, 1965, and Roedder, 1962).

NaCl-H<sub>2</sub>O system. Even when the extreme values given in this example are not considered, ices melting at temperatures below -30°C could point to solutions at least 2.5 times richer in CaCl<sub>2</sub> than in NaCl (Figure 10). Considering that the presence of CaCl<sub>2</sub> in hydrothermal solutions is fairly common, one has to be cautious that the presence of a NaCl daughter mineral is not simply interpreted as evidence for a NaCl dominant solution.

In the present study, the following points have become apparent:

- a) Melting temperature of ice frequently fall below the eutectic point of NaCl-H<sub>2</sub>O system (-21.1°C), and occasionally as low as -60°C.
- b) The majority of inclusions with last melting temperature below -21.1°C contains only liquid + vapour phases, which indicates that the NaCl-H<sub>2</sub>O system is not applicable in these cases.
- c) Some inclusions showed CaCl<sub>2</sub>-hydrates on cooling, the presence of which was later confirmed by scanning electron microscopy.

As CaCl<sub>2</sub> appears to be the dominant species, salinities will be presented mainly as equivalent of CaCl<sub>2</sub> weight percent according to the diagram of the CaCl<sub>2</sub>-H<sub>2</sub>O system (Figure 12).

Several values have been measured which are even below the eutectic temperature of the CaCl<sub>2</sub>-H<sub>2</sub>O system (-49.8°C) or CaCl<sub>2</sub>-NaCl-H<sub>2</sub>O system (-52.0°C) (Yanatieva, 1946; Figures 10 and 11). Values below -52.0°C are probably due to other salts such as: MgCl<sub>2</sub>, KCl, FeCl<sub>2</sub>, and AlCl<sub>3</sub>, all of which have been confirmed by scanning electron microscopy. The eutectic temperatures of each one of these salt-water systems are: HCl-H<sub>2</sub>O: -10.7°C (Figure 9); MgCl<sub>2</sub>-H<sub>2</sub>O: -33.6°C (Figure 13); FeCl<sub>2</sub>-H<sub>2</sub>O: -36.5°C (Figure 14); AlCl<sub>3</sub>-H<sub>2</sub>O: -55°C (Figure 15).

Although no data is available for complex mixtures of these salts, values as low as -60°C are probably the result of a multicomponent eutectic. This idea is supported by phase changes of salt hydrates between -43°C and -35.5°C in calcite of sample A-495-144, in which case one is probably dealing with a system like CaCl<sub>2</sub>-MgCl<sub>2</sub>-FeCl<sub>2</sub>-NaCl-H<sub>2</sub>O.

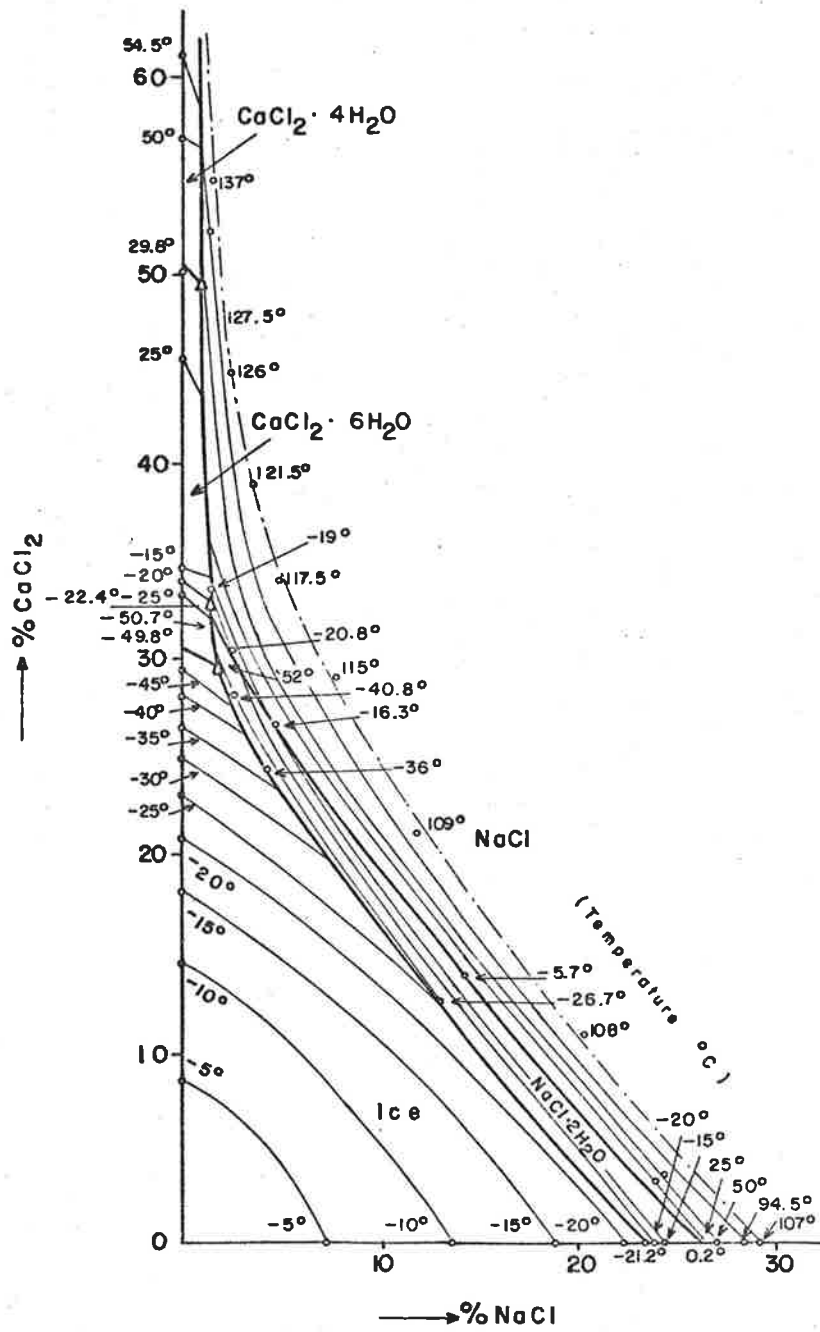


Figure 10: Phase diagram of the system NaCl-CaCl<sub>2</sub>-H<sub>2</sub>O (modified from Yanatieva, 1946).



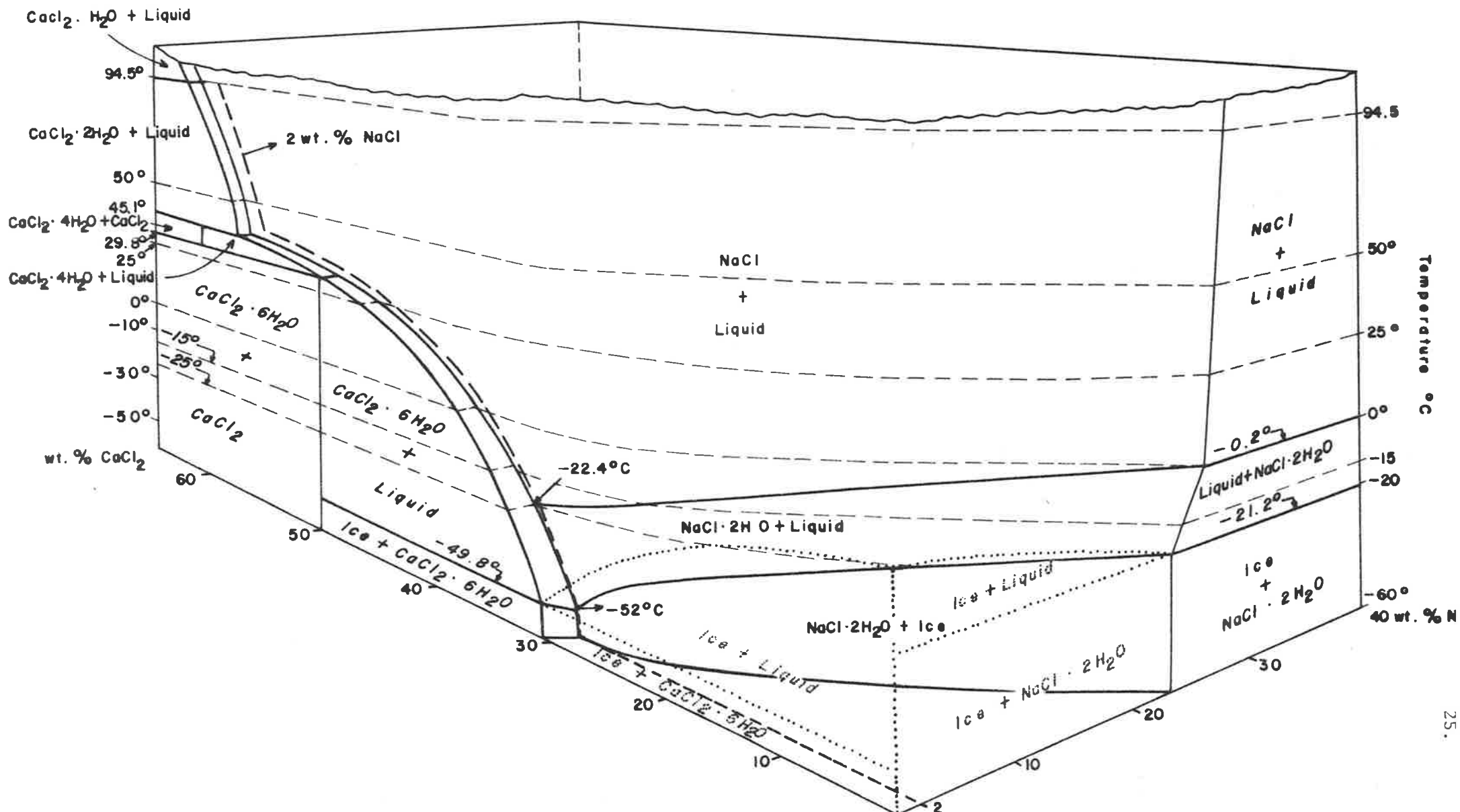


Figure 11: Temperature-composition Model of the System  $\text{CaCl}_2\text{-NaCl-H}_2\text{O}$ . (Modified from Ypma & Fuzikawa, 1979).

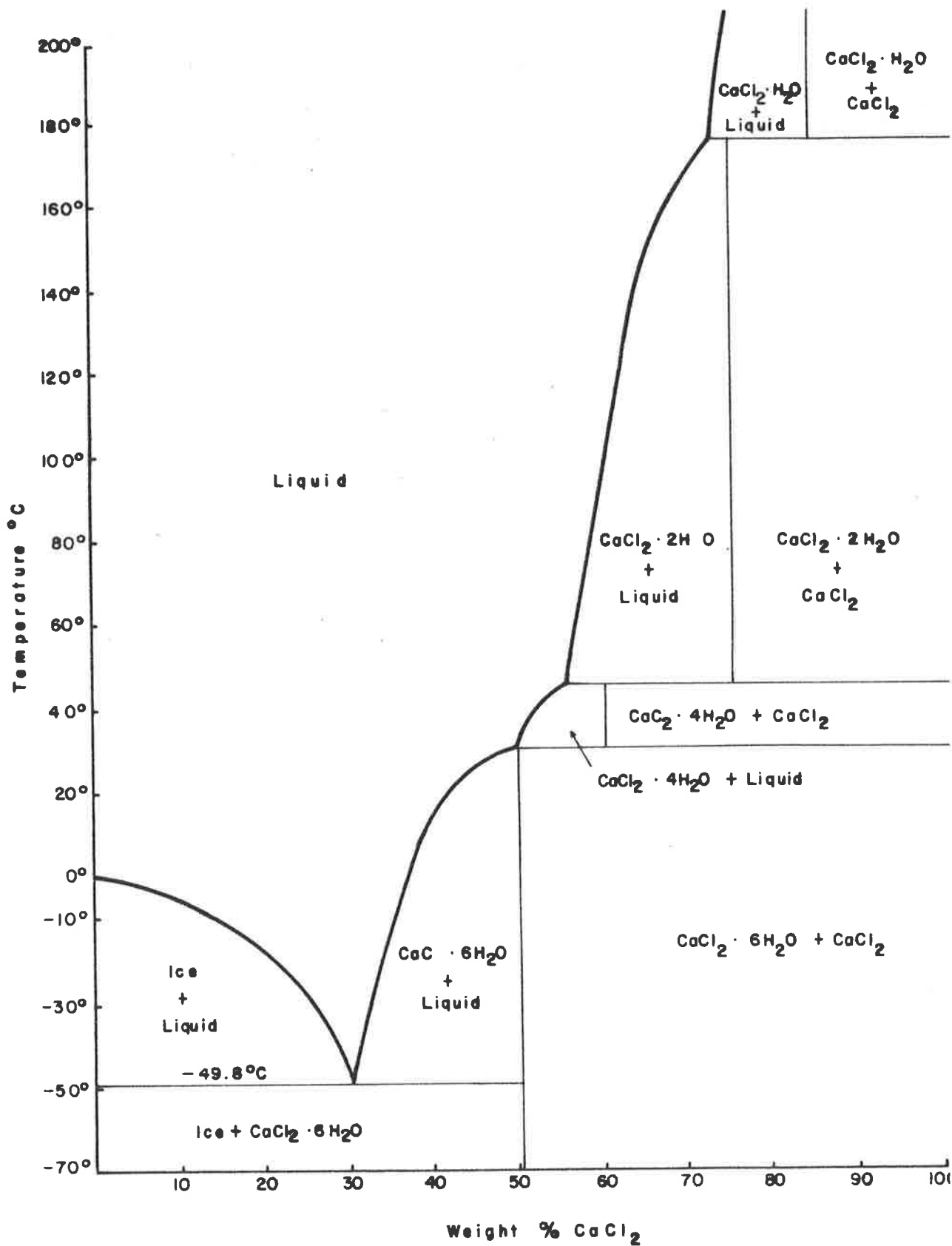


Figure 12: Phase diagram of the system  $\text{CaCl}_2\text{-H}_2\text{O}$  below  $200^{\circ}\text{C}$  based mainly on data from Yanatieva (1946).

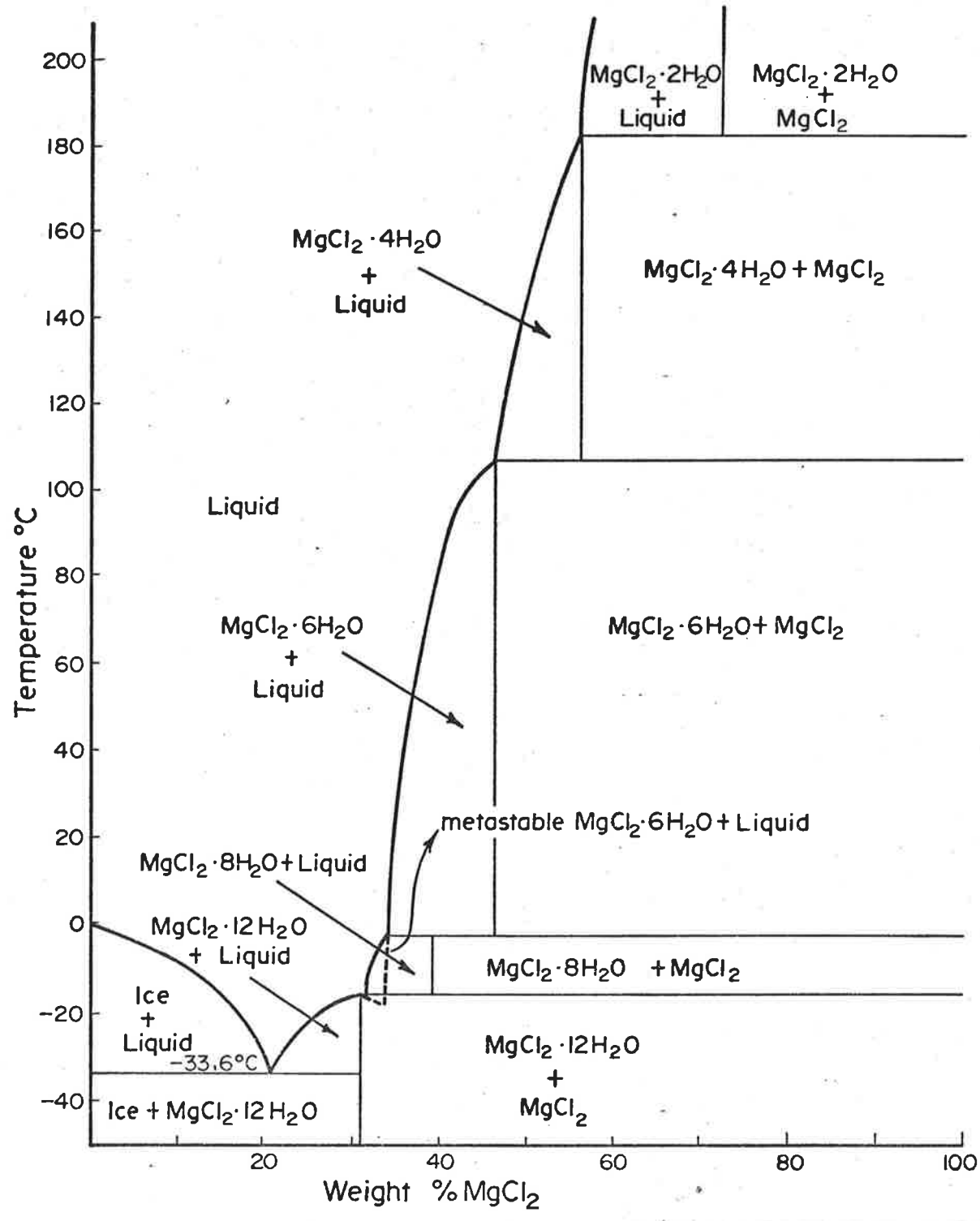


Figure 13: Phase diagram of the system MgCl<sub>2</sub>-H<sub>2</sub>O below 200°C based on data from Yanatieva (1946).

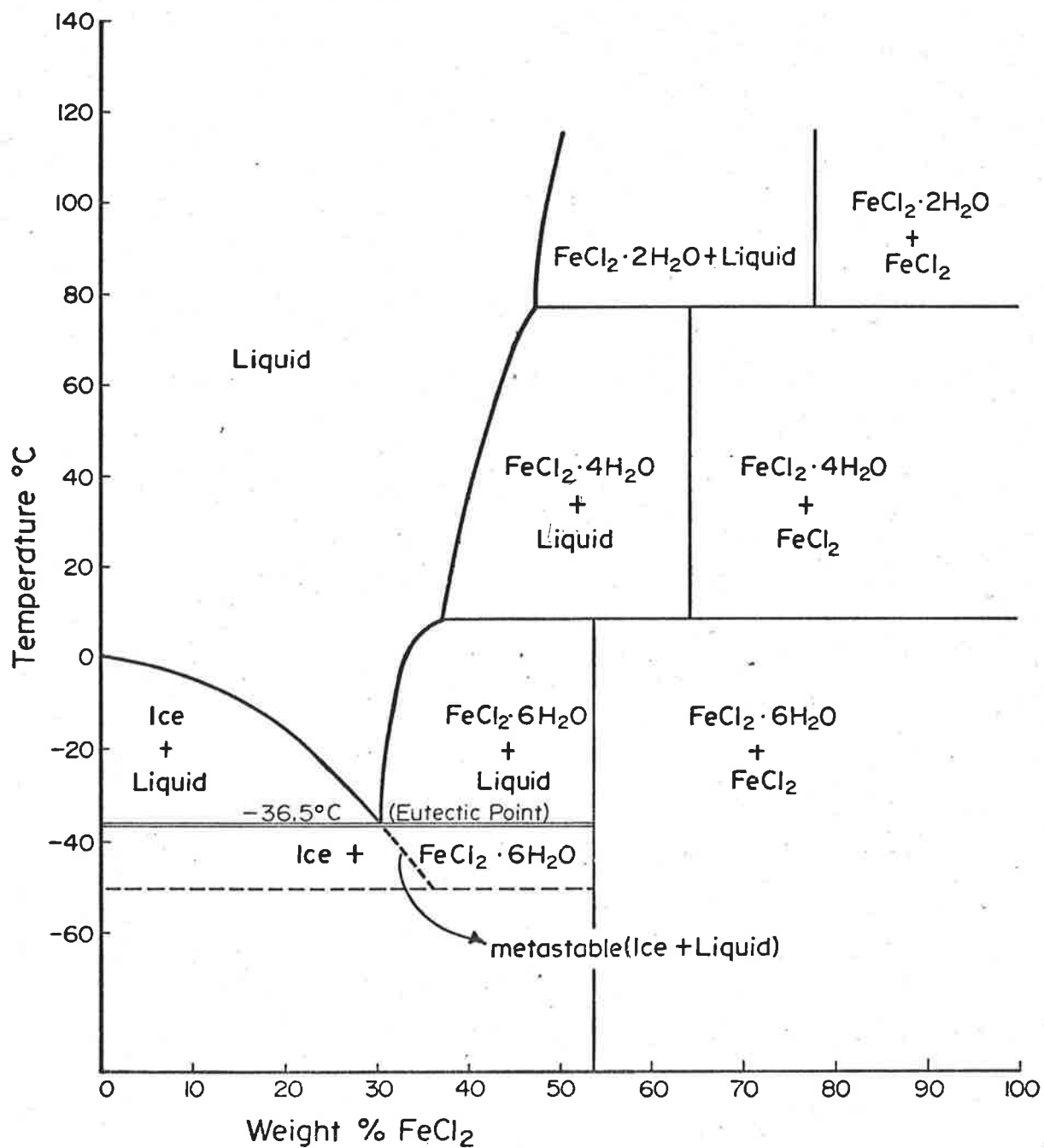


Figure 14: Phase diagram of the system FeCl<sub>2</sub>-H<sub>2</sub>O below 120°C (Data from Linke, 1965).

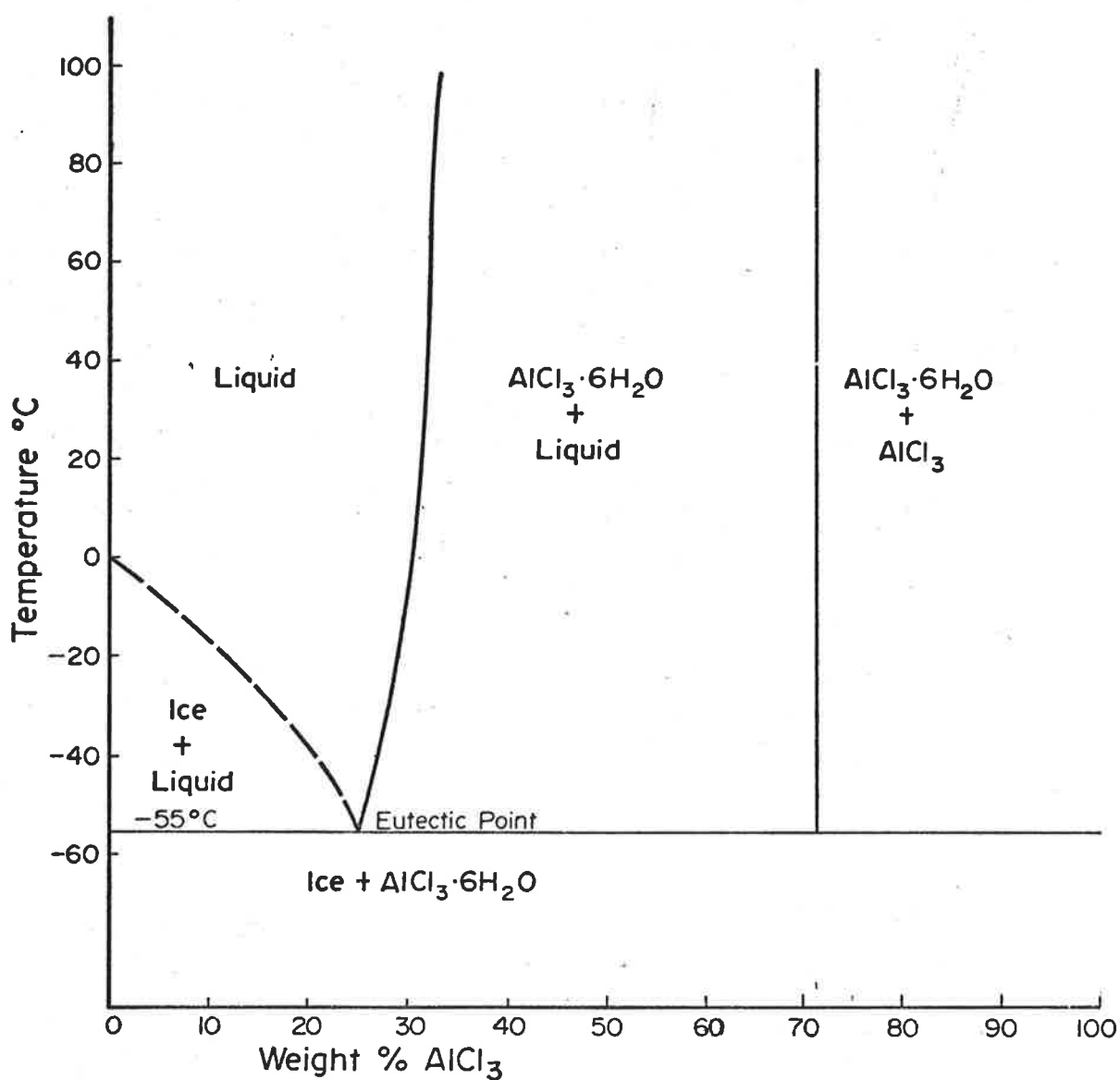


Figure 15: Phase diagram of the system  $\text{AlCl}_3\text{-H}_2\text{O}$  below  $100^{\circ}\text{C}$ .  
(Data from Linke, 1965).

The melting point of  $\text{CO}_2$  ( $-56.6^\circ\text{C}$ ) is another important temperature of reference because the presence of carbon dioxide in fluid inclusions is fairly common. When the melting temperature of solid  $\text{CO}_2$  is lower than  $-56.6^\circ\text{C}$ , the presence of other volatiles with lower critical temperatures are indicated: such as  $\text{CH}_4$ . In a pure  $\text{CO}_2 + \text{CH}_4$  system, the depression of the three phase curves: solid  $\text{CO}_2$ ,  $\text{CO}_2 + \text{CH}_4$  liquid and  $\text{CO}_2 + \text{CH}_4$  vapour, can be used as a property to determine the amount of  $\text{CH}_4$  in this mixture (Figure 16, curve B). The curve B is the locus of triple points of the  $\text{CO}_2 + \text{CH}_4$  mixtures with increasing  $\text{CH}_4$ . But the use of this curve for determining the total amount of  $\text{CH}_4$  in fluid inclusions may not be as simple as proposed by Hollister and Burruss (1976). Upon freezing, these gases will form clathrate compounds. If the amount of  $\text{CH}_4$  and  $\text{CO}_2$  is small, all the molecules of these gases will be tied to the clathrate structure. If they exceed the available amount of  $\text{H}_2\text{O}$  molecules(\*), the  $\text{CO}_2/\text{CH}_4$  ratio of the remaining fluid will probably not correspond to the actual  $\text{CO}_2/\text{CH}_4$  ratio of the inclusion. In this circumstance, the estimated amount of  $\text{CH}_4$  in the  $\text{CO}_2 + \text{CH}_4$  mixture, will not be correct.

Hollister and Burruss (1976) demonstrated that the usefulness of clathrate melting temperatures for determining the fluid composition of inclusions is severely limited by the large range of possible solid solutions among these clathrate hydrates. Clathrates of  $\text{CO}_2$  and  $\text{CH}_4$  are the most common, but other volatiles like  $\text{H}_2\text{S}$ ,  $\text{SO}_2$ ,  $\text{N}_2$ ,  $\text{O}_2$  also form hydrates. They all have the same cubic  $12\text{\AA}$  unit cell structure making the formation of complete, multi-component solid solutions possible. Furthermore, the presence of  $\text{CH}_4$  in a  $\text{CO}_2$ -rich fluid may cause the rise of melting temperature of the corresponding clathrate hydrate (Hollister and Burruss, 1976; figure 2), whereas the presence of  $\text{NaCl}$  causes the opposite effect (figure 17, dashed curves). With such complications the difficulties in interpreting the melting temperatures of clathrate are easily understandable.

(\*) According to Miller (1974)  $\text{CO}_2$  and  $\text{CH}_4$  form hydrates of same structures, and their ideal formula is  $(\text{CH}_4, \text{CO}_2)_{4.5} \cdot \frac{3}{4} \text{H}_2\text{O}$ . In other words the unit cell contains 46 water molecules and  $8 \frac{3}{4}$  cages for  $(\text{CH}_4, \text{CO}_2)$  molecules.

The homogenization temperature is the temperature at which inclusions become filled with a homogeneous fluid. In inclusions with two distinct fluid phases, the homogenization may occur by the disappearance of either phase in consequence of the decrease in volume of that phase or by the sudden disappearance of a phase boundary. In the former case they homogenize into either a vapour or a liquid phase and in the latter, the meniscus separating both fluids remains unchanged until critical phenomena occur. The temperature of homogenization represents, after corrections, the minimal temperature of entrapment of the fluid in the inclusion, or of the formation of the host mineral if the inclusion is primary. The correction to be made is due to the effects of pressure (Klevtsov and Lemlein, 1959; Samoylovich and Khetchikow, 1968).

The critical phenomena - homogenization at the critical point - has more limited use in the study of fluid inclusions, because the fluids rarely consist of a single pure component. So the critical temperatures will generally be those of some unknown multicomponent system. In a few cases the critical phenomena could be helpful, as for example, in the identification of  $\text{CO}_2$  (critical temperature for pure  $\text{CO}_2$ :  $31^\circ\text{C}$ ), or in the estimation of density of fluids and the temperature of trapping of inclusions (Roedder, 1972).

It may also be significant to determine the  $\text{CH}_4$  content in inclusions presenting the  $\text{CO}_2$ - $\text{CH}_4$  mixture. The decrease in the liquid-vapour critical temperature of the above mixture with increasing  $\text{CH}_4$  quantifies  $\text{CH}_4$  content in the  $\text{CO}_2$ -rich phase of a fluid inclusion (Figure 16; Hollister and Burruss, 1976).

In inclusions with saturated solutions (presence of solid salt phases) the temperature of dissolution of salts permits the estimation of the salinity, but this temperature should be interpreted in conjunction with the results of the freezing test, as has been pointed out before. The rate of dissolution may give an indication of the nature of the salt.  $\text{NaCl}$  and  $\text{KCl}$  present different rates of solubility upon heating.  $\text{KCl}$  dissolves more rapidly than  $\text{NaCl}$  (figure 9).

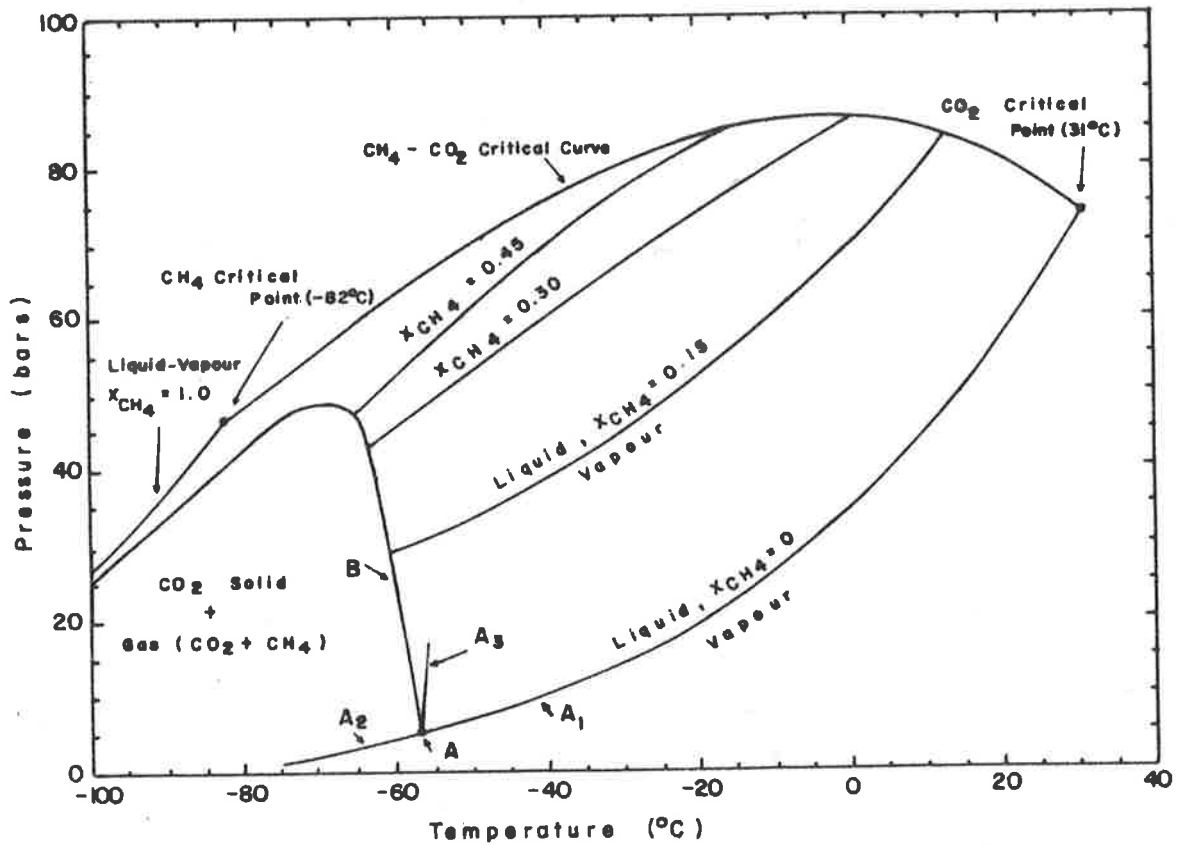


Figure 16: Phase diagram of the system CO<sub>2</sub>-CH<sub>4</sub> at low pressures and temperatures:

- A : pure CO<sub>2</sub> triple-point
  - A<sub>1</sub>: pure CO<sub>2</sub> liquid-vapour coexistence curve
  - A<sub>2</sub>: pure CO<sub>2</sub> solid-vapour coexistence curve
  - A<sub>3</sub>: pure CO<sub>2</sub> solid liquid coexistence curve
  - B : locus of three-phase equilibria (CO<sub>2</sub> solid, CO<sub>2</sub> + CH<sub>4</sub> liquid, and CO<sub>2</sub> + CH<sub>4</sub> vapour) for several CO<sub>2</sub>:CH<sub>4</sub> ratios.
- X<sub>CH<sub>4</sub></sub> : CO<sub>2</sub>-CH<sub>4</sub> liquid-vapour coexistence curves for various molecular percentages of CH<sub>4</sub> (after Hollister and Burruss, 1976).



Inclusions with  $\text{CO}_2$  as liquid and vapour phases (the usual case when this compound becomes distinguishable at room temperature) enable an approximation of the  $\text{CO}_2$  content in the fluid. At  $20^\circ\text{C}$ , the presence of two  $\text{CO}_2$ -rich phases already indicates a solution with more than 1.8 mol.% of  $\text{CO}_2$  based upon the  $\text{CO}_2$ -content of the aqueous solution. This value is the estimated solubility of  $\text{CO}_2$  in water at  $20^\circ\text{C}$  and  $\text{CO}_2$  saturated vapour pressure (Weisbrod et al., 1976). Furthermore, the homogenization temperature of  $\text{CO}_2$  makes possible the estimation of its density, which, associated with the estimated volumes of aqueous and  $\text{CO}_2$ -rich phases, will permit the calculation of  $\text{CO}_2$  content in the fluid (Ypma, 1963).

Theoretically, upon heating, all phases should homogenize into a single homogeneous fluid. In practice, this does not always happen, mainly because of the very low rate of solubilities of some daughter minerals (sulphates, silicates), or because of some leakage of fluids before complete homogenization has been attained.

In addition to the phase changes occurring during the determination of melting points and homogenization temperatures, Roedder (1972) quotes studies where the formation of new immiscible fluid (Kalyuzhnyi, 1958, p.576 in translation; Ermakov et al., 1957, p.494 in translation) and a new vapour phase (Wahler, 1956) were observed upon heating. In the present work, phase changes of daughter minerals and the nucleation of new vapour phase (which subsequently contracted) was observed in some inclusions upon heating (e.g. sample A-495-172B, inclusion No. 1).

#### II.1.1.3 Equipment and calibration

The present study was carried out with equipment built by the Société Chaix-Meca in Nancy, France. The construction of the apparatus was based on research done by the "Équipe de Recherche sur les Équilibres entre Fluides et Minéraux" from "Centre de Recherches Pétrographiques et Géochimiques, Vandoeuvre-les-Nancy", France. A detailed description of this equipment is presented by Leroy (1971), and by Poty et al. (1976) for an improved model.

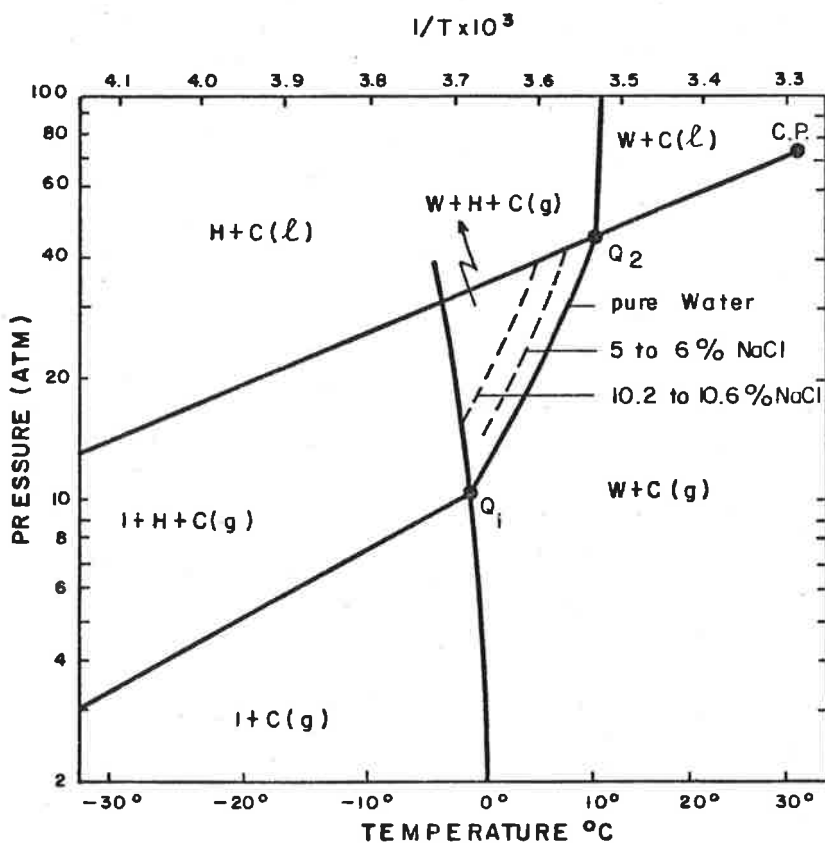


Figure 17: Phase diagram of CO<sub>2</sub> hydrate near 0°C and the influence of NaCl content on the melting temperature of the hydrate.

C.P. - critical temperature of CO<sub>2</sub> (31.0°C and 72.8 atm).

Q<sub>1</sub> - quadruple point (ice + water + CO<sub>2</sub>-clathrate + CO<sub>2</sub> vapour) at -1.77°C and 10.20 atm.

Q<sub>2</sub> - quadruple point (water + CO<sub>2</sub>-clathrate + CO<sub>2</sub> liquid + CO<sub>2</sub> vapour) at 10.20°C and 44.50 atm.

C(g) - CO<sub>2</sub> vapour.

C(l) - CO<sub>2</sub> liquid.

H - CO<sub>2</sub>-clathrate.

I - Ice.

W - Water.

heavy line - modified from Miller (1974).

dashed line - from Bozzo et al (1973).

The unit used is theoretically workable within the temperature range  $-180^{\circ}$  and  $+600^{\circ}\text{C}$ . The stage was calibrated several times during the present work. For low temperatures, the three-phase inclusions with pure  $\text{CO}_2$  in quartz from Calanda, Switzerland (Jehl, 1974), always indicated values of  $-61.4^{\circ}\text{C}$  to  $-61.7^{\circ}\text{C}$  for the triple point of  $\text{CO}_2$  (25x objective). With 10x objective the triple point of  $\text{CO}_2$  for the same inclusion was  $-55.8^{\circ}\text{C}$ . This discrepancy is due to a difference in loss of heat through the metallic body of the objectives when using either the 10x or 25x lenses. The 25x lens has a shorter focal distance - bringing the piece close to the specimen - which causes a thermal gradient. The temperature near the inclusion will always, therefore, be higher than the temperature of the stage. Consequently, whenever possible, after the use of 25x objective, a cross-checking of larger inclusions with 10x objective was made. Especially useful were three inclusions from sample A-495-113 which allowed, in conjunction with other data, the establishment of a temperature calibration diagramme for the 25x and 10x objectives (figure 18). The calibration of other sub-zero temperatures was made with inorganic compounds which have low solubility in water: carbon tetrachloride, chloroform, and toluene, and distilled water itself (Jehl, 1974).

The discrepancies are quite significant, especially at low temperatures, because at  $-60^{\circ}\text{C}$ , for instance, a correction of  $+7^{\circ}\text{C}$  is needed.

For the calibration of high temperatures, a range of organic compounds with known melting points supplied by the Merck Company, was used. The heating tests were done using a thinner silica window and the Reichert Cat. 40x/0.52 250/1.5 Qu reflective objective. The last calibration curve established during the present work, is shown in figure 19. Previous calibrations presented only minor variations from this curve.

The use of an infra-red filter and the exact distance between condensor and stage were always carefully observed. The condensor and infra-red filter are part of the stage. Any change in the conditions under which these accessories are used requires a new calibration curve.

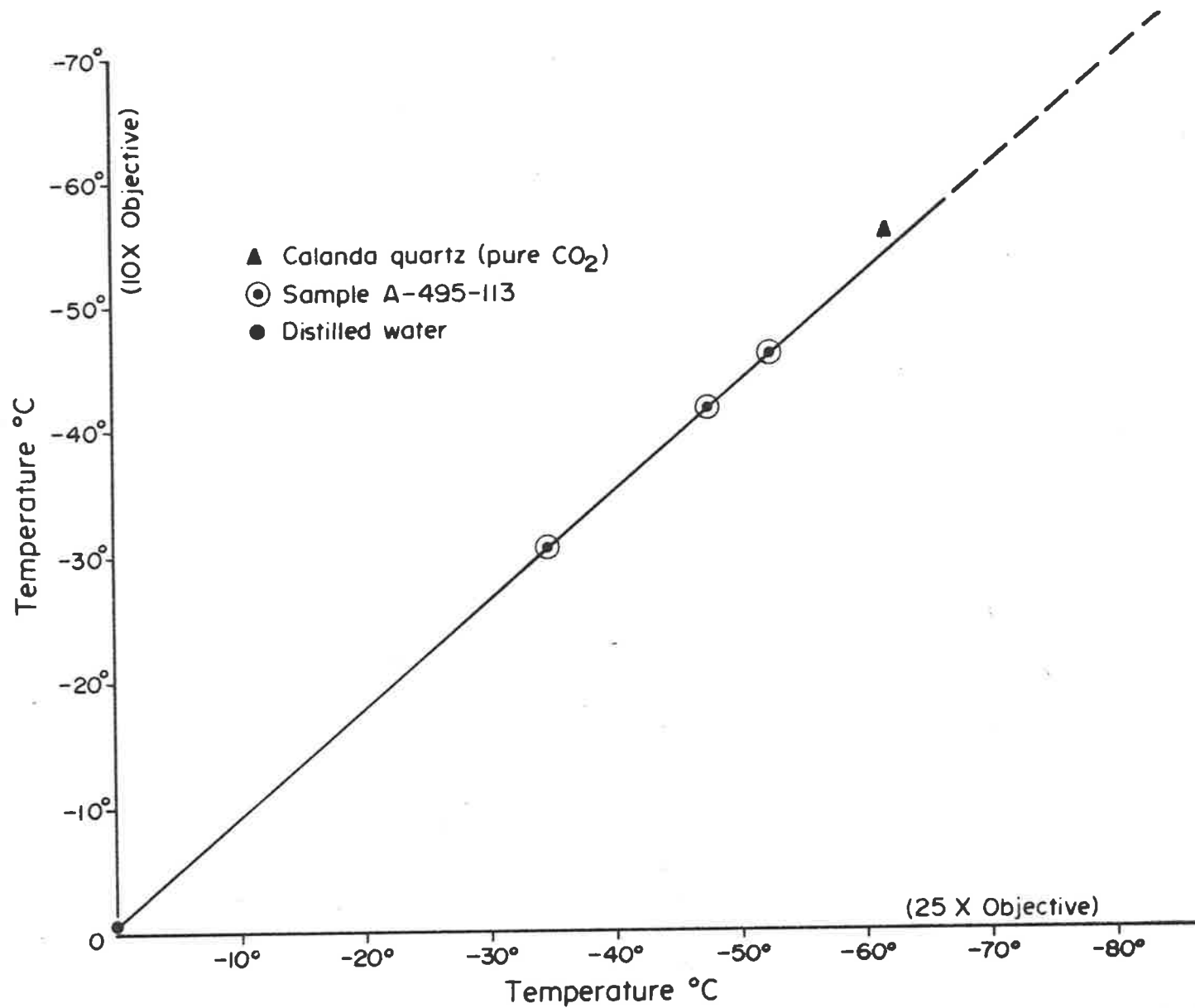


Figure 18: Temperature correlation diagram for freezing temperature measurements made with 25x and 10x microscope objectives.

#### II.1.1.4 Other non-destructive methods

Some other non-destructive methods have been mentioned by Roedder (1972), for example the study by nuclear magnetic resonance (Paré and Ducros, 1964) and micro differential thermal analysis, but they have never been used as routine-methods.

The fluorescence of certain organic substance, under ultraviolet illumination has been used to detect their presence in inclusions (e.g. Ikorskiy, 1964, 1970).

More recently, laser-excited Raman spectroscopy has successfully been applied for the qualitative and quantitative determination of individual phases in fluid inclusions (Rosasco et al., 1975). The method is particularly successful for the determination of sulphates (Rosasco and Roedder, 1976).

#### II.1.2 Destructive methods

The main objective of destructive methods is to obtain qualitative and quantitative data of each component present in fluid inclusions by direct analysis of these components, either by atomic absorption of chemical compounds or by mass spectrometry.

The extraction of the fluid inclusion content involves three stages: the opening of inclusions; separation of the fluids from the host rock, and the collection and concentration of the fluids (Roedder, 1967). Large inclusions (of few mm<sup>3</sup> or more) can be opened with special drilling equipment and the fluids can be extracted by micropipetting. Roedder (1972) reports the successful use of this technique by Kalyuzhnyi (1958, 1960 and 1961), but fluid inclusions of this size are rare. Therefore, the methodology of sample preparation and extraction are most critical with regard to the ultimate analysis. The danger of contamination is very real and not easily prevented (Roedder, 1967 and 1972). One must always be aware of possible pitfalls in any extraction procedure.

In the present study, due to the absence of suitable samples, the extractive methods have not been used. All quartz contains abundant solid inclusions, especially chlorite and/or iron oxides, which would probably cause

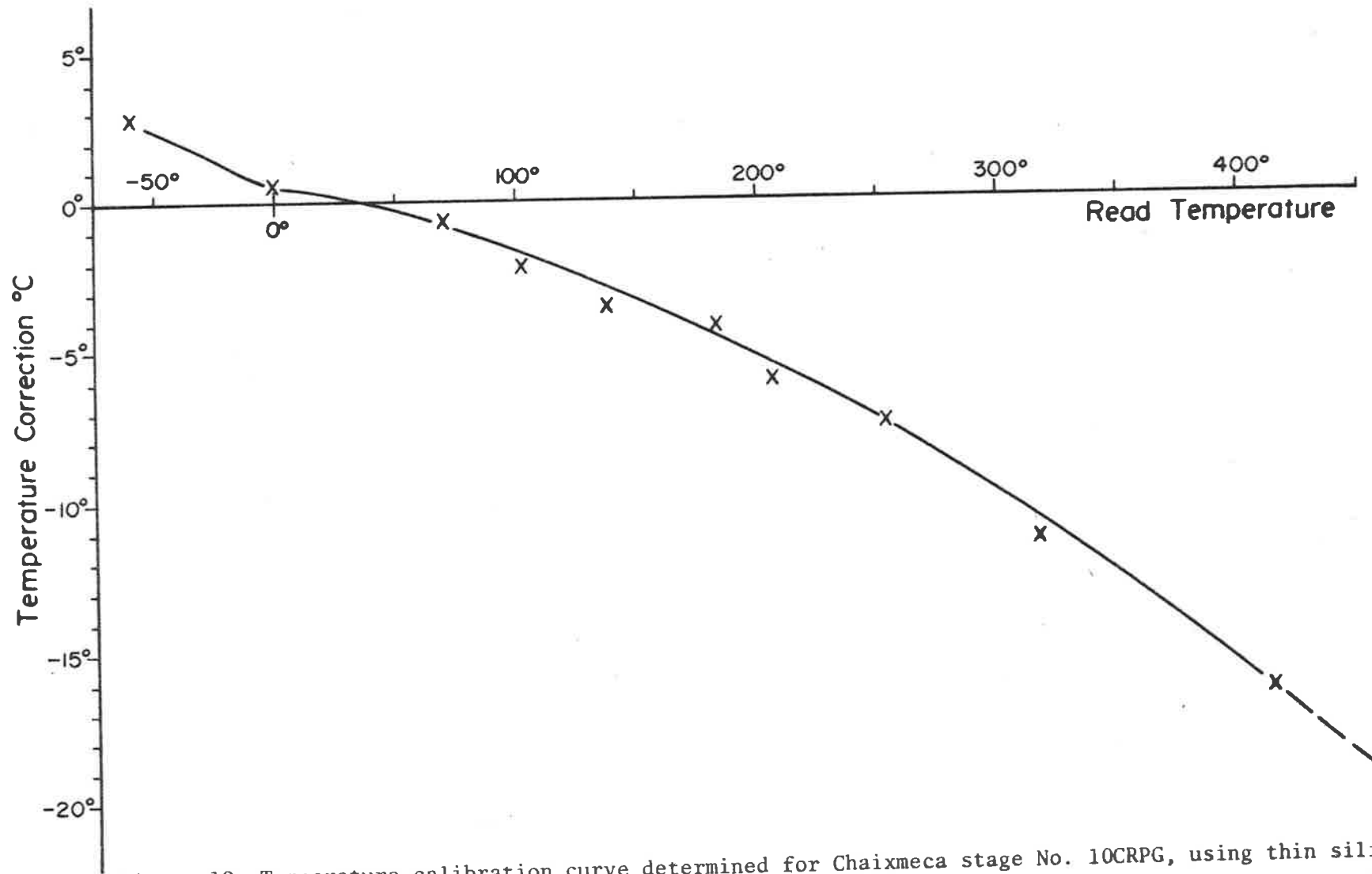


Figure 19: Temperature calibration curve determined for Chaixmeca stage No. 10CRPG, using thin silica window with Reichert Cat. 40/0.52, 250/1.5 Q $\mu$  objective.

contamination to the leaching fluids. Furthermore, of much greater interference to the applicability of the common destructive methods, is the inhomogeneous entrapment of fluid inclusions observed in the many samples. Microscopy and microthermometry indicated samples with inclusions of different generations with different compositions and inclusions of the same generation with different compositions. This fact made any bulk analytical technique completely unsuitable. Therefore, other analytical methods enabling the study of individual inclusions or groups of inclusions were necessary. The crushing test (using a crushing stage) and the S.E.M. (Scanning Electron Microscopy) were the main analytical methods chosen for this study. A more detailed description of each one of these processes will follow.

#### II.1.2.1 The crushing stage

The crushing stage is a simple device which detects gases under pressure in inclusions and permits a qualitative determination of some of these gases, especially CO<sub>2</sub>.

The technique consists of crushing a mineral grain, immersed in an appropriate liquid, between two glass slides fitted into the crushing stage. The comminution process can be observed with the microscope. Deicha (1950) presented his model of a crushing stage which has since been reproduced in a series of new versions with a variety of modifications. The model presented by Roedder (1970), which is basically the model produced by "Société Chaix-Meca" (France), is probably the best known and was used during the present investigation.

A correct use of this stage requires a number of steps which should be carefully observed.

- The mineral grain should be equidimensional, ranging from 630 to 800 microns. The size limit is important because the amount of gas released is compared with a chart to give a relative amount of gas under pressure in inclusions. According to the amount of vapour bubbles developed the gas-release is classified in "very weak", "weak", "medium", "strong" and "very strong" categories (figure 20).

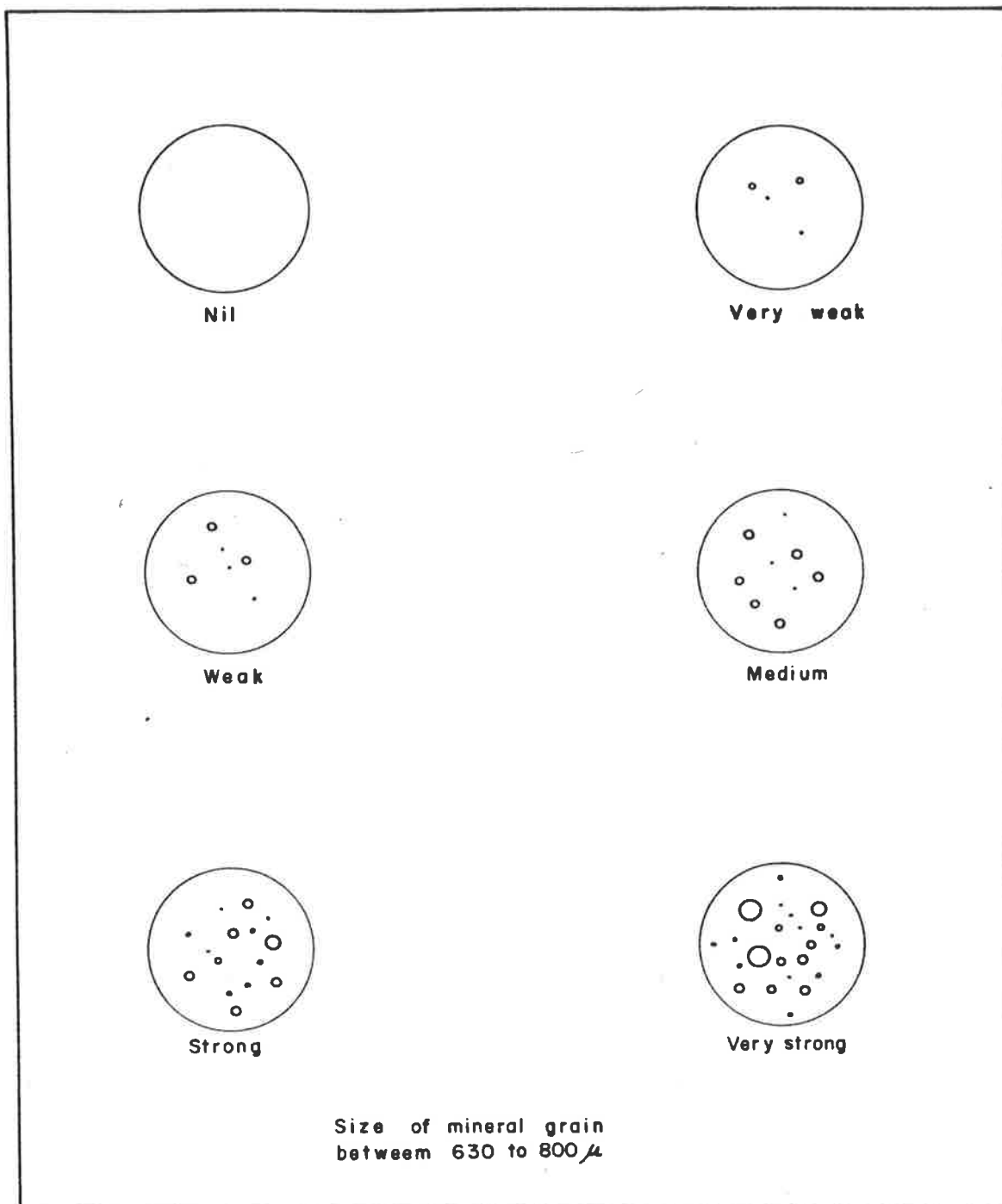


Figure 20: Comparative chart for gases released during a crushing test at a magnification of 35X.  
(From Chaix-Meca instruction booklet).



- An important observation to be made before crushing is the volume of fluids in inclusions in the mineral grain. If there are only few or small inclusions in it, there will obviously be a proportionally smaller amount of gas, which could lead to a misinterpretation of the gas pressure in the inclusions of that particular sample.
- After the immersion of the mineral grain in the liquid, all air-bubbles adhering to the liquid-mineral interface should be removed before crushing.
- The manufacturer recommends a magnification of 35 times as a desirable one for satisfactory observation.

Different kinds of immersion liquids may be used:

- Liquids such as anhydrous glycerine or paraffin oil in which most gases have very low solubility are used to test the presence of a gas or gases under pressure in inclusions (Chaix-Meca, 1973).
- The presence of  $\text{CO}_2$  is detected by crushing the mineral grain immersed in  $\text{Ba}(\text{OH})_2$ . The  $\text{CO}_2$  will react with the barium hydroxide and form  $\text{BaCO}_3$  around each gas-bubble causing shrinkage of the bubble (Rasumny, 1957). If the gas bubble is pure  $\text{CO}_2$ , it will dissolve in the aqueous solution leaving behind a microcluster of barium carbonate crystals.
- Although  $\text{H}_2\text{S}$  was detected by G.R. Helz by testing for the gas with anhydrous glycerol of sodium nitroprusside, the human nose still is the best detector for hydrogen sulphide. Amounts as low as  $10^{-10}$  g of  $\text{H}_2\text{S}$  can be detected by smell (Roedder, 1972).
- Any suspicion of the presence of carbonate minerals such as solid or daughter minerals in fluid inclusions in quartz can be confirmed by crushing this quartz immersed in a  $\text{HCl}$  solution. In the case of calcite, the volume of  $\text{CO}_2$  evolved will be approximately 500 times the volume of the calcite daughter mineral (Rasumny, 1960).

Apart from these tests, determination of the rate of solubility of gas-bubbles in certain solvents may give further information on the nature of gases present in the inclusions. Predominance of one kind of gas in inclusions should show bubbles with similar rates of solubility. The presence of different gases will probably produce different curves of solubility. Cases of complete insolubility of the gas bubble may occur as exemplified during the crushing tests of sample A-495-116.

In the present study, only the solubility of gases in kerosene was considered, because this is a good test for hydrocarbons.

#### II.1.2.2 Crushing under pressure

Ypma (1966) presented an original model of a crushing stage with which thermobarometric readings can be obtained. Essentially the stage is a chamber filled with an appropriate fluid in which the mineral is crushed. The chamber is connected to a hydraulic pump which generates and maintains a constant pressure during the crushing test. The pressure values are indicated by a single gauge. Heating is achieved by a built-in electrical resistance. Cooling could be done, in theory, by circulating cold CO<sub>2</sub>. However the heat capacity of the stage is too large to be cooled effectively. In the present study, the stage was initially cooled in a box with dry-ice.

A major restriction to the use of the barometric crushing stage arises from sample inhomogeneity. In every repetition of the experiment, the mineral grain must contain the same type of inclusions. Therefore, a careful examination and selection of mineral grains before crushing is essential. This is the main reason why the method was applied only to two samples (A-495-176 and A-495-113).

Before mounting the mineral grain in the crushing stage of Ypma (1966) some of the grains were tested in the "Chaix-Meca" stage to observe the amount of gas released. After mounting the grain in the chamber the confining pressure was raised to a value slightly higher than that of the inclusions. In this case, when the mineral is crushed no gas release should be expected. Upon slow release of the confining pressure, the pressure at which

the first gas-bubble appears corresponds to the pressure just below the pressure within the inclusion. Repeating the experiment at different temperatures, different pressure values are obtained. These values allow the construction of the isochore of the inclusion, which will help with the extrapolation of the homogenization temperature to that of the crystallization of the mineral.

Another experiment that can be performed using the geobarometric crushing stage is the determination of the compressibility of the released gas-bubbles. The experiment may be helpful in indicating the composition of these bubbles. The  $\text{CO}_2$  bubbles, for instance, when compressed above  $75 \text{ kg/cm}^2$  must show a phase change (liquefaction) at room temperature (figure 16). The same figure shows that an increasing amount of  $\text{CH}_4$  in  $\text{CO}_2$  depresses the critical temperature of the system  $\text{CO}_2\text{-CH}_4$ . Thus the absence of liquefaction of  $\text{CO}_2$  at  $75 \text{ kg/cm}^2$  may point to the presence of methane or another gas of low critical temperature. This method is particularly instructive when carried out with a cooled crushing stage.

#### II.1.2.3 The scanning electron microscope (SEM)

Scanning electron microscopy of open inclusion cavities has made an important contribution to the morphology of fluid inclusion cavities and the nature of their solutions (Sella and Deicha, 1970; Vasil'ev et al., 1971; Boyarskaya, 1973; Deicha, 1973, Dobrovol'skaya et al., 1973; Gritti-Baudraco, 1975; and Saintives, 1976). When used in conjunction with a solid-stage energy dispersive X-ray detector and a multichannel analyser, the SEM becomes a very useful tool in the direct identification of daughter minerals and other evaporation residues of fluid inclusions.

It has been pointed out that for every destructive method, the major limiting factor in the analysis of inclusions is the problem of contamination due to the small volume of inclusion. The SEM technique permits a reliable analysis in situ of solid phases contained in or originating from cavities of the inclusions, down to the 0.5 micron range (see SEM photos). In consequence, during the last few years the number of researchers using

this method in the study of fluid inclusions has increased steadily (Clocchiati, 1975; Metzger et al., 1975 and 1977; Nesbitt and Keyy, 1975 and 1977; Grant et al., 1976; Le Bel, 1976; Bonev, 1977; and Riese et al., 1978). Especially in the study of Metzger et al. (1977) the reliability of the method for the determination of daughter minerals in fluid inclusions was demonstrated.

The present study was carried out in an AUTOSCAN scanning electron microscope manufactured by the ETEC Corporation. The equipment is attached to an energy dispersive X-ray spectrometer - the Packard Multichannel Analyser - which distributes the X-ray energy over 1024 discrete energy bands.

Before the commencement of the SEM study an important step is the preparation of samples for this purpose. Basically, the samples were prepared following the process described by Metzger et al. (1977). When the specimens presented inclusions of interest, pieces from the same mineral were taken for SEM study. After careful cleaning, the samples were split to open the inclusions. The pieces of this mineral were then mounted on an aluminium substratum with the broken surfaces facing upwards. As soon as feasible, the mounted specimens were coated with a thin conducting film of either carbon or gold. The latter yields better images but the former is preferred in some instances when the interference of X-rays from the gold coating is undesirable.

Upon opening the inclusions by fracturing the specimens, part of the liquid would be lost mainly when the fluids were under pressure. But the amount of liquid remaining in the inclusion cavities, or stuck to the new broken surfaces (because of surface tension) would soon evaporate, either in the air during the cleaving or during the coating process (vacuum), leaving behind a precipitation product. The latter can be seen, for example, in Plate X, photo 2; in Plate XVIII, photo 2; also in: Metzger et al. (1977); and in Bonev (1977).

The freezing of samples in liquid nitrogen, before the opening of inclusions in dry atmosphere, was tried in an attempt to hold as much fluid as possible within the inclusion cavities and, at the same time, to reduce

the possibility of losing daughter minerals from the inclusion cavities. Metzger et al. (1977) states that daughter minerals could be blown out from their cavities due to high internal pressure. It was difficult to prove to what extent the method was successful in retaining the fluids and the daughter minerals because of the difficulty in finding two identical specimens, which, after freezing one of them, could be broken in similar patterns and compared. Nevertheless this technique was used to prepare a new set of specimens for samples A-495-172 and A-495-176. Although it is appreciated that the result might have been merely a coincidence, these specimens prepared after freezing actually showed a larger number of inclusion cavities with daughter minerals.

When highly hygroscopic substances (e.g.  $\text{CaCl}_2$ ) are present in inclusions, like in samples studied, the samples should be kept in a dry atmosphere and studied as soon as possible. The ideal situation would be to split and mount the specimens in a dry atmosphere and take them immediately to the vacuum coating apparatus. The necessity of these precautions was indicated by observations made on the same SEM mount at different times. One of the daughter minerals found at the first time was not present in the same cavity when examined several months later. This crystal had probably dissolved upon absorbing moisture from the air. The high hygroscopy of  $\text{CaCl}_2$  may be the explanation for lesser frequency of this salt during the SEM study of samples which had indicated inclusions rich in birefringent salt hydrates and very low freezing temperatures of ice (e.g. sample A-495-11).

The SEM can be operated in two different modes: the scanning mode and the spot mode.

On the scanning mode, two types of images can be produced on a television screen: 1. The magnified image of the specimen surface. The great depth of focus of the equipment yields excellent images of daughter minerals in the cavities of broken surfaces of mineral specimens (e.g., photos from Plate XVIII. 2. The surface distribution of a selected element can be produced by discriminating with the X-ray spectrometer only for a particular X-ray energy level. A comparison of this image showing the exact location of

chosen elements with the photo-image of the specimen surface may help in the identification of minerals.

On the spot mode, the electron beam can be focused at any single point, and will produce X-rays characteristic of the elements present at that point of the surface of the mineral under consideration (\*). The energy spectrum of the X-rays is graphically displayed on the screen of the multi-channel analyser (e.g. Plate XII, photo 1). The quality of the spectrum depends upon the counting rate and counting time. The spot mode was used by Metzger et al. (1977). The major technical problem with this analytical technique is that, because the electron beam remains stationary, it may, if not carefully operated, cause local burning of phosphorous on the TV screen. In order to avoid this problem greater use was made of the scanning mode which, for a reduced area, could still be made to analyse surfaces as small as  $0.1\mu$ . Obviously, with the scanning mode, there is a greater risk of interference by X-rays generated by the host mineral and/or adjacent minerals, especially when the analysed mineral is smaller than  $0.1\mu$ . On the other hand, scanning of a reduced area produces a reliable spectrum at a much lower counting rate and time.

The present SEM work was usually operated at an accelerating voltage of 20 kV and a condenser lens current of 2.2 A of intensity. A higher voltage (30 kV) was used in the study of heavier elements.

## II.2 Samples Studied

The fluid inclusion study of the Nabarlek uranium deposit was carried out in mineralized and non-mineralized samples in order to compare their results. It has already been mentioned in the study dealing with mineral paragenesis that there was a scarcity of samples with transparent minerals in drill-cores from the main orebody. This required sampling of mineralized specimens from cores drilled at the south-eastern extension of the orebody (Figures 3 and 7). Fluid inclusions in quartz from mineralized and

---

(\*) The method does not respond to elements of atomic number below 11 (Sodium).

non-mineralized samples from core Na77 have been compared with fluid inclusions from other samples.

### II.2.1 Uraniferous samples

Quartz is the only transparent mineral from uraniferous samples suitable for a fluid inclusion study. Apart from drill core NA77 (samples: A-495-172; A-495-171 and A-495-168), drill core Na72 (sample A-495-162) was the only uraniferous sample with quartz. A detailed description and interpretation of fluid inclusion studies of each one of these four samples follows.

Pitchblende was studied by Scanning Electron Microscope (SEM) technique, Energy Dispersive Analyses by X-ray (EDAX), and crushing stage, in the following samples: A-495-110, A-495-116, and A-495-201. The results will be presented following the quartz study.

#### Sample A-495-172

(D.H.Na77; 58.05m)

##### a) Introduction

This sample is a fine-grained quartzite containing an 0.4mm thick quartz vein. Pitchblende was precipitated before, during (photos from Plate III), and after the formation of the quartz vein (Plate IV, photo 2) as demonstrated by emulsion autoradiography. The fluid inclusions studied concerned idiomorphic quartz projecting from the vein walls. The fluid inclusions differed from crystal to crystal. Screening of more than 15 quartz crystals allowed the selection of a crystal with various types of inclusions (Figure 21), and four crystals for microthermometry. These four crystals were numbered as A-495-172A, A-495-172B, A-495-172D and A-495-172F. In general, single phase inclusions with only one liquid dominated.

##### b) Quartz crystal A-495-172A (1x0x1.5mm)

###### Description of inclusions

Twelve inclusions with two or three phases were chosen for microthermometry. They all contained one liquid-phase and a vapour bubble amounting to 5 vol.% of the inclusions. The occasional solid-phase consisted

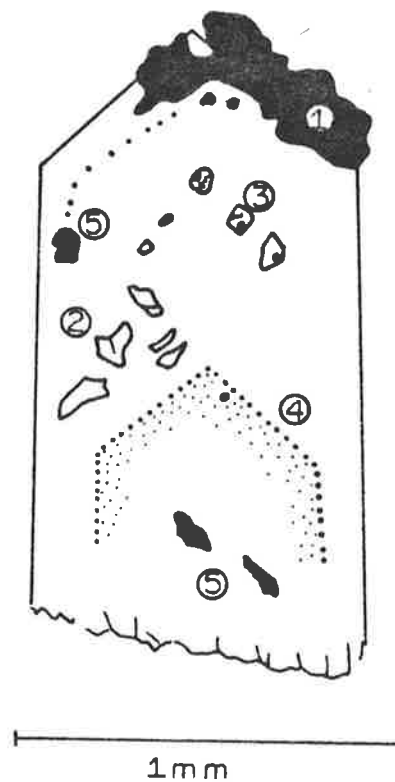


Figure 21: Sample A-495-172 (D.H.Na77; 58.05m)

Inclusions of 3 different generations in quartz crystal.

- (1) Pitchblende on the surface of the crystal;
- (2) one-phase (liquid) inclusions;
- (3) three primary inclusions with two (gas + liquid) and three-phase (gas + liquid + solid) inclusions;
- (4) cluster of tiny two-phase (gas-liquid) inclusions trapped in zone of growth of the crystal;
- (5) pitchblende(?) inside the crystal.

Decreasing temperature during the crystallization of quartz is indicated by the chronology of formation of the fluid inclusions: 4, 3 and 2.



of a cluster of acicular, strongly birefringent crystals or a dark amorphous mineral. The former (Plate V, photo 1) had the appearance of dawsonite ( $\text{NaAlCO}_3(\text{OH})_2$ ) and the latter of pitchblende. In only one exceptionally large inclusion ( $150\mu$ ) were two cubic crystals observed, which jointly amounted to 1 vol.% of the inclusion.

The inclusions used for this study varied in size between  $15\mu$  to  $150\mu$ , but only three of them were larger than  $70\mu$ . The small ones were of an elongated regular shape, increasing in irregularity with size. The inclusions were all isolated and no pattern controlling their arrangement was evident. They all appeared to be primary. Only one inclusion had possibly been subject to post-depositional changes due to a "necking down" process.

#### Microthermometry

The following description is given in detail because of the unusual behaviour of the fluids during the cooling test.

Even rapid cooling to  $-145^\circ\text{C}$  did not produce any freezing. Upon slow warming the inclusions did not suddenly freeze either, which usually happens with dilute solutions. The freezing process occurred at a rather slow pace when the temperature was close to  $-100^\circ\text{C}$ , starting from one point and progressing gradually throughout the whole inclusion. The vapour phase meanwhile had decreased and a second frozen product had formed around the bubble. But in four inclusions, only part of the liquid phase became frozen (partial freezing). Following this, the quartz crystal was cooled again to  $-140^\circ\text{C}$ . Upon warming, the temperature was held at  $-70^\circ\text{C}$  for three hours, but no further change was noticed. After this experiment, the four inclusions presented the following phases (apart from dawsonite(?) and the dark amorphous mineral mentioned earlier):

- two solid phases, one being a large rounded crystal with high relief and the other a microgranular mass adjoining the vapour phase with low relief. Both were isotropic.
- one liquid phase (left after the partial freezing); and
- one vapour phase.

The solid phase with high relief was interpreted as ice initially and the phase with lower relief as a clathrate. Upon further warming the melting point of gas-clathrate in three inclusions were determined as  $+11^{\circ}\text{C}$ ,  $\sim+11^{\circ}\text{C}$ , and  $+14^{\circ}\text{C}$  respectively.

With the temperature held at  $-2^{\circ}\text{C}$  for 30 minutes one inclusion which had formed the high relief solid phase only, showed a change of this solid phase into a birefringent, slightly greenish, hexagonal plate. This phase was probably a  $\text{CaCl}_2$ -hydrate. It melted at  $+13.9^{\circ}\text{C}$  which indicates salinity equivalent to 41 wt.%  $\text{CaCl}_2$ .

In three inclusions which did not form clathrates or hydrates the ice melted at  $-31^{\circ}\text{C}$ ,  $-34.5^{\circ}\text{C}$  and  $-43.0^{\circ}\text{C}$  and these temperatures correspond to salinities equivalent to 26 wt.%, 27 wt.%, and 29 wt.%  $\text{CaCl}_2$  respectively. The melting temperatures of the remaining five inclusions could not be recorded. Figure 22, histogram A-495-172A, indicates the melting points of ice, clathrates and salt hydrate. The presence of small amounts of cubic halides in only one inclusion and the low melting temperatures of ice indicates that the fluids must have been essentially  $\text{CaCl}_2$ -rich brines confirming the observation of  $\text{CaCl}_2$ -hydrates. Partial freezing phenomena are in agreement with highly saline brines postulated by the melting points of ice (Roedder, 1963) and salt hydrates. High melting temperatures for gas-clathrates indicates the presence of  $\text{CH}_4$  in addition to  $\text{CO}_2$  (Hollister and Burruss, 1976).

When the sample was frozen for a second time after homogenization, the inclusions presented a different behaviour. In particular, neither partial freezing nor the nucleation of the two isotropic solid phases was observed. These differences may have been either a result of metastability or the consequence of unnoticed changes (leakage?) in the relative compositions of fluids during the heating process.

Homogenization experiments took into consideration only liquid and vapour phases because of the inconsistent presence of dawsonite (?) and a dark amorphous mineral, which were probably not true daughter minerals but co-precipitated solid phases. Heating of these inclusions for seven hours at  $+150^{\circ}\text{C}$

followed by ten hours at +200°C did not show any perceptible reduction of the above-mentioned minerals.

The homogenization temperatures ranged from 69.5°C to 130.5°C (Figure 23, histogram A-495-172A). The morphology of inclusions seems to rule out disruption of fluid inclusion content after entrapment which therefore cannot be used as an explanation for this wide range of  $T_H$ . These inclusions probably indicate temperature changes during the formation of quartz crystals.

c) Quartz crystal A-495-172B (1.0x1.0mm)

Description of inclusions

This crystal contained seven large inclusions (10 $\mu$  to 120 $\mu$ ) among many small ones. Of these seven inclusions three contained only one liquid phase. The other four inclusions had additional phases. Their descriptions are the following:

Inclusion No.	Size ( $\mu$ )	Approximate shape	No. of phases	Description of phases
1	40	square	2	liquid + isotropic cubic crystal (2 vol.% of the inclusion).
2	55	triangular	3	liquid + vapour (5-10 vol.%) + orange platy mineral.
3	120	elongated irregular	2	liquid + fibrous solid phase (dawsonite?)
4	55	in L	3	liquid + vapour (2-5 vol.%) + hexagonal platy mineral.

Table I: Description of four inclusions from sample A-495-172B.

Microthermometry

All inclusions showed a very strong resistance to freezing. After repeatedly cooling down to -175°C and warming up to -75°C (freezing I, Figure 24), only inclusion Nos. 1 and 2 showed partial freezing, a behaviour similar to some inclusions in crystal A-495-172A. At -100°C the solid had attained a rounded shape (ice rafts), strong relief ( $n > \text{liquid}$ ), and was isotropic. Lowering of temperature to -178°C showed no increase in this solid

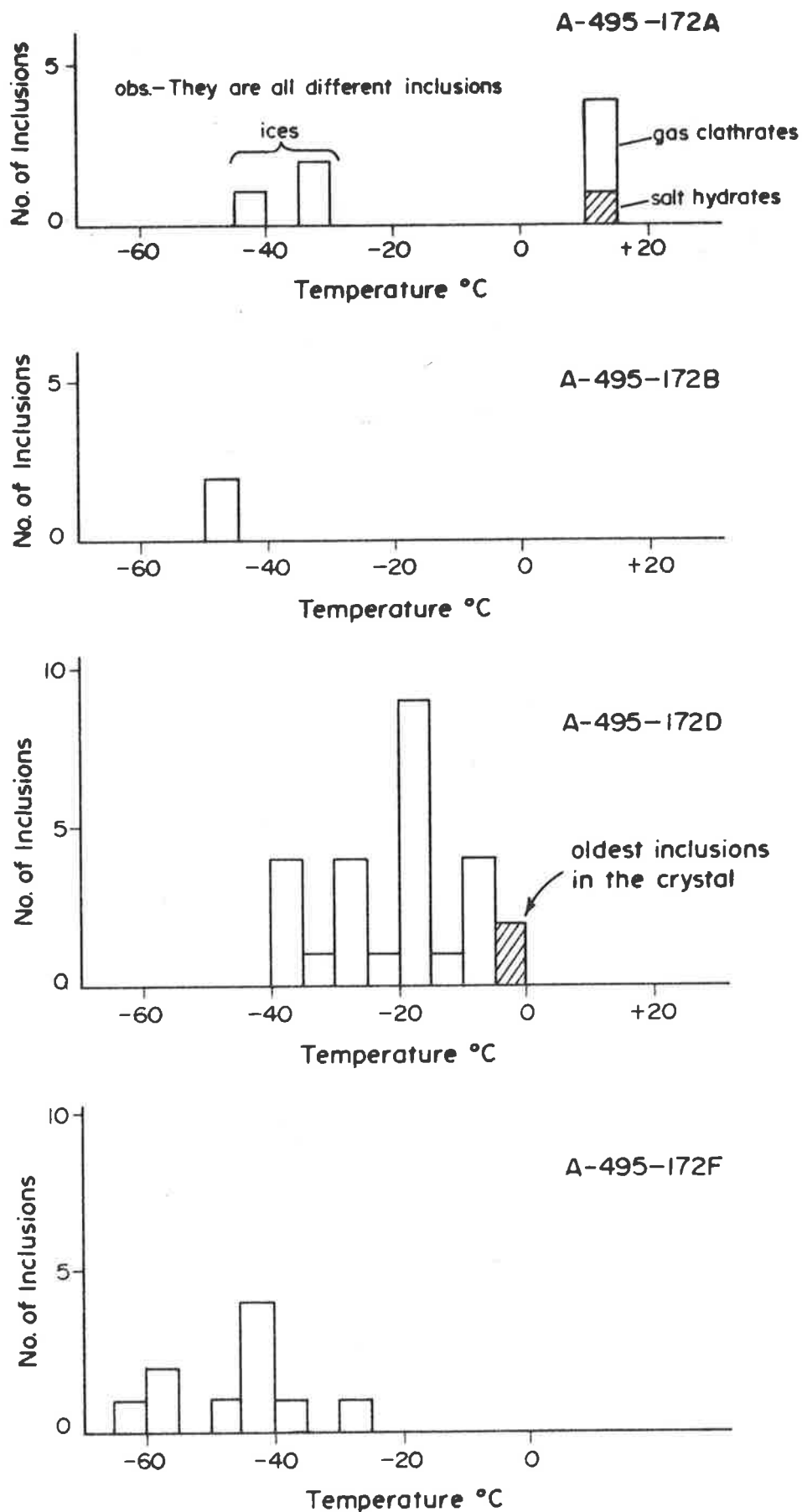


Figure 22: Sample A-495-172.  $T_F$  frequency histograms of fluid inclusions from four late-stage quartz crystal. ( $T_F$  = melting temperatures).

phase, which melted at  $-46^{\circ}\text{C}$  (inclusion No. 1) and  $-46.1^{\circ}\text{C}$  (inclusion No. 2). Although melting at approximately the same temperature, the two inclusions differed in behaviour during the melting stage. In inclusion No. 1, the last three tiny crystals melted very rapidly (similar to the melting of solid  $\text{CO}_2$ ) and at the same time a gas-bubble nucleated, as though we were dealing with a case of incongruent melting. At  $-10^{\circ}\text{C}$  the bubble disappeared leaving the original liquid and the cubic crystal. This cubic crystal remained unchanged during the whole freezing test.

In inclusion No. 2 the main vapour phase was obscured by the ice. Melting occurred more slowly like the melting of ice. At room temperature the bubble had become much larger, indicating leakage and partial loss of liquid during the freezing experiment. Inclusion No. 3, and a few other single-phase inclusions containing a liquid-phase only, showed partial loss of liquid through fractures when the temperature reached  $-55^{\circ}\text{C}$ , although they did not appear to be frozen. Inclusion No. 4 did not freeze.

As mentioned above, inclusion Nos. 2 and 3 had leaked during the first freezing episode (freezing I). Others contained only a liquid-phase. Therefore, these were unsuitable for homogenization tests. In the remaining two inclusions, the cubic crystal of inclusion No. 1 dissolved rapidly and disappeared at  $+89.2^{\circ}\text{C}$  (heating 1, Figure 24); the fluid phases of inclusion No. 4 homogenized into liquid-phase at  $+94.0^{\circ}\text{C}$ , but the orange coloured platy daughter mineral did not change. Upon cooling down to room temperature, inclusion No. 1 formed (at around  $+22^{\circ}\text{C}$ ) many granular, orange-coloured daughter minerals, instead of re-nucleating the cubic crystal. The colours were similar to the hexagonal plate present in inclusion No. 4.

After five months, inclusion Nos. 1 and 4 still exhibited exactly the same phases. In order to understand this behaviour, the crystal was frozen again (freezing II, Figure 24). The temperature was lowered very slowly down to  $-145^{\circ}\text{C}$  but no cubic crystal reappeared in inclusion No. 1. Instead, a bubble of 1 to 2 vol.% suddenly appeared at around  $-80^{\circ}\text{C}$ . The liquid-phase did not freeze at all. Upon warming the newly formed gas-phase disappeared at  $+46.7^{\circ}\text{C}$

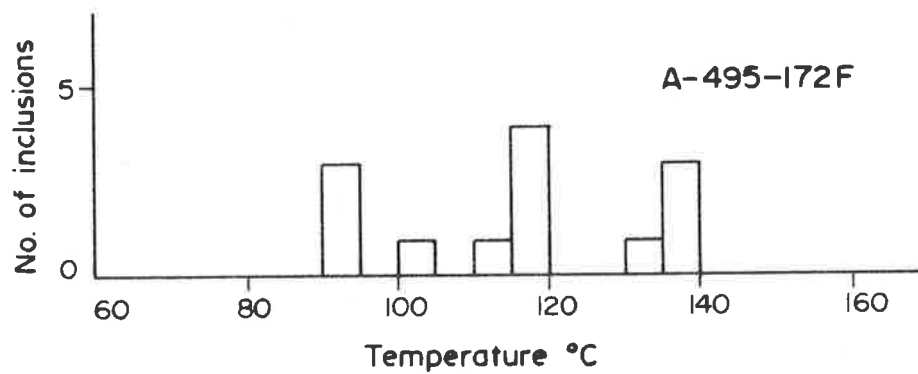
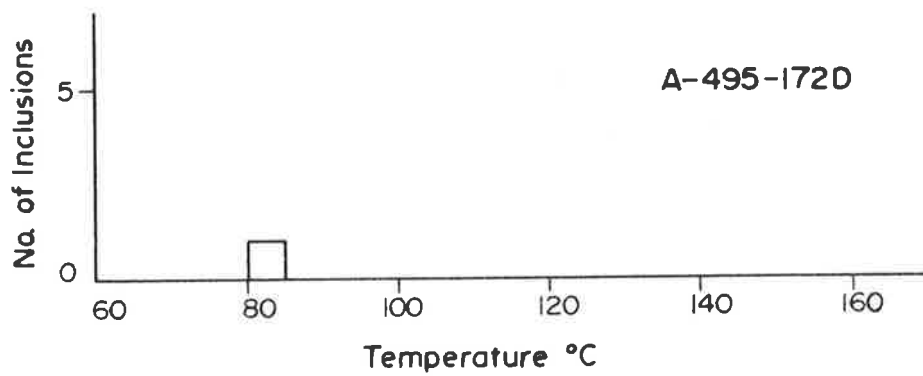
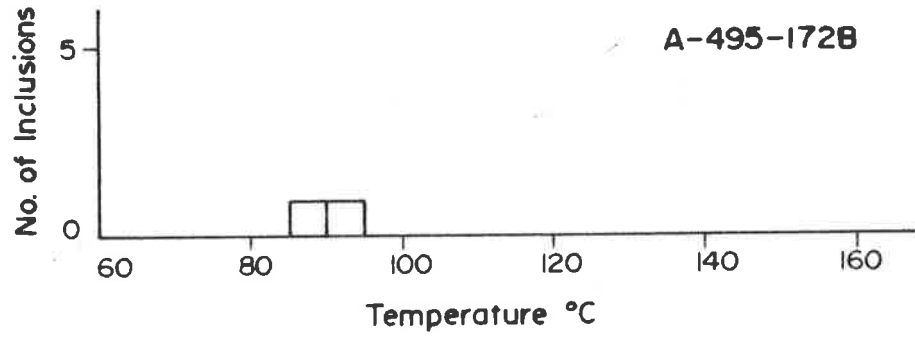
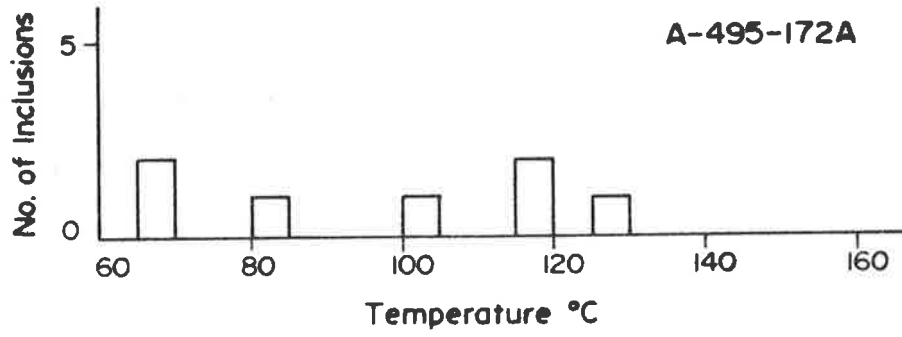


Figure 23: Sample A-495-172.  $T_H$  frequency histogrammes of fluid inclusions in the same four quartz crystals of figure 22. ( $T_H$  = homogenization temperatures).



(heating II). A repetition of the freezing test (freezing III) demonstrated the consistency of this behaviour of inclusion No. 1. Later, before a new attempt to dissolve the orange mineral was made, the quartz crystal was re-examined. Surprisingly, inclusion No. 1 had formed a very large bubble, indicating leakage. When left at  $+150^{\circ}\text{C}$  for 60 hours, no change was noticed in the orange minerals.

The behaviour of inclusion No. 1 is illustrated in Figure 24.

#### Discussion and conclusions

The behaviour of inclusion No. 1 during the microthermometry is not fully understood, yet the partial freezing during the first freezing episode and the presence of a daughter mineral indicate a saturated brine. The rapid incongruent melting behaviour seems to point to a gas clathrate. The inclusion possibly contains a concentrated brine and some dissolved gas in the fluid. The cubic crystal is probably KCl because:

- 1) it did not form hydrates on freezing (Roedder, 1963) and
- 2) it showed a higher rate of solubility than NaCl (Figure 9).

The change in behaviour of inclusion No. 1 after reaching the homogenization temperature was probably the result of a slight leakage of fluids causing irreversible pH or Eh changes. The salinity of the fluid, according to  $T_{\text{H}}$ , would be 35 wt.% of KCl (Figure 9). But its resistance to freezing seems to indicate the presence of  $\text{Ca}^{++}$  ions in the solution. The presence of a KCl daughter mineral at the beginning may be explained by the similar behaviour of the system  $\text{CaCl}_2\text{-KCl-H}_2\text{O}$  to the known system  $\text{CaCl}_2\text{-NaCl-H}_2\text{O}$  which requires less than 3 wt.% NaCl in a  $\text{CaCl}_2$ -rich brine ( $\text{CaCl}_2 > 30$  wt.%) to become saturated with respect to NaCl instead of  $\text{CaCl}_2$  (Figures 10 and 11). Certainly this is at least the case for the temperature range of  $0^{\circ}\text{-}20^{\circ}\text{C}$  (see Linke, 1965, Vol. 1, p.575). The salinity may therefore be presented again as the equivalent of  $\text{CaCl}_2$  in wt.%.

The  $T_{\text{F}}$  of inclusion No. 2 indicates a salinity of 29.5 wt.%  $\text{CaCl}_2$  equivalent. The stubborn resistance of fairly large inclusion No. 4 also indicates a very saline fluid. A  $T_{\text{H}}$  of  $94^{\circ}\text{C}$  indicates the minimum temperature



of the formation of the inclusion. The orange, hexagonal mineral is probably a flake of hematite or goethite, and possibly the product of oxidation of a ferrous-chloride-rich solution, which also explains the new formation of a similar product in inclusion No. 1.

For the purpose of comparison with values found in other crystals, the melting and homogenization temperatures of this quartz crystal are presented in Figures 22 and 23, histograms A-495-172B.

d) Quartz crystal A-495-172D<sup>(\*)</sup>

Description of inclusions

Fluid inclusions from this quartz crystal could be separated into two groups according to their size and location in the crystal: one group of larger inclusions (5 to 25 $\mu$ ) appeared markedly irregular in shape with numerous anastomizing extremities, clearly suggesting a process of "necking down". This process must have occurred at a very low temperature because almost all these inclusions contained only a liquid-phase. They cannot be related to any stage of evolution of the quartz crystal, with two exceptions. These two inclusions were situated in the innermost part of the crystal, and were apparently older than the inclusion of the second group. The inclusions in this second group were smaller ( $\sim 1\mu$ ) and were related to a zone of growth as in Figure 21, No. 4. These tiny inclusions were rounded and only one presented two phases (liquid + vapour). They were certainly primary inclusions.

Microthermometry

During the freezing test the liquid in inclusions of the first group started to freeze at  $-52^{\circ}\text{C}$  and at  $-75^{\circ}\text{C}$  all inclusions were frozen. Excluding the two inclusions in the core of the crystal (oldest inclusions) the last melting temperatures of the ice ranges between  $-9^{\circ}$  and  $-36.8^{\circ}\text{C}$  with four distinct frequency maxima (Figure 22, A-495-172D). The inclusions corresponding with each frequency maximum are spatially associated. This may indicate that each of the groups represents a distinct fluid trapped at different

---

<sup>(\*)</sup> Numbers do not follow in alphabetical order.

time intervals. This was undoubtedly the case for the two oldest inclusions in which the last melting temperature of ice is  $-5.4^{\circ}\text{C}$ . The absence of daughter halides (NaCl) in inclusions with the lowest melting points seems to indicate the presence of concentrated  $\text{CaCl}_2$  brines. The corresponding equivalent values of  $\text{CaCl}_2$  for each group is:

- $5.0^{\circ}\text{C}$ (oldest inclusions)	$9.0^{\circ}$ wt.% $\text{CaCl}_2$ equivalent
- $9.0^{\circ}$ to $-9.5^{\circ}\text{C}$	$13.5^{\circ}$ wt.% $\text{CaCl}_2$ equivalent
- $15.1^{\circ}$ to $-19.5^{\circ}\text{C}$	$18.5^{\circ}$ to $21.0^{\circ}$ wt.% $\text{CaCl}_2$ equivalent
- $25.2^{\circ}$ to $-27.5^{\circ}\text{C}$	$23.5^{\circ}$ to $24.5^{\circ}$ wt.% $\text{CaCl}_2$ equivalent
- $35.2^{\circ}$ to $-36.8^{\circ}\text{C}$	$27.0^{\circ}$ to $27.5^{\circ}$ wt.% $\text{CaCl}_2$ equivalent

The results indicate an increase in salinity from the time of formation of the earliest inclusions to those of the time of formation of later inclusions. This could have been the result of mixing of fluids.

The homogenization temperatures have not been determined as the inclusions had no vapour phase, and even freezing did not nucleate a vapour phase.

In the second group, freezing could not be observed because of the small size of the inclusions. The only two-phase (liquid + vapour) inclusion in this group homogenized at  $+84.8^{\circ}\text{C}$ . Although the result of a single determination, this temperature is significant because this inclusion is of primary origin and, therefore, presents a minimum temperature of formation of quartz-crystal at that particular stage. The absence of vapour-phase in much larger inclusions of the first group is an indication that those inclusions were probably formed at a temperature below  $+84.8^{\circ}\text{C}$ .

e) Quartz crystal A-495-172F

Description of inclusions

This crystal presented numerous inclusions in a prolific combination of different phases, sizes and shapes. The inclusions could present:

- one-phase : liquid only;
- two-phases : liquid + vapour or liquid + solid;
- three-phases: liquid + vapour + solid or liquid + liquid + vapour;
- multiphase : liquid + two solids+vapour or two liquids + vapour+solid.

In some inclusions a change occurred in the number of phases after the freezing or heating tests.

The solid phases included: 1) a cubic isotropic crystal - presumably NaCl; 2) less frequently a birefringent, fibrous mineral and 3) an amorphous, isotropic, dark mineral of undetermined nature (only present in a few inclusions).

The main liquid phase is considered to be a concentrated brine: saturation (cubic salts) and extremely low (last) freezing temperatures (see microthermometry) makes this clear. A second liquid-phase seems to be present occasionally around some vapour bubbles, but the smallness of the bubbles makes this difficult to ascertain. This vapour-phase is approximately  $\sim 2$  vol.%. The suitable inclusions range in size from  $10\mu$  to  $135\mu$  but the majority are between  $20\mu$  to  $40\mu$ . The inclusion shape is highly variable: from rounded to very irregular, elongated forms. A "necking down" process is evident in some inclusions. Many inclusions are situated in planes parallel to the zones of growth of the crystal. This could be considered to be an indication for primary genesis.

#### Microthermometry

The inclusions proved difficult to freeze (see sample A-495-172B). The temperature had to be varied repeatedly between  $-175^{\circ}\text{C}$  and  $-100^{\circ}\text{C}$ . After being left at  $\sim 100^{\circ}\text{C}$  for 30 minutes three different stages of freezing had occurred:

- inclusions with completely frozen brines which, in some cases, were yellowish in colour;
- inclusions with partial freezing resulted into a solid-phase which featured large plates of rounded to elongated shape. These solids are isotropic with higher relief (index of refraction) than that of the remaining liquid;
- inclusions that had resisted freezing.

The unusual characteristic of these frozen products is the extremely low (last) melting temperatures. The highest temperature recorded

was  $-25.5^{\circ}\text{C}$  in one inclusion only (Figure 22, A.495-172F). In five inclusions the last melting point was between  $-43.0^{\circ}$  and  $-48.0^{\circ}\text{C}$  and in three inclusions between  $-57.2^{\circ}\text{C}$  and  $-61.0^{\circ}\text{C}$ .

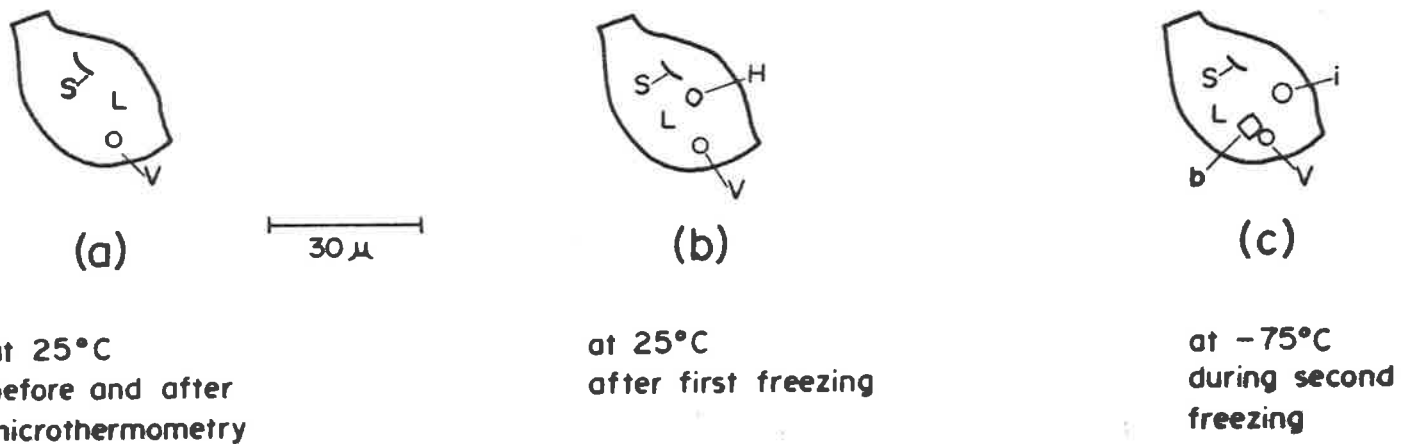
A temperature of  $-61^{\circ}\text{C}$  is below the eutectic of any experimentally known salt-water systems, but could be the result of a mixture of salts such as  $\text{CaCl}_2$ ,  $\text{NaCl}$ ,  $\text{KCl}$ ,  $\text{FeCl}_2$ ,  $\text{MgCl}_2$  and  $\text{AlCl}_3$ .

A similar behaviour was demonstrated by the following inclusion (Figure 25), whose phase relations are typical for inclusions with low freezing temperatures. This inclusion had three phases: liquid, vapour and a tiny speck of a birefringent mineral (dawsonite or any micaceous mineral?) (Figure 25a).

During the first freezing test a hydrate was left after all ice had melted (temperature not recorded). This feature is not unique but has also been in other inclusions with very low last melting temperature ( $-50.5^{\circ}\text{C}$ ). After slow warming the presumed hydrate did not melt before  $0^{\circ}\text{C}$ , indicating that it could not have been  $\text{NaCl}\cdot 2\text{H}_2\text{O}$ . Further warming produced at  $+45^{\circ}\text{C}$ , a phase change into a strongly birefringent and green-coloured solid (Figure 25b). With continuous heating this solid finally dissolved at  $103^{\circ}\text{C}$ . Data from Linke (1965) indicate that  $+45.1^{\circ}\text{C}$  is the temperature at which  $\text{CaCl}_2\cdot 4\text{H}_2\text{O}$  changes into  $\text{CaCl}_2\cdot 2\text{H}_2\text{O}$  in the presence of a saturated solution.

The persistence of the hydrate up to  $103^{\circ}\text{C}$  is probably a metastable event, as the salinity corresponding with this temperature (62.5%  $\text{CaCl}_2$ ) would have required the whole inclusion to consist of  $\text{CaCl}_2\cdot 6\text{H}_2\text{O}$  at  $-61^{\circ}\text{C}$  (see Figure 12). The metastable persistence of  $\text{CaCl}_2\cdot 2\text{H}_2\text{O}$  is probably the result of a fluid composition close to the eutectic of water- $\text{CaCl}_2$  and other halides. The presumed metastability was supported by a second freezing test in which no metastable phases were observed.

The salinity of a fluid composition close to the eutectic water- $\text{CaCl}_2$  is nevertheless the highest concentration of  $\text{CaCl}_2$  ever recorded (30.5%  $\text{CaCl}_2$ ). Obviously, the result of this single inclusion cannot be accepted as being representative for fluid compositions during the crystallization of this quartz. However, the results from other inclusions undoubtedly



S=solid (dawsonite or mica?); L=liquid; V=vapour; H=hydrate  
 i=ice-like solid; b=birefringent solid

Figure 25: Typical phase changes during the microthermometry of one inclusion from quartz crystal A-495-172F.

indicate the presence of extremely concentrated brines (Figure 22, A-495-172F). The association of such solutions with uranium deposits is unknown to date.

This high salinity inclusion homogenized into a liquid-phase at  $+119^{\circ}\text{C}$ , except for the tiny birefringent, fibrous solid which remained unaffected. Cooling to room temperature did not nucleate any other solid-phase.

During the second freezing test the temperature was brought down to  $-179^{\circ}\text{C}$ . Upon warming up to  $-133^{\circ}\text{C}$  the liquid started to form dendritic crystals which grew slowly at the expense of the liquid and expanded over the whole inclusion (with the exception of the vapour-phase) in a few minutes. At  $-75^{\circ}$  the solids recrystallized into larger rounded ice rafts and one square-shaped birefringent crystal (Figure 25c).

Both solid phases melted at  $-59^{\circ}\text{C}$ . This is most likely the true eutectic temperature of the system, at which composition the probability increases that hydrates are formed, which persist metastably beyond the minimum melting temperature.

Apart from these fluid inclusions, another seven inclusions contained cubic daughter minerals which occupy less than 5 vol.% of inclusion. Upon freezing, all inclusions formed granular hydrates which melted near  $0^{\circ}\text{C}$ , pointing to hydrates of NaCl. The low last melting temperatures of the ice-phase ( $-44.5^{\circ}$  to  $-50.5^{\circ}\text{C}$ ) indicate a  $\text{CaCl}_2$ -rich solution.

The homogenization temperatures of these inclusions range between  $+93.5^{\circ}$  and  $+142^{\circ}\text{C}$ , with values clustered into five groups:  $+93.5^{\circ}\text{C}$ ,  $+115^{\circ}$  to  $120^{\circ}\text{C}$ , and  $+134^{\circ}$  to  $+142^{\circ}\text{C}$  (Figure 23, A-495-172F). These clusters may be an indication of a temperature sequence although the possibility of later disruption cannot be excluded.

#### f) Crushing tests

Several quartz grains were crushed while immersed either in anhydrous glycerine or in barium hydroxide solution. The major limitation of the test was the difficulty in finding quartz grains with a sufficiently large number of inclusions. As might be expected, grains with few inclusions did

not release any noticeable gas. Grains with some inclusions similar to those previously described released very few gas bubbles, which formed a  $\text{BaCO}_3$  precipitate in barium hydroxide solution.

g) Scanning electron microscopy

The SEM search for daughter minerals and evaporation residue on freshly broken surfaces was not always successful, due to the difficulty of sample preparation. It is difficult to break small (1mm) quartz crystals exactly across an area containing a cluster of inclusions. Although the microthermometry strongly suggested the presence of  $\text{Ca}^{++}$  in fluids, the SEM did not identify any  $\text{CaCl}_2$  crystals as was the case in other samples. The presence of  $\text{Ca}^{++}$  ions was only found on the surface of micaceous minerals from Plate VIII, photo 1.

The most common minerals found in inclusion cavities were micaceous minerals which, according to the X-ray energy dispersive analysis, were probably sericites and chlorites (Plate VIII, photos 1 and 2).  $\text{NaCl}$  was the most common daughter mineral (Plate VIII, photo 3), which confirms the observation of  $\text{NaCl}$  daughters in inclusions from sample A-495-172F. The fibrous mineral found in sample A-495-172F, shown in Plate V, photo 1, could possibly be a hydrated calcium silicate daughter mineral. Apart from these minerals, the elements: K, Fe, Ni and Cl have been detected within the cavities as coatings of micaceous minerals, pointing to the presence of alkali and metal chlorides.

h) General conclusions for sample A-495-172

- The study of fluid inclusions from four individual crystals from vein quartz indicates that the inclusions contained a variety of compositions. These differences are well characterized when comparison is made between inclusions from crystal A-495-172D and inclusions from the other three (A-495-172A, A-495-172B and A-495-172F). The large sizes of inclusions in crystals A-495-172A and B permitted a detailed observation of the unusual phase changes during microthermometry, of which the observation of  $\text{CaCl}_2$ -hydrates and their phase changes has been the most significant one.

- The freezing test indicates that fluids from inclusions in crystal A-495-172D have lower salinity than the other three samples. Fluids from inclusions of these three samples are extremely resistant to freezing and many of them only obtained partial freezing. In general, they have a last melting temperature of less than  $-40^{\circ}$  (i.e. salinity  $>28.3$  wt.%  $\text{CaCl}_2$  equivalent), whereas inclusions in A-495-172D have a melting temperature above  $-40^{\circ}\text{C}$  (Figure 22).

- The  $T_F$  determination also indicates that within the crystal A-495-172D, the inclusions have different salinities which vary with time of formation.

- These rapid changes in solution chemistry within a small vein quartz sample are most readily explained by the mixing of hypersaline brines with more dilute solutions during the crystallization of the host. The association of pitchblende with this quartz vein implies similar changes in condition during precipitation of pitchblende.

- The  $T_H$  presented values from  $<70^{\circ}\text{C}$  to  $140^{\circ}\text{C}$ . The occurrence of inclusions of totally different  $T_H$ 's (A-495-172D and A-495-172F) within one small sample also supports the hypothesis of the mixing of fluids of different origin and temperature.

- The SEM confirmed the presence of NaCl and chlorides of K, Ca, and possibly Fe. The occurrence of sericite and chlorite in cavities in this vein quartz is highly significant with respect to the genesis of these sheet silicates, which are so common in the ore alteration zones which accompany the uranium ores of the Pine Creek Geosyncline uranium deposits.

- The crushing test indicated small amounts of  $\text{CO}_2$  in inclusions, but the test cannot be considered as conclusive because of small sample size.

#### Sample A-495-168

(D.H.Na77; 46.80m)

#### Description of inclusions

This sample is similar to A-495-172 but the host rock is brecciated, forming small cavities where idiomorphic quartz have grown. Only a few of



these crystals are suitably transparent. Inclusions situated in the core of the crystals were of irregular shape containing a liquid-phase only and measuring around  $10\mu$ . Few of these inclusions contain unidentified solid phases such as an orange-coloured platy mineral, a dark amorphous substance and a rectangular mineral.

A series of inclusions marking growth zones of the quartz host have a highly variable liquid to vapour ratio: from pure liquid to pure vapour. Two broad categories can be recognized: (Figure 26; Plate II, photos 1 and 2):

Type (a) (liquid-rich inclusions): inclusions with vapour-phase of less than  $\sim 20$  vol.%; and

Type (b) (vapour-rich inclusions): inclusions with a vapour-phase of more than  $\sim 20$  vol.%.

Their average size is  $3\mu$ , although some large ones may reach  $7\mu$ . The sample contains pitchblende mineralization. Emulsion autoradiography showed  $\alpha$ -track sources in the central area of the quartz crystal, indicating that uraniferous solid inclusions are coeval with the formation of the present fluid inclusions (Plate II, photos 3 and 4).

#### Microthermometry

The freezing test indicated melting temperatures ranging from  $-11^{\circ}$  to  $-33.5^{\circ}\text{C}$  for the liquid-rich inclusions, while the gas-rich inclusion indicated have the last ice disappear at  $-20.2^{\circ}\text{C}$ .

Partial freezing could be observed in one inclusion from the low melting temperature cluster. Other inclusions from this cluster did not freeze. The recorded range of temperature indicates salinity of 15.5 wt.% to 27.0 wt.%  $\text{CaCl}_2$  (equivalent) (Figure 27,  $T_F$ ).

During the freezing test three inclusions nucleated a vapour phase which was not present before. On heating these bubbles disappeared between  $95.5^{\circ}$  and  $108^{\circ}\text{C}$  (Figure 27,  $T_H$ ). This range of temperature could be significant with regard to the temperature of formation of the host.

#### Crushing test

Quartz grains with Type (b) inclusions always presented a "very strong" release of gas. A few of the gas bubbles dissolved in  $\text{Ba}(\text{OH})_2$  solution,

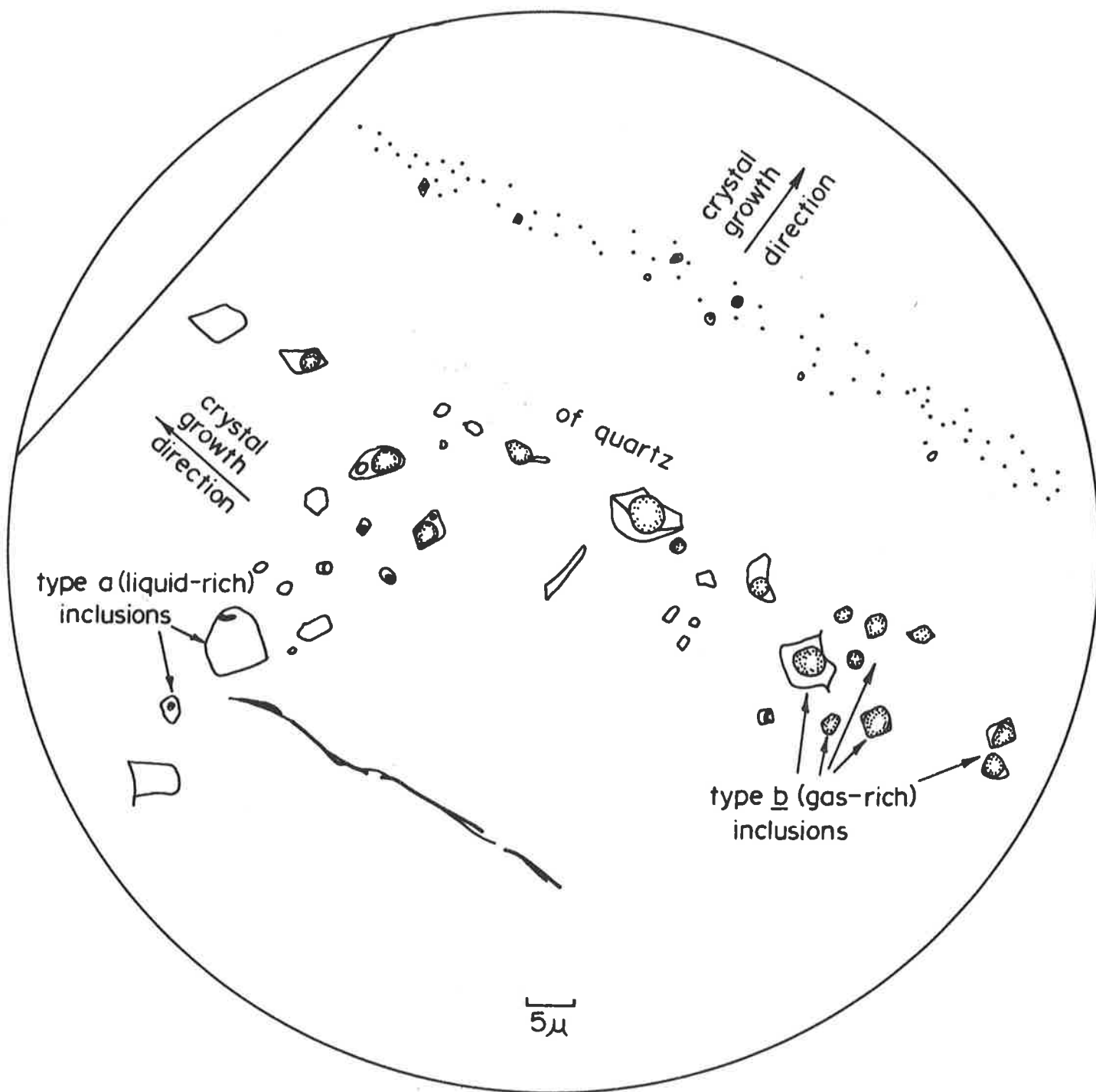


Figure 26: Sample A-495-168.

Type (a) (liquid-rich) and type (b) (vapour-rich) inclusions from zone of growth of a quartz crystal. Also see Plate II, photos 1 and 2.

forming a  $\text{BaCO}_3$  precipitate, while the majority dissolved only very slowly. Some bubbles showed a partial reaction, i.e., the bubble shrank only partially upon reaction with  $\text{Ba(OH)}_2$  and remained stable thereafter.

Conclusions for sample A-495-168

- The low melting temperatures of some frozen products, partial freezing, and the resistance to freezing clearly indicate the presence of highly saline brines (presumably Ca and alkali chlorides).
- The variation of salinity within one small crystal seems to indicate the mixing of different fluids.
- The mixing could also explain the formation of types (a) and (b) inclusions through the exsolution of gas, at the stage that a low salinity  $\text{CO}_2$ -rich fluids mixes with a concentrated brine.
- The low melting temperature of the gas-rich inclusions ( $-22.2^\circ\text{C}$ ) excludes the possibility of boiling as the cause of variable liquid-vapour ratios. A vapour-rich phase when cooled could not have resulted into a saline brine because of the very limited salinity of water vapour even at high temperatures (Sourirajan and Kennedy, 1962). Moreover the high overall salinity and the generally low homogenization temperatures exclude boiling in the present case. The most likely explanation for the varying liquid/vapour ratio is the mixing of a saline brine with a more dilute  $\text{CO}_2$ -rich solution which lost its capacity to carry  $\text{CO}_2$  in solution on contact with the brine.
- The crushing test seems to point to a gas composition similar to that of sample A-495-176 (see in later description):  $\text{CH}_4$ -rich +  $\text{CO}_2$  gas phase.
- The homogenization temperature of inclusions, the content of which was probably not the result of mixing, points to deposition of pitchblende at around  $100^\circ\text{C}$  or even lower, which conclusion is in agreement with the range of temperatures found in sample A-495-172.

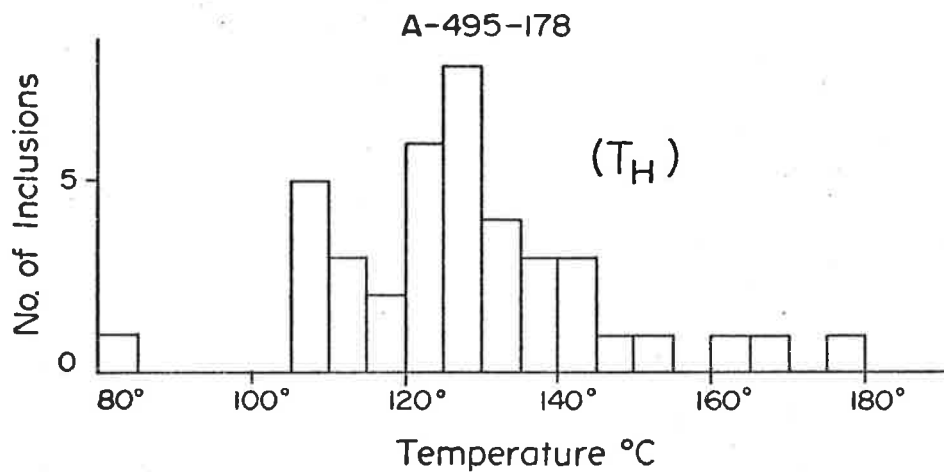
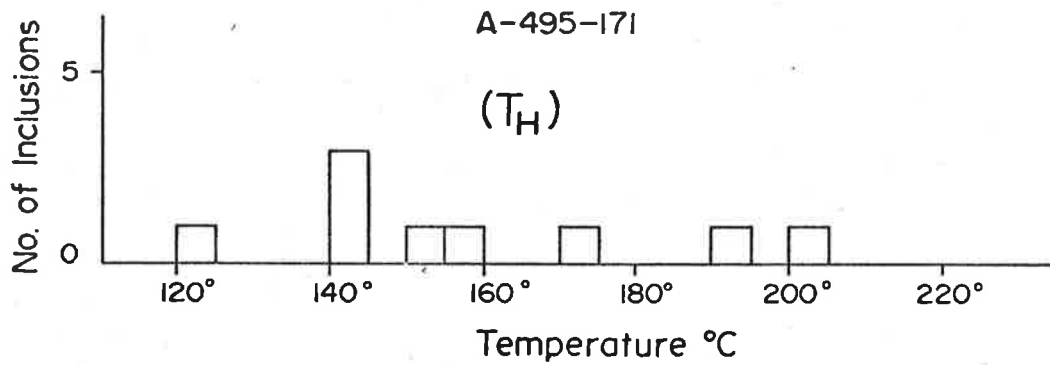
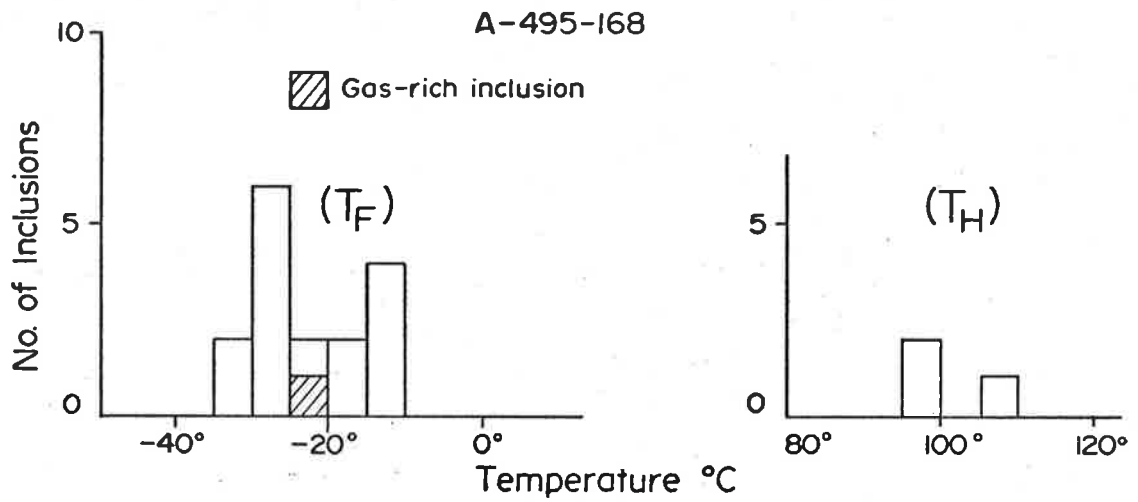


Figure 27: Frequency histograms of microthermometry of fluid inclusions in quartz from samples A-495-168 (late-stage), A-495-171 (early-stage) and A-495-178 (late-stage).

Sample A-495-171

(D.H.Na77; 56.70m)

Description of inclusions

In this sample the late-stage idiomorphic quartz contains a larger number of inclusions. They are nearly all of one-phase (liquid) type with many of them situated along zones of growth. Few inclusions were rich in vapour. The average size of these inclusions is  $15\mu$

The early-stage quartz is generally milky and too fractured to contain inclusions suitable for study. However, in a few small vugs completely filled with quartz crystals, some grains of early-stage material could be examined. The inclusions contained two-phase (liquid + vapour) type inclusions, with some evidence of "necking down". The average size of these inclusions was  $10-15\mu$  with a vapour bubble of 1-5 vol.%.

Microthermometry

One cluster of one-phase inclusions from late-stage quartz was immersed in liquid nitrogen in an attempt to nucleate a gas-phase. But the test did not show any change in appearance of inclusions. This could be an indication that these inclusions were formed at low temperatures ( $<70^{\circ}\text{C}$ ).

A cluster of two-phase inclusions from the early-stage quartz presented  $T_H$  ranging from  $120^{\circ}$  to  $200^{\circ}\text{C}$ . Five inclusions out of 40 did not homogenize below  $220^{\circ}\text{C}$ . "Necking down" could be partially responsible for this large range of  $T_H$ . Although a statistically significant number of measurements could not be made, a maximum at  $140^{\circ}\text{C}$  is shown in Figure 27. It is interesting to notice that on cooling to room temperature, eight inclusions did not re-nucleate a vapour-phase. This points to the possibility of metastable conditions for many liquid or liquid-vapour inclusions. One of the inclusions that did not re-nucleate a vapour phase, homogenized earlier at a temperature of  $\sim 190^{\circ}\text{C}$ . With such an extensive metastability, one wonders how many one-phase inclusions from late-stage quartz were in fact inclusions with a "stretched" liquid at room temperature having actual entrapment temperatures between 120 and  $200^{\circ}\text{C}$ . However, the homogeneity of the liquid composition of

the one phase inclusions and the persistent absence of any nucleation of a vapour-phase - even after immersion in liquid nitrogen - seems to rule out this possibility. It is more likely that differences in temperature of formation between inclusions of the two quartz stages are the result of different entrapment temperatures as will be pointed out in reference to samples A-495-174 and A-495-176.

Sample A-495-162

(D.H.Na72; 29.6m)

Description of inclusions

This hematite-stained quartz-chloritic rock was collected at the lower limit of the main orebody. It is one of the rare samples available from the ore-zone which contains suitable fluid inclusions.

The pitchblende was contemporaneous with hydrothermally-formed quartz and chlorite (Plate I, photo 1). Black minerals - probably pitchblende - were present as solid inclusions (Plate I, photo 2). The quartz contained numerous chlorite inclusions and fluid inclusions, giving the host a clouded aspect. The inclusions could be separated into two types: (a) liquid-rich; (Plate I, photo 3) and (b) vapour-rich; (Plate I, photo 4). Among type (b) inclusions only one showed a second liquid-phase. A few type (a) inclusions contain only a liquid phase, and daughter minerals are rare. In this group there was one exceptionally large inclusion (150 $\mu$ ) with polyhedral morphology (Plate I, photo 3). The average size of the inclusions was between 10 to 15 $\mu$ .

Microthermometry

Freezing indicated last melting temperatures ranging from very low salinities for the majority of inclusions ( $T_F = -0.9^\circ\text{C}$  to  $-0.3^\circ\text{C}$ ) - including the large one ( $T_F = -3.8^\circ\text{C}$ ) - to a few high salinities ( $T_F = -30.5^\circ\text{C}$  to  $-13.5^\circ\text{C}$ ) (Figure 28,  $T_F$ ).

Two inclusions formed clathrates of  $\text{CO}_2 + \text{CH}_4$  (?), which melted between  $-31.5^\circ$  and  $-28.3^\circ\text{C}$ .

As  $\text{CO}_2 \cdot 5 \frac{3}{4} \text{H}_2\text{O}$  and  $\text{CH}_4 \cdot 5 \frac{3}{4} \text{H}_2\text{O}$  form isomorphous solid solutions (Poty and Stalder, 1970), we are probably dealing with a mixed hydrate melting

at a pressure of around  $10 \text{ kg/cm}^2$ . These pressures are in marked contrast to melting temperatures of gas-clathrates recorded in literature (op. cit.) where pressures of around  $150 \text{ kg/cm}^2$  have been postulated with corresponding melting temperatures ranging between  $+15$  and  $+20^\circ\text{C}$ .

Homogenization temperatures are presented in Figure 28. Inclusions with  $T_H$  above  $200^\circ\text{C}$  showed a loss of fluid during the test, presumably because of temperatures exceeding the entrapment temperature. The result is that the number of significant  $T_H$  measurements is rather small. The large range of  $T_H$  distribution is probably due to post-entrapment phase changes: differential transfer of liquid and vapour phases.

#### Crushing test

The crushing test clearly indicated the presence of gas under pressure. This consisted of  $\text{CO}_2$  and hydrocarbons, as demonstrated by the reaction of  $\text{CO}_2$  with a  $\text{Ba}(\text{OH})_2$  solution and the dissolution of  $\text{CH}_4$  in kerosene.

#### Scanning electron microscopy

The SEM and EDAX investigation of cavity fillings indicated the presence of chlorides:  $\text{CaCl}_2$  (Plate VI, photo 4),  $\text{NaCl}$  (Plate VII, photo 1a);  $\text{NaCl} + \text{KCl}(\text{?})$  (Plate VII, photo 1b); micaceous minerals, probably sericite (Plate VII, photos 1b and 2), and clay-minerals of the kaolinitic group (Plate VI, photos 1, 2 and 3); kaolinite was very common and sericite was also frequent. Chlorides were less frequent, because the number of inclusions containing brines of high salinity was probably small. The micaceous minerals may have been trapped as a solid phase during the crystallization of quartz, or possibly deposited as a daughter mineral from the less saline brines, in the same way in which chlorides form daughter minerals in concentrated brines.

The identification of kaolinite was based on the platy morphology of the crystal, its hexagonal outlines and perfect basal cleavage: all criteria which identify the mineral as a sheet silicate (Plate VI, photo 2). The EDAX analysis indicated only silica and aluminium, which seems to suggest kaolinite. Sericite plates have a distinct K-peak. The instruments low sensitivity to sodium implies that the presence of alkali-deficient illite cannot be completely

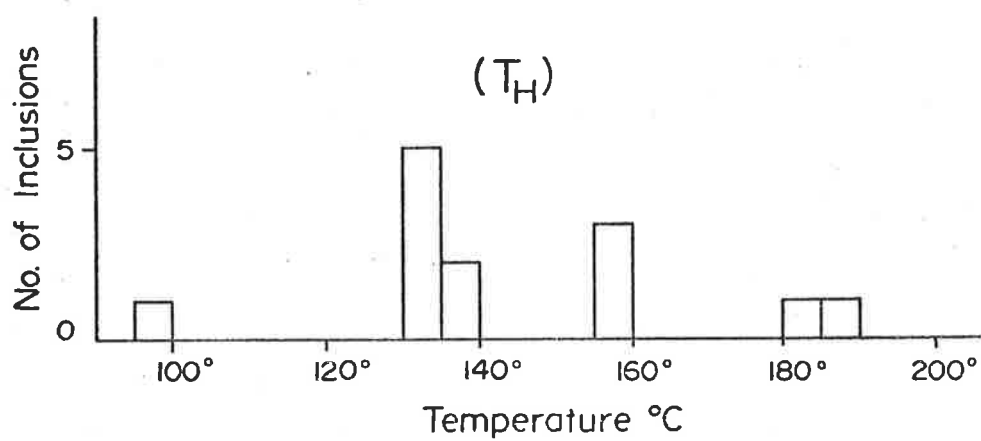
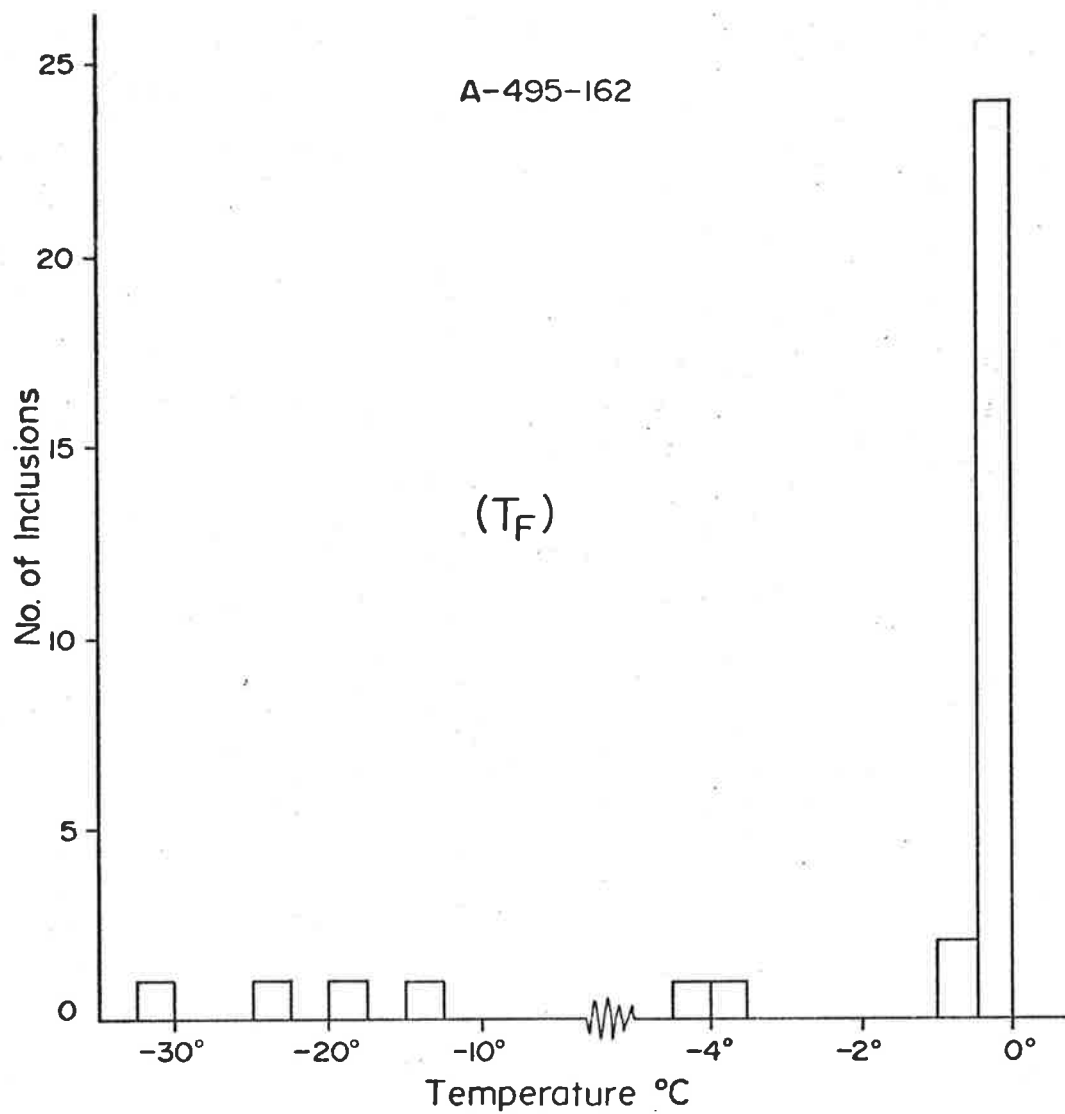


Figure 28: Sample A-495-162. T<sub>F</sub> and T<sub>H</sub> frequency histogrammes of fluid inclusions in hydrothermal quartz.



ruled out.

#### Conclusions for sample A-495-162

- Although few fluid inclusions indicated high salinity, the vast majority (24 inclusions) pointed to a solution of constant 0.4 wt.% NaCl. This is the lowest value of all samples considered in this study and strongly supports the hypothesis of the mixing of solutions of grossly different salinities.

- The frequency of kaolinite daughter minerals is highly relevant because of the distinct retrograde metamorphic aureole around the Nabarlek and Jabiluka deposits (Binns et al. 1979). The observation of kaolinite and other sheet silicates in fluid inclusions, places the predominance of chlorite-sericite-clay mineral alteration in uraniferous rocks into direct relation with the low temperature brine solutions. In other words it would appear that hydration of country-rock minerals and U-mineralization are coeval.

#### Pitchblende samples

##### Introduction

Inclusions in pitchblende obviously cannot be studied by ordinary microscopy. In an attempt to obtain at least some information from inclusions in pitchblende, three samples were selected and examined with SEM/EDAX techniques and crushing stage (samples A-495-110, A-495-116, and A-495-201). Bonev (1977), demonstrated the feasibility of an SEM study of galena. Freshly broken surfaces of pitchblende were studied for solid inclusions, daughter minerals and residues of evaporation. Both daughter minerals and evaporation residues could give information on the composition of fluids involved in pitchblende formation. The crushing test supplies the same kind of information obtained for transparent minerals. The only complication is the opacity of the mineral. In the event of "weak" gas release the bubbles would remain obscured behind mineral fragments.

##### Scanning electron microscopy

Apart from the presence of inclusions of galena (probably of radiogenic origin) and micaceous minerals (identified as chlorite), the

minerals most frequently found in pitchblende inclusion cavities were calcite and dolomite (Plate XV, photos 1 and 2). The calcite from sample A-495-110 may be the product of a later event coeval with the introduction of fibrous calcite veinlets cutting across the pitchblende. Furthermore, there is the possibility of gypsum as a solid inclusion (Plate VI, photo 3).

Although 8 SEM-samples of pitchblende have been studied, only the presence of  $\text{Ca}^{++}$  could be established. The presence of numerous empty cavities without a fringe of evaporation products points to dilute brines in the inclusions.

#### Crushing test

The crushing of pitchblende grains always presented the strongest release of gas in minerals from the Nabarlek uranium deposit, indicating gases under pressure. Many gas bubbles precipitated  $\text{BaCO}_3$  with a  $\text{Ba(OH)}_2$  solution pointing to the presence of  $\text{CO}_2$ . Almost all bubbles dissolved fairly rapidly in kerosene. The rate of solubility varied. Figure 29 shows some of these different rates of solubility. Curves b, c, and d have different patterns which indicate bubbles with different gas composition. For example, two bubbles with the same diameter of 3.5 units ( $\sim 70\mu$  and a volume of  $\sim 1.796 \times 10^{-4} \text{ mm}^3$ ) presented totally different rates of dissolution: one bubble dissolved at half the rate of the other. The bubble with the higher rate of dissolution clearly indicated a rate change during the first 30 seconds, pointing to a mixture of two gases of different solubilities. A third bubble with 5 units ( $\sim 100\mu$  or a volume  $\sim 5.235 \times 10^{-4} \text{ mm}^3$  which is nearly 3 times the volume of the previous two) presented a rate of dissolution different from them both. These different solubilities point to the existence of at least three different gas compositions. Apart from hydrocarbons and  $\text{CO}_2$ , these gases probably contain helium also, as a product of uranium decay.

Pitchblende impregnated by porous mica-chlorite aggregates may contain microvoids filled with air. In order to settle this question the solubility of air bubbles in kerosene was measured (Figure 29, curve a). These tests pointed to a complete insolubility of the air for at least the time

period covered by the experiment. The initial increase in the size of the air-bubble was the result of expansion due to heat from microscope light.

In conclusion, it seems certain that the pitchblende contained at least carbon dioxide, hydrocarbons and helium under high pressure.

## II.2.2 Non-uraniferous samples

Quartz was also the main mineral for the fluid inclusion study of non-uraniferous samples. The selected specimens are (Figure 7):

II.2.2.1.1 - sample A-495-176

II.2.2.1.2 - " A-495-174

II.2.2.1.3 - " A-495-178 from drill-hole Na77

II.2.2.1.4 - " A-495-179

II.2.2.2 - sample A-495-157 (drill-hole Na55) which is a vein-quartz in altered dolerite.

II.2.2.3.1 - sample A-495-113 (drill-hole Na1) and

II.2.2.3.2 - " A-495-156 (drill-hole Na55) from areas where strong hydrothermal action is located just below the main orebody.

II.2.2.4.1 - sample A-495-144 (drill-hole Na23) and

II.2.2.4.2 - " A-495-191 (drill-hole Na83) which contain alteration products and are situated inside and at the bottom of the dolerite sill.

II.2.2.5.1 - sample A-495-186 (drill-hole Na83) consisting of hydrothermal quartz collected between the dolerite sill and the granitic body.

II.2.2.6.1 - sample A-495-144. Only two calcites from non-uraniferous host rocks were available (drill-hole Na23) and

II.2.2.6.2 - " A-495-220 (drill-hole Na176).

II.2.2.1.1 Sample A-495-176

(D.H.Na77; 67.35m)

### a) Introduction

This sample is a non-mineralized quartz-chlorite schist containing the only large quartz-vug found in drill-cores from Nabarlek. The vug contains good material for fluid inclusion studies. As mentioned previously, the size of the present sample made it possible to distinguish between

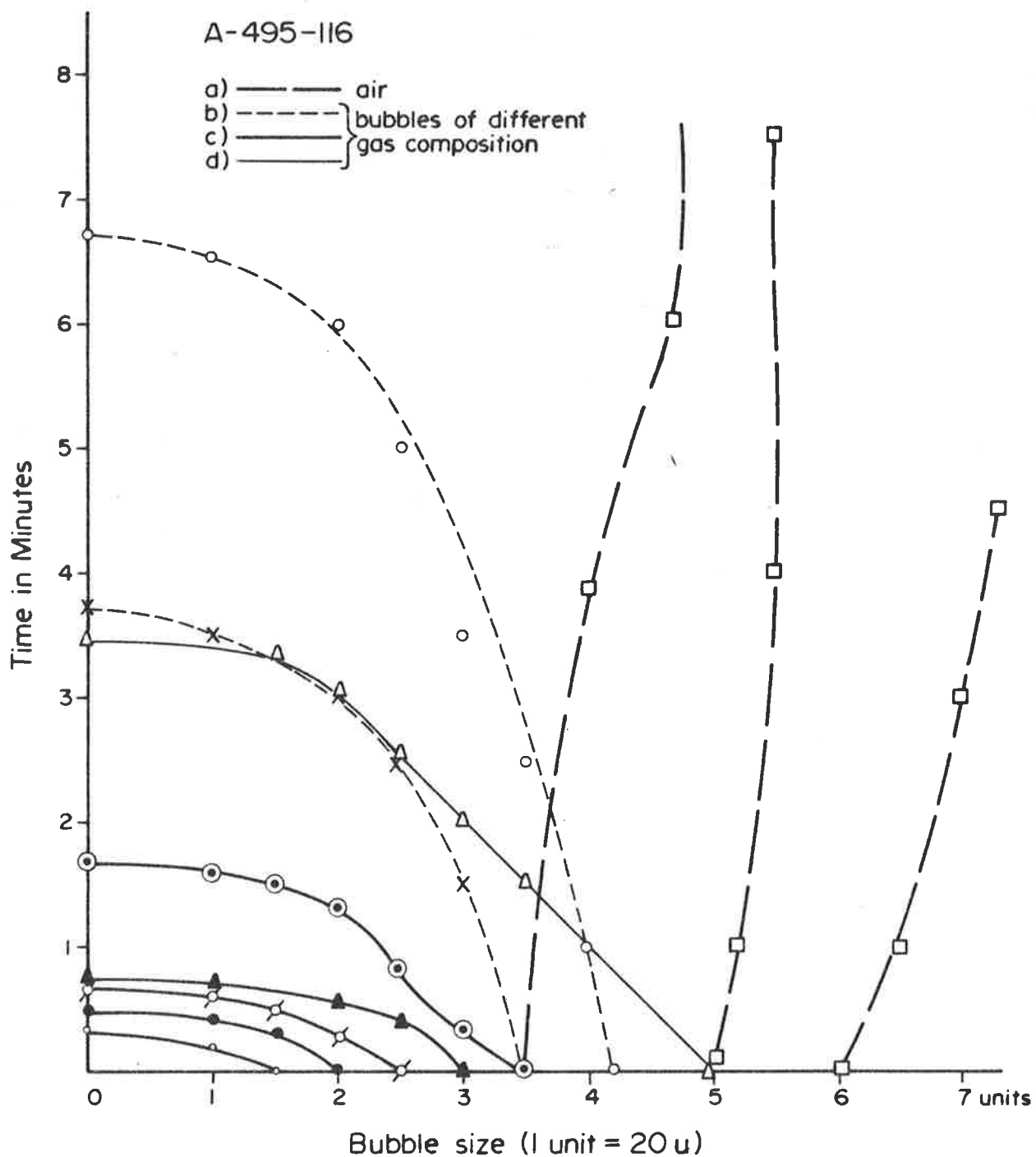


Figure 29: Solubility in kerosene of gas bubbles released by pitchblende during crushing test (1 scale unit equals 20 micron bubble diameter).

idiomorphic quartz (late-stage) and non-idiomorphic quartz formed at an earlier-stage (Plate V, photo 3). Therefore a careful study of several clusters of fluid inclusions from both stages of quartz (Plate V, photo 4) could be carried out. It was not possible to differentiate between the fluid inclusions from the two stages purely by inclusion morphology. The early-stage quartz is generally milky and fractured (Plate V, photo 4). As a result, it does not contain very large inclusions, but only material between 10 and 15 microns.

The selection of the material produced two idiomorphic quartz crystals of the late-stage and four groups of inclusions of the early-stage in xenomorphic quartz. Each of the hosts was studied individually by microthermometry. In general, the inclusions contain two phases (liquid + vapour) in variable ratios which have been classified into two types: (a), liquid-rich (Plate IV, photo 3) and (b) vapour-rich as established in sample A-495-168 (Plate II, photo 2).

With the exception of one sample, nearly all microthermometric studies were based on type (a) inclusions. Type (b) inclusions were not suitable because:

- Inclusions with very large bubbles are, in general, very dark. The liquid-phase consists of a thin lining of the cavity only, while the bubble obscures any phase changes of the liquid.
- Liquid/gas ratios are highly variable. In consequence, the  $T_H$  will also vary, does not indicate nor bear any resemblance to inhomogeneous entrapment temperatures of the host (e.g. A-495-176-E).
- As the formation of substantial amounts of clathrates increases the salinity of the remaining solutions, with the exception of saturated liquids, the determination of actual salinities is not possible by non-destructive means.

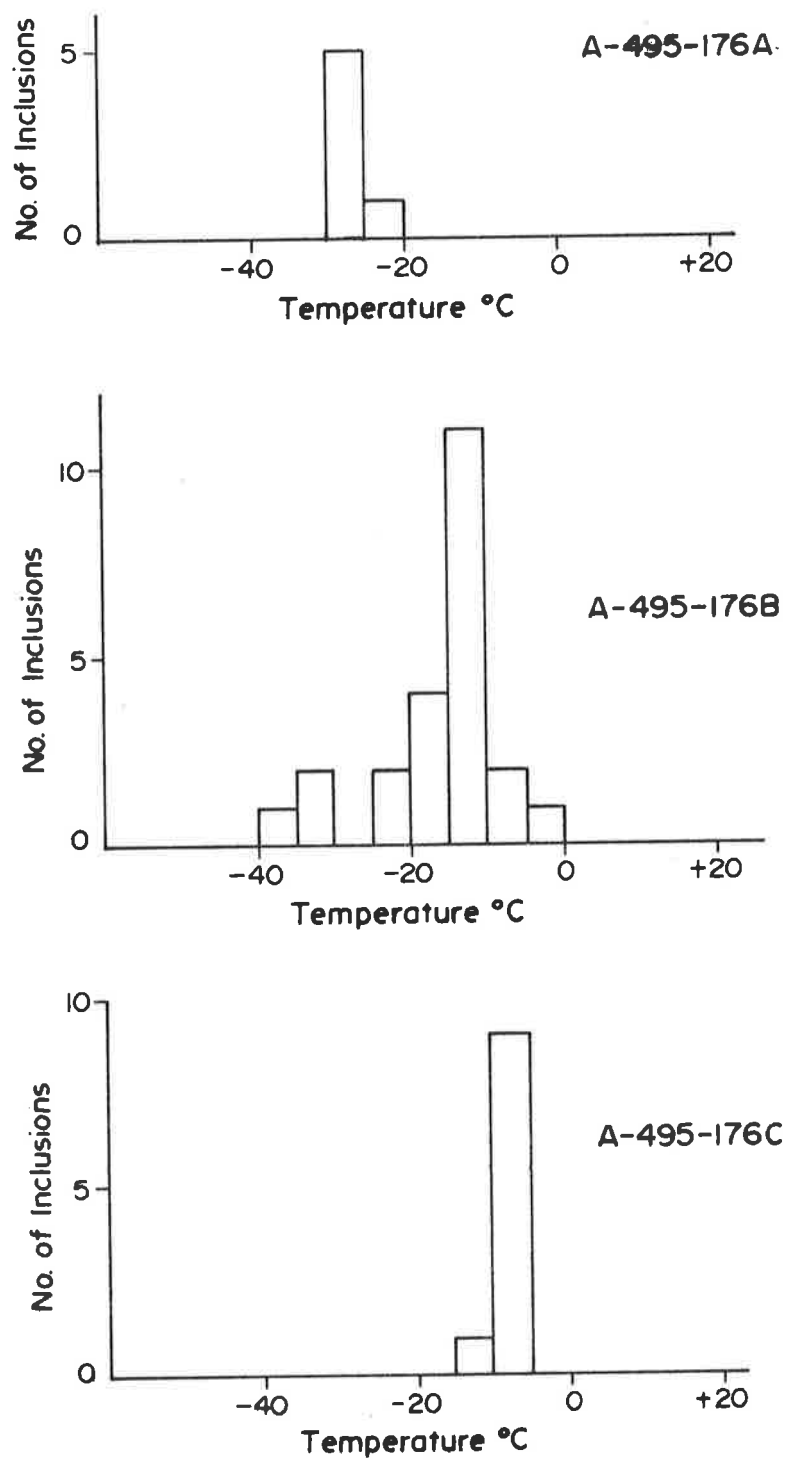


Figure 30: Sample A-495-176.  $T_F$  frequency histograms of fluid inclusions in three different early-stage quartz samples of a non-mineralized area.

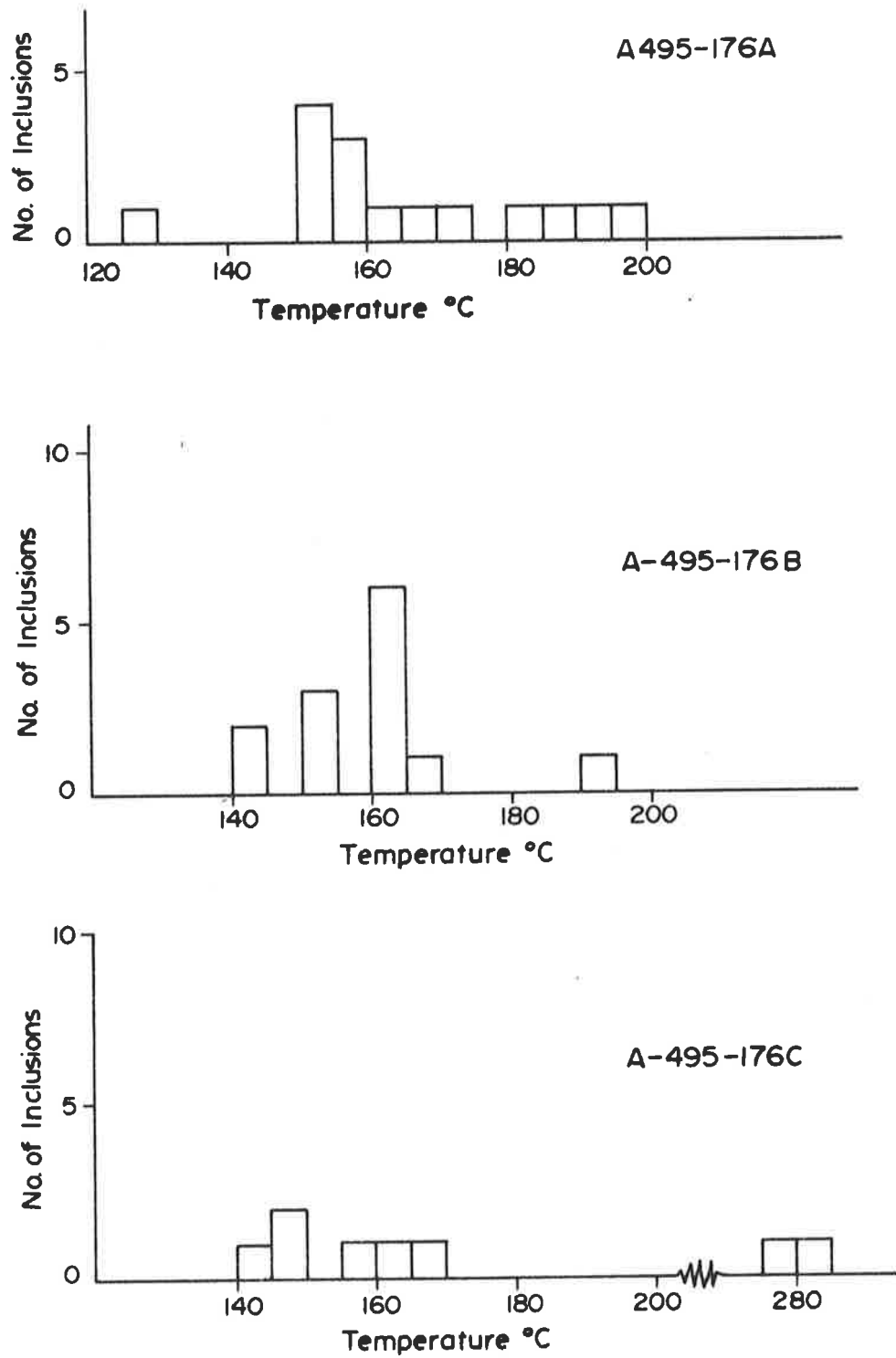


Figure 31: Sample A-495-176.  $T_H$  frequency histograms of fluid inclusions in the same quartz samples of figure 30.

b) Early-stage quartzb.1 Quartz A-495-176-ADescription of inclusions

In a cluster of more than 30 inclusions, the type (a) inclusions presented a vapour-phase varying between 1 and 5 vol.%, whereas the type (b) normally had a vapour-phase exceeding 40%. Liquid-rich inclusions ranged from 1 to 30 $\mu$ . The larger ones were more irregular in shape. Vapour-rich inclusions occurred in rows probably indicating a secondary origin. These were not studied.

Microthermometry

The inclusions appeared to be extremely resistant to freezing. After cooling several times to -175 $^{\circ}$ C, only one cluster of six type (a) inclusions were frozen. Five of them had a last melting temperature of about -28 $^{\circ}$ C and one at -24 $^{\circ}$ C (Figure 30, A-495-176-A). These temperatures indicate a salinity of 26 to 29.5 wt.% CaCl<sub>2</sub> equivalent. The reason for their resistance to freezing is not obvious, but the small size of inclusions, their high salinity and lack of nucleating agents could have played a role. The heating experiment indicated a wide range of T<sub>H</sub>, with a distinct frequency maximum between 150 $^{\circ}$  and 160 $^{\circ}$ C (Figure 31, A-495-176A). The wide range of T<sub>H</sub> could have been a consequence of post-entrapment changes.

b.2 Quartz A-495-176-BDescription of inclusions

Essentially, the inclusions were similar to those described in A-495-176-A. Additional characteristics were:

- both types of inclusions may have contained cubic daughter minerals;
- some type (b) inclusions (gas-rich) have negative-crystal shape and seemingly contain only gas;
- post-entrapment redistribution of inclusion content "necking-down" was conspicuous in some large type (a) inclusions.



### Microthermometry

During a stepwise cooling, some inclusions formed a thin condensed phase around the vapour bubbles at  $+6^{\circ}\text{C}$  pointing to liquified gas.

At  $-60^{\circ}\text{C}$  many inclusions were frozen, but two larger ones ( $15\mu$ ), which will be named inclusion (1) and inclusions (2), presented different behaviours. At room temperature, inclusion (1) contained a fairly large gas-phase ( $\sim 10\%$  by volume); whereas inclusion (2) presented a vapour-phase of 5 vol.% and a cubic mineral of similar volume. At  $-40^{\circ}\text{C}$  both inclusions started nucleating daughter products (presumably salt hydrates). When kept at  $-80^{\circ}\text{C}$  for 30 minutes, these daughter products aggregated into a single-phase solid. Inclusion (2) resisted complete freezing (Plate IV, photo 4). Upon warming, the solids seemed to undergo a phase change because of the change in birefringency. Phase changes are unknown for  $\text{NaCl}\cdot 2\text{H}_2\text{O}$ .  $\text{KCl}$  does not normally form hydrated products. Melting of these phases has escaped attention. It was surprising to note that ice in the saturated brine solution of inclusion (2) persisted up to  $-13.4^{\circ}\text{C}$ , the temperature of which does not correspond to the eutectic of either  $\text{KCl}-\text{H}_2\text{O}$  or  $\text{NaCl}-\text{H}_2\text{O}$ , and is well above any eutectic of a system involving  $\text{CaCl}_2$ .

The frequency histogram of two-phase (liquid + vapour) inclusions is presented in Figure 30, A-495-176B. It points to an average salinity of 17.5 wt.%  $\text{CaCl}_2$  equivalent. The three inclusions presenting a  $T_F$  below  $-30^{\circ}\text{C}$  may have originated at a different stage as they form an isolated cluster. Their temperatures indicate salinities of 26.5 to 28 wt.%  $\text{CaCl}_2$  equivalent. Freezing of gas-rich inclusions was not observed.

The  $T_H$  of two phase inclusions is presented in Figure 31, A-495-176B. Temperatures ranged from  $+142.5^{\circ}$  to  $+165^{\circ}\text{C}$ , grouped in two frequency maxima. Inclusion (2) was heated up to  $+286^{\circ}\text{C}$  but the daughter mineral did not dissolve. The high temperature at which the last ice melted ( $=13.4^{\circ}\text{C}$ ) seems to suggest a brine saturated with  $\text{KCl}$ . However, the absence of solubility of the daughter mineral clearly indicates the contrary. The only solution to

this problem is 1) the presence of a substance other than KCl and NaCl, or 2) the coating of a NaCl crystal by an insoluble substance (silicates?). In either case the daughter mineral is possibly an heterogeneously trapped phase. The fact that most of the inclusions presented last melting temperatures around  $-15^{\circ}\text{C}$ , as indicated in Figure 30, A-495-176B, seems to support a non-soluble accidentally trapped solid.

### b.3 Quartz A-495-176C

#### Description of inclusions

All inclusions except one belong to the liquid-rich type. Their main characteristics were:

- much lower relief than the previous groups of inclusions;
- ~~the absence~~ of daughter minerals or solid phases;
- highly irregular shapes: amoeboid, anastomatic resulting in "necked down" inclusions with only a liquid-phase.

#### Microthermometry

The melting temperature of ice (Figure 30, A-495-176C) indicated an average salinity of 13.5 wt.%  $\text{CaCl}_2$  equivalent, which is the lowest salinity determined for sample A-495-176.

The high homogenization temperatures of some inclusions ( $\sim 280^{\circ}\text{C}$ ) is the result of post-entrapment changes in liquid-vapour ratios. Normal values were in the same  $T_H$  range as previously studied early-stage quartz (Figure 31, A-495-176C).

### b.4 Quartz A-495-176D

This piece of quartz was selected from close to the wall-rock of the vug and is likely to be quartz of the earliest-stage (Plate V, photo 4, point D). Because the aggregate was highly fractured, only small inclusions were preserved. The majority of inclusions are of the liquid-rich type. The heating test indicated a wide range of  $T_H$  (Figure 32, A-495-176D), which could be the consequence of post-entrapment changes resulting in the formation of inclusions with variable gas/liquid ratio, or alternatively, the trapping of inclusions at different temperatures. Notwithstanding the large

range of  $T_H$ , the histogram shows frequency maxima at  $\sim 160^\circ\text{C}$  and at  $\sim 185^\circ\text{C}$ . This interval could be taken as the likely range of temperature at which this quartz was formed.

c) Late-stage quartz

Fluid inclusions in two idiomorphic quartz crystals were studied by microthermometry.

c.1 Quartz crystal A-495-176E

Description of inclusions

This specimen was selected because it contained a cluster of type (b) vapour-rich inclusions. Only 3 out of 38 inclusions were of the liquid-rich-type. This crystal was one of the rare samples with type (b) inclusions suitable for microthermometry. Most of these type (b) inclusions studied so far, showed a high relief of contrast vapour bubbles which precluded the observation of two fluid phases inside the bubble. The inclusions of sample A-495-176E showed elongated to irregular shapes which facilitated observation. A few inclusions contained an amorphous solid phase which could not be identified.

Microthermometry

Freezing of type (b) inclusions

A few inclusions with lower than normal bubble relief (due to the particular geometry of the inclusion) showed a second liquid phase on cooling. At  $-70^\circ\text{C}$  all inclusions were frozen; the first melting started at  $-66^\circ\text{C}$ ; the last melting temperatures of ice are shown in Figure 32, A-495-176E. The corresponding salinities are in the range of 22.0-30.5 wt.%  $\text{CaCl}_2$  equivalent. The actual salinity may be slightly lower than these figures because of the presence of  $\text{CO}_2$  which may have formed clathrates, although their presence could not be ascertained.

Freezing of type (a) inclusions

The melting temperatures of ice from three type (a) inclusions were also between  $-28.2$  to  $-30.5^\circ\text{C}$ , the same range of temperature as for type (b) inclusions. This again, is a strong indication against the

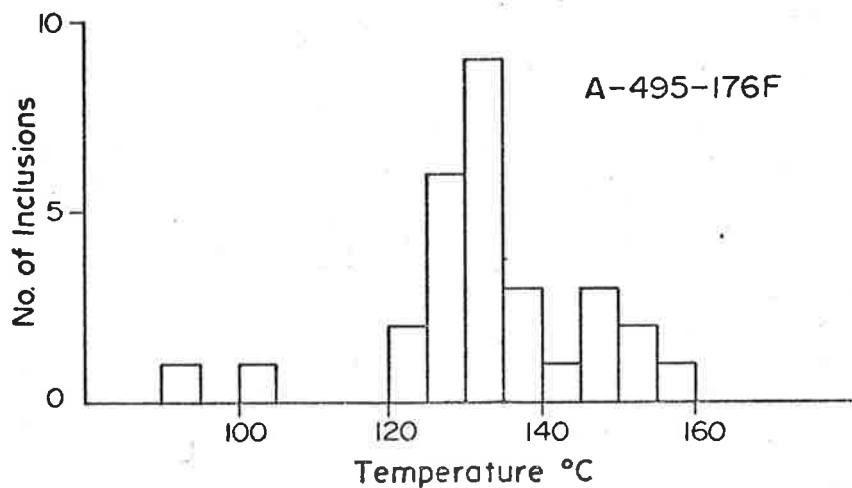
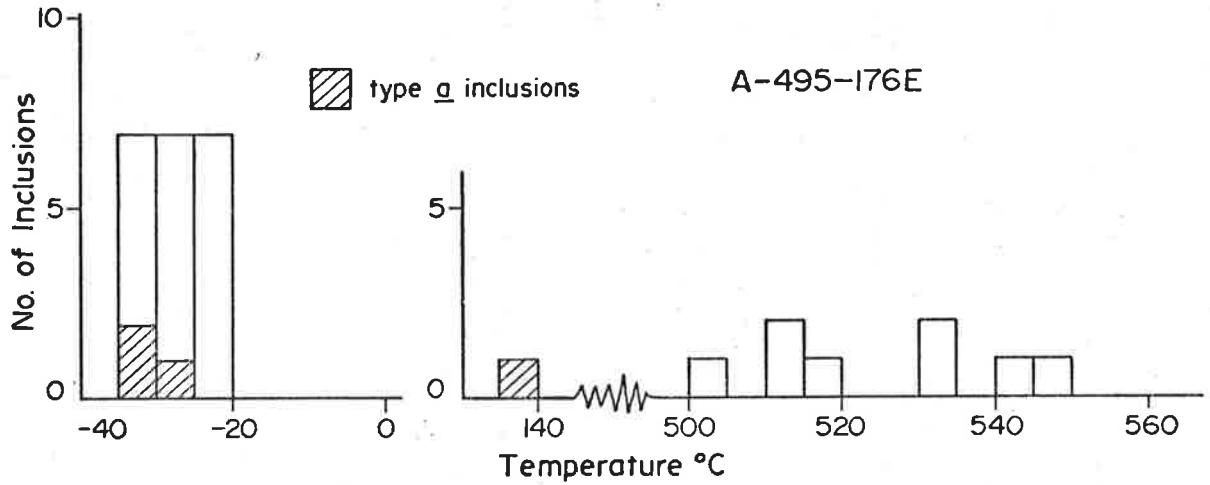
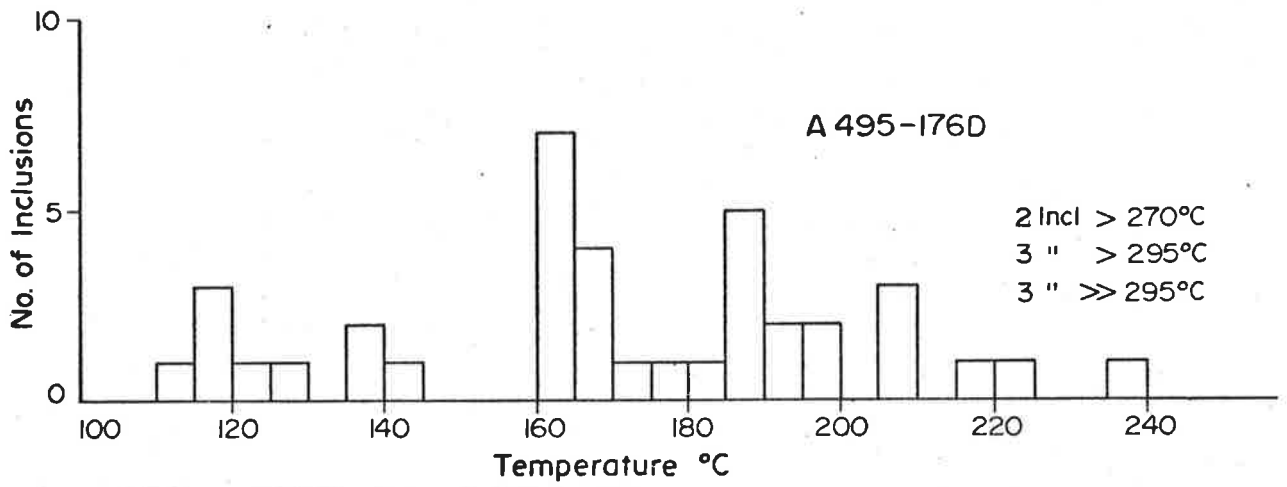


Figure 32: Frequency histogrammes of microthermometry of fluid inclusions in early-stage (A-495-176D) and late-stage (A-495-176E and F) quartz of a non-mineralized area (quartz pod in chlorite rock)

boiling model as a possible explanation for the formation of gas-rich inclusions.

#### Heating tests

During the heating test the inclusions behaved as follows: One type (a) inclusion homogenized into a liquid-phase at  $+133.4^{\circ}\text{C}$ . Some type (b) inclusions homogenized only between  $+500^{\circ}$  and  $+550^{\circ}\text{C}$  (Figure 32, A-495-176E). The majority of type (b) inclusions did not homogenize at all even at these high temperatures. Obviously these  $T_{\text{H}}$  cannot be considered as an entrapment temperature of this quartz crystal because, if the present late-stage quartz had been formed at such high temperatures, this certainly should have shown up in other mineralogical and petrological evidence. The most obvious interpretation for these abnormal  $T_{\text{H}}$  is that the gas bubbles were a heterogeneous entrapment product due to exsolution of gas during the mixing of brines of different salinities and gas compositions. This interpretation had already been proposed for sample A-495-168. Therefore the only homogenization temperature representing homogeneous entrapment is the one from type (a) inclusion ( $+133.4^{\circ}\text{C}$ ).

#### c.2 Quartz crystal A-495-176F

##### Description of inclusions

This idiomorphic quartz was chosen because its fluid inclusion content was fairly representative of inclusions connected with the late-stage quartz of sample A-495-176. This crystal showed only type (a) inclusions. With the exception of 3 inclusions which contained a solid phase (fibrous or amorphous mineral), all inclusions were of the liquid + vapour-phase type. The shapes of inclusions varied from regular (this includes a "negative" crystal) to elongated, and randomly shaped. The average size used for this study varied between 20 to  $30\mu$ .

##### Microthermometry

The frequency histogram of  $T_{\text{H}}$  of these inclusions is shown in Figure 32, A-495-176F. The temperatures range from  $+120^{\circ}$  to  $+155^{\circ}\text{C}$  with frequency maximum of  $+130^{\circ}\text{C}$ . This value of  $130^{\circ}\text{C}$  seems to be a recurrent

temperature, and therefore could reasonably be considered the minimum temperature of formation of the late-stage quartz.

d) Crushing tests of sample A-495-176

The crushing test with the Chaix-Meca stage showed a "very strong" gas release from every quartz grain containing type (b) (gas-rich) inclusions. Approximately 20% of the released gases reacted with  $\text{Ba(OH)}_2$  to form  $\text{Ba(CO)}_3$ . The remaining 80% dissolved very slowly in  $\text{Ba(OH)}_2$  solution. The opposite occurred in kerosene: the majority of bubbles dissolved very rapidly while a few did not dissolve at all. Measurements of the rate of dissolution in kerosene indicated that a bubble with a diameter of, for instance,  $60\mu$  dissolved in less than 15 seconds, whereas another bubble of only  $15\mu$  was only partially dissolved after 3 minutes. These differences in gas solubility support the results of the precipitation reactions with  $\text{Ba(OH)}_2$  suggesting  $\text{CO}_2$  as a minor component and hydrocarbons (probably methane) as a major component of the combined gas-phase. This result agrees with the relatively minor amount of liquid  $\text{CH}_4\text{-CO}_2$  formed during the freezing test (A-495-176B and A-495-176E), in spite of the evidence of major amounts of gas released during the crushing test. Figure 33 shows the curve of solubility in kerosene of five gas-bubbles. They indicate a fairly homogeneous mixture with hydrocarbons probably the predominant component.

When quartz grains containing mainly type (a), liquid-rich, inclusions were crushed, the gas-release was only "weak" to "very weak". The behaviour of these gas-bubbles in  $\text{Ba(OH)}_2$  solution and kerosene was similar. The compressibility of gases released from gas-rich inclusions was measured in the microbarometric stage. Their data are presented in Figure 34. The gases show high compressibility up to  $20 \text{ kg/cm}^2$ . Beyond this pressure the rate changes. At  $50 \text{ kg/cm}^2$  the compressibility rapidly decreased. Compression up to  $150 \text{ kg/cm}^2$  did not produce any evidence of liquid condensation. This is a further indication of  $\text{CH}_4$ -rich gas-phase in the inclusions, for, if carbon dioxide had been a major component, it should have condensed as liquid  $\text{CO}_2$  at pressures above  $80 \text{ kg/cm}^2$  and  $20^\circ\text{C}$  (Figure 16.). The compression test, although

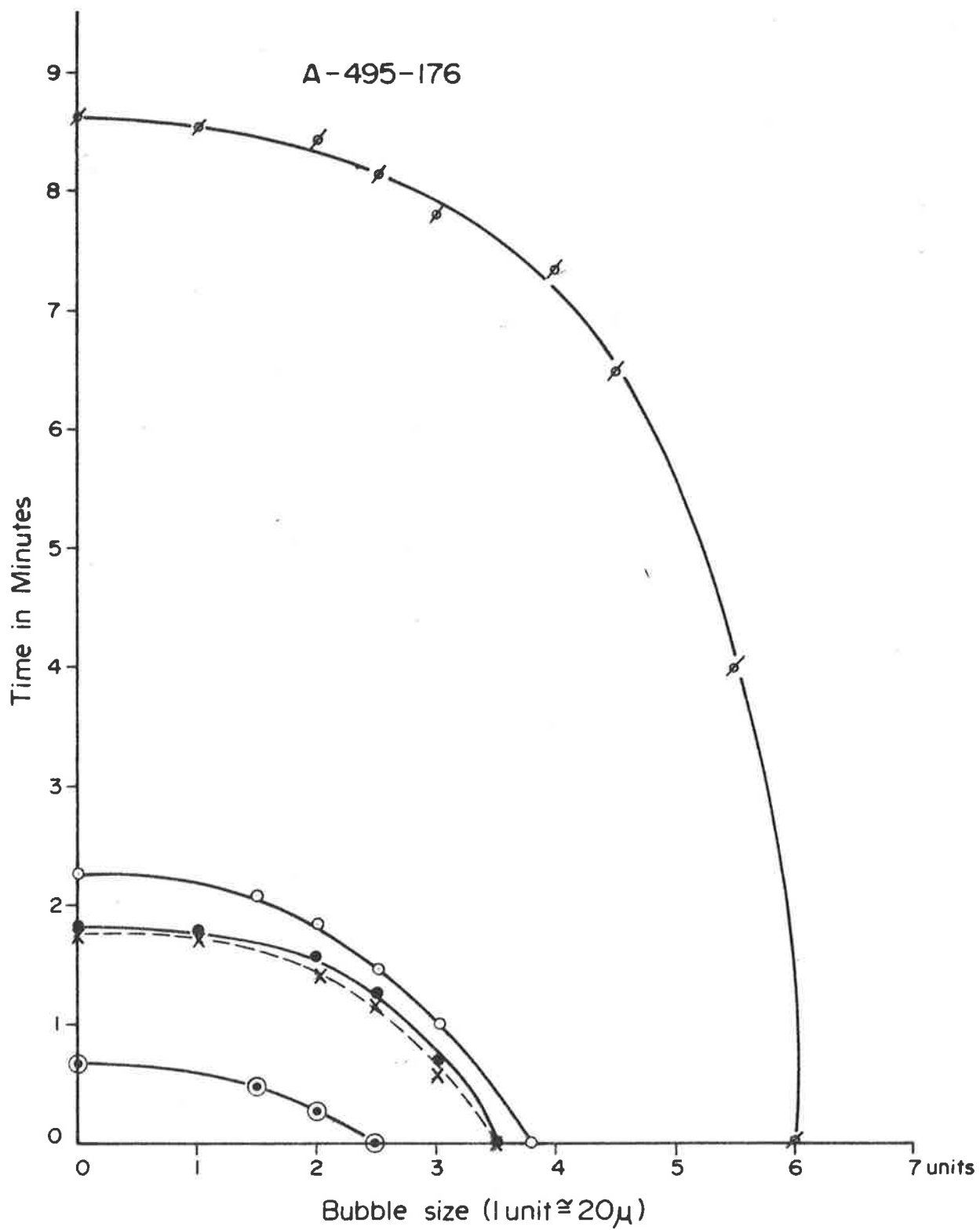


Figure 33: Solubility in kerosene of gas bubbles released by crushing of a quartz grain with type (b) vapour-rich inclusions.

carried out below the critical T of  $\text{CO}_2$  ( $31^\circ\text{C}$ ) failed to produce a liquid "gas" phase.

e) Scanning Electron Microscopy

The SEM and the EDAX of the early-stage quartz indicated the presence of chlorides of Ca, Na and K as residues of evaporation. Sericite and kaolinite (?) (Plate IX, photo 1) were very common and seemed to have been trapped as extraneous solid phases. In the late-stage quartz, similar evaporation residues were found. In addition the following minerals were identified: sylvite (Plate X, photo 2),  $\text{FeSO}_4$  hydrate (?) (Plate X, photo 1), and  $\text{CaCO}_3$  (Plate XI, photo 1). Minerals like those in Plate IX, photos 2, mineral (b), and photo 3, and Plate X, photo 3, are not easily identifiable, notwithstanding chemical information which does not conform to a unique mineral composition. The inclusion on Plate XI, photo 2, seems to contain dolomites and ankerites.

f) General conclusions for Sample A-495-176

In this sample, fluid inclusions from two chronologically different types of quartz (early- and late-stage) have been studied. In both quartz stages inclusions could be separated into two groups: Type (a) (liquid-rich) and type (b) (gas-rich) inclusions.

The freezing test of early-stage quartz indicated inclusions with brines of salinities varying from 13.5 to 28.0 wt.%  $\text{CaCl}_2$  equivalent. A difference in salinity found in different clusters of inclusions points to the mixing of fluids (Figure 30). Some inclusions present strong metastability (phase retardation) and others partial freezing phenomena. Salinities in late-stage quartz proved to be within the same range as the early-stage quartz.

The SEM and EDAX confirmed the presence not only of  $\text{CaCl}_2$  but of carbonates,  $\text{FeSO}_4$  hydrate,  $\text{NaCl}$ ,  $\text{KCl}$ , and possibly Al, Mg, and Ba chlorides as well. Apart from these salts, sericite, chlorite and kaolinite occurred in fluid inclusion cavities.

The microbarometric crushing and the crushing under different liquids pointed to a "very strong" gas-release from type (b) inclusions and a "weak" gas-release from type (a) inclusions. In both cases the amount of  $\text{CH}_4$



seemed to be larger than the  $\text{CO}_2$ .

The heating test indicated that  $T_H$  of type (b) inclusions were due to inhomogeneous entrapment. The  $T_H$  from type (a) inclusions indicated a change of temperature in time from  $>150^\circ\text{C}$  of the early-stage quartz to  $<130^\circ\text{C}$  for the late-stage quartz.

#### II.2.2.1.2 Sample A-495-174

(D.H.Na77; 61.70m)

##### Description of inclusions

This sample presented mainly two-phase type (a) inclusions similar to those studied in sample A-495-176. The inclusions are from quartz collected in small veins and vugs of a quartz-chlorite breccia. The sample material could be separated into early- and late-stage (idiomorphic) origin. Inclusions from both generation of quartz were similar in appearance. They are fairly regular in shape (rounded or negative crystals), they rarely contain daughter minerals, and they average 5 to  $8\mu$  in size. Two early-stage and one late-stage quartz were studied.

##### Microthermometry

Because of their small size, the homogenization was difficult to observe in some instances. Nevertheless, the histograms of distribution of  $T_H$  show a marked difference in temperatures between early- and late-stage quartz. In the latter, (Figure 35, A-495-174A),  $T_H$  values are concentrated between  $75.0$  and  $95.5^\circ\text{C}$ . At  $120^\circ\text{C}$  all inclusions had homogenized into a liquid-phase.

In the early-stage quartz (Figure 35, A-495-174B and A-495-174C), the  $T_H$  values are mainly between  $110$  and  $160^\circ\text{C}$ , similar to other samples previously mentioned. Because no changes seem to have occurred after entrapment, the spread in values may have been the result of different entrapment temperatures, or possibly be due to retardation of phase changes, apparently a common phenomenon for very small inclusions. Similar  $T_H$  ranges were observed in the samples A-495-172F and A-495-176D. The sample A-495-174C of early quartz shows a distinct frequency maximum near  $130^\circ\text{C}$ , the temperature of which coincides with that of the late quartz of A-495-176. However, the difference

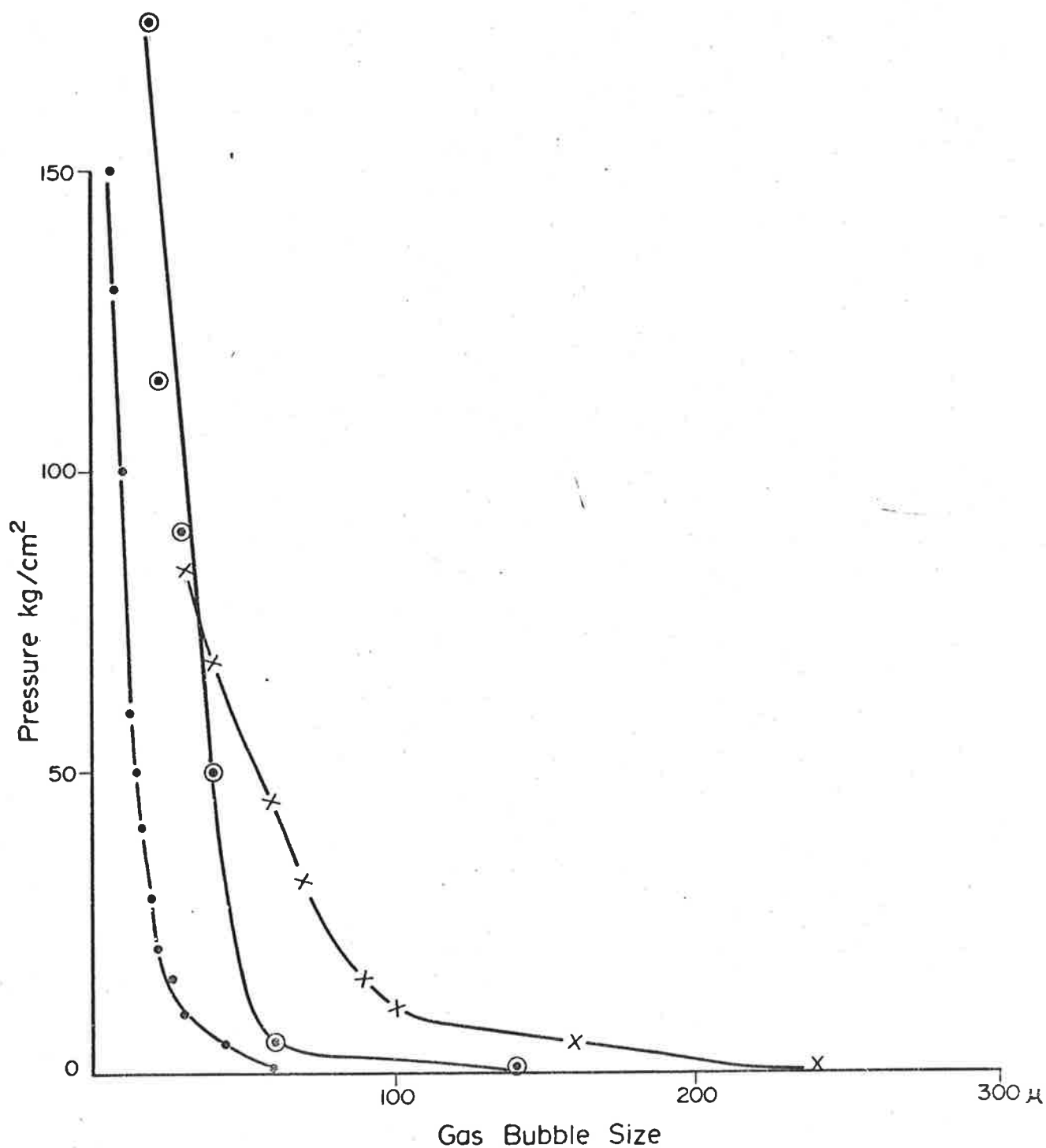


Figure 34: Compressibility curves of three gas bubbles released upon crushing a quartz grain with type (b) inclusions from sample A-495-176. The sharp rate change points to supracritical "liquefaction" of the gas. Compression at 20°C.

in  $T_H$  between the two quartz generations within this sample still exists and points to a decrease in temperature between the time of formation of early- and late-stage quartz.

#### II.2.2.1.3 Sample A-495-178

(D.H.Na77; 104.4m)

##### Description of inclusions

This sample is from a quartz-chlorite breccia. Because the early-stage quartz could not be physically separated from the late-stage quartz, the fluid inclusions study was restricted to the latter. Liquid-vapour inclusions of type (a) were clustered in the central part of the crystal, whereas pure liquid-filled inclusions were generally situated near its perimeter. There are very few gas-rich inclusions. The average size of inclusions is  $10\mu$ , but some are as large as  $35-40\mu$ . Only a few inclusions presented shapes that could have been the result of "necking down".

##### Microthermometry

At  $200^{\circ}\text{C}$  the majority of inclusions had become homogeneous. Figure 27, A-495-178, indicates the frequency histogram of  $T_H$  of the inclusions. The diagram shows two maxima:  $110^{\circ}\text{C}$  and  $130^{\circ}\text{C}$ . A  $T_H$  above  $140^{\circ}\text{C}$  might have been the result of post-entrapment changes. The presence of single-phase inclusions could indicate that the temperature of formation had dropped to  $70^{\circ}\text{C}$  towards the end of crystallization. Therefore, the bi-modal  $T_H$  distribution may also indicate entrapment during a temperature gradient.

#### II.2.2.1.4 Sample A-495-179

(D.H.Na77; 11.43m)

##### Description of inclusions

The fluid inclusions in this quartz differed from previous samples from drill-hole Na77, because this quartz was probably a product of metamorphogenic emplacement preceding the formation of hydrothermal quartz.

The inclusions can still be classified into type (a) and type (b), but their compositions are different from inclusions studied in the hydrothermal quartz. Type (a) inclusions (liquid-rich) were variable in shape and size.

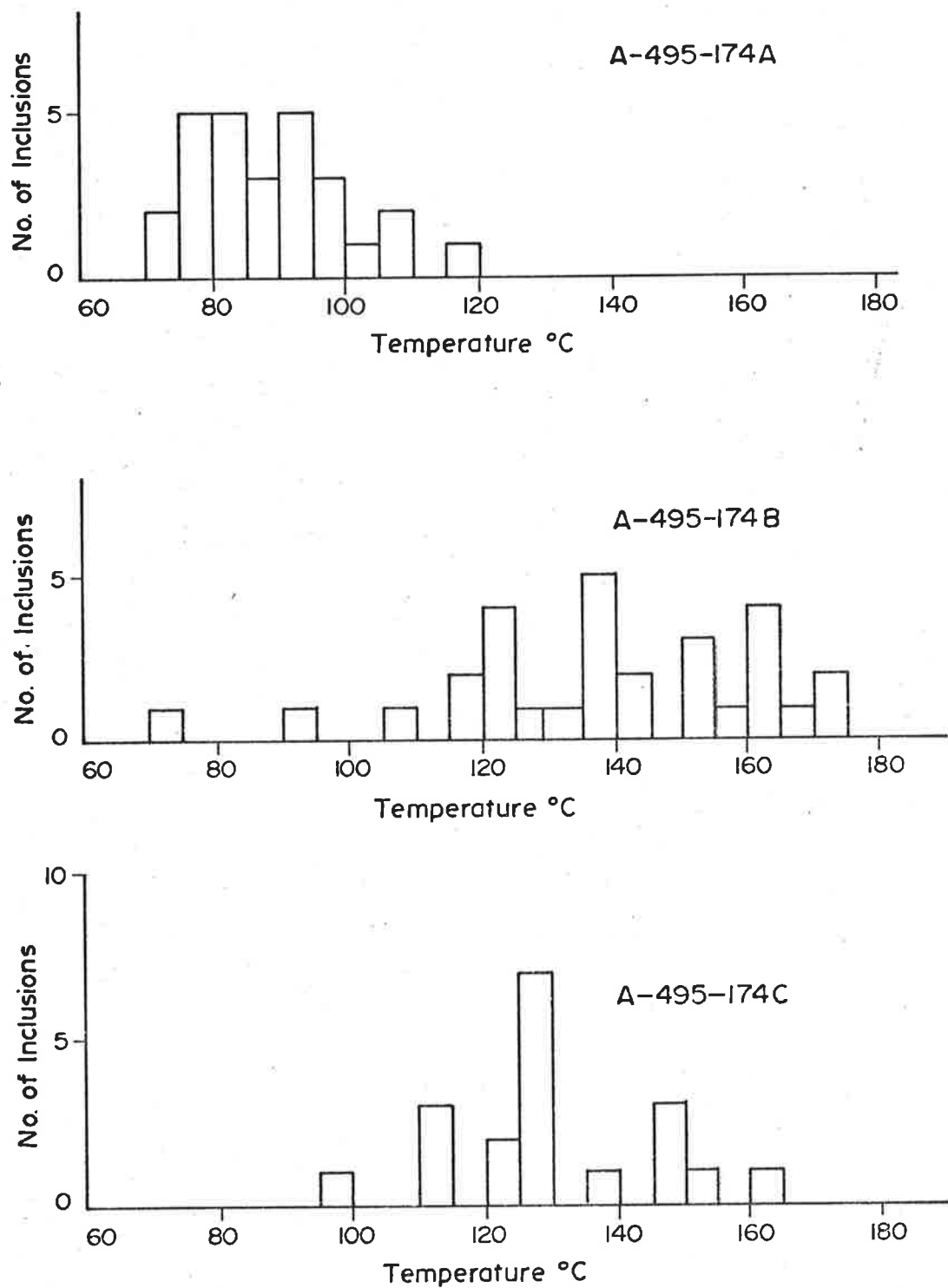


Figure 35: Sample A-495-174.  $T_H$  frequency histogrammes of fluid inclusions in late-stage (A-495-174A) and early-stage quartz (A-495-174B and C). Non-mineralized quartz of chlorite breccia and alteration zone.

Their average size ranges between 10 and 15 $\mu$ . A few type (a) inclusions present unusual size and daughter minerals content (Figure 36). These are very irregularly shaped and contained a set of at least three (sometimes up to seven) enclosed minerals apart from the liquid and vapour phases.

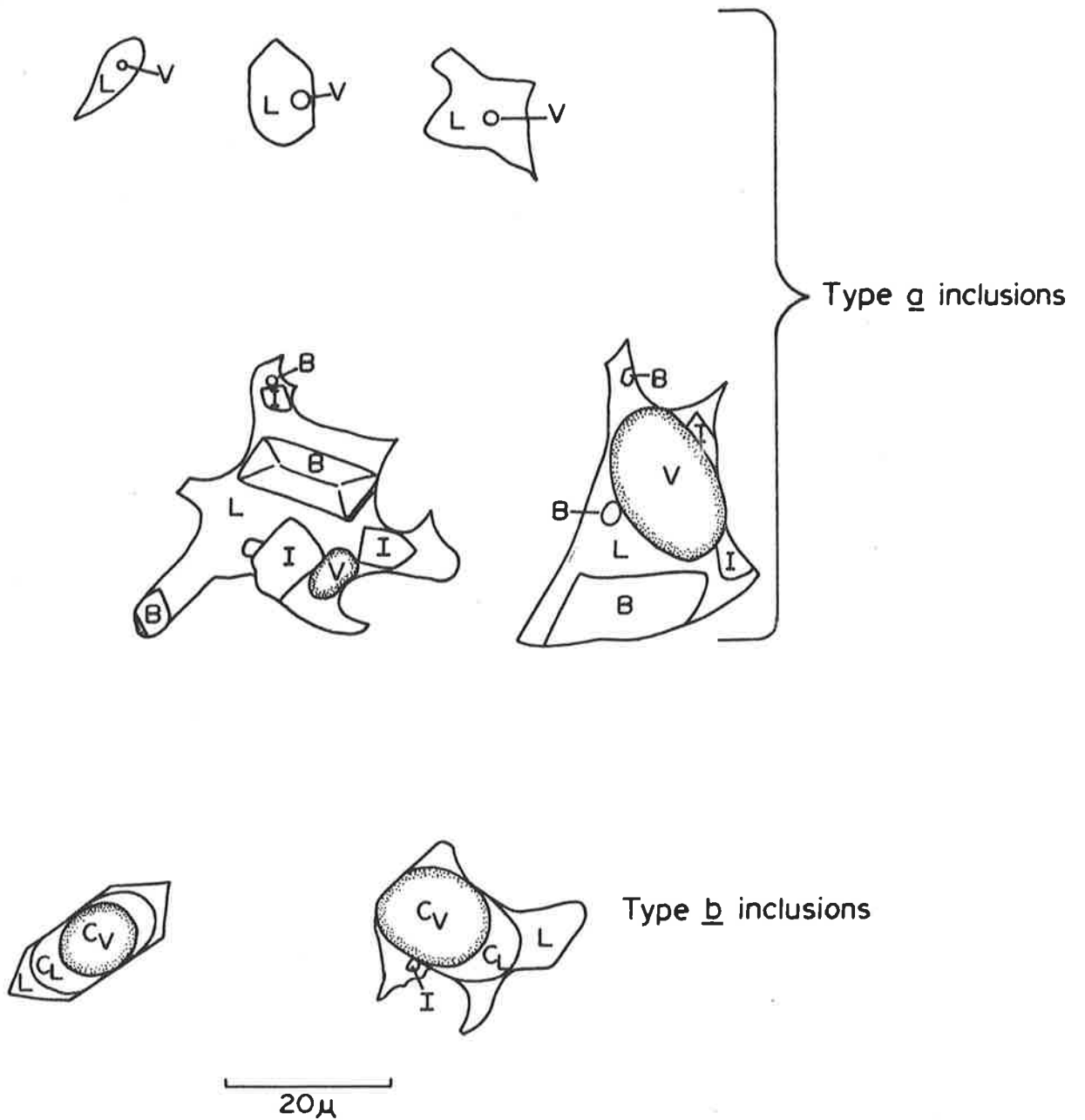
The daughter minerals include isotropic minerals (up to three phases) of NaCl, and/or KCl, and several anisotropic phases, the proper nature of which has not been established, but will be discussed under SEM studies. The size of these inclusions was in the order of 50 $\mu$ . Their particular shape, low frequency and the unusual volume of solid phases could indicate inhomogeneous entrapment or changes after nucleation of daughter minerals.

The type (b) inclusions presented the most characteristic differences from similar inclusions in hydrothermal quartz. They were much larger in size (20-30 $\mu$ ), were more numerous, and always had a CO<sub>2</sub> liquid-phase (Figure 36). Entrapped solids were rare and small.

Inclusions with liquid CO<sub>2</sub> and inclusions with daughter minerals seemed to be mutually exclusive. Even in a cluster containing both types of inclusions, CO<sub>2</sub>-rich inclusions very seldomly contained daughter minerals and vice versa. This feature is normally considered to be an indication of boiling but could also be due to exsolution.

#### Microthermometry

Cooling produced an increase in CO<sub>2</sub> liquid-phase in type (b) inclusions. At -53°C some type (a) inclusions started to freeze and at -100°C type (b) inclusions were also frozen. Upon warming to just below -55°C, the solid CO<sub>2</sub> suddenly melted in all type (b) inclusions, indicating almost pure CO<sub>2</sub> (Figure 37, T<sub>F</sub> (a)). In type (a) (two phase-liquid + gas) inclusions, the last ice melted at near -21°C (Figure 37, T<sub>F</sub> (b)), which indicates a salinity of 22 wt.% of CaCl<sub>2</sub> equivalent. The gas-rich inclusions formed clathrates which melted between +8.4 and +10.9°C (Figure 37, T<sub>F</sub> (c)). The salinity of the CO<sub>2</sub>-rich inclusions was not determined, because the formation of clathrates affects the salinity of the remaining solution. The CO<sub>2</sub>-rich phases homogenized into a gas-phase between 25.7 and 30.9°C with a frequency maximum of 28.5°C. This temperature could indicate CO<sub>2</sub> pressures between 62 and



- B - birefringent mineral
- C<sub>L</sub> - Carbon dioxide-rich liquid
- C<sub>V</sub> - Carbon dioxide + hydrocarbon vapour
- I - Isotropic mineral
- L - Liquid
- V - Vapour

Figure 36: Types of fluid inclusions present in quartz (metamorphogenic) from sample A-495-179, at an observation temperature of 20°C.

72 kg/cm<sup>2</sup> at that temperature, or equal pressure but varying amounts of CH<sub>4</sub>. The T<sub>H</sub> histogram shows major frequency of type (a) inclusions homogenizing at 140 and 160°C (Figure 37, T<sub>H</sub>). However, if the liquid-rich portion of these inclusions were the result of splitting from a former CO<sub>2</sub>-rich brine, these temperatures would indicate only the temperature of re-sealing of an inclusion after separation of the CO<sub>2</sub>-rich phase. Inclusions rich in daughter minerals decrepitated before dissolution could be completed, which is possibly a further indication of inhomogeneous entrapment. Type (b) inclusions homogenized into gas-phase, but the exact T<sub>H</sub> of each inclusion was difficult to establish because of a decrease in visibility at higher temperatures. It was only possible to see that at 370°C all observable type (b) inclusions had become homogeneous. A further limitation on the reliability of this temperature was the observation that in some inclusions the bubble size had increased after the heating cycle, indicating leakage. In only one inclusion could a temperature of 366.5°C be considered as a reliable observation. It is doubtful whether the inclusions rich in daughter minerals could be made to homogenize at all. One became almost homogeneous at 347°C but decrepitated at 417°C. In all cases the vapour-phase disappeared before dissolution of daughter minerals.

#### Crushing test

In agreement with the microthermometric data the crushing test indicated a "very strong" gas release from type (b) inclusions. The gas bubbles consisted largely of CO<sub>2</sub> and probably some CH<sub>4</sub>, judging from the Ba(OH)<sub>2</sub> and kerosene solubility test. The high density of the CO<sub>2</sub>-rich phase (0.65 grammes CO<sub>2</sub>/Cm<sup>3</sup>) at 31°C postulates a minimum pressure of 450kg/cm<sup>2</sup> at 150°C of the brine-rich inclusions and a pressure of 1.4 Kb at the homogenization temperature of the CO<sub>2</sub>-rich inclusions. These pressures are considerably higher than the pressure domain of the hydrothermal quartz data discussed so far.

#### Scanning Electron Microscopy

The SEM showed a few good images of some unusual "daughter minerals". Chlorides are abundant: NaCl, CaCl<sub>2</sub> (Plate XII, photo 1, mineral b; and Plate XIII, photo 1) and KCl is common; FeCl<sub>2</sub>·2H<sub>2</sub>O (Plate XII, photo 2) a

most interesting constituent and is found for the first time among the samples of Nabarlek. Next to chlorides, carbonates were the most frequent daughter minerals: viz. ankerite (Plate XIII, photo 2, mineral b), calcite (Plate XIV, photo 2), and dolomite (Plate XIV, photo 3). A calcium-rich mineral from Plate XIII, photo 2, mineral c, and Plate XIV, photo 1, mineral a, is probably a Ca-silicate because the EDAX peaks of Si are much stronger than the normal background present when measuring carbonates (e.g. compare with Plate XIV, photos 2 and 3). The most unusual mineral found in an inclusion cavity of this sample is presented in Plate XII, photo 1, mineral a and c. The mineral is probably a sulphate of Zn, Na, Fe, and Cu, but could also be a complex sulphide of the same metallic ions.

A CaAl-silicate (anorthite?) was found in one inclusion (Plate XI, photo 3). Apart from these minerals, other daughter minerals such as muscovite (Plate XIII, photo 2, mineral a) haematite and a possible zeolite (Plate XIV, photo 1, mineral b) have been found.

#### Conclusions

The fluid inclusions present in quartz of sample A-495-179 are quite distinct from those found in hydrothermal vein quartz associated with uranium mineralization. The differences include: 1) higher CO<sub>2</sub> content; 2) more complex (NaCl-rich) brines; 3) higher homogenization temperatures; 4) higher total pressures.

This more complex aspect could reflect a metamorphogenic origin for this quartz, with a slight overprint by hydrothermal solutions.

#### II.2.2.2 Sample A-495-157

(D.H.Na55, 89.00m)

#### Description of inclusions

The inclusions studied were from quartz in a 2-5mm thick vein cutting throughout an altered dolerite. The vein itself is probably the product of the hydrothermal process which caused the alteration of the dolerite. The quartz has numerous fluid inclusions and solid inclusions of chlorite. The fluid inclusions are rather small in size - 3 to 10 $\mu$ , occasionally reaching



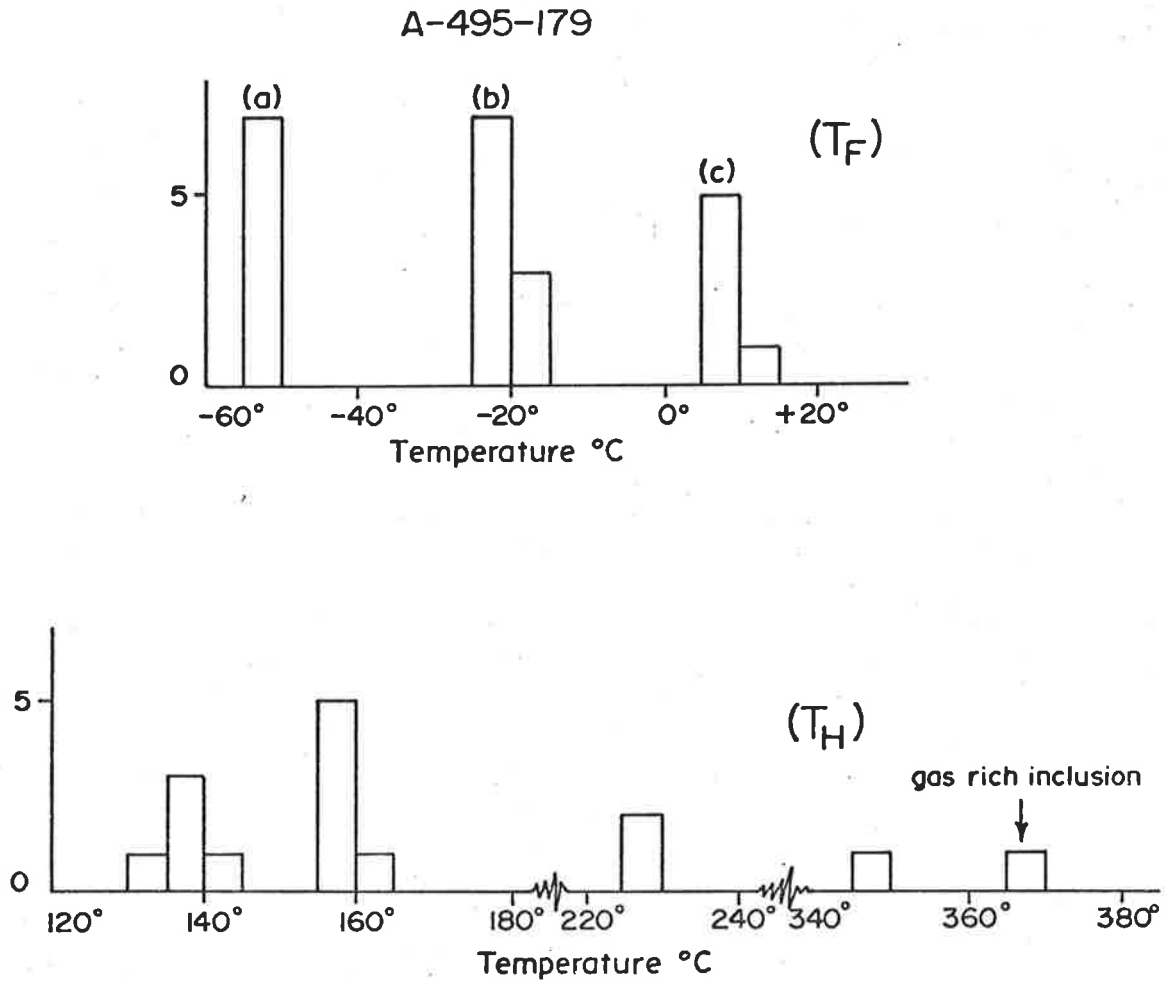


Figure 37: Sample A-495-179. T<sub>F</sub> and T<sub>H</sub> frequency histograms of fluid inclusions in metamorphogenic quartz.

T<sub>F</sub>(a) refers to melting of CO<sub>2</sub> solid;

(b) refers to melting of last ice;

(c) refers to disappearance of CO<sub>2</sub>-clathrates.

15 $\mu$  or more. Their shapes are irregular with a tendency towards elongated forms. Indications of "necking down" are apparent in some of the larger inclusions. Some inclusions were situated along fractures but the majority are randomly distributed in the crystal or occurred along zones of growth. However, no characteristic distinction separated the two. The majority of inclusions are bi-phased (liquid + gas) a few are single-phased (liquid), others are tri-phased (liquid + gas + solid). The liquid/gas ratios are fairly regular. The gas-bubbles represent  $\sim 2\%$  by volume of inclusions. The most common daughter mineral is a birefringent fibrous mineral. Less frequently is an isotropic cubic crystal. The latter is probably NaCl while the former has the aspect of dawsonite.

#### Microthermometry

Upon cooling, the formation of a double ring condensed vapour (CO<sub>2</sub>) within the vapour phase was observed in only one inclusion, and the nucleation of NaCl(?) in a few others, at around  $-40^{\circ}\text{C}$ . The majority of inclusions were frozen at  $-110^{\circ}\text{C}$ , the sample having been cooled down to  $-160^{\circ}\text{C}$ . A few inclusions did not freeze at all and one, which had a  $T_F$  of  $-58^{\circ}\text{C}$ , was only partially frozen. The first melting started at around  $-80^{\circ}\text{C}$ . A few inclusions formed two solid phases on freezing: a rounded, isotropic, low-relief solid which is probably ice, and a prismatic, birefringent mineral with strong relief which could be a salt hydrate. Unfortunately, the melting point of both solids was not observable. However, their behaviour was similar to that of many inclusions from the quartz of the ore zone (described above), apart from featuring the lowest  $T_F$  found so far. In fact four inclusions presented  $T_F$ 's even lower than the eutectic point of the system CaCl<sub>2</sub>-NaCl-H<sub>2</sub>O ( $-49.8^{\circ}\text{C}$ ) indicating the presence of other ions (Mg<sup>2+</sup>, Al<sup>3+</sup>, Fe<sup>2+</sup>). The distribution of  $T_F$  of all inclusions is presented in Figure 38 which indicates again a large range of freezing temperatures. The corresponding salinities range from 25 to  $>30$  wt.% of CaCl<sub>2</sub> (equivalent).

The heating test indicated a multi-modal frequency distribution. The temperatures were in the range of  $100^{\circ}$  to  $160^{\circ}$  (Figure 38,  $T_H$ ).

The  $T_F/T_H$  diagram points to an inverse relationship which contravenes the normal tendency for the solubility of salts to increase with increasing temperature (Figure 38,  $T_F/T_H$ ). This unusual relationship can be explained by the high heat of solution of  $\text{CaCl}_2$ , which, upon entering in solution, drops the temperature of the brine. This is not a very likely explanation as  $\text{CaCl}_2$  is not known from any geological environment. Another reason for the inverse relationship is the fact that  $\text{CaCl}_2$ -rich brines can only be generated in a cool environment, any increase in temperature will immediately result in dissolution of the much more readily available  $\text{NaCl}$ . The problem of generation of  $\text{CaCl}_2$ -rich brines will be discussed later.

#### Crushing test

The crushing of several quartz grains always released "weak" to "very weak" amounts of gas. This result is in agreement with the absence of gas-rich inclusions. The gas released was mainly  $\text{CO}_2$ .

#### Scanning electron microscopy

An exhaustive investigation of quartz grains mainly revealed empty inclusion cavities. Only one cavity showed minerals which, according to EDAX analysis, were probably chlorite and Ca+K chloride.

#### II.2.2.3.1 Sample A-495-113

(D.H.Nal, 59.80m)

#### Description of inclusions

In the main pitchblende orebody at Nabarlek, no samples with quartz suitable for fluid inclusion studies have been found. All material discussed in the first part of this chapter came from ore zones that are peripheral to the main body. This sample was collected from below the main orebody and is situated very close to it. The fluid inclusion host is a hydrothermal quartz with inclusions of various sizes (<5 to 100 $\mu$ ) occurring in a large variety of shapes. The classification into type (a) and type (b) inclusions used for other specimens is again applicable. The occurrence of fibrous and amorphous daughter minerals was fairly common, while isotropic cubic minerals and orange-coloured flakes were only occasionally present.

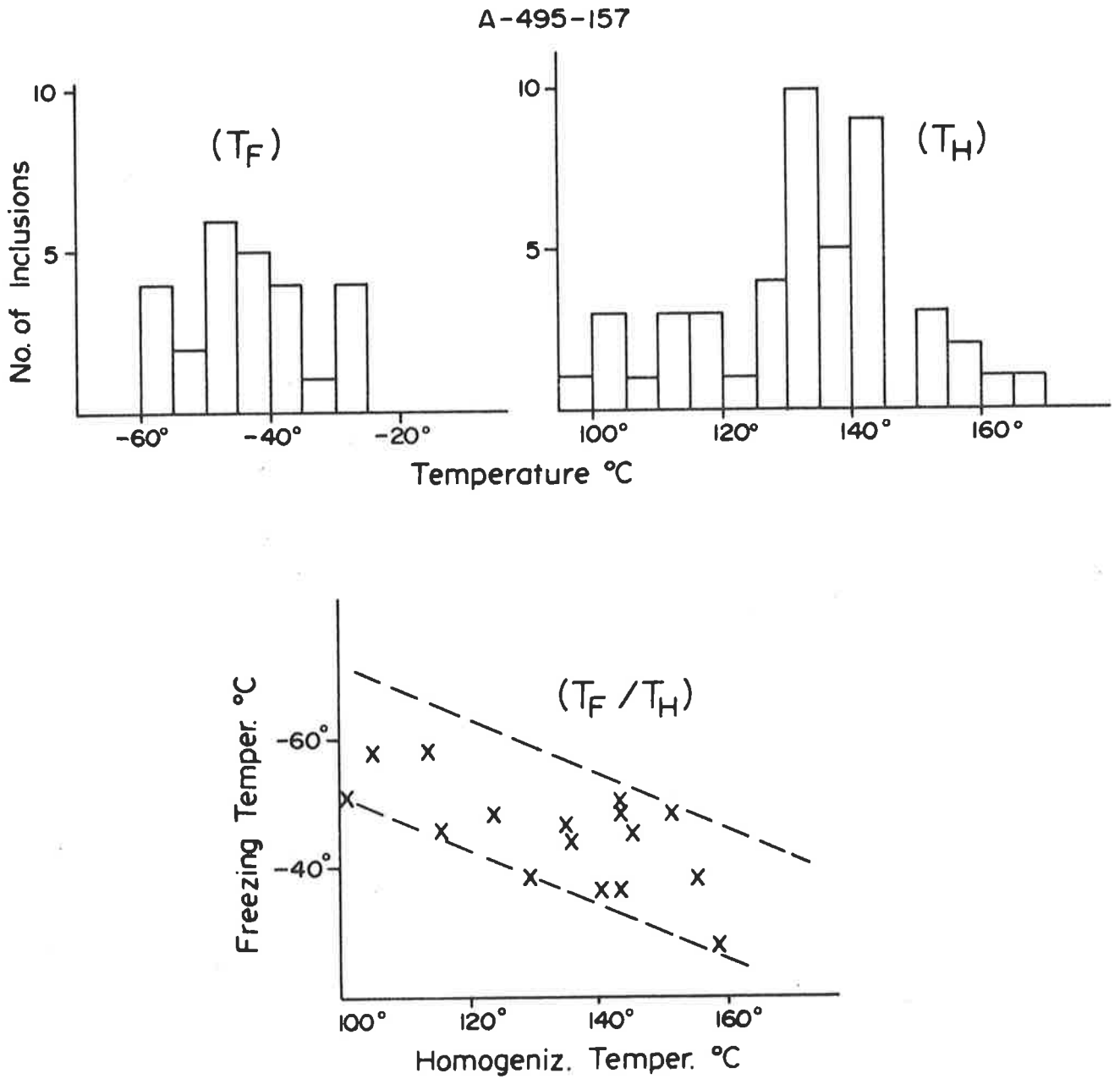
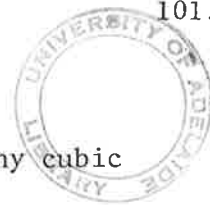


Figure 38: Sample A-495-157.  $T_F$  and  $T_H$  frequency histogrammes of fluid inclusions in quartz and the relation  $T_F/T_H$ . Quartz from vein cutting altered dolerite dyke.



### Microthermometry

The freezing experiment showed the nucleation of tiny cubic daughter minerals in some inclusions at  $\sim +3^{\circ}\text{C}$ . The formation of gas clathrates expected for many type (b) inclusions did not occur. Instead, some inclusions formed greenish cubic and prismatic salt hydrates which in two cases were observed to melt at  $-8^{\circ}$  and  $+4^{\circ}\text{C}$ . The frequency distribution of freezing temperatures is shown in Figure 39, ( $T_F$ ). This distribution is clearly bimodal, suggesting the presence of two different fluids. The salinities fall in the following groups:

- 1)  $T_F$  values  $-7^{\circ}$  to  $-21.5^{\circ}\text{C}$  (11.5 to 21.5 wt.%  $\text{CaCl}_2$  equivalent).
- 2)  $T_F$  values between  $-41.0^{\circ}$  to  $-46^{\circ}\text{C}$  (28.5 to 29.5 wt.%  $\text{CaCl}_2$  equivalent) and
- 3) inclusions which showed salt hydrates (presumably  $\text{CaCl}_2 \cdot 6\text{H}_2\text{O}$ ) which melted at  $-8^{\circ}\text{C}$  and  $+4^{\circ}\text{C}$  respectively. In theory this would correspond to a solution with 36 and 38 wt.%  $\text{CaCl}_2$  respectively if equilibrium conditions existed. However, as the melting temperatures of the last ice were found to be  $-34.7^{\circ}$  and  $-30.5^{\circ}\text{C}$  respectively, and such would correspond to a salinity of 32 and 33 wt.%  $\text{CaCl}_2$  respectively, a stable  $\text{CaCl}_2 \cdot 6\text{H}_2\text{O}$  phase could not exist. These temperatures do not correspond to the eutectic composition of the system  $\text{CaCl}_2$ - $\text{H}_2\text{O}$  but could correspond to a eutectic of  $\text{CaCl}_2$  plus some other compounds of lower solubility. However, even if  $-34.7^{\circ}$  and  $-30.5^{\circ}\text{C}$  did correspond to a multi-component eutectic, the amount of  $\text{CaCl}_2 \cdot 6\text{H}_2\text{O}$  still should have been in the order of 50-60 vol.% at a temperature below the eutectic. As this has not been observed the possibility of metastable persistence of salt hydrates still exists, as in sample A-495-172F.

The  $T_H$  histogram of the same inclusions indicated a multi-modal distribution in a wide range of temperatures (Figure 39,  $T_H$ ). In the present case, post-trapment changes seem unlikely to have been the cause of the wide

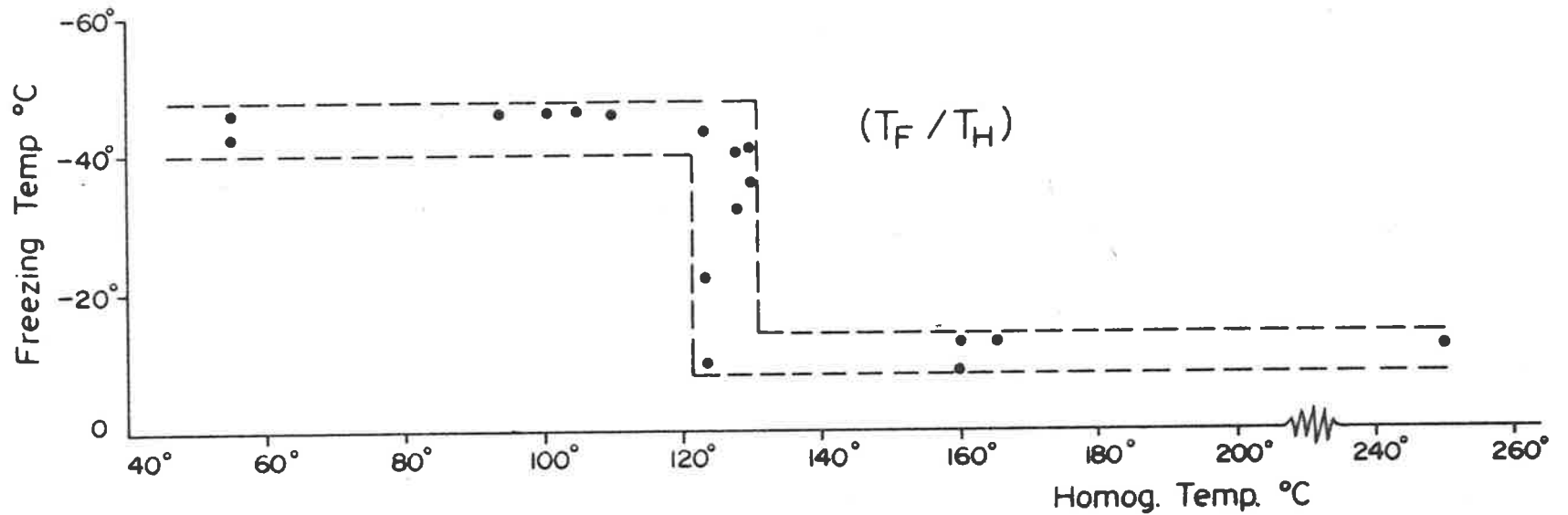
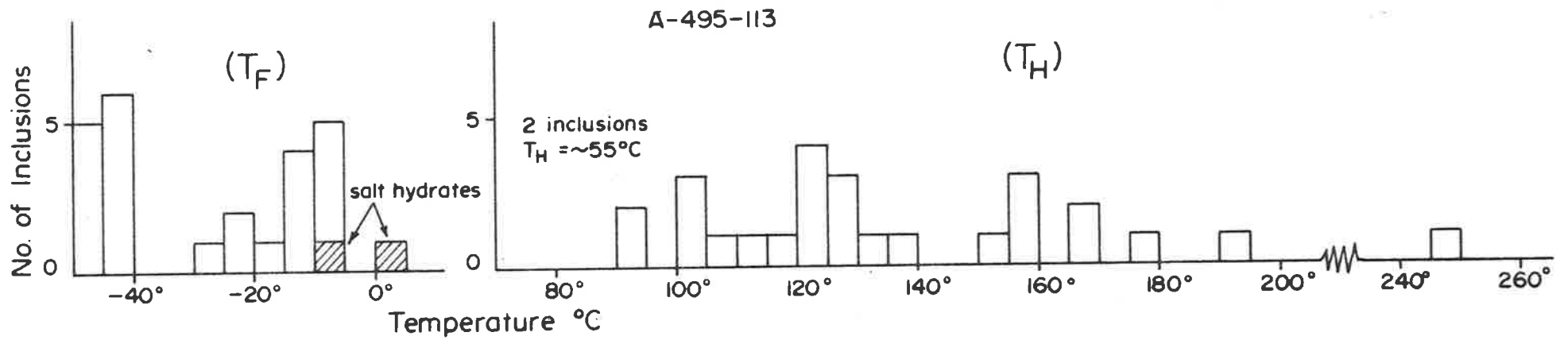


Figure 39: Sample A-495-113.  $T_F$  and  $T_H$  frequency histograms of fluid inclusions in quartz and the relation  $T_F/T_H$ . Quartz from veins spatially closely associated with the main Nabarlek orebody.

range of  $T_H$ . In relating the  $T_F$  to  $T_H$  of each inclusion, it becomes evident that those with a  $T_H$  higher than  $130^{\circ}\text{C}$  present lower salinities (high  $T_F$ ) and those with a  $T_H$  lower than  $120^{\circ}\text{C}$  present much higher salinities (low  $T_F$ ), contravening the normal tendency of salt solubility as a function of increasing temperatures (Figure 39,  $T_F/T_H$ ). This inverse relationship of  $T_F/T_H$  could be more readily explained by mixing of fluids. Furthermore, the  $T_F/T_H$  ratios indicate that this mixing of fluids probably occurred between  $120^{\circ}$  and  $130^{\circ}\text{C}$ . The heating of another cluster of inclusions (A-495-113B) indicates a narrower range of  $T_H$  but the range is still within the multi-modal distribution pattern (Figure 40, A.495-113B,  $T_H$ ).

#### Crushing tests

Quartz grains with inclusions similar to those studied in microthermometry, always showed on crushing, a "strong" to "very strong" gas release. Reactions with  $\text{Ba}(\text{OH})_2$  solution and solubility in kerosene indicate that  $\sim 25\%$  of the volume of the bubbles was  $\text{CO}_2$  and the remaining 75% were probably hydrocarbons. Timing of the rate of solubility of gases showed that bubbles as large as  $60\mu$  in diameter dissolved in kerosene in about one minute. Whereas another bubble, as small as  $5\text{-}10\mu$  in diameter, remained undissolved for five minutes. The conclusion is that bubbles of the first type contained hydrocarbons while the second type contained  $\text{CO}_2$ . Figure 41 shows the curve of solubility in kerosene of six bubbles of different sizes. These bubbles indicate a fairly homogeneous composition with hydrocarbons as the main component. The presence of a component with faster dissolution characteristics can be seen in the initial dissolution of the bubble with 3.5 units size.

The compressibility of two large bubbles was tested in the microbarometric stage (Figure 42). Even at a pressure of  $150\text{ kg/cm}^2$  the bubbles remained in a fluid phase. This is a further indication of the presence of hydrocarbons - probably methane - in fluid inclusions. If the gas bubbles had been  $\text{CO}_2$  vapour, they should have condensed into liquid  $\text{CO}_2$  under pressures higher than  $\sim 70\text{ kg/cm}^2$  at room temperature ( $22^{\circ}\text{C}$ ), (Figure 16).

In a further experiment with this stage, one quartz grain was crushed under  $100\text{ kg/cm}^2$  external hydrostatic pressure. No gas bubbles were

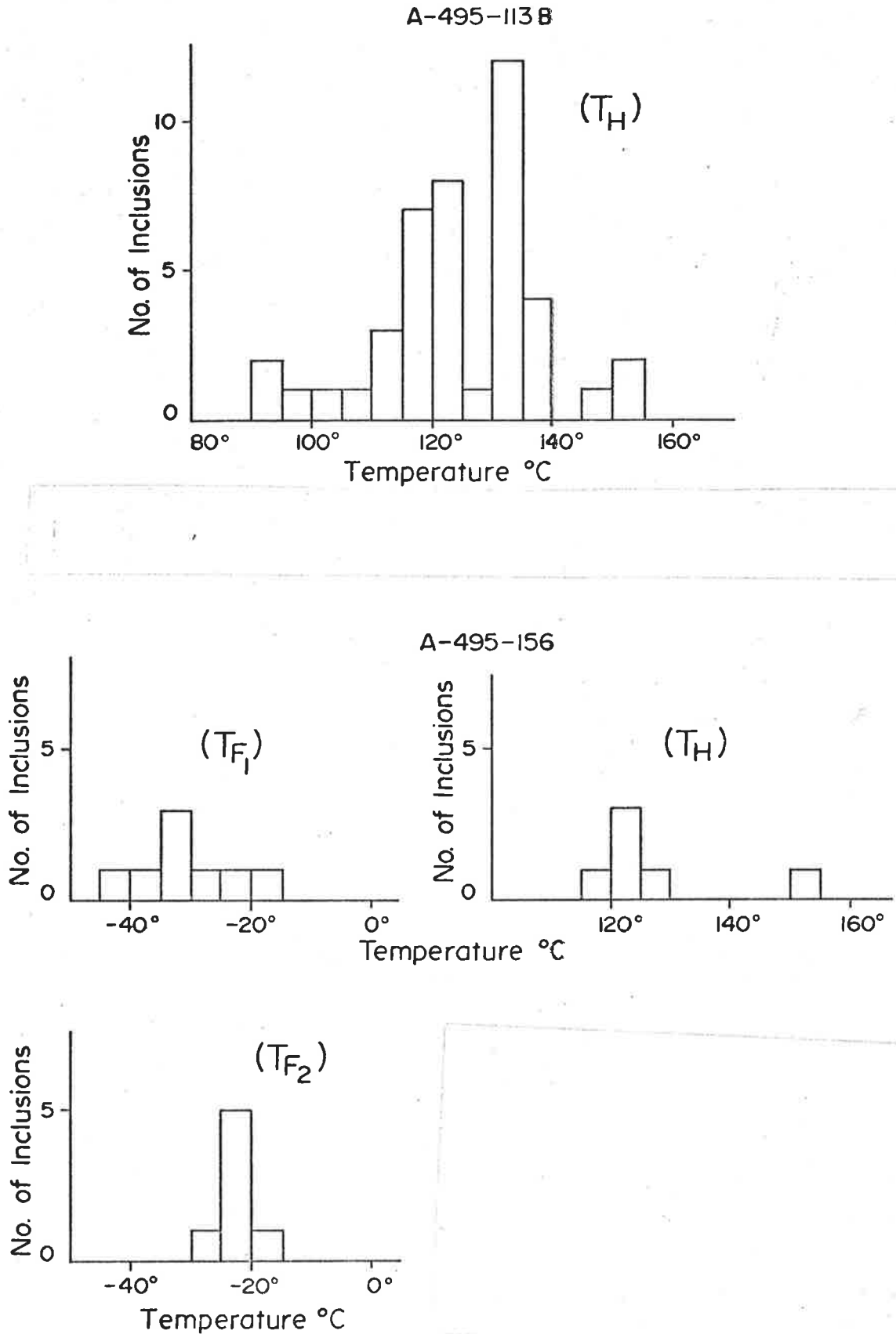


Figure 40: Frequency histogrammes of microthermometry of fluid inclusions in quartz from sample A-495-113B and in quartz from sample A-495-156. Both are from vein quartz spatially closely associated with the main Nabarlek orebody.  $T_{F1}$  refers to the last melting temperature of bi-phase inclusions,  $T_{F2}$  refers to the melting temperature of mono-phase inclusions.



observed. Releasing the pressure slowly, the first bubble became visible at a pressure of  $60 \text{ kg/cm}^2$ . This was probably the pressure present within the fluid inclusions of quartz from sample A-495-113 at room temperature ( $22^\circ\text{C}$ ).

The next experiment with the microbarometric stage involved cooling down to  $<-10^\circ\text{C}$  and the compression of bubbles under a hydraulic pressure of  $90 \text{ kg/cm}^2$ . Even then, no sign of condensation of liquid-phase in the bubbles was observed. These data point to the occurrence of more than 40 mol.% of  $\text{CH}_4$  in the mixed  $\text{CO}_2$ - $\text{CH}_4$  gas-phase (Figure 16), corroborating the results of crushing in kerosene and  $\text{Ba}(\text{OH})_2$  solution.

#### II.2.2.3.2 Sample A-495-156

(D.H.Na55; 83.90m)

##### Description of inclusions

As with sample A-495-113, this quartz-haematite-chlorite rock was collected below the main orebody, the only difference being that this sample was situated much closer to the dolerite sill. The quartz is fine-grained or presents a near-fibrous texture. It only contains type (a) inclusions. Because of this host grain size the inclusion's size is rather small. The larger ones ( $\sim 30\mu$ ) are very irregular in shape and contain haematite, chlorite and quartz (?) as a solid phase. The smaller ones are of a more regular or negative-crystal form. The inclusions are single-phase (liquid) or two-phase (liquid + gas). The single-phase inclusions had a very low relief. The distribution of inclusions in the quartz is fairly homogeneous with no trends or structural control. The density of distribution of the inclusions is much lower than in sample A-495-113.

##### Microthermometry

Freezing indicated different  $T_F$  values and some metastability. Three large ( $>50\mu$ ) inclusions, among many others, did not freeze even after being submitted to a temperature as low as  $-172^\circ\text{C}$  for 15 minutes. Inclusions with two phases presented a lower  $T_F$  than those with a single phase (Figure 40,  $T_{F1}$  (two phases) and  $T_{F2}$  (single phase)). An average  $T_F$  of  $-33.0^\circ\text{C}$  for  $T_{F1}$  and  $-22^\circ\text{C}$  for  $T_{F2}$  indicated salinities of approximately 26.5 and 22.0 wt.%

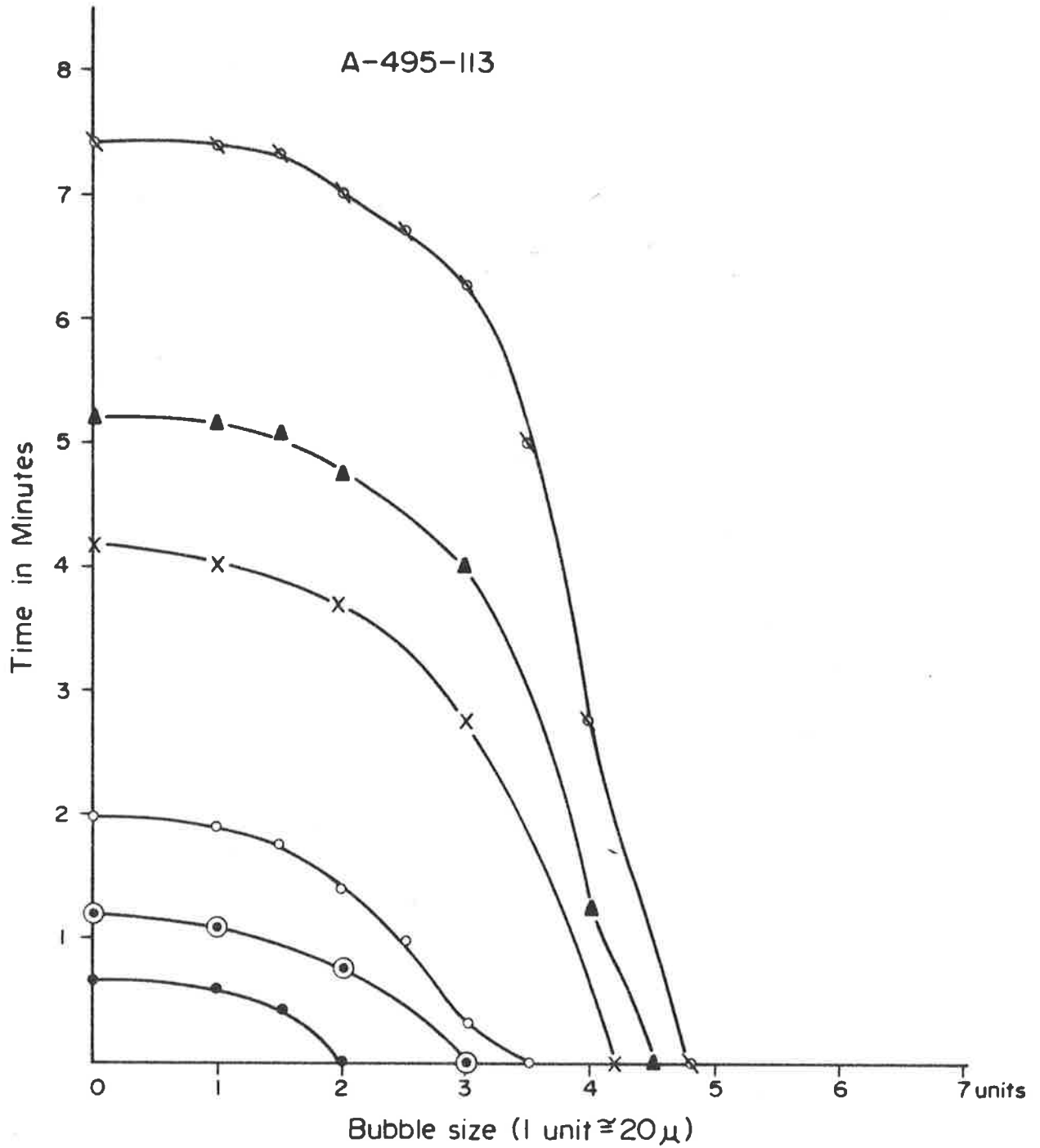


Figure 41: Solubility in kerosene of gas-bubbles released by crushing of quartz from a vein spatially closely related to the main Nabarlek orebody.

CaCl<sub>2</sub> equivalent respectively. The different salinities may be an indication of inclusions which had trapped fluids of different origin. However, because the number of measurements is relatively small, the inclusions cannot unambiguously be subdivided into two groups as has been the case in sample A-495-113.

T<sub>H</sub> of the few inclusions that have been measured clustered around +120°C (Figure 40, T<sub>H</sub>). One large one-phase inclusion nucleated a gas bubble upon freezing. The bubble disappeared again before +50°C, indicating that these inclusions were effectively trapped at a very low temperature (<70°C).

#### Crushing test

The inclusions released gas-bubbles of "weak" to "medium" intensity. This result is in agreement with the visual absence of gas-rich inclusions in the sample. The released gas bubbles showed the presence of CO<sub>2</sub>.

#### II.2.2.4.1 Sample A-495-144 (Quartz)

(D.H.Na23: 305.55m)

#### Description of inclusions

The quartz sample is derived from a core intersecting the contact between schists and a dolerite sill. The quartz contained only one-phase (liquid) inclusions. A fibrous birefringent mineral is present in some inclusions. They have low relief and are irregular in shape. In some cases they are situated in planes parallel to zones of growth of the quartz host. Grain sizes of this daughter mineral range from <1μ to 35μ.

#### Microthermometry and crushing

The fluids presented T<sub>F</sub> from -1.2 to -22.0°C and had a major frequency of values between -11.5 and -12°C which points to salinities of 15.0 to 16.0 wt.% of CaCl<sub>2</sub> equivalent (Figure 43). The inclusions did not nucleate a gas-phase upon freezing.

The crushing test was completely negative. No sign of gas release was noticed, which is in agreement with the apparent absence of gas-rich inclusions. The results point to fluids trapped at temperatures below +70°C.

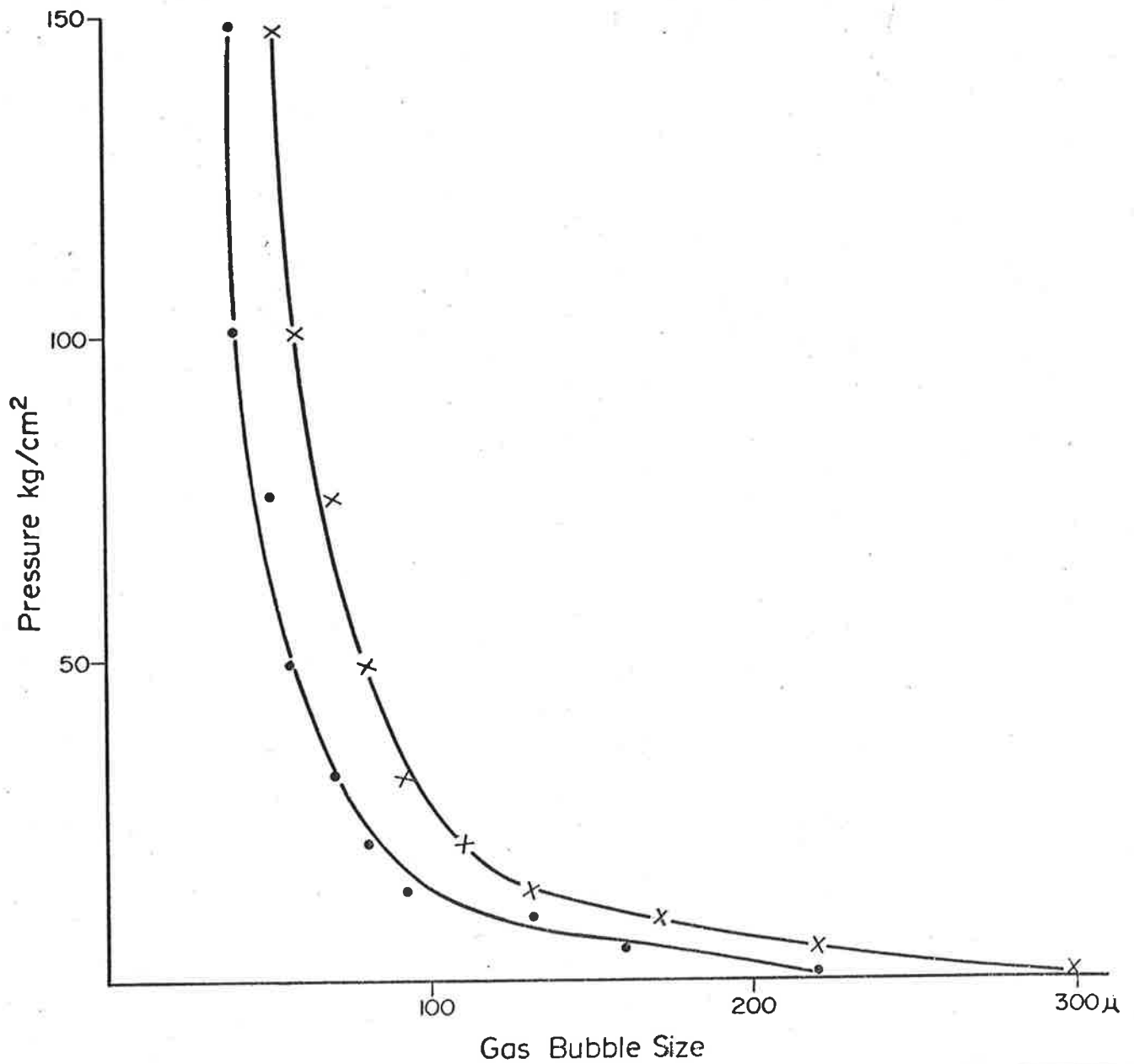


Figure 42: Compressibility of two gas bubbles at 22°C released upon crushing a quartz grain from sample A-495-113. Quartz from vein associated with main orebody at Nabarlek. Note the steep rate of pressure increase at a density which corresponds to that of a liquid (fluid CH<sub>4</sub>?).

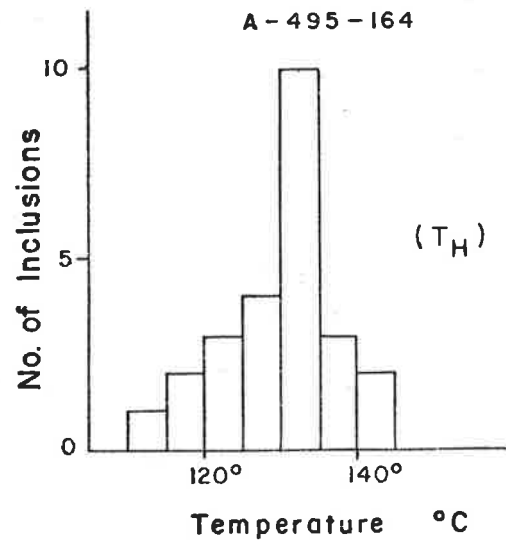
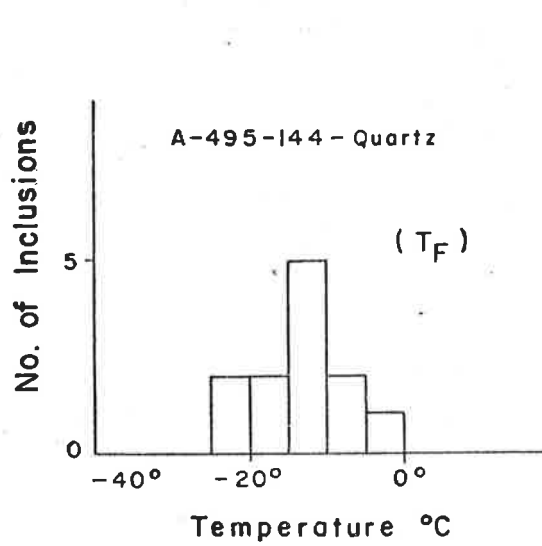
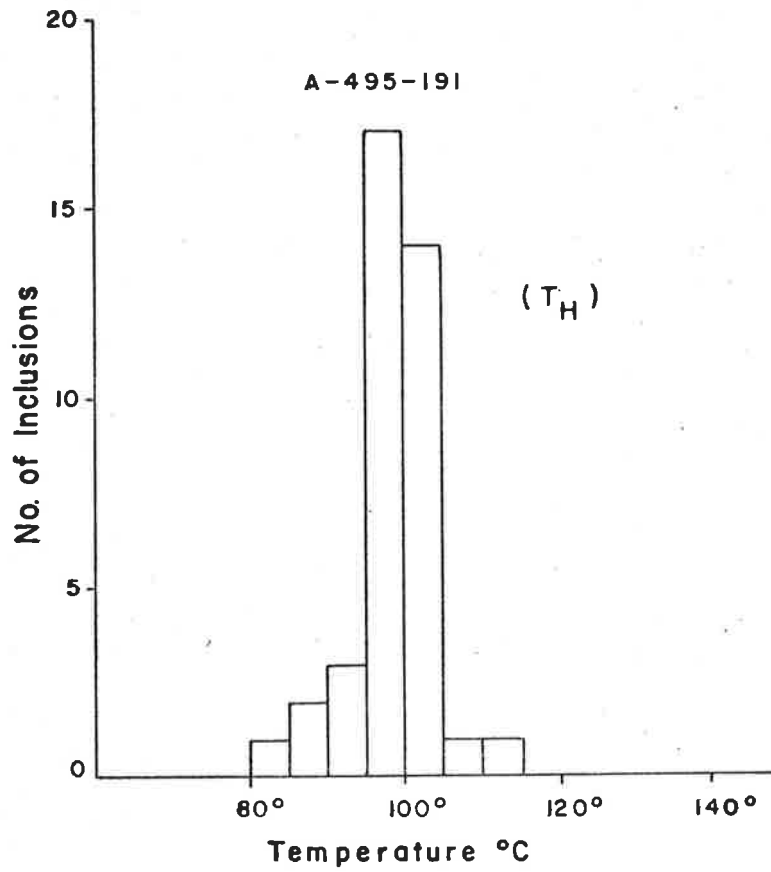


Figure 43: Frequency histogrammes of microthermometry of fluid inclusions in quartz from samples A-495-191, A-495-144, and A-495-164 (late-stage).

#### II.2.2.4.2 Sample A-495-191

(D.H.Na83: 93.30m)

This quartz vein came from quartz chlorite-xenolith 40m inside the dolerite, as measured from the dolerite intersection. All inclusions are markedly homogeneous in composition (liquid + gas) and in liquid/gas ratios (2-5% gas by volume). A few inclusions presented small elongated isotropic daughter minerals. No gas-rich inclusions were observed. The average fluid inclusion size is rather small, ranging from  $<1\mu$  to  $10\mu$ , and only a few measure more than  $10\mu$ . The distribution of the inclusions throughout the idiomorphic quartz crystal is not structurally controlled and they are probably of primary origin.

The heating test indicated a fairly precise  $T_H$  of  $\sim +100^\circ\text{C}$  (Figure 43). As was to be expected for these types of inclusions, the crushing test always indicated a "very weak" gas release.

#### II.2.2.5.1 Sample A-495-186

(D.H.Na83: 416.4)

This sample is a hydrothermally altered chlorite-muscovite-quartz schist. The quartz is very fine-grained, cloudy and fractured. Hence, the remaining inclusions are all very small ( $\sim 1\mu$ ), with the largest one being only  $5\mu$ . The majority of them, which were situated along fractures, are of secondary origin. In a few quartz grains, isolated clusters of fluid inclusions are probably of primary origin. These are similar to those studied in other specimens with liquid-rich and gas-rich inclusions. No microthermometry was attempted because of the smallness of the inclusions and the poor transparency of the mineral.

The crushing test indicated a "very strong" gas release which largely dissolved in kerosene, suggesting again, the presence of hydrocarbons.

#### II.2.2.5.2 Sample A-495-164

(Na74; 39.55m)

The early-stage quartz from this sericite-quartz breccia were too fractured and did not present suitable fluid inclusions for study. The late-

stage quartz presented essentially inclusions with liquid + vapour phases. They could easily be classified in type (a) and type (b) inclusions. The heating test of type (a) (liquid-rich) inclusions indicated a fairly precise  $T_H$  of  $130^{\circ}\text{C}$  (Figure 43). This value agrees very much with the temperature of the hydrothermal event indicated by other samples.

#### II.2.2.6.1 Sample A-495-144-Calcite

(D.H. Na23: 305.55m)

##### Description of inclusions

This is the only sample with a quartz-calcite association. Paragenetically, the quartz has been formed before the calcite. A comparison of their fluid inclusion content should have proved to be interesting. In general, however, the calcite presents only a few inclusions which are confined to some sparsely scattered clusters. These are situated along a plane (of growth?) and always contain liquid + gas. They are probably primary, because larger isolated inclusions ( $\sim 30\mu$ ), which are undoubtedly primary, show the same composition and  $T_H$  (Plate V, photo 2). Their sizes range from 5 to  $20\mu$  and the bubble represented 5-10% by volume. Their shapes are fairly regular with a tendency to elongation.

##### Microthermometry

The homogeneous behaviour of all inclusions during the freezing test brought about a better understanding of super-saline fluids hitherto studied. At  $-50^{\circ}\text{C}$  many one-phase (liquid) inclusions started nucleating a bubble and a solid-phase which is isotropic with strong relief. The latter, where observable, is cubic in shape. Between  $-65^{\circ}\text{C}$  and  $-70^{\circ}\text{C}$  almost all inclusions presented these three phases which were accompanied by a change of index of refraction of the liquid - probably due to a change in density. The relief of inclusions decreased accordingly. When the temperature was dropped to  $-155^{\circ}\text{C}$  and kept at this level for 30 minutes, the inclusions remained only partially frozen. The liquid-phase did not decrease, nor did the solid-phase increase. At  $-80^{\circ}\text{C}$  the solid-phase started to melt, however re-cooling again to  $-175^{\circ}\text{C}$  did not change the relative volume of the phases. During the warming process

the cubic solid melted incongruently between  $-43^{\circ}$  and  $-33.5^{\circ}\text{C}$  (Plate V, photo 2) and formed a greenish, birefringent mineral of varying shape: hexagonal, cubic and/or elongated. This newly formed daughter mineral all melted at temperatures between  $-3^{\circ}$  and  $-2^{\circ}\text{C}$  (Figure 44). These phase changes point to the predominance of  $\text{Ca}^{++}$  in combination with other ions in the solution. The solid-phase that nucleated upon cooling to  $-50^{\circ}\text{C}$  is most likely a salt hydrate. The reason for the extreme metastability of the remaining brines is not clear. The temperature of incongruent melting may be an indication of metastable  $\text{CaCl}_2$ -hydrates in weak  $\text{NaCl}$  solutions (see Figure 10). The newly formed minerals could be  $\text{NaCl}$  (cubic) and the other product from incongruent melting:  $\text{CaCl}_2 \cdot 6\text{H}_2\text{O}$ . The fact that all melting temperatures of the hydrates fell between  $-3^{\circ}$  and  $-2^{\circ}\text{C}$  indicates a constant salinity of  $\sim 37$  wt.%  $\text{CaCl}_2$  equivalent.

Upon heating, the majority of inclusions homogenized into one liquid phase between  $96^{\circ}$  and  $104^{\circ}\text{C}$  (Figure 44). The freezing test and heating test indicated the trapping of a homogeneous fluid which had not been disturbed since its entrapment.

#### Crushing test

The crushing of more than 10 calcite grains indicated a "very weak" release of gas in only two grains. The result is in agreement with the type (a) inclusions as observed.

#### Scanning Electron Microscopy

Although an exhaustive search on freshly fractured surfaces has been made, no residues of evaporation were found, although there were many completely empty inclusion cavities. The apparent conflict between the absence of evaporated salts and the presence of strong brines in fluid inclusions is not well understood but could be the result of a reaction of  $\text{CaCl}_2$  solutions with  $\text{CO}_2$  of the atmosphere to form calcite. In this case the newly formed calcite would not be distinguishable from the host mineral.

#### Conclusions for sample A-495-144 (calcite)

The fluid inclusion study of calcites showed quite a drastic change in fluid composition which had taken place since the deposition of



A-495-144

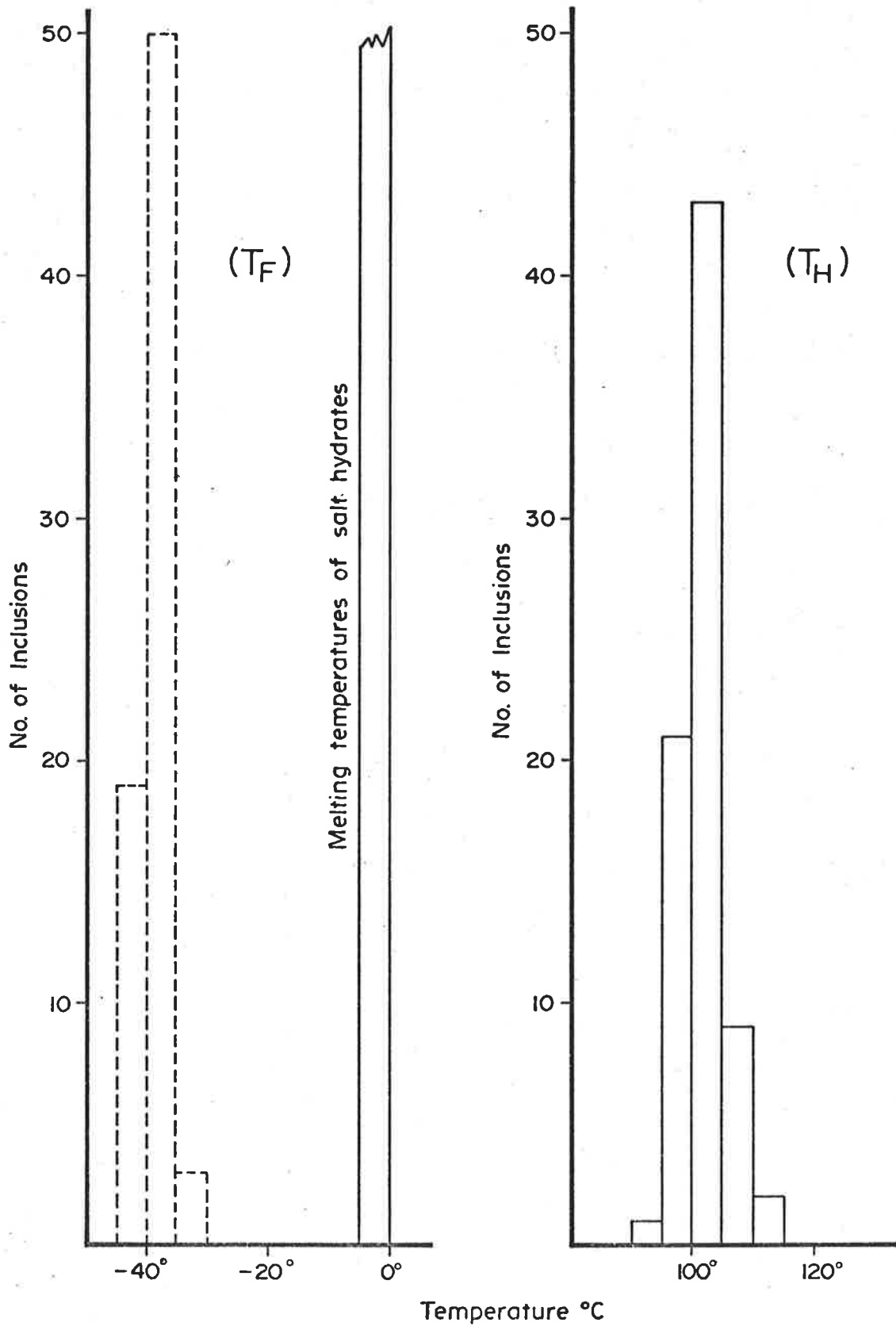


Figure 44: Sample A-495-144.  $T_F$  and  $T_H$  frequency histograms of fluid inclusions in calcite. Note the homogeneity of the results.

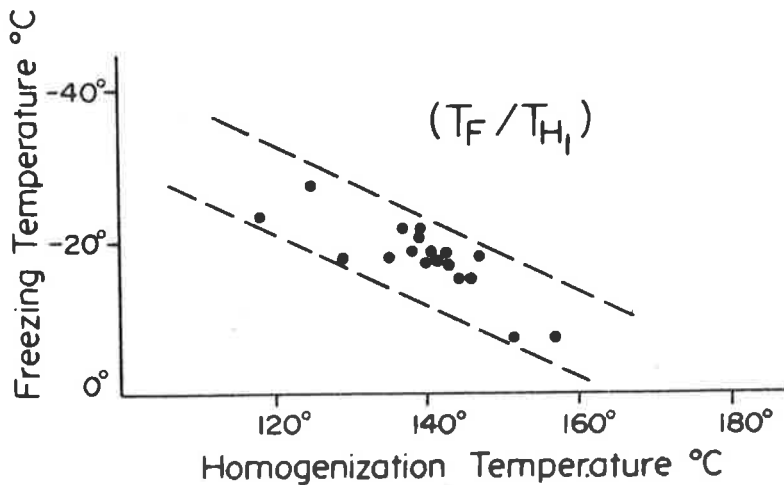
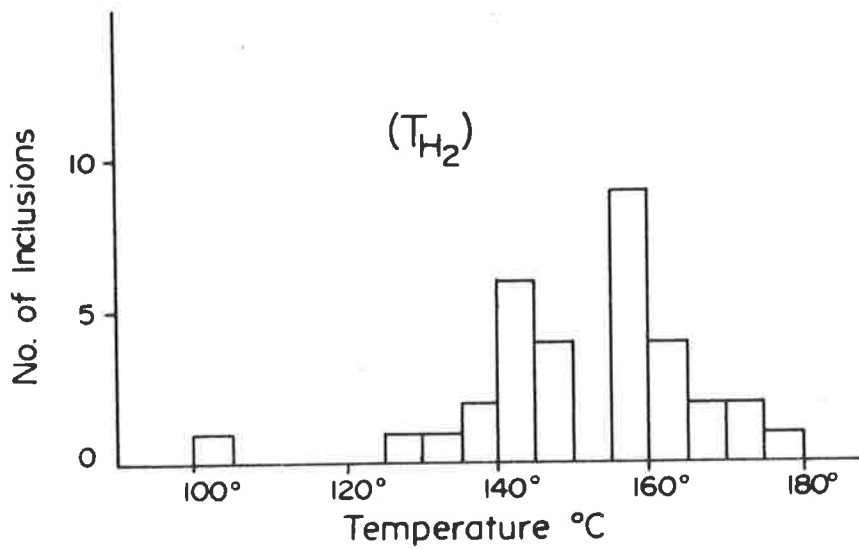
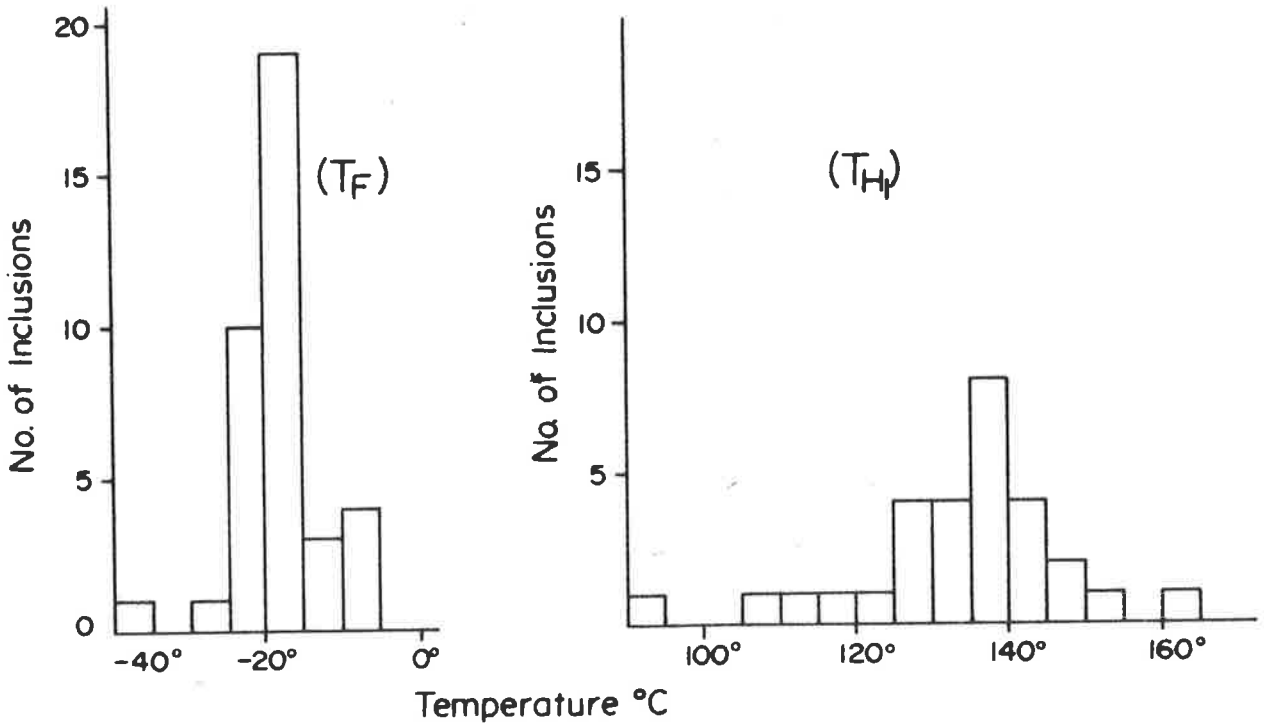


Figure 45: Sample A-495-220.  $T_F$  and  $T_H$  frequency histogrammes of fluid inclusions in calcite and the relation  $T_F/T_H$ .  $T_H$  refers to results from the first group of inclusions.  $T_{H1}$  refers to the results from a second group of inclusions.  $T_{H2}$  Both results are repeatable within 1.0°C.

quartz. The salinity increased from 15-16 wt.% during the quartz formation to 37 wt.%  $\text{CaCl}_2$  equivalent during calcite deposition; during the same period the temperature increased from  $\sim 70^\circ\text{C}$  to  $100^\circ\text{C}$ .

#### II.2.2.6.2 Sample A-495-220

(D.H.Na176; 44.0m)

##### Description of inclusions

This sample is an altered feldspar-actinolite-schist with an 0.2 mm calcite vein cutting across the drill core. The calcite was broken into small crystals and examined for inclusion contents. The sample contains fluid inclusions similar in shape, size and phases to calcite from sample A-495-144. The calcite grains selected for microthermometry contain numerous type (a) inclusions in several planes parallel to the face of the crystal (zone of growth), they are possibly of primary origin.

##### Microthermometry

The  $T_F$  presents a major frequency around  $-20^\circ\text{C}$ , which indicates a salinity of 23.0 wt.%  $\text{CaCl}_2$  equivalent (Figure 45,  $T_F$ ). The main  $T_H$  distribution ranges from  $+125^\circ$  to  $+150^\circ\text{C}$  with a major concentration of values around  $+140^\circ\text{C}$  (Figure 45,  $T_{H_1}$ ). To determine whether other inclusion domains had different  $T_H$  values, the calcite was turned over and heated for the second time. Surprisingly, the  $T_H$  histogram showed a bimodal pattern with the main mode around  $160^\circ\text{C}$ , which is  $20^\circ\text{C}$  above the temperature  $T_{H_1}$  (Figure 45,  $T_{H_2}$ ). These results might be taken as proving either that the inclusions were trapped at different temperatures, or that leakage occurred during the first heating test. The possibility of leaking introducing a permanent change was pointed out by Larson et al. (1973) for inclusions in fluorite from the Young Mine, East Tennessee, and sphalerite from the Laisvall deposit, Sweden. In order to investigate these possibilities, the first group of inclusions ( $T_{H_1}$ ) was heated a third time. The new results exactly matched the results of the former determination. The differences recorded were within  $1.0^\circ\text{C}$  which confirmed the absence of leakage. It seems clear that some variation of temperature must have occurred between the time of formation of the inclusions in the first

group ( $T_{H_1}$ ) and those in the second ( $T_{H_2}$ ). Furthermore, the  $T_F/T_H$  negative correlation similar to the one in sample A-495-157, points to possible fluid mixing during the formation of the vein (Figure 45,  $T_F/T_H$ ).

#### Crushing and Scanning Electron Microscopy

The crushing of several calcite grains which contain fluid inclusions always showed a "weak" gas release which proved to be  $CO_2$ . The SEM showed only empty inclusion cavities and the EDAX analysis revealed that minerals from one cavity contained elements indicative of chlorides of Ca(?) and K (Plate VII, photo 3, mineral a).

#### II.2.3 General conclusions on fluid inclusions

- (a) The majority of samples from an early to late-stage quartz indicated the presence of two types of inclusions:
- 1) type (a), liquid-rich and 2) type (b), gas-rich.
- (b) The inclusions indicated a wide range of salinities, i.e. values between 0.4 wt.%  $CaCl_2$  equivalent in quartz from sample A-495-162 to 37 wt.%  $CaCl_2$  in calcite from sample A-495-144. Phase changes, such as incongruent melting and the appearance and melting of hydrates, the very early melting of ice ( $-80^{\circ}C$ ) and very low temperature of the last melting of ice are internally consistent with a fluid with very high Ca-content. These very saline fluids commonly presented partial freezing phenomena. As the salinities varied widely within a single crystal, the spread in values is unlikely to have been the result of the generation of brines of different salinities, but rather an indication of the mixing of fluids. The indication of mixing is also provided by inclusions from different quartz grains of the same sample (A-495-172), and even by inclusions trapped at different stages in the same quartz grain (e.g. A-495-172D). Further evidence of fluid mixing is indicated by the inverse correlation between  $T_F$  and  $T_H$ , i.e. a higher salinity in inclusions with lower  $T_H$  (samples A-495-157

and A-495-220). In the case of sample A-495-113 it was even possible to estimate the temperature at which the mixing had occurred (120-130°C).

- (c) Crushing with Chaix-Meca stage and the microthermobarometric measurements of type (b) inclusions in hydrothermal quartz indicated pressures of 60-70 kg/cm<sup>2</sup> at room temperature (20°C). By a combination of freezing data with crushing results, the presence of CO<sub>2</sub> could be established as a minor component of the gas-phase, with hydrocarbons as major components. Different rates of solubility of the gases in kerosene pointed to a mixture of gases where hydrocarbons seemed to be the major component. Pressure-condensation measurements are consistent with a gas phase consisting predominantly of CH<sub>4</sub>.
- (d) The co-genesis of inclusion types (a) and (b) in the same sample or same growth zone is interpreted as the product of exsolution of gases caused by the mixing of fluids of different salinities, according to data presented by Takenouchi and Kennedy (1965). Boiling has normally been invoked as the major explanation for the simultaneous entrapment of vapour and liquid rich inclusions. However, this process can be ruled out on the following grounds: 1) Both fluid-rich and vapour-rich inclusions have similar salinities. 2) The salinity of the solutions is, in all cases, too high to have allowed boiling at the homogenisation temperatures observed (120-160°C). 3) All vapour phases are gases under pressure and not a low pressure water vapour.
- (e) The heating test indicated T<sub>H</sub> from +70°C to +200°C. The distinction between early- and late-stage quartz indicated that: the older quartz presented a higher frequency of T<sub>H</sub> >+150°C while in the younger quartz T<sub>H</sub> was below +150°C, pointing to a temperature gradient with time. At the same time, there is an

inverse salinity gradient. High  $T_H$ 's correspond with lower salinities and vice-versa. The crystallization of quartz at temperatures below  $+70^{\circ}\text{C}$  is suggested by samples with fluid inclusions containing a liquid-phase only, and by some inclusions which, after nucleating a vapour-phase during the freezing test, homogenized again into liquid-phase at low temperatures (e.g. A-495-172A, A-495-156).

- (f) The freezing experiment indicated and the SEM-EDAX confirmed the presence of  $\text{Ca}^{++}$ ,  $\text{Na}^+$ ,  $\text{K}^+$  and, less frequently  $\text{Fe}^{++}$  chlorides. Carbonates - calcite, dolomite and ankerite - and probably calcium silicates - have also been detected. Sericite and chlorite were the most common micaceous minerals, probably trapped as solid phases but were contemporaneous with the fluids. Kaolinite was fairly common and could be a daughter mineral (Plate VI, photos 1 and 2). The presence of dawsonite was suspected in some inclusions (A-495-172), but not confirmed by SEM-EDAX.
- (g) Contemporaneity of fluid inclusions and uranium mineralization was indicated by an autoradiographic study. The occurrence of uranium mineralization in samples with strong (e.g. A-495-172, A-495-168) and weak (A-495-162) brines indicated that the salinity variations were not directly responsible for uranium precipitation. The common presence of hydrocarbons - a strong reductant - must have played a major role in the precipitation of uranium from solutions containing the uranyl complexes. This aspect will be discussed further in Chapter IV.

## CHAPTER III

OXYGEN ISOTOPE STUDYIII.1. Principles and TechniquesIII.1.1 Introduction

Isotopic fractionation is a common phenomenon of many natural processes. In the last three decades, the isotopic fractionation of hydrogen, carbon, sulphur and oxygen in minerals have been applied to the study of geological processes with increasing frequency and detail. The theoretical background of the geochemistry of stable isotopes is based on the works of Urey (1947) and Bigeleisen and Mayer (1947). The accurate measurements of isotopic variations of the above-mentioned elements became feasible because of the development of precise mass spectrometry by Nier (1947) and McKinney and others (1950). Among the various fields of application of oxygen isotope fractionation studies, those concerning the study of hydrothermal mineral deposits and their fluid transport mechanism has acquired an increasing importance (e.g. see Garlik<sup>c</sup><sub>λ</sub> and Epstein, 1966; Rye, 1966; Rye and O'Neil, 1968; Hall, 1969; Ohmoto and Rye, 1970; Addy, 1973; Landis and Rye, 1974; Rye and Sawkins, 1974; Sheppard and Gustafson, 1976; Ford and Green, 1977). There are three main aspects of oxygen isotope studies which can be investigated by determining the oxygen isotopic composition of minerals in a given assemblage. These aspects are (Taylor, 1967):

- (a) investigation of isotopic equilibrium or non-equilibrium between two or more mineral pairs;
- (b) determination of temperatures of formation of these mineral pairs;
- (c) information about the nature, origin, and volume of hydrothermal fluids involved in the formation of a particular mineral assemblage.

The published papers on the application of oxygen isotope studies to hydrothermal uranium deposits are relatively rare and are mainly limited

to some Canadian deposits (Sassano et al., 1972; Robinson and Ohmoto, 1973; Robinson and Badham, 1974). Ayres and Eadington (1975) published results of sulphur isotope studies on the South Alligator River uranium deposits. Stable isotope studies on uranium ores of the Pine Creek Geosyncline have been published in a special volume dealing with uranium deposits of the Pine Creek Geosyncline (Ferguson, 1980).

The significance of oxygen isotope studies to geological problems is greatly enhanced by the dominance of oxygen in the earth's crust. Being the major constituent of the majority of minerals - silicates, sulphates, carbonates and oxides - considerations of mass transfer are largely possible through oxygen isotope studies. Water is of special importance for hydrothermal and surface processes. The relative abundance of the three stable isotopes in the oxygen of air was determined by Nier (1950). They are  $^{16}\text{O} = 99.759\%$ ,  $^{17}\text{O} = 0.0374\%$  and  $^{18}\text{O} = 0.2039\%$ . In ocean water the values are slightly different:  $^{16}\text{O} = 99.763\%$ ,  $^{17}\text{O} = 0.0327\%$ , and  $^{18}\text{O} = 0.1995\%$  (Garlick, 1969). In nature, the range of variation of the  $^{18}\text{O}/^{16}\text{O}$  ratio is as large as 10%.

### III.1.2 Isotopic Notation

The oxygen isotopic data are reported in parts per mil deviation of the sample from a standard, by the conventional  $\delta$ -notation:

$$\delta^{18}\text{O} \text{ sample } (\%) = \frac{^{18}\text{O}/^{16}\text{O} \text{ sample} - ^{18}\text{O}/^{16}\text{O} \text{ standard}}{^{18}\text{O}/^{16}\text{O} \text{ standard}} \times 1000$$

(e.g. see Devereux, 1968; or Hudson, 1977).

For example, if a quartz has  $\delta^{18}\text{O} \text{ quartz} = 15\%$  SMOW means that this quartz is 15 per mil (1.5 per cent) richer in  $^{18}\text{O}$  than the Standard Mean Ocean Water, the adopted standard for the present study. Or, if a hydrothermal solution has  $\delta^{18}\text{O} \text{ solution} = -7\%$  SMOW means that this solution is 0.7 percent poorer in  $^{18}\text{O}$  than the SMOW. The difference in oxygen isotope content between two oxygen-bearing compounds (in equilibrium or not) is known as fractionation ( $\alpha$ ). Generalizing, the fractionation factor between two chemical species or minerals A and B, ( $\alpha_{A-B}$ ) is defined as:



$$\alpha_{A-B} = \frac{({}^{18}\text{O}/{}^{16}\text{O})_A}{({}^{18}\text{O}/{}^{16}\text{O})_B}$$

$\alpha_{A-B}$  relates to  $\delta$  in the following way:

$$10^3 \ln \alpha_{A-B} \approx \delta_A - \delta_B = \Delta_{A-B}$$

which approximation is valid for  $\delta$ -values  $< |10\%|$ . Theoretical calculations and experimental determinations have demonstrated that fractionation between two oxygen compounds is inversely proportional to the square of the absolute temperature:  $1/T^2$ . As this also applies to water-mineral fractionations, calculated and experimentally determined  ${}^{18}\text{O}/{}^{16}\text{O}$  fractionation curves are presented as plots of  $10^3 \ln \alpha$  against  $10^6/T^2$  (Taylor, 1974).

### III.1.3 Experimental Determinations of Isotopic Fractionations

The theory developed for isotopic fractionation calculations is essentially derived from ideal gases (Urey, 1947; Bigeleisen and Mayer, 1947).

The slow exchange kinetics, where isotopic equilibrium between two solids in contact is concerned, makes experimental isotope fractionations below  $500^\circ\text{C}$  very difficult (Bottinga and Javoy, 1973). To avoid this problem, determinations have been made equilibrating the mineral with an aqueous phase at a certain temperature, and measuring the mineral-water fractionation ( $\alpha$  mineral-water). The fractionation between two minerals is then calculated by combining the mineral-water fractionations for each mineral. Several experimental fractionation curves have been determined in this way. In another approach, Blattner (1975) used natural minerals grown in springs of known temperature to determine calibration curves for quartz and feldspar. Blattner (op. cit) used two calibration points to construct the quartz-K-feldspar geothermometer. He used one natural quartz-K-feldspar pair from a hydrothermal environment for  $275^\circ\text{C}$  (Broadlands geothermal field, N.Z.) and the  $600^\circ\text{C}$  experimental quartz-K-feldspar fractionation of Blattner and Bird (1974). In this way, Blattner obviated the need of analyses of solution with their inherent complications. From the quartz-K-feldspar curve he derived the quartz-muscovite and the quartz-calcite curves (see Blattner, 1975, for details). The present study used low temperature extrapolations of these curves,

assuming linearity between  $\Delta$  and  $1/T^2$ .

The equation by Blattner (1975), Blattner and Bird (1976), other mineral-water fractionation equations, and other mineral-mineral fractionation equations obtained by combination, were used in the present study.

They are:

$$\Delta \text{ quartz-water} = 3.65 (10^6/T^2) - 2.59 \text{ (Blattner, 1975)} \quad (1)$$

$$\Delta \text{ calcite-water} = 2.78 (10^6/T^2) - 3.39 \text{ (O'Neil et al., 1969)} \quad (2)$$

$$\Delta \text{ quartz-K-feldspar} = 0.74 (10^6/T^2) + 0.82 \text{ (Blattner, 1975)} \quad (3)$$

$$\Delta \text{ quartz-muscovite} = 1.27 (10^6/T^2) + 1.30 \text{ (Blattner, 1975)} \quad (4)$$

$$\Delta \text{ quartz-calcite} = 0.88 (10^6/T^2) + 0.37 \text{ (Blattner, 1975)} \quad (5)$$

$$\Delta \text{ chlorite-water} \sim 1.56 (10^6/T^2) - 4.70 \text{ (Wenner and Taylor, 1971)} \quad (6)$$

$$\Delta \text{ muscovite-water} = 2.38 (10^6/T^2) - 3.89 \text{ (O'Neil and Taylor, 1969)} \quad (7)$$

Combining equations (4) and (5), and (6) and (7), calcite-muscovite and muscovite-chlorite geothermometers are respectively obtained.

$$\Delta \text{ calcite-muscovite} = 0.39 (10^6/T^2) + 0.93 \quad (8)$$

$$\Delta \text{ muscovite-chlorite} \sim 0.82 (10^6/T^2) + 0.81 \quad (9)$$

Wenner and Taylor (1971) have also obtained the following equations:

$$\Delta \text{ quartz-chlorite} \sim 2.01 (10^6/T^2) + 1.99 \text{ and} \quad (10)$$

$$\Delta \text{ chlorite-magnetite} \sim 1.69 (10^6/T^2) + 1.68 \quad (11)$$

Other mineral pairs such as: quartz-plagioclase, quartz-muscovite, plagioclase-pyroxene, quartz-magnetite, and muscovite-magnetite fractionation curves have been compiled by Friedman and O'Neil (1977).

### III.1.4 Analytical Procedures

#### III.1.4.1 Selection of rock samples

Samples of granite, dolerite, amphibolite schist and their correspondent altered equivalents were selected for oxygen isotopic analyses. Major emphasis was placed on the study of alteration products because they seem to be related to the uranium mineralization. All samples are from drill-cores. The complete list of selected samples with their provenance

and brief petrographical description is given in Appendix 1.

#### III.1.4.2 Mineral separation

The coarse-grained samples were broken into small pieces, ground, and the minerals were hand-picked. The grains were then cleaned in an ultrasonic bath. When necessary, further grinding was carried out. For finer grained samples grinding and sieving separated the 250-90 $\mu$  fraction. After ultrasonic cleaning, the samples were dried and the magnetite separated with a hand magnet. The use of a Frantz magnetic separator and heavy liquids completed the separation of other minerals. Chlorite and sericite formed by alteration of pyroxene and feldspar from dolerites were difficult to separate because of the ophitic texture of the rock causing intimate intergrowths between the mineral pair. Only in porphyritic dolerites and in a few samples rich in chlorite could a satisfactory separation of pure minerals be achieved. The pitchblende always carried an impurity of chlorite. The two samples that were analysed contained 5% chlorite. The purity of mineral separates was always checked under a binocular microscope and in a few samples, by X-Ray diffraction.

#### III.1.4.3 Analytical Techniques

The analyses - oxygen extraction and subsequent mass spectrometry - were carried out at the Institute of Nuclear Sciences, of the Department of Scientific and Industrial Research in Lower Hutt, New Zealand, on two different occasions. Oxygen from silicates and oxides were extracted by a process differing from that for carbonates.

##### (a) Silicates and oxides

The oxygen of these minerals was extracted by reaction with bromine-pentafluoride ( $\text{BrF}_5$ ) in nickel reaction tubes. Basically, the method is the one described by Clayton and Mayeda (1963).

Two types of errors can be introduced during oxygen extraction: incomplete O-extraction with the attendant danger of fractionation and the addition of extraneous oxygen due

to contamination. The two main sources of contamination are air and moisture. To minimize any possible effects from these sources, the samples were loaded inside a dry box (dry nitrogen atmosphere) where the humidity was equal to or lower than 25%. The sample tubes, after being connected to the extraction line, were evacuated at room temperature for at least one hour and heated to  $\sim 150^{\circ}\text{C}$  for  $\sim 20$  minutes to drive out any condensed water in the line. When cooled to room temperature, the extraction line was pre-treated with  $\text{BrF}_5$  for roughly two minutes and then evacuated. Details of the entire procedure are described by Devereux (1968).

Because the reactions require several hours for completion, they generally took place overnight. Reaction took place at  $550^{\circ}\text{C}$  with the exception of magnetite and haematite for which a temperature of  $700^{\circ}\text{C}$  is required.

The amount of sample necessary for each analysis is a weight that could yield approximately 150 micro-moles of  $\text{CO}_2$ .

For minerals and rocks analysed, these weights correspond to:

9mg - quartz;

10mg - sericite, granite, and altered dolerite;

11mg - feldspars and dolerite;

12mg - chlorite, biotite, pyroxene, and actinolite;

16mg - haematite; and

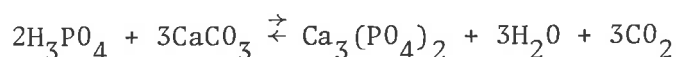
35mg - pitchblende.

The reactions having been completed overnight, the next step was the conversion of oxygen to  $\text{CO}_2$ . This was achieved by circulating the extracted oxygen over a hollow graphite rod connected to a coil of platinum wire which

was heated by a Radio Frequency furnace. The resultant  $\text{CO}_2$  was frozen in a liquid nitrogen trap and - after expansion - measured in a manometer. Devereux (1968) gives a detailed description of the process. The only difference in our procedure being the deletion of a Toepler pump for gas transfer.

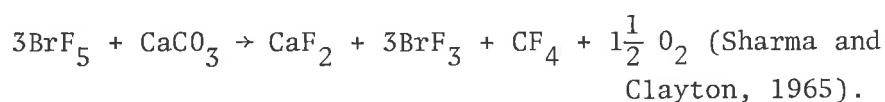
(b) Carbonates

$\text{CO}_2$  from calcites was extracted by reacting the mineral with 100% phosphoric acid, at  $25^\circ\text{C}$ , in vacuum, following the procedures described by McCrea (1950). The reaction can be expressed by the following relationship:



The  $\text{CO}_2$  and  $\text{H}_2\text{O}$  were both collected in a liquid nitrogen trap.  $\text{H}_2\text{O}$  was separated by retaining it in a coiled trap immersed in a slurry of dry ice-alcohol. Carbon dioxide was then transferred to the manometer where its volume was measured and it was finally collected in a bottle with a valve for mass spectrometry. The weight of calcite used in each run was 11-13 mg.

Carbonates can also be analysed by the bromine pentafluoride method. The theoretical advantage of this method is the possibility of extracting 100% of the oxygen from carbonates. Three variations of analytical procedure have been described by Sharma and Clayton (1965). The high temperature procedure was tried during this study. This variation consists of a reaction between carbonate and bromine pentafluoride at  $700^\circ\text{C}$ , according to the following equation:



However, in this study, the oxygen yield was always incomplete (70% and 85%) with a remaining gas pressure after the conversion of  $O_2$  to  $CO_2$ . As the reaction in the tube was apparently incomplete, the above-mentioned equation may not be fully correct. For this reason, the method was abandoned.

#### III.1.1.4 Mass Spectrometry and Standards

The isotopic composition of the  $CO_2$  gas derived from carbonates, silicates and oxides was measured with a Nuclide Analysis Associates (NAA) Mass Spectrometer which is a 15 cm.  $60^\circ$ , double-collector mass spectrometer of the type described by Nier (1947).

Carbon dioxide from Te Kuiti Limestone (TKL) was used as Standard. Upon standardization with respect to SMOW (Blattner and Houlston, 1975) this limestone  $CO_2$  has the following composition:

$$\delta^{18}O_{TKL} = 26.6\% \text{ (with respect to SMOW and } \alpha_{CO_2-H_2O}^{25^\circ C} = 1.0407).$$

The conversions of results from mass spectrometry (NAA) into the SMOW scale were made according to the following equation (Blattner, 1972):

(a)  $BrF_5$  method, (Fig. 46),

$$\delta^{18}O \text{ vs. SMOW (1.0407)} = 1.0408 \delta R_{46} \text{ vs. TKL} + 0.0100 \\ \delta R_{45} \text{ vs. TKL} + 36.58$$

where:  $\delta R_{46}$  vs. TKL is the result from the balancing panel,

$$\delta R_{45} \text{ vs. TKL} = 0.22, \text{ and}$$

$$1.0407 \text{ is the assumed value of } \alpha_{CO_2-H_2O}^{25^\circ C};$$

(b) in the case of calcite samples treated with 100%  $H_3PO_4$ ,

$$\delta^{18}O \text{ calcite vs. SMOW (1.01025, 1.0407)} = 1.0302 \delta R_{46} \text{ vs.} \\ \text{TKL} + \text{TKL} + \delta R_{45} \text{ vs. TKL} + 26.06$$

where: 1.01025 is the kinetic fractionation factor for calcite.

These relationships include correction for 0.30% inlet valve mixing.

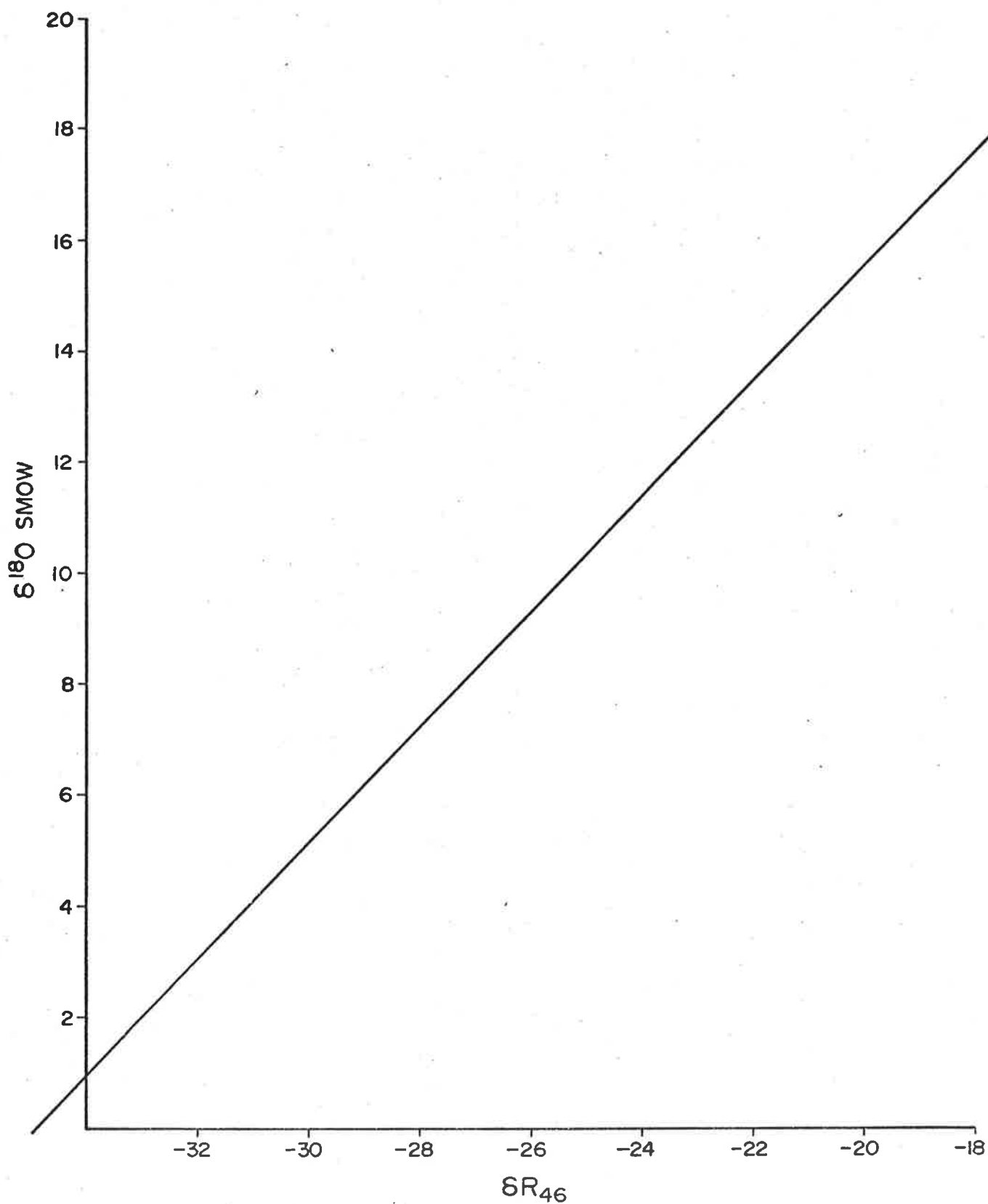


Figure 46: Correlation curve between the results from mass spectrometry (NAA) unit from the Institute of Nuclear Science, Lower Hutt, N.Z. ( $\delta R_{46}$ ) and the SMOW scale for the  $\text{BrF}_5$  method is used.

Quartz sample R4150 of the Institute of Nuclear Sciences laboratory was used as the working standard for silicates and oxides. The  $\delta^{18}\text{O}$  value of this quartz was determined to be  $7.9 \pm 0.5\%$  SMOW for the samples analysed in the first group and  $8.2 \pm 0.3\%$  SMOW for the second group. After correction, these values are in the same scale range as NBS28 = +9.8 (Blattner, 1975).

The mass spectrometer has an analytical precision of approximately  $\pm 0.15\%$  in results from individual samples. Taking into consideration the results of the working standard R4150, the margin of error for  $\delta$  values from both sample groups are respectively 0.5% and 0.3% for the first and second group of samples (\*).

### III.2 Samples Studied

#### III.2.1 Previous Oxygen Isotope Works on Hydrothermal Uranium Deposits

The number of oxygen isotope studies of hydrothermal uranium deposits is fairly small. Sassano et al., (1972) published the  $\delta^{13}\text{C}$  (PDB) and  $\delta^{18}\text{O}$  (SMOW) results of carbonate gangue minerals from uranium deposits of Eldorado, Saskatchewan. For hydrothermal dolomites of early generation, with no apparent significant recrystallization, they found  $\delta^{18}\text{O}$  values of +9.5 to +11.0% SMOW. Late-stage calcites presented  $\delta^{18}\text{O} = +13.2$  to +14.5% SMOW. The authors concluded that the deposits were generated by metamorphic hydrothermal fluids with an initial  $\delta^{18}\text{O}$  value of +6 to +8% SMOW.

Robinson and Ohmoto (1973) studied the oxygen isotopic composition of some minerals from Echo Bay U-Ni-Ag-Cu deposits of Northwest Territories, Canada. In view of temperatures obtained from fluid inclusion temperature studies, the authors came to the conclusion that the hydrothermal ore-forming fluid had almost constant oxygen isotopic composition throughout the entire depositional event with  $\delta^{18}\text{O}$  values in the range  $1.0 \pm 2.5\%$  SMOW, which suggests a very small contribution, if any, of magmatic water.

---

(\*) During the study of samples of the first group, the oxygen extraction line presented a rather difficult problem of leakage, giving less precise results.



The stable isotope geochemistry of the Great Bear Lake silver deposits of Northwest Territories, Canada, were studied by Robinson and Badham (1974). The constant  $\delta^{18}\text{O}$  value is 15‰ SMOW for dolomites of all paragenetic stages is considered to be indicative of relatively constant temperature of deposition, which is estimated as 200°C. For the ore-fluid a value of  $\delta^{18}\text{O} = +2\%$  SMOW was calculated which was considered to be a possible indication of connate water.

As is the case for many base metal deposits, where more extensive stable isotope studies are available (e.g. Addy, 1973, p.71), the oxygen isotope studies of these few hydrothermal uranium deposits seemed to point to the importance of surface waters and the negligible contribution made by magmatic waters for uranium-bearing solutions.

### III.2.2 Analytical Results and Discussion

#### III.2.2.1 Quartz from D.H.Na77

The oxygen isotopic analyses of the three types of quartz considered in Chapter I, showed some interesting features. The most important of them was the marked difference in  $\delta^{18}\text{O}$  values between the late- and early-stage quartz, which was particularly well defined in some samples from drill-hole Na77. The late-stage quartz yielded  $\delta^{18}\text{O}$  values range of 14 to 16.5‰ SMOW while in the early-stage quartz, these values were in a lower range of 9.3 to 11.0‰ SMOW. Actually, the former range might be narrower because the late-stage quartz from sample A-495-171 which yielded a  $\delta^{18}\text{O}$  value of 14‰ SMOW was contaminated by ferruginous material, which was difficult to be completely removed during mineral separation. The iron oxide contamination would have lowered the isotopic composition of the quartz. In any case, the isotopic difference between both types of quartz is beyond any doubt and it clearly indicates an increase of the  $\delta^{18}\text{O}$  of hydrothermal quartz with time (Table 2). This difference could be a consequence of:

- a) enrichment of  $^{18}\text{O}$  content of the mineralizing solution with time while the temperature remained constant;
- b) constant  $^{18}\text{O}$  content of the mineralizing solution but decrease

in temperature - and, as a result, an increase of the quartz-water equilibrium fractionation;

c) an interaction of these two possibilities.

Those differences in  $\delta^{18}\text{O}$  values from the two mentioned stages of quartz were clearly observed in the samples A-495-171, A-495-174, A-495-174A and A-495-176 (Table 2). In sample A-495-176 the two stages of quartz formation are clearly distinguishable on the basis of paragenetic sequence, which enabled a complete physical separation of the two stages. The analyses show a markedly higher  $\delta^{18}\text{O}$  value for the late-stage quartz.

Fluid inclusion microthermometry of this sample also showed different homogenization temperatures ( $T_{\text{H}}$ ) for each type of quartz:

- +160° to +210°C for the early-stage types and
- +125° to +150°C for the late-stage types (Table 2).

Although these values represent a broad range of temperatures, they show a decrease of temperature with time of crystallization. Hence, the different  $\delta^{18}\text{O}$  values seem to be at least to some extent, the consequence of decreasing temperature of the solutions leading to the formation of two types of quartz. However, a change in  $\delta^{18}\text{O}$  value of the solutions cannot be completely ruled out because mixing of solutions was indicated during the fluid inclusion study. These different solutions, with different salinities, certainly have had different  $\delta^{18}\text{O}$  values and thus account for, at least partially, for the difference in  $\delta^{18}\text{O}$  of the two stages of quartz. The calculated  $\delta^{18}\text{O}$  of the solutions, using equation (1) and the  $T_{\text{H}}$  of fluid inclusions, shows values from -5.8‰ to -1.0‰ SMOW (with a mode of -5.5‰ SMOW) for solutions in isotopic equilibrium with the early-stage quartz and values from -4.5‰ to -0.2‰ SMOW (with a mode of -3.7‰ SMOW) for mineralizing solutions of the late-stage quartz (Table 2). Both ranges of values show an overlap which favours the idea of decreasing temperature during the crystallization as the major reason for different  $\delta^{18}\text{O}$  of quartz, as opposed to a major change in  $\delta^{18}\text{O}$  value of the solution.

A similar comparison can be drawn between two quartz samples

SAMPLE No. A-495-	DEPTH (m)	$\delta^{18}\text{O}$ quartz (% SMOW)			$T_H$ ( $^{\circ}\text{C}$ )	CALCULATED $\delta^{18}\text{O}$ SOLUTION (% SMOW)	MODE VALUE	SALINITY Mol-CaCl <sub>2</sub>	CORRECTED $\delta^{18}\text{O}$ SOLUTION (% SMOW)	MODE VALUE
		METAMORPH.	EARLY-STAGE	LATE-STAGE						
167	44.6	-	9.5 $\pm$ .1	-	-	-	-	-	-	-
168	46.8	-	15.5 $\pm$ .1	-	-	-	-	-	-	-
168	46.8	-	-	15.9 $\pm$ .1	100	-9.7	-	2.5	-7.2	-7.2
171	56.7	-	9.5 $\pm$ .5	-	140	-9.3	-	-	-	-
171	56.7	-	-	14	(~70)	(-14.4)	-	-	-	-
172	58.0	7.1 $\pm$ .5	-	-	(300)	(- 1.4)	-	-	-	-
172	58.0	-	-	16	85-140	-11.8 to -4.8	-7.0	4.0	-7.8 to -0.8	-3.0
174	61.7	-	10.1 $\pm$ .5	-	120-165	-12.0 to -6.5	-9.4	-	-	-
174	61.7	-	-	16.1 $\pm$ .1	80-100	-12.2 to -9.1	-	-	-	-
174-I	61.8	-	9.3 $\pm$ .1	-	-	-	-	-	-	-
174-I	61.8	-	-	15.2 $\pm$ .1	-	-	-	-	-	-
176	67.4	-	11.0 $\pm$ .1	-	160-210	- 5.8 to -1.0	-5.5	2.2	-5.8 to -1.0	-5.5
176	67.4	-	11.0 $\pm$ .1	16.0 $\pm$ .5	125-150	- 6.5 to -2.2	-5.7	3	-4.5 to -0.2	-3.7
178	104.4	-	-	16	105-145	- 9.2 to -6.8	-8.1	-	-	-
179	111.4	10.3 $\pm$ .5	-	-	(~300 $^{\circ}$ )	(+1.7)	-	2.5	+4	-

Table 2:  $\delta^{18}\text{O}$  values of quartz from drill-hole Na77. The corresponding values for solutions was calculated using equation (1) (Blattner, 1975). The corresponding values of solutions corrected for temperatures and salinities was made according to the curves of figure 49. Values in brackets are estimated.

separated from sample A-495-174. The early-stage quartz presents  $T_H$  in the range  $120^{\circ}$ - $165^{\circ}$ C and  $\delta^{18}O = 10.1\%$  SMOW while the late-stage one presents  $T_H$  in the range  $80^{\circ}$ - $100^{\circ}$ C and  $\delta^{18}O = 16.1\%$  SMOW. The calculated  $\delta^{18}O$  solution values are in the range  $-12.0\%$  to  $-6.5\%$  SMOW and  $12.2\%$  to  $-9.1\%$  SMOW respectively, which again shows a good correlation between  $\delta^{18}O$  of quartz and homogenization temperatures.

The calculated  $\delta^{18}O$  of the solutions for these two specimens seems to point against magmatic origin. Assuming that the time at which the Nabarlek uranium mineralization occurred, ocean-water had an isotopic composition approximately similar to present-day sea-water (Taylor, 1977; p.551), the above-mentioned  $\delta^{18}O$  solution values indicate more precisely waters of meteoric origin (Taylor, 1974; p.849). The reason for the different ranges of  $\delta^{18}O$  solution values as calculated for both samples is not clear, but in view of the possibility of mixing of solutions - discussed in the fluid inclusions chapter - either 1) the meteoric water involved in the crystallization of quartz A-495-174 may have come from sources differing from those involved in the crystallization of quartz A-495-176, or 2) alternatively, the reason may be due to the different salinities of the solutions leading to different isotopic fractionations (see below), or a combination of both factors.

Further samples from drill-hole Na77 which contain the pair of early- and late-crystallized quartz with distinctly different  $\delta^{18}O$  values are the A-495-171 and A-495-174-I. The latter was collected at practically the same depth as sample 174. The main macroscopic difference between these two lies in the higher radioactivity of A-495-174-I. The quartz did not contain fluid inclusions suitable for study, but their  $\delta^{18}O$  values, although lower than the  $\delta^{18}O$  values of 174, are still within the ranges of early- and late-stage quartz. In sample A-495-171, although no precise  $T_H$  could be determined, the calculated (but uncorrected for salinity)  $\delta^{18}O$  value of the solutions were  $-9.5\%$  SMOW and  $-14.4\%$  SMOW for early- and late-stage quartz, respectively.

Sample A-495-168 presented only a slight difference in  $\delta^{18}O$  values between the two stages of quartz (see Table 2). Because of the absence

of suitable fluid inclusions, the  $T_H$  of early-stage quartz could not be determined. But, if the same variation of  $T_H$  between early- and late-stage quartz in previous samples is assumed, this smaller than normal difference in  $\delta^{18}O$  between the two stages of quartz A-495-168, (in view of the accuracy of both analyses), may be an indication of mixing of meteoric waters of different  $^{18}O$  content, as has been demonstrated above. The same explanation may be applicable to the  $\delta^{18}O$  values in the quartz of samples A-495-164 and A-495-191 (Table 3), although in these cases, the analytical precision was not as good as for A-495-168. Perhaps the most obvious explanation for this narrow range in isotopic values is that the early- and late-stage quartz, although physically distinct in these samples were actually formed at approximately the same temperature from the same solution.

In the samples A-495-167, A-495-172 and A-495-178, the hydrothermal quartz could not be assigned to a specific stage of mineralization. But they all yielded  $\delta^{18}O$  values that would fit within the range of either early- or late-stage quartz. The  $\delta^{10}O$  values of these quartz crystals for which a reliable  $T_H$  was determined always pointed to a solution with  $\delta^{18}O$  values indicative for waters of meteoric origin (Table 2).

#### III.2.2.2 Metamorphic quartz

The two metamorphic quartz samples (A-495-172 and A-495-179) presented  $\delta^{18}O$  values which are closer to that of early-stage hydrothermal quartz. Although the  $T_H$  of the fluid inclusions were not completely reliable, type (b) - gas-rich - inclusions indicate homogenization temperatures occurring above  $300^{\circ}C$ . The mineral assemblage at Jabiluka points to a temperature of  $300^{\circ}C$  for the retrogressive metamorphic stage (Binns et al., 1979). Assuming this temperature, the isotopic composition of a solution in equilibrium with the metamorphic quartz would be  $\delta^{18}O \sim +2$  and  $\delta^{18}O = -1$  for samples A-495-179 and A-495-172, respectively.

The salinity of sample A-495-179 (22 wt.%  $CaCl_2$  or approximately 2.5 Moles as determined by microthermometry) requires at  $300^{\circ}C$  a correction of  $\delta^{18}O = +2$  (Figure 49) for the isotopic composition of the solution (see

further details at III.2.2.4). This would give a total value of  $\delta^{18}\text{O} \sim +4$  for the solution present during retrogressive metamorphism. This figure is only an approximation but is not unrealistic and indicates a change in isotopic composition of the solutions since the period of retro metamorphism.

### III.2.2.3 Other quartz (Table 3)

A random sample of quartz from other drill-holes other than Na77 were also analysed for oxygen isotopic composition in order to test the isotopic compositional uniformity of the area. The results conform fairly well with those of drill-hole Na77. In particular, the four quartz specimens from veins and vugs of samples A-495-144, A-495-156, A-495-157 and A-495-191 present  $\delta^{18}\text{O}$  values which are similar to those of the late-stage quartz of Na77.

The  $\delta^{18}\text{O}$  values of quartz displayed in Table 3 point to  $\delta^{18}\text{O}$  solution values which confirm the presence of surface waters during their hydrothermal genesis. Samples A-495-157 and A-495-191 are from quartz veins within the dolerite sill. Results of their analyses and their corresponding  $\delta^{18}\text{O}$  solution values are indicative of the action of meteoric water even 40m within the dolerite sill.

An explanation for the  $\delta^{18}\text{O}$  values of sample A-495-164 has already been considered in discussing sample A-495-168.

The results from sample A-495-162 are important because this quartz crystallized from a very weak solution (0.4 weight % NaCl or 0.5 wt %  $\text{CaCl}_2$  equivalent). This means that the calculation of  $\delta^{18}\text{O}$  of the corresponding solution: (-7.6‰ to -4.5‰ SMOW) does not require a correction for salinity and it serves as a further proof of the strong influence of meteoric waters in the hydrothermal processes in the Nabarlek deposit area.

Summarising the discussions above, the oxygen isotopic composition and the homogenization temperatures of the fluid inclusions in quartz from the Nabarlek uranium deposit, indicate the following:

- 1) The hydrothermal quartz shows an increase of  $^{18}\text{O}$  content with time of crystallization, i.e. the  $\delta^{18}\text{O}$  quartz values increase from early-

DRILL HOLE No.	SAMPLE No. A-495-	DEPTH (m)	$\delta^{18}\text{O}$ QUARTZ (% SMOW)	$T_H$ ( $^{\circ}\text{C}$ )	CALCULATED $\delta^{18}\text{O}$ SOLUTION (% SMOW)	MODE VALUE	SALINITY Mol. $\text{CaCl}_2$	CORRECTED $\delta^{18}\text{O}$ SOLUTION (% SMOW)	MODE VALUE
Na 23	144	305.5	16.8 $\pm$ .1	~100	-7.5	- 7.5	1.7	-5.5	-5.5
Na 55	156	83.9	15.1 $\pm$ .5	120	- 8.5 to -7.5	- 8.0	2.4	-6.0 to -5.0	-5.5
Na 55	157	89.0	17.0 $\pm$ .5	100-145	- 9.0 to -1.8	- 4.6	3.9	-7.0 to +0.2	-2.6
Na 83	191	93.3	15.5 $\pm$ .5 (late-stage)	90-110	-10.8 to -9.4	-10.2	-	-	-
Na 83	191	93.3	15 (early-stage)	-	-	-	-	-	-
Na 83	186	416.4	10.8 $\pm$ .5	-	-	-	-	-	-
Na 74	164	39.5	13.8 $\pm$ .5 (late-stage)	120-140	- 9.2 to -6.8	- 7.5	-	-	-
Na 74	164	39.5	12.8 $\pm$ .5 (early-stage)	-	-	-	-	-	-
Na 72	162	22.5	12.3 $\pm$ .5	130-160	- 7.6 to -4.5	- 7.5	0.0	-7.6 to -4.5	-7.5

Table 3:  $\delta^{18}\text{O}$  values of quartz and the corresponding solutions calculated and corrected as in table 2.

to late-stage quartz.

2) This enrichment in  $^{18}\text{O}$  seems to be the consequence of increasing quartz-water fractionation due to decreasing temperature in the system, although a change in the isotopic composition of the fluids, because of the mixing of brines, cannot be ruled out completely.

3) All calculated  $\delta^{18}\text{O}$  values for corresponding solutions clearly indicate the presence of meteoric waters.

4) Small fluctuation of  $\delta^{18}\text{O}$  values of solutions from the general trend may be the result of mixing of brines due to different mixing ratios.

#### III.2.2.4 Calcite

Only three samples of calcite were available in drill-cores from Nabarlek deposits: a-495-110, A-495-144 and A-495-220. Although restricted in number, they were studied for oxygen isotopic composition because of their significance to hydrothermal alteration (A-495-220); their association with quartz of hydrothermal origin (A-495-144), and their association with pitchblende (A-495-110). These calcites represent the very last phase of hydrothermal mineralization, not only in each of these samples but in the whole paragenetic sequence as well. They are probably not contemporaneous, because of different homogenization temperatures of their fluid inclusions. Using the  $T_H$  and the equation (2), samples 220 and 144 point to  $\delta^{18}\text{O}$  values of the hydrothermal solutions within the range of surface waters. However, if salinity corrections are considered (see III.2.2.5) the indications of surface origin become less evident (Table 4). The corrected values may even indicate solutions of metamorphogenic origin (Taylor, 1974). This is probably the result of a very large rock/water ratio affecting the isotopic composition of the last hydrothermal solutions. Although sample A-495-110 did not contain fluid inclusions, its  $\delta^{18}\text{O}$  value is clearly in the range of fresh water limestone or the lower range of marine limestones (Taylor, 1967). This very fact is an indication of crystallization at low temperature (<50°C). As such, this temperature fixes the lower limit for the deposition of pitchblende and again indicates a  $\delta^{18}\text{O}$  solution value of surface water.



DRILL-HOLE No.	SAMPLE No.	DEPTH (m)	$\delta^{18}\text{O}$ CALCITE (% SMOW)	$T_H$ ( $^{\circ}\text{C}$ )	$\delta^{18}\text{O}$ SOLUTION (% SMOW)			SALINITY (Mol. $\text{CaCl}_2$ )
					CALCULATED (EQUATION (2))	CORRECTED FOR $\text{NH}_4\text{Cl}$	CORRECTED FOR SALINITY EFFECT	
Na- 1	A-495-110	39	$22.5 \pm .1$	(50)	-0.7	-0.2	<-0.2	?
Na- 23	A-495-144	305	$13.1 \pm .1$	95-105	-4.0 to -3.0	-2.8 to -1.8	-0.3 to +0.7	3
Na-176	A-495-220	38	$13.2 \pm .1$	125-165	-1.0 to +2.1	+1.0 to +4.1	+2.0 to +4.1	2

Table 4: Oxygen isotope values of calcites and corresponding brines calculated and corrected for temperature and salinity.

Another interesting feature of sample 144 is that it is the only one with quartz-calcite association. A temperature of 240°C can be derived from the fractionation of this mineral-pair using equation (5) and the corresponding  $\delta^{18}\text{O}$  determinations. The inferred temperature is completely at variance with the  $T_{\text{H}}$  of fluid inclusions from both minerals. As the  $T_{\text{H}}$  measured for primary inclusions in calcite (105°C) is considered to be a reliable value and the estimated  $T_{\text{H}}$  for inclusions in quartz ( $\sim 100^\circ\text{C}$ ) are generally acceptable, the quartz-calcite fractionation temperature rather indicates that these minerals were not in isotopic equilibrium at the time that each was formed.

### III.2.2.5 Calculation of $\delta^{18}\text{O}$ of parent solutions

The calculation of  $\delta^{18}\text{O}$  of solutions in equilibrium with oxides is based on  $\delta^{18}\text{O}$  values of minerals and homogenization temperatures ( $T_{\text{H}}$ ) of its fluid inclusions.

Although the analytical error in oxygen isotope ratios was rather poor in some instances and the  $T_{\text{H}}$  of inclusions in some samples presented a wide range of temperatures, nevertheless the corresponding  $\delta^{18}\text{O}$  values of the solutions are all within the range for surface water even when extreme  $\delta^{18}\text{O}$  mineral and  $T_{\text{H}}$  values of each case (Figure 47, Tables 2, 3 and 4, calculated values) are taken into consideration. As described by Taylor (1967), all these  $\delta^{18}\text{O}$  solution values are in the range of surface waters, and are most probably of meteoric origin.

Points of major concern regarding the reliability of calculated  $\delta^{18}\text{O}$  solution are the corrections which must be added to these values, due to the isotopic effect of:

- (a) the nature of the electrolyte used for establishing mineral-water fractionation factor;
- (b) the concentration of salts.

Experiments by Taube (1954) indicated that, although there is not a simple mathematical relationship between ionic potential and the ionic radius of the cations to calculate their effects on isotope fractionation,

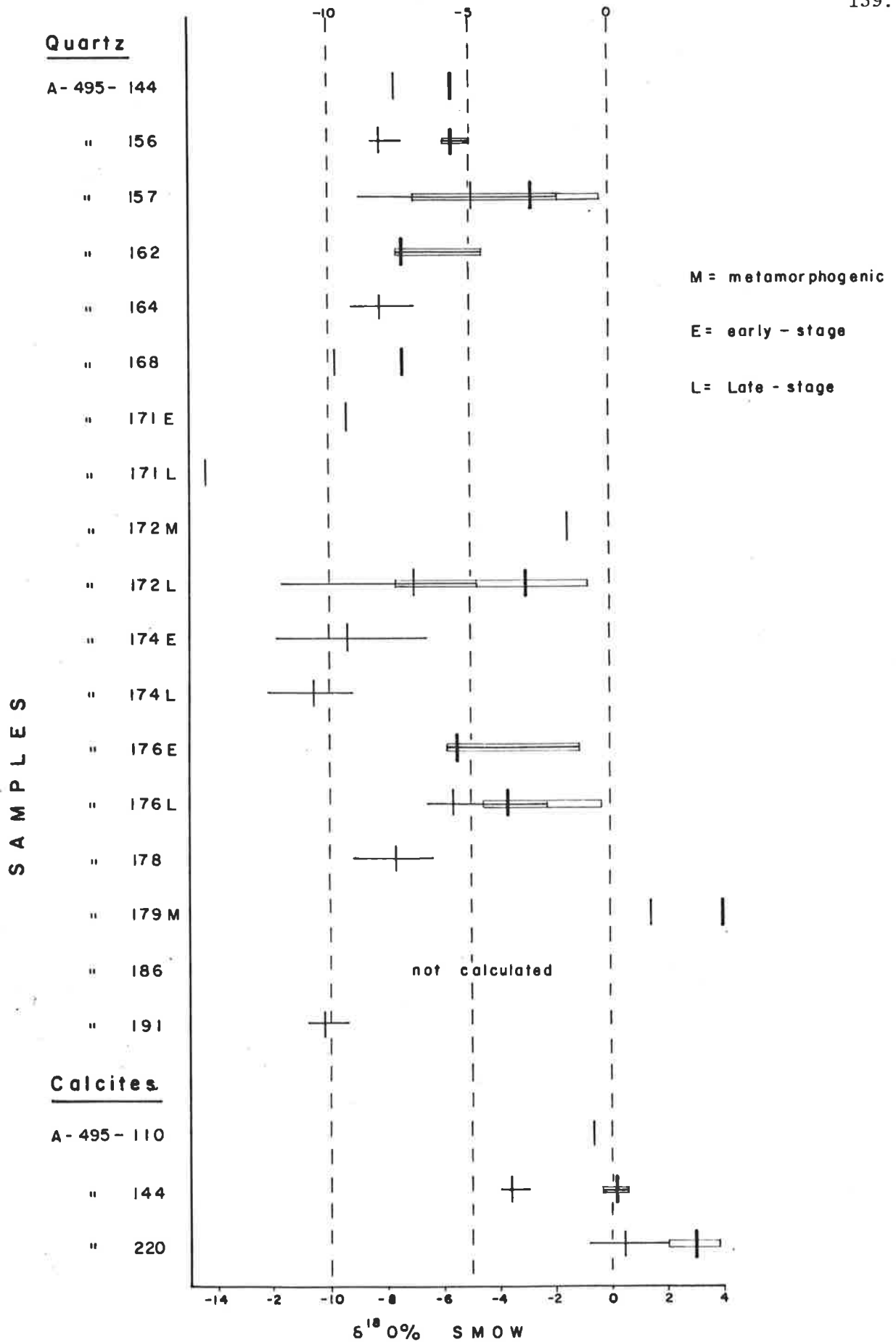


Figure 47: Calculated  $\delta^{18}O$  values of solutions in equilibrium with quartz and calcite of the Nabarlek uranium deposit. (Double line: values corrected for salinity effect).

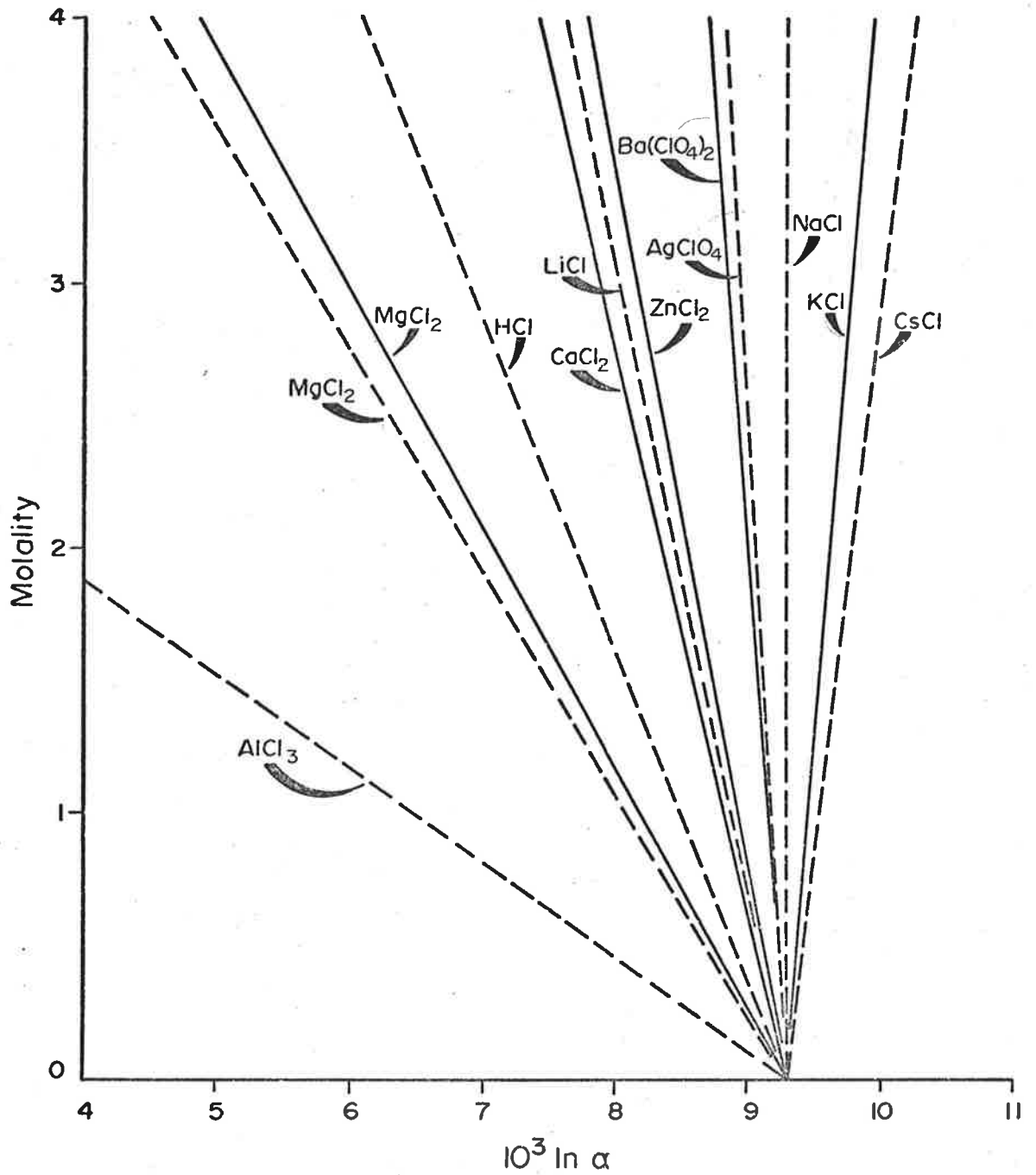


Figure 48: Water(liq.) - water vapour solute fractionation for salt solutions at 25°C (from Friedman and O'Neil, 1977. Dashed lines from Taube, 1954, and solid lines from Sofer and Gat, 1972).

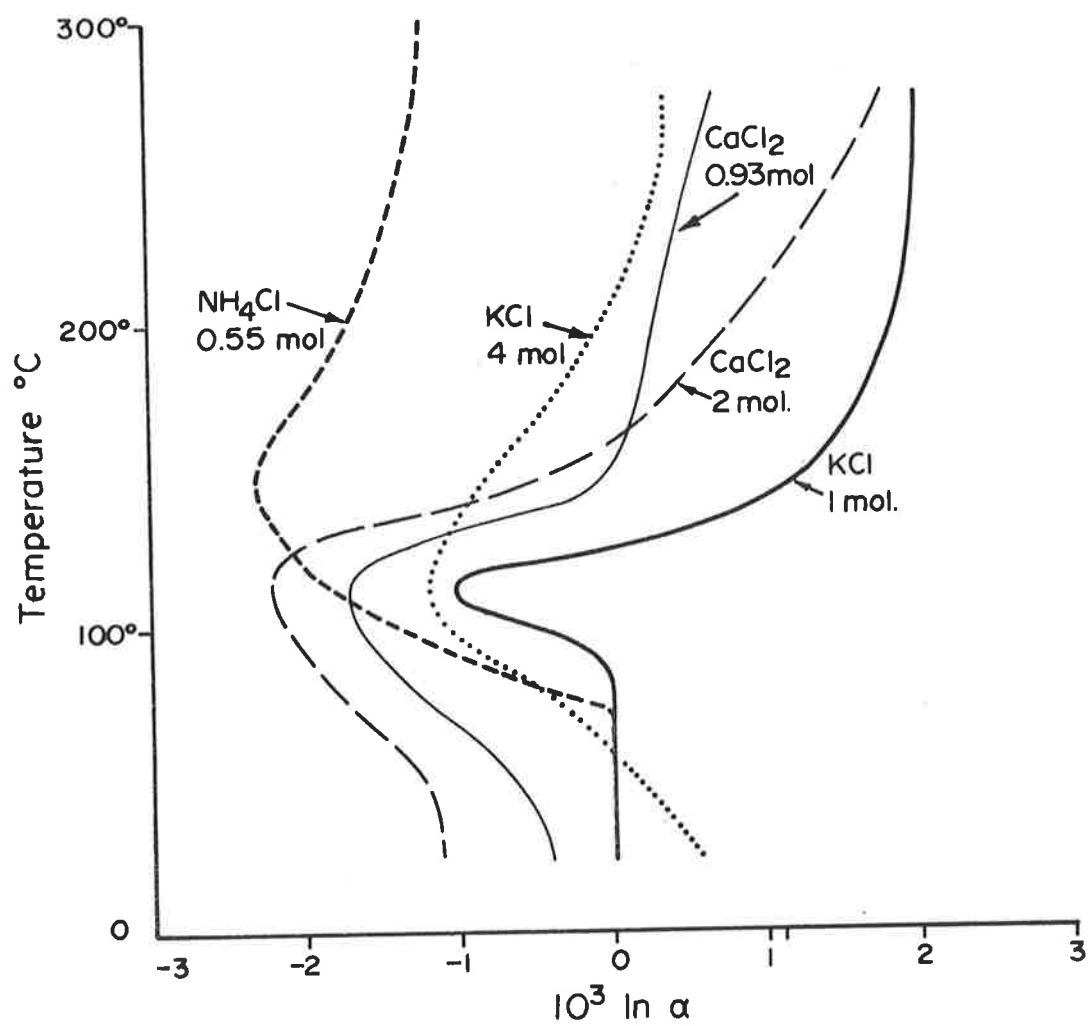


Figure 49: Isotopic effects of  $\text{NH}_4\text{Cl}$ ,  $\text{KCl}$ , and  $\text{CaCl}_2$  solutions (liq.)-water (liq.) between  $25^\circ\text{C}$  and  $275^\circ\text{C}$ . (Modified from Friedman and O'Neil, 1977).

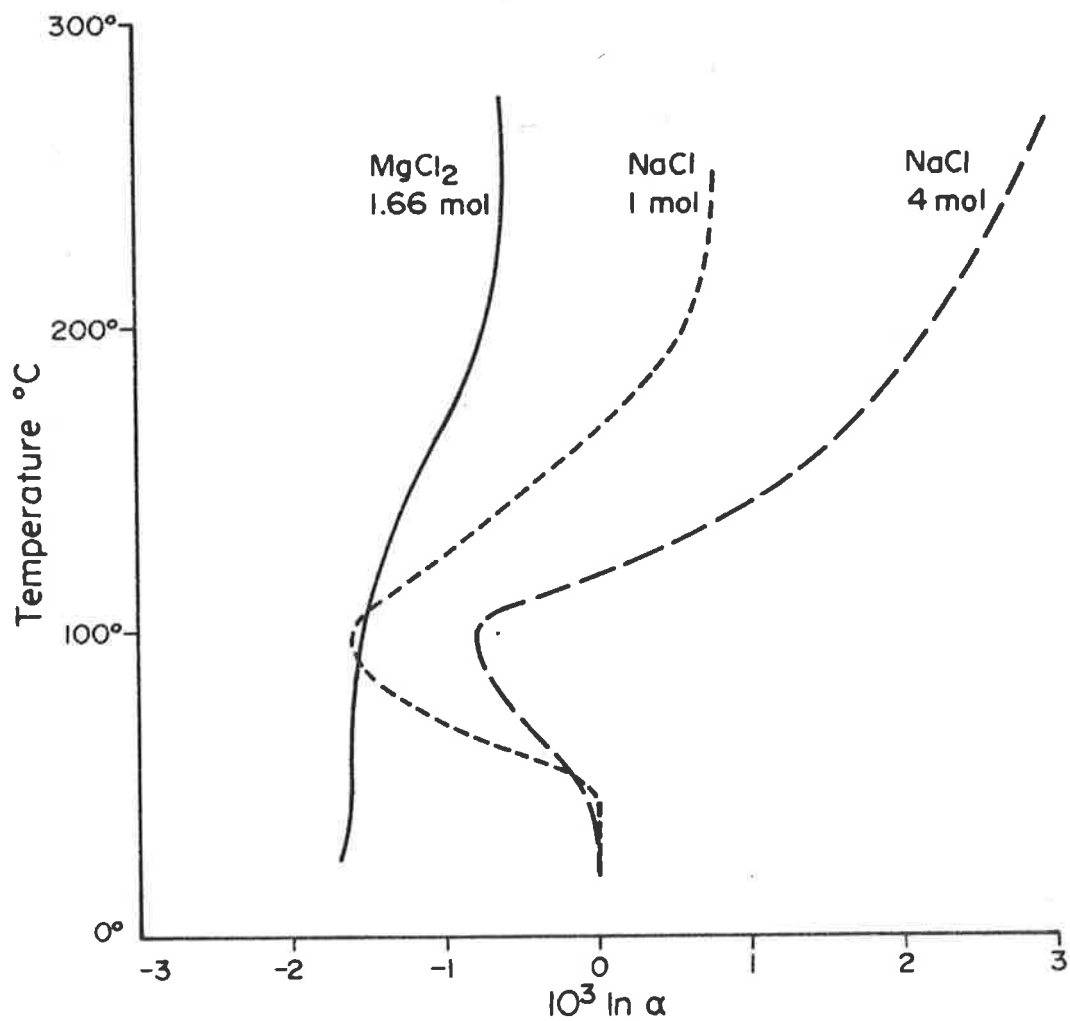


Figure 50: Isotopic fractionation between NaCl and MgCl<sub>2</sub> solutions (liq.) and pure water (liq.) between 25°C and 275°C. (From Friedman and O'Neil, 1977).

ionic radius and ionic potential are the major factors effecting the fractionation. Cations like  $\text{Al}^{3+}$  and  $\text{Mg}^{2+}$  were shown to produce the largest positive fractionation effects, i.e. concentrated  $^{18}\text{O}$  with respect to some other phase, while for others like  $\text{Cs}^+$  and  $\text{K}^+$  the effect was negative (Fig. 48). These data also show that  $\text{Na}^+$  solutions have no effect even at very high concentrations (up to 16 molar), and also that anions in general did not exert a major influence on isotope fractionation. Sofer and Gat (1972) extended the study of the isotopic effect of other cations including  $\text{Ca}^{2+}$  and  $\text{K}^+$ .

Both Taube's and Sofer and Gat's results are for  $25^{\circ}\text{C}$  and one would expect different fractionation values at higher temperatures. Truesdell (1974) carried out experiments to show the isotopic effects up to  $275^{\circ}\text{C}$ . It is interesting to see how the fractionation changes quite drastically with temperature for the majority of cations. At Nabarlek the hydrothermal solutions contain many cations which, from microthermometric and SEM studies, proved to be mainly  $\text{Ca}^{2+}$ ,  $\text{Na}^+$  and  $\text{K}^+$ . Truesdell's (op. cit) and Friedman and O'Neil's (1977) data give the general trend for fractionation between pure water and a saline solution as a function of temperature and concentration. The curves indicate maximal negative  $\Delta$  values in the  $100^{\circ}$ - $120^{\circ}\text{C}$  (Figures 49, and 50), and a change to positive  $\Delta$  values between  $130^{\circ}$  and  $200^{\circ}\text{C}$ .

The calcite-water fractionation was calculated as if the cumulative effects of  $\text{CaCl}_2$  and  $\text{NaCl}$  are the equivalent of an 0.55 mol  $\text{NH Cl}$  solution (O'Neil et al., 1969), which would require corrections as in Figure 49, Table 4. Difficulty in correcting for salinity is the fact that all experimental fractionation values were determined for solutions containing only one electrolyte whereas natural solutions contain at least several ions, such as:  $\text{Ca}^{2+}$ ,  $\text{Na}^+$  and  $\text{K}^+$ . The question is: would the isotopic effect of the solutions be the sum of effects due to each electrolyte? The thermodynamics of partitioning would seem to give an affirmative answer. Studies of isotopic fractionation caused by a complex solution at different temperatures have not been carried out. Therefore, the corrections were made assuming the salini-

ties to be  $\text{CaCl}_2$  equivalent and extrapolating the isotopic effects for an average molality of each sample. This assumption is reasonable in the present case because all the samples had salinities which are richer in  $\text{CaCl}_2$  than other chlorides, and because even  $\text{NaCl}$ , which has no isotopic effect at  $25^\circ\text{C}$ , requires negative correction around  $100^\circ\text{C}$ , the same as  $\text{CaCl}_2$  and  $\text{KCl}$  (Fig. 50). In other words, they all show the same trend in the range of temperature considered. Furthermore, the extent of the corrections, due to solute fractionation would not change our interpretation a great deal, regarding the source of hydrothermal solutions involved in the mineralization (Figure 47). Only in the case of one calcite would the correction have taken the  $\delta^{18}\text{O}$  solution value into the range of marine or metamorphic waters.

Finally, a further support for the meteoric origin of the hydrothermal solutions comes from a case where no corrections were needed for salinities: i.e. quartz sample A-495-162, because of the very dilute nature of the brine (as discussed on page 105). The calculated  $\delta^{18}\text{O}$  value of this solution is in the range of  $-7.6\%$  to  $-4.5\%$  SMOW, which points to meteoric origin of water.

#### III.2.2.6 Dolerite

Almost all dolerite samples are altered to a certain degree. Only drill-holes reaching the center of the sill provided intersections with nearly fresh rocks. These samples were analysed to check for any similarity with the alteration effects as studied at Skye, Scotland, by Taylor and Forester (1971).

Samples A-495-138 and A-495-143 are representative of unaltered dolerites. Although sample A-495-143 was slightly more altered than sample A-495-138, both yielded similar  $\delta^{18}\text{O}$  total rock values:  $+6.8 \pm .5\%$  and  $+6.6 \pm .1\%$  SMOW respectively. These figures are typical for the range of values of basic igneous rocks.

The altered dolerites show  $\delta^{18}\text{O}$  total rock values roughly in the same range as the unaltered ones. This is probably an indication that the alteration process took place within a closed system, with a large total rock over water ratio, a situation very different from Skye. The indication of



volumetrical dominance by dolerite, and a small volume of a hydrous component is in agreement with the observed preservation of the dolerite texture in altered rocks (Chapter I, p.8). According to Spry (1976) the "preservation of palimpsest igneous texture.... is favoured by low stress and an absence of intergranular fluid". This conclusion also points to the role of a residual hydrous phase as the major agent of alteration of the dolerite. If the alteration had been the product of newly introduced water the  $\delta^{18}\text{O}$  values of minerals and whole rock should present a pattern similar to those found at Skye.

Different  $\delta^{18}\text{O}$  total rock values observed in some altered samples, such as A-495-136 =  $+9.2 \pm 0.5\%$  SMOW or A-495-132 =  $+4.2 \pm 0.1\%$  SMOW (Appendix 1), are the result of their mineralogical composition. Although the number of individual mineral analyses is small, yet the alteration of plagioclase into sericite indicates the kind of changes to be expected - an increase of  $\delta^{18}\text{O}$  from  $7.8 \pm 0.5\%$  to  $10.2 \pm 0.1\%$  SMOW. Inversely, alteration of mafic minerals (mainly pyroxene,  $\delta^{18}\text{O} = +5.7 \pm 0.5\%$  SMOW) into chlorite involves a lowering of  $\delta^{18}\text{O}$  ( $\delta^{18}\text{O}$  chlorite =  $+4.8 \pm 0.1\%$  SMOW). Figure 51 shows that wholesale mineralogical changes have effected the total  $\delta^{18}\text{O}$  value of the rock as this is controlled by relative amounts of sericite and opaques, and not by interaction of extraneous fluids with the dolerite.

### III.2.2.7 Quartz-actinolite-schist

Although only one pair of retrogressed (A-495-211) and non-retrogressed (A-495-207) quartz-actinolite-schist was analysed, the samples showed an isotopic behaviour similar to that of dolerite. The  $\delta^{18}\text{O}$  values of whole rock samples are roughly the same. The mineralogical alteration follows the same pattern as dolerites: the feldspars break down into sericite and the actinolite into chlorite. The actinolite-chlorite alteration indicated a decrease in  $\delta^{18}\text{O}$  values. Quartz in both samples presented very similar  $\delta^{18}\text{O}$  values (Appendix 1). Obviously, these samples having been collected in an area closely related to the dolerites and the granites, one would expect the same type of alteration to have been operational in these schists.

### III.2.2.8. Granitic rocks

The role of the granite emplacement with regard to uranium mineralization at Nabarlek is not clear. Some genetic tie might have existed but if it ever existed it was probably obliterated by the later Oenpelli dolerite intrusion in the area. In drill-cores below the dolerite sill, only background radioactivity has been observed. Nevertheless, the oxygen isotope values of fresh and altered granite could shed some light on the derivation of uranium. For instance, a similarity between oxygen isotope ratios between granite alteration and mineralization could point to the leaching of granite as a source of uranium.

No absolutely fresh samples were available from the two core samples of granite. The sample A-495-181 is the least altered one. The whole rock  $\delta^{18}\text{O}$  value of this sample and the values of other granites show, more or less, only a slight difference between them (Table 5). The variation of  $\delta^{18}\text{O}$  is even smaller than that of the dolerites. Again, this is evidence that the alteration process occurred in a closed system with little, if any, influence from external fluids.

Quartz seems to be able to retain the isotopic composition it acquired during the crystallization of the granite (see III.2.2.9), although the fluid inclusions in the quartz gives evidence for the introduction of fluids of secondary origin. As is the case for the dolerites, sericite is the alteration product of feldspar. The granite feldspars show  $\delta^{18}\text{O}$  values in the same range as those of sericites, the  $\delta^{18}\text{O}$  values of which seem to be too high to be in equilibrium with the above-mentioned quartz (see Taylor, 1967) at temperatures normally associated with sericitic alteration. The feldspars probably were isotopically re-equilibrated during the alteration process.

The whole-rock  $\delta^{18}\text{O}$  value of sample A-495-181 is higher than that of the individual minerals (Table 5). The analyses were repeated but the results persisted. The actual reason for this inconsistency remains unknown.

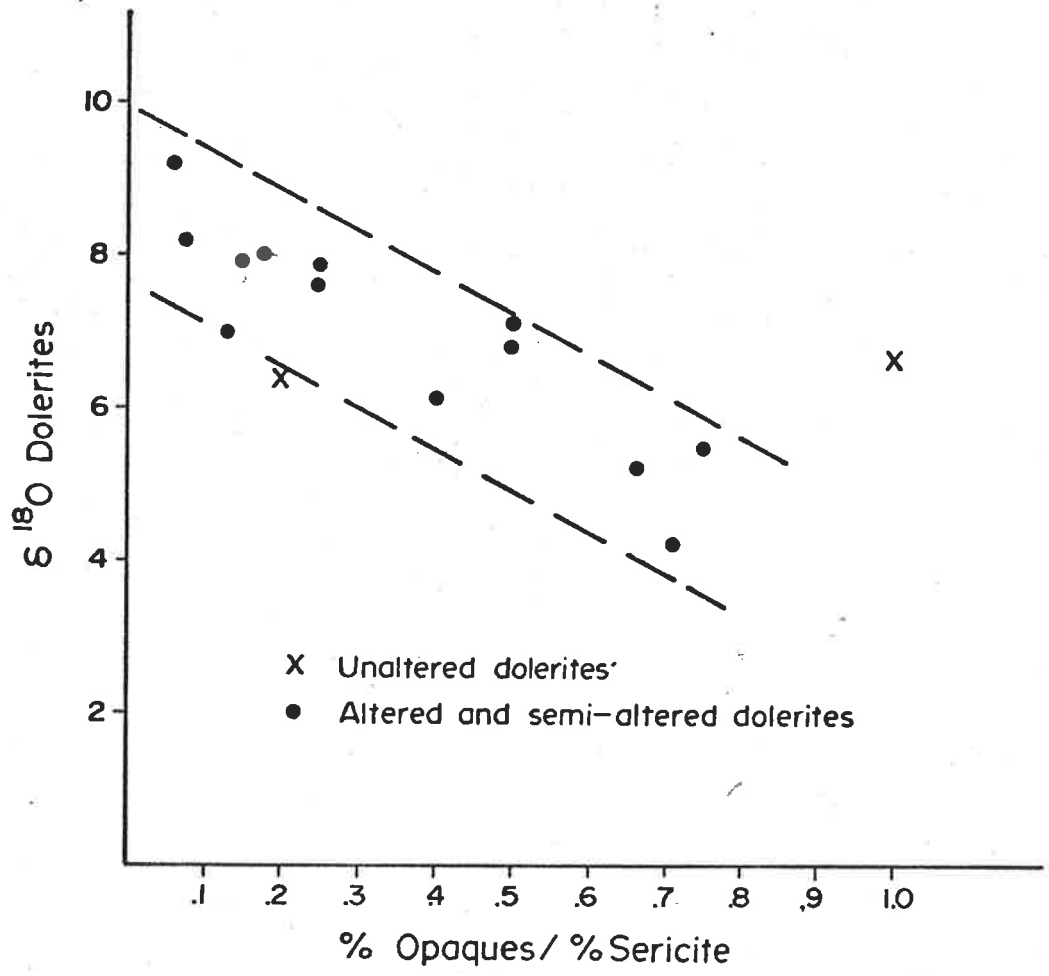


Figure 51: Variation of  $\delta^{18}\text{O}$  values of altered and unaltered dolerite as a function of whole-sale mineralogical changes in dolerite because of alteration. The diagram points to alteration in a closed system.

DRILL-HOLES	DEPTH (m)	SAMPLE No.	$\delta^{18}O$ (‰ SMOW)						
			WHOLE ROCK	QUARTZ	K-FELDSPAR	PLAGIOCLASE	SERICITE	CHLORITE	BIOTITE
Na-83	488.05	A-495-181	11.3 $\pm$ .1	10.9 $\pm$ .1	10.3 $\pm$ .5	-	10.2 $\pm$ .1	-	-
Na-83	469.90	A-495-182	10.3 $\pm$ .5	10.8 $\pm$ .1	-	10.4 $\pm$ .5	-	3.9 $\pm$ .5	6.3 $\pm$ .5
Na-83	451.75	A-495-183	-	11.5 $\pm$ .1	-	-	-	-	-
Na-23	487.1	A-495-146	10.5 $\pm$ .5	10.5 $\pm$ .5	-	-	9.3 $\pm$ .5	-	-
Na-23	481.8	A-495-147	10.3 $\pm$ .5	10.7 $\pm$ .1	10.9 $\pm$ .1	-	9.4 $\pm$ .1	-	-

Table 5: Oxygen isotope analyses of granitic rocks and their individual minerals.

### III.2.2.9 Pitchblende

Oxygen isotopic compositions of two different pitchblende-rich samples: A-495-110 and A-495-201 and one massive vein-pitchblende from Echo Bay, Canada, have been determined. The specimen from Echo Bay was used for comparison, because of its high purity. The  $\delta^{18}\text{O}$  values of the three samples indicated large depletion of  $^{18}\text{O}$  in pitchblende (Table 6). These values are in agreement with the theoretical prediction of strong  $^{18}\text{O}$  depletion in compounds with weak oxygen-cation bonds and heavy cation mass.

Higher  $\delta^{18}\text{O}$  values of pitchblende from sample A-495-201 may reflect the higher state of oxydation of the sample.

The  $\text{CO}_2$  yield was always larger than the ideal value for  $\text{UO}_2$  (Table 6). This may indicate an oxydation state of pitchblende higher than  $\text{UO}_{2.3}$  as used in the calculations. Furthermore, the samples from Nabarlek may have contained more than the estimated 5% impurities (such as: chlorite in sample A-495-110 and sericite in sample A-495-201).

Because of these complications,  $\delta^{18}\text{O}$  determinations of pitchblende samples were limited to those reported here.

### III.2.2.10 Temperatures and isotopic equilibrium

Oxygen isotopic temperatures were calculated from the few mineral-pairs separated from various samples.

In minerals from granitic rocks, an attempt to use quartz-sericite pairs gives a maximum  $\Delta$  quartz-muscovite of 1.3 for the sample A-495-147. This value is too small to be compared with any of the experimental quartz-muscovite of 1.3 for the sample A-495-147. This value is too small to be compared with any of the experimental quartz-muscovite curves: Taylor (1967, p.125), Blattner (1975), or Friedman and O'Neil (1977, Fig. 24). Extrapolation would indicate temperatures above  $800^\circ\text{C}$  which is too high to be in agreement with the petrological reality. Only in the case of sample A-495-146, Table 7, when taking into account the standard deviation of each mineral in opposite directions in order to give the largest  $\Delta$ , could the temperature be calculated as low as  $610^\circ\text{C}$ , using the calibration curve presented by Friedman and O'Neil

Sample No.	Drill-hole	Depth(m)	CO <sub>2</sub> yield (%)	$\delta^{18}\text{O}_{\text{‰}}$ SMOW
A-495-201	Na 1	44.4	126	-4
A-495-110	Na94	42.1	129	-7.5
Echo Bay	-	-	112	-8

Table 6:  $\delta^{18}\text{O}$  values of some pitchblendes.

(1977, Fig. 24, curve B). These apparent temperatures are indications that the quartz and sericite are not in isotopic equilibrium. Apparently the quartz did not change from its original  $\delta^{18}\text{O}$  composition to any great extent, while sericite acquired an isotopic composition corresponding to the alteration process. By the same argument the temperature calculated from the quartz-chlorite mineral pair becomes meaningless. The quartz-biotite pair has not been used because of a possible contamination by chlorite and the fact that the calibration curves by Shiek and Taylor, 1969, hinge on the values of muscovite, which is useless in our case.

In dolerites and schists, the mineral pairs with quartz always yielded temperatures that were well above the homogenization temperatures of fluid inclusions in corresponding vein quartz (Table 7). The reason for this discrepancy is probably due to the fact that the minerals from each pair were not coeval. This has been proven to be the case for the hydrothermal quartz veins where early- and late-stage quartz were identified. Furthermore, minerals like calcite and chlorite may have exchanged  $^{18}\text{O}$  after their formation, while quartz is less affected by isotopic re-equilibration.

An independent indication of the lack of isotopic equilibrium, even among hydrothermally formed minerals is given by the samples A-495-157, A-495-156, and less specifically by A-495-144. The mineral-pairs, quartz-sericite, quartz-magnetite, and sericite-magnetite from the first sample, quartz-chlorite and chlorite-magnetite from the second sample, and quartz-sericite, quartz-calcite, and calcite-sericite from the last sample, show temperatures that are in conflict with each other (Table 7). This lack of equilibrium may be the consequence, not only of the temperature change during the alteration process, but also of the mixing of solutions as indicated by fluid inclusion studies, and kinetic factors in establishing equilibrium during low temperature genesis.

The feldspar-pyroxene pair presented a temperature range which, at its upper limit, may represent the actual temperature of crystallization of the dolerite. However, at high temperatures the feldspar-pyroxene equilibrium

SAMPLE No.	MINERAL PAIR	TEMPERATURE °C	CURVES AND EQUATIONS (p. 93) USED
<u>Granites</u> (see Table 5)			
A-495-181	quartz-K-feldspar	>1000	(3)
	quartz-muscovite	>1000	(4)
A-495-182	quartz-plagioclase	> 950	(Figure 25)*
	quartz-chlorite	370± 40	(10)
A-495-146	quartz-muscovite	> 800	(4)
	quartz-muscovite	> 610	(Figure 24)*
A-495-147	quartz-muscovite	>1000	(4)
	quartz-muscovite	800± 50	(Figure 24)*
<u>Dolerites and schists</u> (see Appendix 1)			
A-495-136	muscovite-chlorite	150± 10	(9)
A-495-138	feldspar-pyroxene	500±180	(Figure 25)*
A-495-144	quartz-muscovite	275	(4)
	quartz-calcite	240± 15	(5)
	calcite-muscovite	395	(8)
A-495-156	quartz-chlorite	220± 30	(10)
	quartz-magnetite	445± 40	(Figure 22)*
	chlorite-magnetite	impossible	(11)
A-495-157	quartz-muscovite	245± 50	(4)
	quartz-magnetite	300± 20	(Figure 22)*
	muscovite-magnetite	380± 35	(Figure 22)*
A-495-176	quartz-chlorite	225± 20	(10)
A-495-186	quartz-muscovite	>1000	(4)
A-495-211	quartz-chlorite	285± 20	(10)

\* see Friedman & O'Neil, 1977.

Table 7: Oxygen isotope geothermometry of samples from Nabarlek uranium deposit.



curve becomes very steep and the estimation of temperatures becomes inaccurate. The high standard deviation of the mineral pair in sample A-495-138 makes the temperature estimate ambiguous (see Friedman and O'Neil, 1977, Fig. 25).

As sericite and chlorite are both products of the same hydrothermal process, this implies that temperatures derived from this mineral pair might be of significance, assuming that equation (9) is correct. The temperature of  $150 \pm 10^\circ\text{C}$  as calculated for this mineral pair from sample 136, is indeed in the middle to upper range of temperatures found for fluid inclusions in quartz associated with this mineral pair. Because the analyses were very accurate, this temperature probably constitutes a confirmation of the temperature hydrothermal processes or of isotopic re-equilibration of these minerals during the declining temperature.

### III.3 Summary and Conclusions

A summary of the oxygen isotope study of minerals and rocks from Nabarlek indicates that:

- Quartz and calcite of hydrothermal origin can be distinguished on the basis of their isotope ratios into two stages of deposition. Quartz of an early-stage yields  $\delta^{18}\text{O}$  values within the range +9 to +11‰ SMOW. Quartz of a late-stage has  $\delta^{18}\text{O}$  values within the range of +14 to +17‰ SMOW. The two earlier calcites yield a  $\delta^{18}\text{O}$  value of +13.1‰ SMOW, whereas a later calcite has a  $\delta^{18}\text{O}$  value of +22.5‰.
- The differences in  $\delta^{18}\text{O}$  values between early- and late-stage quartz within a single sample, seems to be the consequence of increasing  $\alpha_{\text{quartz-water}}$  with decreasing temperature and to a lesser extent the result of fractionation effects due to variations in salinity.
- Calculated and corrected  $\delta^{18}\text{O}$  values of solutions in isotopic equilibrium with hydrothermal quartz at the time of their formation indicate a strong influence from meteoric waters. Differences in the range of  $\delta^{18}\text{O}$  values of solutions from different samples may be an indication of the influence of meteoric waters from different

sources and/or the mixing of solutions of different origin.

Solutions of different origin may be suggested by  $\delta^{18}\text{O}$  solution values calculated and corrected from the  $\delta^{18}\text{O}$  value of calcite.

- Fresh and altered total rock analyses of granite and dolerite point to very small relative water volumes involved in the alteration, the alteration being the result of an essentially closed system.
- Isotopic composition of pitchblende are difficult to interpret but probably point to higher than ideal oxydation stages  $\text{UO}_{2-n}$ , where  $n$  is larger than 0.7.
- Almost all temperature determinations showed values indicative of early silicates and alteration products. Only where the isotopic fractionation between two alteration products was given, a reliable temperature of  $150 \pm 10^\circ\text{C}$  was the result (sericite and chlorite).

## CHAPTER IV

DISCUSSIONS AND CONCLUSIONSIV.1 Introduction

Although the major uranium deposits of the Alligator River areas have been considered to be vein-type deposits (IAEA, 1974), or metamorphic hydrothermal deposits (Cornelius, 1976), in consequence of their close proximity to a major unconformity, they are generally classified in conjunction with similar Canadian deposits, as unconformity-related uranium deposits (Beck, 1977; Mathews, 1978). After an extensive discussion of their genesis, Mathews (1978) classified these deposits as the uranium deposits of uncertain genesis. In spite of all studies and extensive data material, a general agreement on the genesis of unconformity-related type of uranium deposits has not yet been reached.

The initial genetic controversy ranged from a "per descensum" model of origin (e.g. Knipping, 1974; Langford, 1974) to a deep-seated "per ascensum" model of origin (e.g. Beck, 1969; Little, 1974). Later concepts of genesis suggested a polygenetic origin in which diagenetic processes, occurring during and after the deposition of undeformed, arenaceous unconformity sediments, played a major role (e.g. Hoeve and Sibbald, 1978; Langford, 1978; Dahlkamp, 1979).

The results of these fluid inclusion and oxygen isotope studies of the Nabarlek deposit seem to favour some aspects of the polygenetic model and have yielded new data which may be useful for the understanding of the formation of these deposits.

IV.2 The Common Characteristics of Unconformity-related Uranium Deposits

The most conspicuous characteristic of this kind of deposit is obviously the close spatial association with a regional unconformity of Proterozoic age where psammitic to psephitic sediments of terrestrial facies overly Lower Proterozoic metasediments. The latter are usually the main host rocks of the mineralization. The degree of metamorphism and deformation

of these metasediments is variable. The most common hostrock lithologies are graphite and/or chlorite-bearing schists. Other lithologies include quartzites, sericite schists, and carbonates, but these are normally unmineralized. The overlying sedimentary cover has - apart from some faulting - undergone no deformation.

In the case of the Alligator River area, it has been shown that the mineralization is confined to the metasedimentary Cahill Formation, immediately underlying the Kombolgie Formation. The present ground level at Nabarlek is very close to the original unconformity (Figure 4), confirming its close association to the deposit. At Jabiluka the proximity to the unconformity is still more evident.

The second, also remarkable, characteristic is the association of the mineralization with a localized structural complexity which includes: fracturing, faulting, brecciation, collapse structures, shear zones and mylonitization. Alteration processes are usually associated with them. The latter is well represented at Nabarlek. These stratigraphically bound tectonic disruption zones have been the most likely channelways for solutions. This concept has also been supported by Needham and Stuart-Smith (1976) and Mathews (1978).

According to ore chemistry the orebodies can be categorized into monometallic or polymetallic. The former contains almost exclusively uranium while the latter contains significant amounts of Ni, Cu, Ag, Au or Bi. Some of these metals may have economic value. Both types of deposits have in common a very low Th content. This is an important chemical characteristic and indicates the transport of uranium in the hexavalent state (Mathews, 1978). Nabarlek is a monometallic deposit while Jabiluka contains Cu, Pb, Au, Ag, Bi, and Ni. Only gold has economic value (Hegge, 1977).

The geochronological data (Hegge, 1977; Table 3) of unconformity-related deposits place the formation of the ores well after the deposition of overlying sediments. This implies deposition of uranium under an arenaceous cover of at least a few hundreds of metres (Smart et al., 1975). The deposi-

tion of Kombolgie sandstone in the Pine Creek Geosyncline, occurred between 1688 and 1370 m.y. whereas the age of the last alteration event affecting the Nabarlek area (which is related to the uranium mineralization) can be bracketed between 850 and 1000 m.y., (Page et al., 1979). Hills and Richards (1976) found no uranium older than 900 m.y. at Nabarlek and Jabiluka. These ages - if they are equilibrium ages - clearly indicate the formation of these two deposits under the Kombolgie sandstone cover.

#### IV.3 Data of the Present Work and the Conditions of Uranium Mineralization

The data obtained during the present work are not comprehensive enough to allow the formulation of a precise genetic model for the Nabarlek uranium deposit. Nevertheless in combination with other data, they are significant and can be used to explain the formation of the Nabarlek deposit.

##### a) Mixing of very saline and dilute solutions

The fluid inclusion study clearly points to prevalence of mixing of fluids of different composition during the crystallization of hydrothermal quartz closely associated with uranium mineralization in the Nabarlek orebody and its environments. This conclusion is particularly supported by the salinities of inclusions in sample A-495-162 and in many others, especially A-495-172 and A-495-176. Quartz from these last two samples indicated fluid inclusions with concentrated brines of variable salinities (9.0 to 30.5 wt.%  $\text{CaCl}_2$  equivalent). Another proof for varying salinities follows from the inclusion in sample A-495-172D (p. 42) where fluid inclusions of different entrapment ages presented a salinity gradient. Other samples which confirmed this conclusion is sample A-495-133, which demonstrated salinities as high as 38.0 wt.%  $\text{CaCl}_2$  equivalent. Comparing this value with sample A-495-162 with 0.5 wt.%  $\text{CaCl}_2$  equivalent, demonstrates the wide range of salinities within one crystal or group of crystals (see Appendix 2).

In contrast to this variation, metamorphogenic quartz seems to present only saturated brines according to data of sample A-495-179 from Nabarlek and sample A-495-11 (Appendix 5) from Jabiluka.

Further indications of mixing of fluids were suggested by an inverse correlation of  $T_H$  and  $T_F$  of inclusions in some samples and the coexistence of  $CO_2$  and  $CH_4$ -rich inclusions in the same sample. Temperature and salinity usually present a positive correlation, the higher the temperature of the solution, the more salt can be dissolved. However, the solutions of fluid inclusions in two hydrothermal quartz samples (A-495-113 and A-495-157) and one calcite sample (A-495-220) - in all samples numerous microthermometric measurements were performed - presented a negative correlation: the salinities were higher (low  $T_F$ ) for low  $T_H$ . The coexistence of vapour- and liquid-rich inclusions is normally explained by boiling of the solution at the point of entrapment, resulting into inhomogeneous entrapment (Roedder and Coombs, 1967; Cuney, 1974). In the case of boiling, the liquid phase in a gas-rich inclusion must be a dilute solution because of low salt solubility in the vapour phase. In the present study, however, this was not the case, vapour-rich inclusions could contain a concentrated brine. Moreover, the low  $T_H$  of inclusions with high salinity would exclude boiling in any way (A-495-168). Thus, the only explanation for the presence of these volatile saline brine inclusions contemporaneous with  $CH_4$  or  $CO_2$ -rich inclusions seems to be an exsolution of these volatile compounds carried by dilute solutions upon mixing with saline brines.

Samples which provide evidence of this mixing process of brine and  $CO_2$ -rich solutions are concentrated along a shear zone with the main orebody (Figure 7), which occurrences suggest mixing in zones of high permeability.

b) Chemical composition of the concentrated and dilute  $CO_2$  or  $CH_4$ -rich solutions

There seems to be an initial difference in fluid chemistry between inclusions in quartz of metamorphogenic or hydrothermal origin. Both display inclusions with high salinities. The hydrothermal quartz, however, has a large range of salinity and variety of chlorides. Most common are chlorides of Ca, Na and K, and less frequently of Mg, Al and Fe.

These widely varying salinities, which were exhaustively investigated by microthermometry and SEM, are probably the main characteristics of fluid inclusions associated with uranium mineralization at Nabarlek and Jabiluka. The presence of true daughter minerals (in the genetic sense), is generally limited to NaCl. Its presence in  $\text{CaCl}_2$ -rich brines is interesting, as brines have normally been described as NaCl-rich brines. It has been demonstrated that these NaCl daughters in the  $\text{CaCl}_2$ -NaCl- $\text{H}_2\text{O}$  system only constitute a minority component.

The SEM has identified other solid phases. Chlorite, sericite, kaolinite, hematite, and carbonate were the more frequent ones. Their random occurrence in inclusions point to an heterogeneous entrapment. These minerals were probably formed during the alteration process that formed the hydrothermal quartz. The autoradiography suggested the presence of pitchblende in some fluid inclusions indicating the contemporaneity of fluid mixing, alteration process and mineralization.

Ordinary microscopy has detected liquid  $\text{CO}_2$  mainly in metamorphogenic quartz. Liquid  $\text{CO}_2$  was only rarely seen in hydrothermal quartz, although low liquid/gas ratios are frequent. The crushing of the host mineral for this type of inclusions always yielded a very prominent release of gas. Reaction with  $\text{Ba}(\text{OH})_2$  solution (indicating  $\text{CO}_2$ ) and dissolution of the gas bubble in kerosene (test of  $\text{CH}_4$ ) indicated that hydrocarbons are more common than  $\text{CO}_2$ . Melting temperature of gas hydrates and the use of a thermo-barometric crushing stage confirmed the predominance of  $\text{CH}_4$  over  $\text{CO}_2$ .

### c) Origin of fluids

Considering the common occurrence of mixing of fluids of different salinities, a point of major interest is the origin of each fluid. The oxygen isotope data from Nabarlek indicated a strong influence of meteoric waters in the formation of hydrothermal quartz. The  $\delta^{18}\text{O}$  value of water in isotopic equilibrium with metamorphogenic quartz (A-495-179) is in the range of metamorphic fluids (Figure 47). The  $\delta^{18}\text{O}$  value of water in isotopic equilibrium with calcites was higher than those in equilibrium with hydro-

thermal quartz. As the calcites seem to represent the last mineral in the paragenetic sequence, the  $\delta^{18}\text{O}$  value of water in equilibrium with these calcites may have at that stage, re-equilibrated isotopically with the metamorphic rocks and their alteration products. This trend thus reflects the demise of the influx of meteoric water. The reverse situation occurred during the formation of the early hydrothermal quartz as the mixing with metamorphogenic fluids would probably have increased the  $\delta^{18}\text{O}$  of early-stage meteoric waters.

In conclusion, the calculated  $\delta^{18}\text{O}$  values of different aqueous solutions show evidence of mixing of meteoric and metamorphogenic fluids.

d) Formation of highly saline solutions

Both at Jabiluka and Nabarlek the presence of saturated saline solutions was clearly indicated by fluid inclusion data. At Nabarlek the fluid inclusion and the oxygen isotope data indicated a mixing of aqueous solutions of different salinities where the dilute brines certainly had a meteoric origin and the concentrated ones were of metamorphic origin.

According to Crick and Muir's (1979) model of ore genesis in the Pine Creek Geosyncline, the formation of concentrated brines at Jabiluka could have been the result of dissolution of evaporites if one considers their arguments of carbonate crystal morphology as valid for evaporite origin. However, at Nabarlek no carbonate units are known. An alternative explanation is a possibility that these highly saline metamorphogenic fluids have been formed from  $\text{Ca}^{++}$  and  $\text{Na}^{++}$  released during the retrogressive alteration of the Oenpelli Dolerite and amphibolite schists. Chemical analyses of fresh and altered rock-types show a nearly total depletion of Ca and Na in the altered state (Appendix 4). These analyses indicate a release of 286 kg of Ca and 47 kg of Na by the alteration of 1 cubic meter of dolerite. This could also explain why the major fluid constituent is Ca instead of Na and the almost complete absence of Mg as determined by SEM. Although Mg is more frequent at Jabiluka, SEM studies still indicate that Ca is the more impor-



tant component of the fluid inclusions (Plate XVIII).

e) Temperature and pressure

No precise temperature determinations were possible for metamorphic quartz (A-495-179) but the temperature was well above that of crystallization of hydrothermal quartz.  $T_H$  values of  $CO_2$ -rich inclusions in sample A-495-179, and the temperature indicated by the mineral assemblage for the retrogressive metamorphism at Jabiluka (Binns, et al., 1979) suggest  $300^\circ C$  as the minimum estimate for the recrystallization of quartz. Data from sample A-495-179 indicate pressure of 1 kbar for  $300^\circ C$ .

During the formation of hydrothermal quartz, evidence for temperature changes were recorded in some samples: A-495-172 (different  $T_H$  in different quartz crystals); A-495-176 (different temperature between early- and late-stage quartz); or even in fluid inclusions from single quartz crystal (A-495-172A). The range of  $T_H$  for hydrothermal quartz is  $69.5^\circ C$  to  $150^\circ C$ . The presence of many large primary inclusions containing only a liquid phase suggest temperatures even lower than those obtained by microthermometry. The decrease of temperature could have been due to the regional cooling of the whole area but could also have a result of mixing of fluids of different temperatures. Microbarometric crushing stage data indicated fluid pressures above  $60 \text{ kg/cm}^2$  (= 58.8 bars).

IV.4 Genetic Models

A combination of geological, fluid inclusion and oxygen isotope data results into a general model which conforms to the type of hydrothermal uranium deposits, as presented by Rich et al. (1977), p.70 and 71:

- a) The deposit has a very limited vertical extent.
- b) A very close spatial relationship with the unconformity between the Kombolgie sandstone and the metasedimentary Cahill Formation.
- c) Fluid inclusion homogenization temperatures of hydrothermal quartz and oxygen isotope temperature of chlorite-sericite mineral pair, indicate low temperature and pressure.
- d) Fluid inclusion data indicate that mineralization took place at

the confluence of very dilute solutions with low CO<sub>2</sub> content and concentrated saline brines.

- e) The deposit is essentially monometallic and presents very simple gangue minerals: chlorite and sericite and small amounts of iron oxide and quartz.
- f) The age of uranium mineralization is much younger than the unconformity.
- g) The calculated  $\delta^{18}\text{O}$  value of the fluid in equilibrium with hydrothermal quartz, which contain the fluid inclusions, indicate a predominance of meteoric water.
- h) The topography of the orebody pinches out at shallow depth which suggests formation by a descending ore fluid.

The agreement with the Rich et al. (1976) model may support the supposition of a thin arenaceous cover during the process of ore formation. Actually the true thickness of the Kombolgie Formation at the time of ore deposition is difficult to derive from present data. A few kilometres to the northwest and also to the south, the Kombolgie escarpments indicate thicknesses of more than 50m, but the amount of sandstone eroded is not known. At Green Ant Hill, the nearest Kombolgie sandstone outcrop (Figure 4), the estimated present thickness is less than 20m, but similarly, the amount of sediments eroded is unknown.

Considering these observations and the great stability of the basement since Carpentarian time, the original thickness of the Kombolgie Formation was probably not more than two hundred metres.

At Jabiluka, the Kombolgie Formation varies between 20-260m (Hegge, 1977), that is: under present (eroded) conditions.

Langford (1978) proposed the formation of ore during deposition of the initial cover rocks and subsequent changes after deep burial. But his concept of restricted permeability in the metasediments by chlorite and sericite seems to be in conflict with the concept of fluid loss which influenced Pb-isotope ratios. Furthermore, at Nabarlek and Jabiluka (Ypma and

Fuzikawa, 1979; and present study) the numerous fluid inclusions with  $T_H$  values well below  $100^{\circ}\text{C}$  cannot be considered as a relict of low temperature as suggested by Langford (1978). Moreover, these two deposits have no radiometric age determination older than 900 m.y. which does not support Langford's proposed genesis.

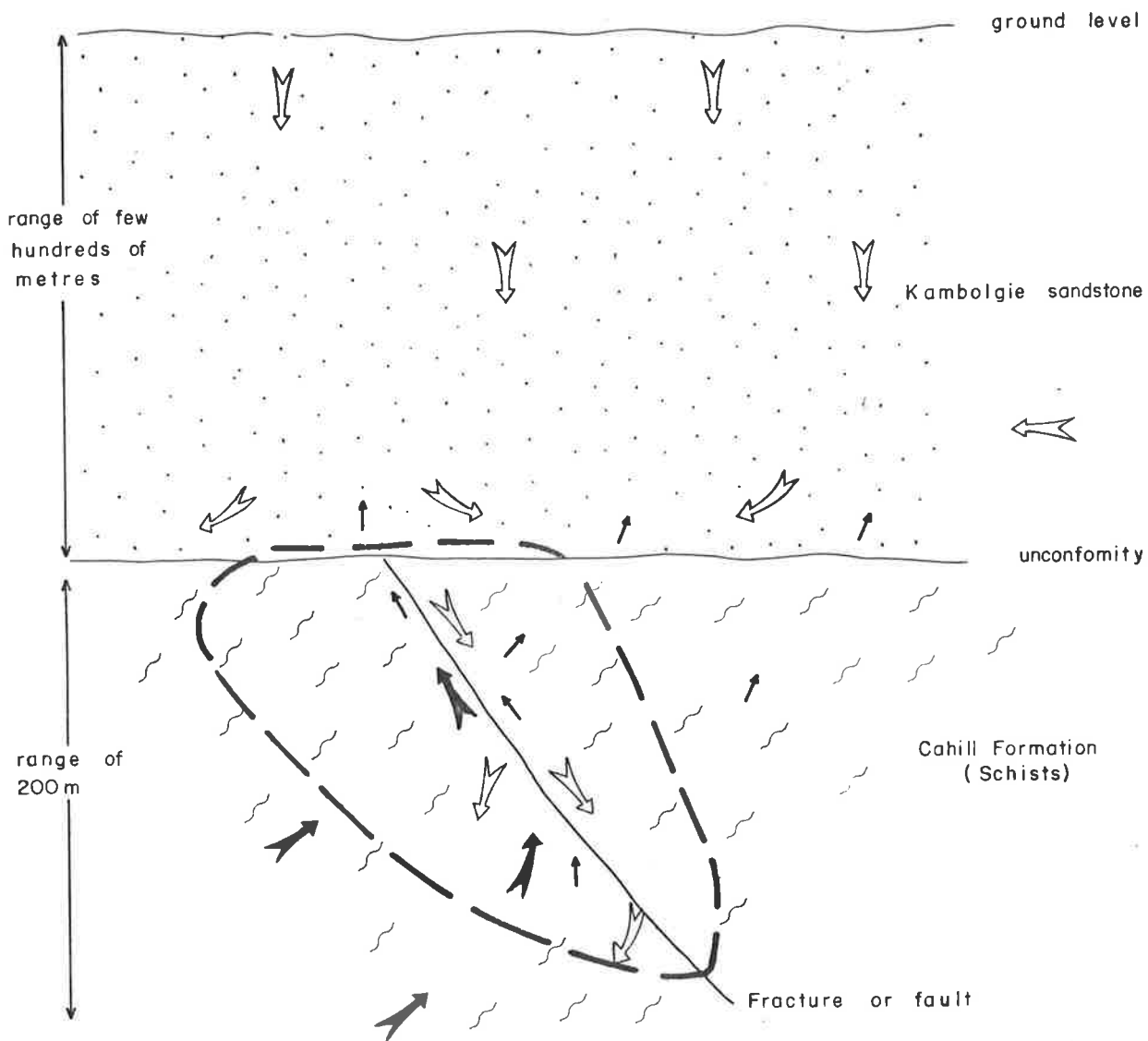
Ferguson's (1979) model of paleokarst and Crick and Muir's (1979) model of diapiric breccia as the basis for surface bound genesis of the Alligator River uranium deposits cannot be generally applicable because even at Jabiluka, for instance, 80% of ore occurs in schists and at Nabarlek no carbonate units are known.

The data of present work supports a hydrothermal emplacement as a consequence of meteoric waters mingling with low temperature-hydrothermal fluids as proposed by Ryan (1979). The only ingredient that is missing in this model is the derivation of mineralizing fluids from granitization, anatexis, and expulsion of metal-bearing connate waters, which, at Nabarlek, is not supported by geological and geochronological data. At the time of ore formation no such igneous or metamorphic events were present.

Considering the geological framework of the Alligator River Uranium Province, the most obvious place for the mixing of different aqueous solutions to occur is the unconformity and the tectonic disturbance spatially associated with the unconformity, because these structural discontinuities were the obvious channelways for the circulating solutions (Figure 52).

A conclusion of the present study is that the presence of an arenaceous cover seems to be the essential factor in the location of uranium deposits near unconformities, because the conditions for the mixing of fluids is greatly facilitated at this interface. The common presence of "injected chlorite" near the base of the Kombolgie Formation strongly supports this conclusion. There is little doubt about the good permeability and porosity of the Kombolgie sandstone. This had already been noted by Ryan (1979). It is an ideal aquifer for waters of meteoric origin.

Waters percolating and residing in the Kombolgie sandstone would







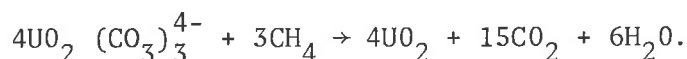
-  Flow of Meteoric waters
-  Flow of saline solutions
-  Flow of gases (CH<sub>4</sub> + CO<sub>2</sub>)
-  Area of mixing of solutions and U deposition

Figure 52: Schematic presentation of the environment of U deposition at Nabarlek.

have a low probability of  $^{18}\text{O}$  isotopic reequilibration with quartz of the sandstone because Si-O-Si bonds are the strongest in the silicate structures (Taylor, 1967). The  $\delta^{18}\text{O}$  values of meteoric waters would, therefore, not be significantly altered and would fractionate accordingly during crystallization of hydrothermal quartz.

Although the basement rocks near unconformities are usually more radioactive, the presence of less permeable sediments overlying an unconformity would prevent a large-scale circulation and mixing of meteoric waters with solutions present in underlying basement. Such radiometric anomalies tend to be small and uneconomic, whereas a permeable cover (such as the Kombolgie Formation) would allow scavenging solutions to accumulate large deposits.

Meteoric waters percolating downwards through porous and permeable sediments reaching an unconformity will follow permeable strata and brittle structures such as breccias and cataclastic shear zones. These tectonic disturbances in the metasediments are places where the meteoric waters can penetrate more easily and mingle with metamorphogenic fluids of high salinity containing uranium as uranyl complexes. The flow of fluids may be caused by gravity (such as a gently dipping unconformity); a thermal gradient, or disparity in solution densities (Rich et al., 1977). The system as a whole, due to variations in temperature, pH, and the exsolution of gases could lead to the precipitation of uranium. Methane and other light hydrocarbons as present in the dilute fluids are strong reductants and may have played a major role in the reduction of uranyl complexes. The oxydation of  $\text{CH}_4$  to  $\text{CO}_2$  is capable of reducing  $\text{U}^{6+}$  to  $\text{U}^{4+}$  and precipitating pitchblende (Langmuir, 1978) through a reaction similar to:



The Jabiluka mineralization is slightly different from Nabarlek and the fluid inclusion data are not enough to indicate a proper model. Nevertheless, fluid inclusion data of seven drusy dolomite and quartz samples indicated a fairly reliable  $T_{\text{H}}$  of 110-130°C. For the dolomites, Sun (1979, written communication) found  $\delta^{18}\text{O}$  values ranging from +15‰ to +26.4‰ SMOW.

The corresponding  $\delta^{18}\text{O}$  water are -4.2‰ SMOW and +7.2‰ SMOW. These data suggest again the occurrence of mixing of dilute meteoric and concentrated metamorphic waters in a range of temperature equivalent to Nabarlek.

A P P E N D I C E S

APPENDIX 1

List of studied samples from Nabarlek uranium deposit with  $\delta^{18}\text{O}$  values.

<u>Drill-hole No.</u> Depth(m)	Sample No.	Description	Minerals	$\delta^{18}\text{O}$ (% SMOW)
<u>Na 1</u> 44.37	A-495-110	Massive pitchblende in chlorite rock w/fibrous calcite veinlets.	calcite pitchbl.	+22.5 $\pm$ .1 -7
	A-495-113	Massive chlorite rock w/quartz. The quartz contain inclusions of chlorite.	not analysed	
<u>Na 4</u> 42.40	A-495-116	Massive pitchblende in chlorite rock.	not analysed	
<u>Na 5</u> 80.1	A-495-120	Altered dolerite (chlorite = 50%; sericite = 40%; opaques = 10%; and quartz = 2%).	total rock	+ 7.6 $\pm$ .5
<u>Na19</u> 67.85	A-495-127	Altered dolerite (chlorite = 50%; sericite = 30%; and opaques = 20%).	total rock	+ 5.2 $\pm$ .5
	A-495-130	Altered dolerite (chlorite = 60%; sericite = 20%; biotite = 10%; and opaques=10%).	total rock	+ 7.1 $\pm$ .5
<u>Na22</u> 67.85	A-495-132	Altered dolerite (chlorite = 35%; sericite = 35%; biotite = 5%; and opaques (large amount of haematite flakes) = 25%).	total rock	+ 4.2 $\pm$ .1
	A-495-133	Altered dolerite (chlorite = 20%; sericite = 50%; biotite = 10%; and opaques = 20%).	total rock	+ 6.1 $\pm$ .5
	A-495-134	Altered dolerite (chlorite = 50%; sericite = 40%; biotite = 1%; and opaques = 3%).	total rock	+ 8.2 $\pm$ .5



APPENDIX 1 (cont'd) List of studied samples from Nabarlek uranium deposit with  $\delta^{18}\text{O}$  values.

Drill-hole No. Depth(m)	Sample No.	Description	Minerals	$\delta^{18}\text{O}$ (‰ SMOW)
<u>Na22</u> (cont'd)				
79.03	A-495-135	Semi-altered dolerite (plagioclase = 20%; pyroxene = 50%; olivine = 3%; sericite = 20%; biotite = 1%; and opaques = 3%).	total rock	+ 7.9 $\pm$ .1
110.6	A-495-136	Altered dolerite (chlorite = 50%; sericite = 45%; opaques = 3%; and biotite = 1%).	total rock sericite chlorite	+ 9.2 $\pm$ .5 +10.2 $\pm$ .1 + 4.8 $\pm$ .1
161.2	A-495-137	Altered dolerite (composition similar to A-495-134. opaques = 5%).	total rock	+ 7.0 $\pm$ .1
211.6	A-495-138	Dolerite (plagioclase = 40%; pyroxene = 50%; olivine = 5%; sericite = 3%; and opaques = 3%).	total rock plagioclase pyroxene	+ 6.6 $\pm$ .1 + 7.8 $\pm$ .5 + 5.7 $\pm$ .5
<u>Na23</u>				
285.0	A-495-143	Dolerite (plagioclase = 30%; pyroxene = 50%; olivine = 3%; sericite = 10%; and opaques = 5%).	total rock	+ 6.8 $\pm$ .5
305.5	A-495-144	Quartz-calcite veinlet in chlorite-sericite schist.	quartz calcite sericite	+16.1 $\pm$ .1 +13.1 $\pm$ .1 +11.3
487.1	A-495-146	Altered granite (quartz = 40%; sericite = 50%; chlorite = 5%; and opaques = 1%).	total rock quartz sericite	+10.5 $\pm$ .5 +10.5 $\pm$ .5 + 9.3 $\pm$ .5
481.8	A 495-147	Altered granite (quartz = 50%; feldspar+sericite = 50%; and zircon+biotite = <1%).	total rock quartz K-feldspar sericite	+10.3 $\pm$ .5 +10.7 $\pm$ .1 +10.9 $\pm$ .1 + 9.4 $\pm$ .1

APPENDIX 1 (cont'd) List of studied samples from Nabarlek uranium deposit with  $\delta^{18}\text{O}$  values.

<u>Drill-hole No.</u> Depth(m)	Sample No	Description	Minerals	$\delta^{18}\text{O}$ (‰ SMOW)	
<u>Na55</u>	83.9	A-495-156	Quartz-sericite-haematite-chlorite rock (quartz = 10%; sericite = 20%; haematite+magnetite = 30%; and chlorite = 40%).	quartz chlorite haematite + magnetite	+15.1 $\pm$ .5 + 4.8 $\pm$ .5 + 5.0 $\pm$ .5
	89.0	A-495-157	Altered dolerite w/quartz vein (quartz = 1%: chlorite = 50%; sericite = 40%; and haematite = 7%).	total rock (no quartz from vein) quartz(vein) sericite haematite	+8  +17.0 $\pm$ .5 +10.8 $\pm$ .5 + 2.2 $\pm$ .5
<u>Na72</u>	22.2	A-495-162	Chlorite-sericite-quartz rock(w/pitchblende)	quartz	+12.3 $\pm$ .5
<u>Na74</u>	39.55	A-495-164	Sericite-quartz breccia	early-st.qtz. late-st. qtz.	+12.8 $\pm$ .5 +13.8 $\pm$ .5
<u>Na77</u>	44.6	A-495-167	Chlorite-sericite-quartz breccia w/pitchblende mineralization.	early-st.qtz.	+ 9.5 $\pm$ .1
	46.8	A-495-168	Chlorite-sericite-quartz-breccia w/pitchblende mineralization.	early-st.qtz. late-st. qtz.	+15.5 $\pm$ .1 +15.9 $\pm$ .1
	56.7	A-495-171	Oxidized chlorite-sericite-quartz-breccia w/ pitchblende mineralization. (late-stage quartz $\delta^{18}\text{O}$ value should be taken as minimum value because the quartz was ferruginous).	early-st.qtz. late-st. qtz.	+ 9.5 $\pm$ .5 +14
	58.0	A-495-172	Quartzite w/quartz-vein.	quartzite late-st. qtz.	+ 7.1 $\pm$ .5 +16

APPENDIX 1 (cont'd) List of studied samples from Nabarlek uranium deposit with  $\delta^{18}\text{O}$  values.

Drill-hole No. Depth(m)	Sample No.	Description	Minerals	$\delta^{18}\text{O}$ (% SMOW)
<u>Na77</u>	61.7	A-495-174	Chlorite-sericite-quartz breccia with quartz vugs.	early-st. qtz. +10.1 $\pm$ .5 late-st. qtz. +16.5 $\pm$ .1
	61.8	A-495-174-I	Similar to A-495-174 with pitchblende mineralization.	early-st. qtz. + 9.3 $\pm$ .1 late-st. qtz. +15.2 $\pm$ .1
	67.4	A-495-176	Chlorite-sericite-quartz breccia w/quartz vugs.	early-st. qtz. +11.0 $\pm$ .1
	104.4	A-495-178	Sericite-chlorite-quartz breccia	late-st. qtz. +16
	111.43	A-495-179	Quartz-sericite-chlorite-biotite-schist. (Retrometamorphosed amphibolite schist).	quartz +10.3 $\pm$ .5
	<u>Na83</u>	488.05	A-495-181	Altered granite(quartz = 30%;sericitized feldspar = 60%: chloritized biotite = 10%;and zircon <1%)
469.9		A-495-182	Altered granite (quartz = 20%; sericitized plagioclase = 70%;muscovite+biotite+chlorite = 10%).	total rock +10.3 $\pm$ .5 quartz +10.8 $\pm$ .1 sericite- plagioclase +10.4 $\pm$ .5 chlorite + 3.9 $\pm$ .5 biotite + 6.3 $\pm$ .5
451.75		A-495-183	Altered granite(quartz = 70%; altered plagioclase = 30%)	quartz +11.5 $\pm$ .1
416.4		A-495-186/	Muscovite-quartz schist (quartz 80%; muscovite/sericite = 20%).	total rock +11.1 $\pm$ .5 quartz +10.8 $\pm$ .5 muscovite +10.5 $\pm$ .5
205.1		A-495-189	Dolerite (plagioclase = 40%; pyroxene = 40%; sericite = 10%; olivine = 3%; opaques = 2%; sphene = 1%).	total rock + 6.4 $\pm$ .1

APPENDIX 1 (cont'd) List of studied samples from Nabarlek uranium deposit with  $\delta^{18}\text{O}$  values.

<u>Drill-hole No.</u> Depth(m)	Sample No.	Description	Minerals	$\delta^{18}\text{O}$ (‰ SMOW)
<u>Na83</u>				
105.46	A-495-190	Semi-altered dolerite (plagioclase-sericite = 40%; chlorite+pyroxene = 50%; and opaques = 5%).	total rock	+ 7.9 $\pm$ .1
93.3	A-495-191	Quartz-chlorite rock with quartz veins and vugs.	quartz (veins)	+15.5 $\pm$ .5
37.1	A-495-196	Altered dolerite (sericite+chlorite = 70%; opaques+haematite = 30%).	total rock	+ 5.5 $\pm$ .5
<u>Na94</u>				
42.1	A-495-201	Ferruginous muscovite schist w/blebs of pitchblende	total rock pitchblende	+11.7 - 3.2
<u>Na111</u>				
80.7	A-495-207	Actinolite schist (actinolite = 70%; sericite = 20%; quartz = 5%; and opaques = 5%).	total rock quartz actinolite	+10.1 $\pm$ .5 +12.2 $\pm$ .5 + 7.9 $\pm$ .5
136.95	A-495-211	Altered actinolite schist (sericite = 70%; quartz = 20%; chlorite = 10%; and opaques = 2%).	total rock quartz chlorite	+ 9.8 $\pm$ .5 +13.1 $\pm$ .1 + 5.6 $\pm$ .5
<u>Na176</u>				
43.00	A-495-220	Feldspar-actinolite schist (altered into chlorite-biotite-feldspar schist with a calcite vein).	calcite	+13.2 $\pm$ .1
-	-	Massive pitchblende from Echo Bay (Canada)	pitchblende	-8.0

APPENDIX 2

FLUID INCLUSION STUDY OF SAMPLES FROM NABARLEK URANIUM DEPOSIT

(gas-release upon crushing: n = none; w = weak; s = strong; v.s. = very strong)

SAMPLES A-495	MICROTHERMOMETRY				SALTS PRESENT	SALINITY CaCl <sub>2</sub> wt% (equivalent)	E.D.A.X. Minerals + elements	CRUSHING
	PHASES AT 25°C	PHASES (UPON FREEZING)	MELTING TEMP. (°C)	HOMOGEN. TEMP. (°C)				
Quartz 172 A	liquid + vapour, cubic crystal, dawsonite (?), and dark amorphous min.	ice → salt hydrate →	-49 +14	+ 70 to 130	CaCl <sub>2</sub> +NaCl	30	sericites,  chlorites,	w.
172 B	liquid only or liquid + vapour, cubic crystal, dawsonite (?), and hematite	ice	-46	KCl → 89 94	CaCl <sub>2</sub> +KCl	29.5	ca-silicate,  NaCl,	
172 D	liquid only (Few liquid + vapour)	ice	- 5 - 9 to -9.5 -15.1 to -19.5 -25.2 to -27.5 -35.2 to -36.8	85	CaCl <sub>2</sub> +NaCl	9.0 13.5 18.5-21.0 23.5-24.5 27.0-27.5	K,  Fe,	
172 F	liquid + vapour (cubic crystals)	new cubic crystals CaCl <sub>2</sub> hydrates ice	-44 to -61	93 to 142	NaCl+CaCl <sub>2</sub>	28.0-30.0	Ni, and Cl	

SAMPLES A-495	MICROTHERMOMETRY				SALTS PRESENT	SALINITY CaCl <sub>2</sub> wt% (equivalent)	E.D.A.X. Minerals + elements	CRUSHING
	PHASES AT 25°C	PHASES (UPON FREEZING)	MELTING TEMP. (°C)	HOMOGEN. TEMP. (°C)				
176 A	liquid + vapour	ice	-24 to -28	150-200	NaCl+CaCl <sub>2</sub>	26.0-29.5	sericite,	v.s.
176 B	liquid + vapour (cubic crystals)	ice salt hydrate	- 5 to -40	140-170	NaCl+CaCl <sub>2</sub>	average 17.5	kaolinite(?), CaCl <sub>2</sub> ,	
176 C	liquid + vapour	ice	- 3 to -15	140-280	NaCl+CaCl <sub>2</sub>	average 13.5	NaCl, KCl,	
176 D	liquid + vapour	-	-	110-240	-	-	FeSO <sub>4</sub> (?),	
176 E	liquid + vapour (amorphous solid)	ice	-20 to -35	133.4 > 500	-	22-30.5	CaCO <sub>3</sub> , dolomite,	
176 F	liquid + vapour (fibrous or amorphous solid)	ice	-	120-160 (fr.max=130)	-	-	ankerite, Ba	
179	liquid, liquid CO <sub>2</sub> , and vapour (up to 7 daughter minerals)	ice salt hydrates	-21	366.5	Ca,Na,K,Fe chlorides carbonates sulphates	22	NaCl,CaCl <sub>2</sub> , KCl,FeCl <sub>2</sub> , ankerite, calcite, dolomite, Ca-silicate, sulphate(?), of Zn, Na, Fe, Cu. Ca + K, and chlorides	v.s.

SAMPLES A-495	MICROTHERMOMETRY				SALTS PRESENT	SALINITY CaCl <sub>2</sub> wt% (equivalent)	E.D.A.X. Minerals + elements	CRUSHING
	PHASES AT 25°C	PHASES (UPON FREEZING)	MELTING TEMP. (°C)	HOMOGEN. TEMP. (°C)				
168	liquid or liquid + vapour	ice	+11.0 to -33.5	95-108	NaCl+CaCl <sub>2</sub>	15.5-26.5	-	v.s.
171	liquid or late-stage qz) liquid + vapour (early-stg.qz)			< 70 120-200				
162	liquid or liquid + vapour	ice clathrate	-0.3 to -0.9 -30.5	95-190	CaCl <sub>2</sub> +NaCl +KCl(?)	0.5 25.5	kaolinite sericite CaCl <sub>2</sub> , NaCl, KCl (?)	s.
110, 116, 201							galena chlorite calcite dolomite gypsum Ca	v.s.

SAMPLES A-495	MICROTHERMOMETRY				SALTS PRESENT	SALINITY CaCl <sub>2</sub> wt% (equivalent)	E.D.A.X. Minerals + elements	CRUSHING
	PHASES AT 25°C	PHASES (UPON FREEZING)	MELTING TEMP. (°C)	HOMOGEN. TEMP. (°C)				
157	liquid + vapour + few cubic crystals	ice + salt hydrates	-26 to -58	100-160	Ca,Na,K chlorides	24.0-31.0	Ca + K chlorides	w.
156	liquid + vapour	ice	-20 to -36	120	Na + Ca chlorides	21.0-27.0	-	w.
113	liquid + vapour + few cubic crystals	ice salt hydrates →	- 7 to -46 +4	110-140	NaCl+CaCl <sub>2</sub>	28.5-38.0	-	v.s.
144	liquid only	ice	-12	-	NaCl+CaCl <sub>2</sub> ?	16.0	not detected	n.
<u>Calcite</u> 144	liquid + vapour	ice hydrates	- 3 to - 2 (salt-hydrates)	96-104	Na + Ca chlorides	33.8		-
220	liquid + vapour	ice	- 7 to -23	125-170	CaCl <sub>2</sub> +KCl	9.0-22.5	Ca, K, Cl	w



## APPENDIX 3

## AUTORADIOGRAPHIC STUDIES

Introduction

The study of radioactive minerals by autoradiography is a technique described and applied by many authors. Coppens (1950) presented an extensive work where quantitative and qualitative data were obtained studying  $\alpha$ -tracks in photographic emulsion. Bowie (1951) gives an account of autoradiographic techniques in geological research.

In the present study the main interest was focused in the detection of pitchblende among opaque minerals and in fluid inclusions in quartz. For this purpose, liquid emulsion radiomicrographic technique was used. Piccioto (1952), Baranov and Tleuberghenova (1956), and Baranov et al. (1962) among others demonstrated the advantages of the method.

The liquid emulsion and application technique

The used liquid emulsion was the Ilford Nuclear Research Emulsion type K.5 which is sensitive to all charged particles of any energy and has the grain diameter of  $0.21\mu$ . The emulsion is stored at a temperature slightly above  $0^{\circ}\text{C}$  and must be handled only in safelight illumination for non colour sensitive materials. The substance which is a white mass at storage temperature must be removed from the bottle into a glass or stainless steel vessel in amounts needed for immediate use. The separated emulsion is warmed up in water-bath to about  $50^{\circ}\text{C}$ . During the process the emulsion melts into a milky liquid. Local overheating and froth formation must be avoided by gentle stirring. Return of unused emulsion back to the bottle must never be allowed.

The samples coated with this emulsion were either fluid inclusion thin sections (~200 $\mu$  thickness) or petrographic thin sections without cover glass. A small amount of emulsion were dropped in one edge of thin section and allowed to run off slowly over the thin section. When the emulsion had evenly covered the specimen the glass was held in the vertical position for few minutes in order to drain the excess of the emulsion. Afterwards the emulsion covered thin sections were kept in horizontal position in a dark-box and let do dry. To hasten the drying process the box may be taken to a stove for slight warming. The thin sections were left for variable period of time to be impressed by  $\alpha$ -rays. This period of time is merely empirical, depending on the intensity of radioactivity. At last, the thin sections were processed according to the instructions of the leaflet (Ilford Photographic Emulsions for Nuclear Research Y44.1).

#### Results obtained

The autoradiography made possible the distinction between pitchblende and other opaque minerals (e.g. Plate III, photo 2). The presence of  $\alpha$ -tracks clearly indicated the precipitation of pitchblende before, during and after the crystallization of hydrothermal quartz (Plate I, photo 1; Plate II, photos 3 and 4; Plate III, photo 2; and Plate IV, photo 2).

With the liquid emulsion autoradiography it was also possible to determine the approximate thickness of quartz capable of obstructing the  $\alpha$ -rays. The observation of  $\alpha$ -tracks from pitchblende inclusion like the one illustrated in figure 53 and from other pitchblende grains at different distances from the surface of the thin section indicated that 10-12 $\mu$  of quartz was sufficient to block all  $\alpha$ -rays.

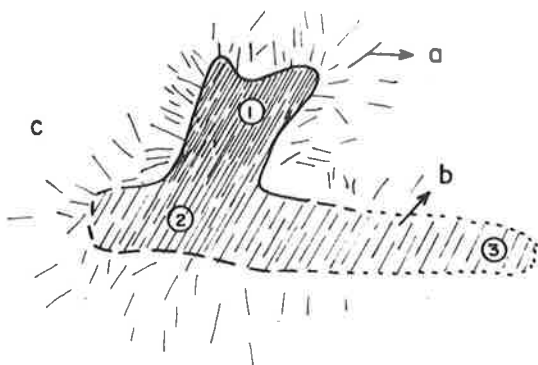


Figure 53: Sample A-495-162. Autoradiography of pitchblende inclusion in quartz.

a -  $\alpha$ -tracks; b - pitchblende; and c - quartz. The specimen was coated with photographic emulsion. The pitchblende outcropping at the surface of the thin section (1), produced more numerous and intense  $\alpha$ -tracks. At point (2) where the pitchblende is  $5\mu$  below the surface the  $\alpha$ -tracks are shorter and less numerous. At (3) the pitchblende is  $18\mu$  below the surface which thickness is enough to obstruct all  $\alpha$ -rays. Measurements from other pitchblende grains in this sample and others indicated that  $10-12\mu$  of quartz are enough to obstruct the  $\alpha$ -rays.

In this circumstances, the attempt to obtain  $\alpha$ -tracks from opaque solid phases present in fluid inclusions was fruitless because of major difficulty in the preparation of an appropriate specimen (Plate I, photo 2 and Plate III, photo 3). Nevertheless there is a favourable ground to believe that these black minerals were pitchblende because of their habit (botryoidal) and because of the high frequency of pitchblende inclusions in the same quartz crystals (Plate I, photo 1 and Plate III, photo 2). In the other hand, tiny fluid inclusion from the same area of the quartz crystal, in which no opaque minerals were distinguishable, seem to have been the source of  $\alpha$ -tracks (Plate III, photo 4). In any case, the observations indicate the contemporaneity of entrapment of fluid inclusions and the precipitation of pitchblende.

## APPENDIX 4

## CHEMICAL COMPOSITION OF SOME SAMPLES FROM NABARLEK AREA

X-ray fluorescence and flame photometry ( $\text{Na}_2\text{O}$ ) analyses determined the major elements of some typical samples from Nabarlek area.

Samples of actinolite schist, dolerite, and granitic rocks were analysed to compare the results between altered and unaltered or less altered rocks of each type. The most representative sample of each group was selected for this purpose. The altered samples were chosen in such way that their mineralogical composition before alteration was as similar as possible to the unaltered or less altered ones. This correlation was possible because:

a) The major mineralogical alterations were of feldspars to sericite and mafic minerals to chlorite (Chapter 1).

b) The altered samples had preserved the texture of the original rocks.

The results are presented in table 8.

The main observations discernible from this data are:

- 1 - Strong depletion of  $\text{CaO}$  and  $\text{Na}_2\text{O}$  in altered samples. Considering the conspicuous alteration in the Nabarlek area (up to 40 m deep in the case of dolerite for instance) a enormous amount of Ca and Na was released during the process. Only the alteration of dolerite would have been able to liberate several millions of tons of these elements. In granitic rocks the process was less pronounced because the feldspars were potassic and already altered to a certain degree.

- 2 - The behaviour of  $K_2O$  was variable. K-rich rocks like the granites and the actinolite schist showed only partial depletion probably because part of K was retained by sericite. In low  $K_2O$  sample like the dolerite the sericitization probably required an addition of potassium.
- 3 - The enrichment of MgO in altered samples was obviously a requirement necessary for chloritization, but this Mg metasomatism represented a less drastic change than the Ca + Na depletion.
- 4 - From  $SiO_2$ ,  $Al_2O_3$ , and  $Fe_2O_3$  only the second had a significant increase in altered actinolite schist, which may be the consequence of sericitization. Si and Fe did not show significant changes.

MAJOR ELEMENTS	ACTINOLITE SCHISTS		DOLERITES		GRANITES		
	Less altered	Altered	Fresh	Altered	Less altered	Less altered	Altered
	A-495-207	A-495-211	A-495-138	A-495-136	A-495-181	A-495-147	A-495-146
SiO <sub>2</sub>	51.96	51.63	48.74	42.72	72.15	72.53	75.67
Al <sub>2</sub> O <sub>3</sub>	14.15	19.24	18.04	17.81	13.25	13.80	13.65
Fe <sub>2</sub> O <sub>3</sub>	12.33	11.29	9.98	11.95	1.90	1.76	1.62
MnO	0.20	0.03	0.15	0.10	0.04	0.02	0.01
MgO	6.13	7.52	6.80	14.31	0.99	1.88	1.43
CaO	5.97	0.09	11.85	0.35	0.45	0.38	0.13
Na <sub>2</sub> O	1.47	0.08	2.31	0.46	1.57	0.17	0.08
K <sub>2</sub> O	4.58	3.27	0.48	2.93	6.75	6.24	4.07
TiO <sub>2</sub>	0.99	0.77	1.00	1.43	0.18	0.24	0.24
P <sub>2</sub> O <sub>5</sub>	0.13	0.06	0.09	0.12	0.04	0.07	0.06
Loss	2.07	5.95	0.95	7.78	2.16	2.66	2.66
Total	99.98	99.93	100.39	99.96	99.48	99.75	99.62

Table 8: Major element (wt.%) analyses of some samples from the Nabarlek area.

## APPENDIX 5

FLUID INCLUSION STUDY OF SAMPLES FROM  
JABILUKA URANIUM DEPOSIT.

Fluid inclusion study of four samples from Jabiluka uranium deposit was performed in an attempt to find possible similarities with the results from Nabarlek deposit. The four samples were selected from the following lithological units: Upper Graphite Series (A-495-1), Hanging Wall Series (A-495-3), and Main Mine Series (A-495-5 and A-495-11).

Excepting samples A-495-3, the quartz from other samples always showed metamorphic imprints on it. The non mineralized sample A-495-3 presented idiomorphic quartz crystals, and could be equivalent of hydrothermal quartz from Nabarlek.

Sample A-495-1

(D.H.143: 67.80m)

This sample was a piece of uraniferous quartz-carbonaceous-chlorite-schist from Upper Graphite Series. The selected mineral for fluid inclusion study was quartz from a vug. Although highly fractured and somewhat recrystallized the hexagonal sections in many grains were still preserved. Iron oxide and carbonaceous matter had been introduced in some of these fractures.

Description of inclusions

Although indicating somewhat different fluid inclusions from Nabarlek, the inclusions from sample A-495-1 could also be grouped into two types:



type (a): liquid-rich and

type (b): gas-rich inclusions.

Type (a) inclusions were irregularly distributed, presented irregular shape, and had sizes ranging between 10 to 20 $\mu$ . Occasionally they reached 50 $\mu$ . When present, the daughter minerals were cubic, amorphous, and orange to reddish flaky, minerals. The first was probably NaCl and the last was very likely to be hematite. The vapour phase occupied between 2 to 5 vol.%.

Type (b) inclusions were probably secondary, for the majority were located along fractures crosscutting the boundaries of quartz grains. The vapour phase was much larger (~50 vol.%) and almost always presented a fringe of liquid CO<sub>2</sub>. The CO<sub>2</sub> liq./H<sub>2</sub>O liq. ratio was approximately one. The shape was more regular (negative crystals) and an average size of 3 $\mu$ .

#### Microthermometry

The freezing test indicated two different salinities for type (a) inclusions. One group of inclusions presented salinity of around 18wt.% of NaCl or CaCl<sub>2</sub> equivalents (last ice melting around -16°C, Figure 54). The second group formed salt hydrates which dissolved only at +26°C. This temperature indicates a very dense brine of 46 wt.% CaCl<sub>2</sub> equivalent (Figure 12, and 54). The hydrate always presented birefringence and hexagonal shape like in Plate XVIII, photo 4. This seems to be indicative of a calcium rich chloride hydrates.

Type (b) inclusions presented a solid phase melting at -54°C and gas-clathrate between +6°C to +6.5°C (Figure 54). These values are indicative of carbon dioxide. In one inclusion with high CO<sub>2</sub>liq./H<sub>2</sub>O liq. ratio the distinction between solid CO<sub>2</sub>(completely

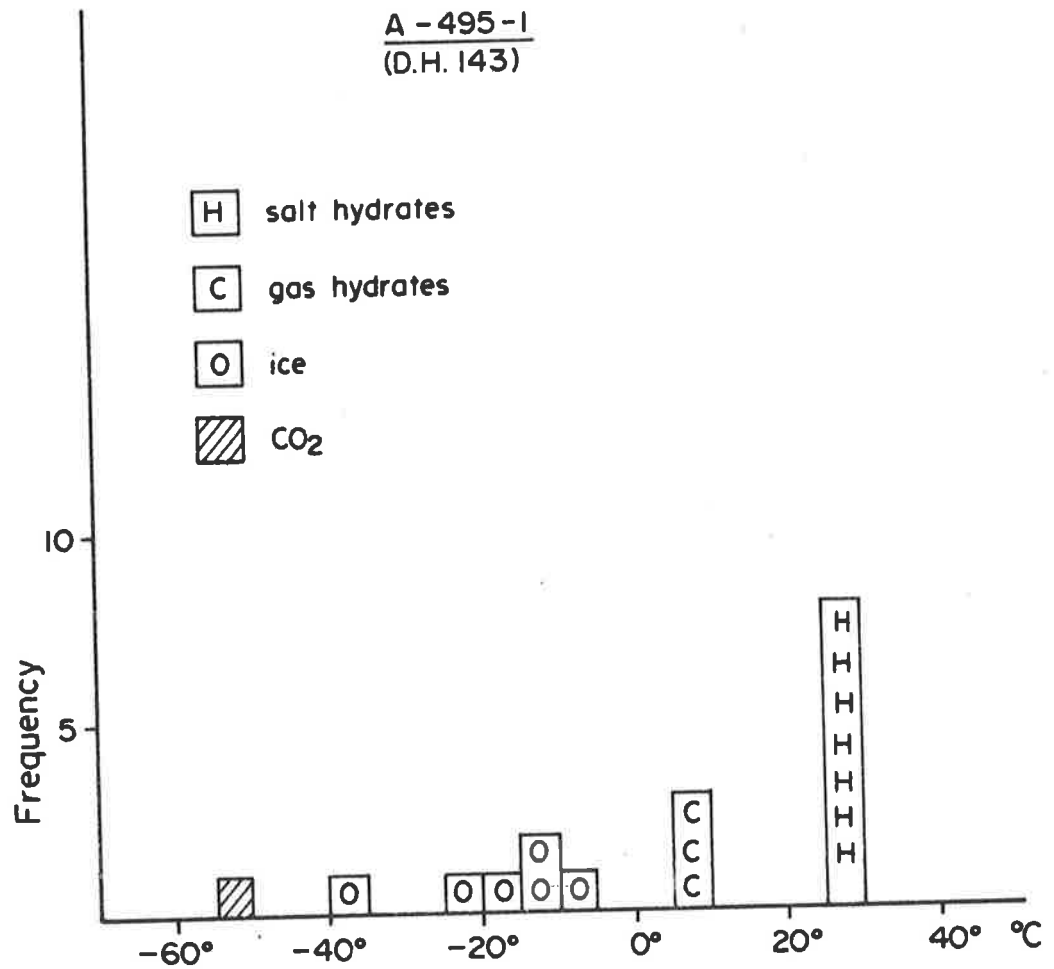


Figure 54:  $T_F$  frequency histogram of fluid inclusions in quartz.

transparent) and CO<sub>2</sub> clathrate (mushy) was possible. Their melting temperatures were very close to the values above mentioned. The formation of clathrates precludes the determination of the salinity of inclusions.

The presence of graphite in the sample and in fractures of the quartz suggests the formation of CO<sub>2</sub>-rich inclusion by the reaction of graphite and water (French, 1966).

Sample A-495-3

(D.H.143: 104,0m)

Description of inclusions

The studied quartz crystals were collected from a vug in quartz-chlorite-sericite schist of Hanging Wall Series. The crystals were idiomorphic and did not show fracturing or evidences of recrystallization. Among the four samples studied this quartz represents the latest phase in the paragenetic sequence.

The inclusions studied were probably of primary origin. They were large and isolated or from zones of growth of quartz. The crystals were stained by hematite. Inclusions in the innermost part of the crystal were larger and irregular in shape while those closer to the surface of the crystal along zones of growth were smaller and elongated. The majority of inclusions presented two phases (liquid + gas) and, as in the case of Nabarlek, could be separated into two groups: type (a) with larger liquid-phase and type (b) with larger gas-phase. The latter was smaller in number. A thin ring of liquid CO<sub>2</sub> could be suspected around the bubble in some inclusions. In some type (a) inclusion the gas-phase was absent possibly as a consequence of "necking down" process. Only few inclusions contained solid phases which were orange flake

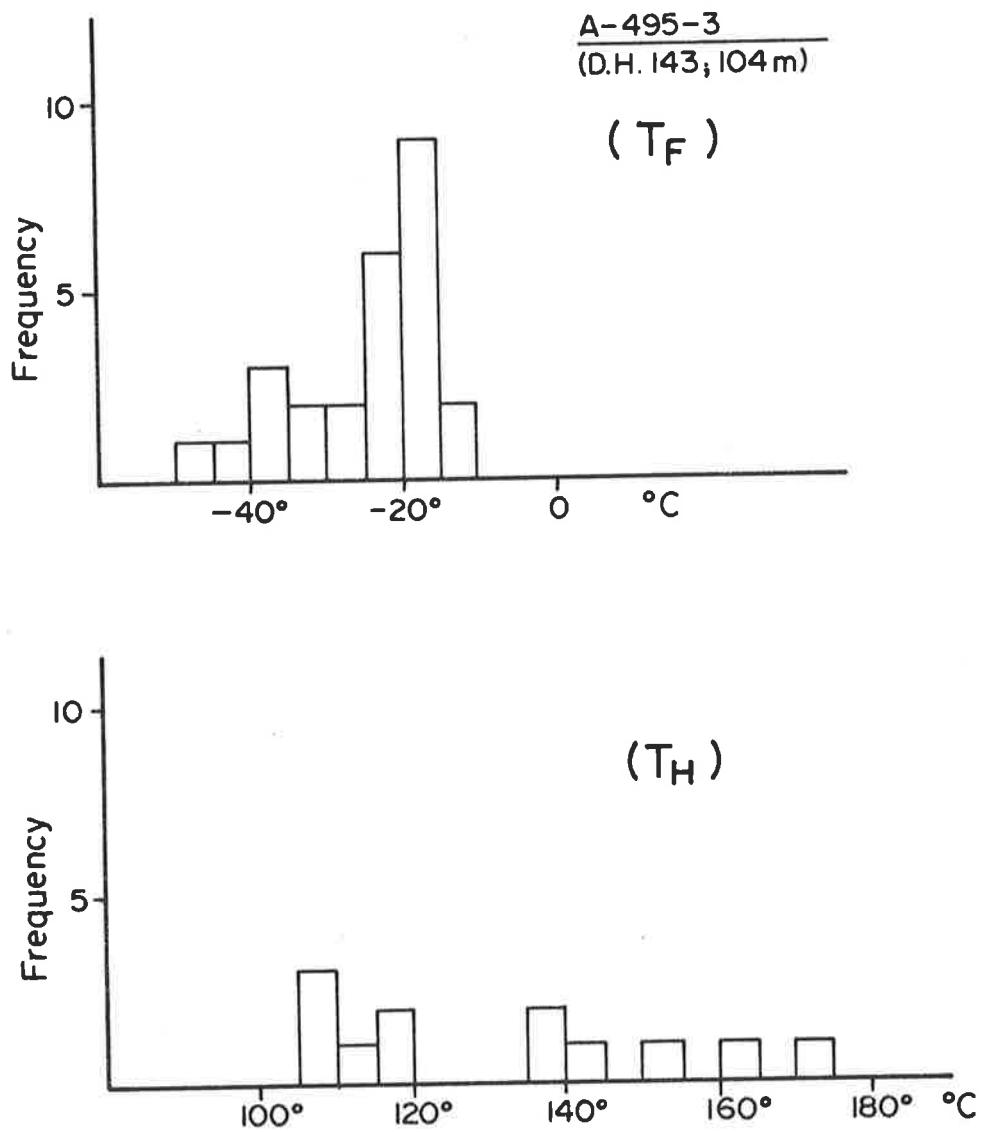


Figure 55:  $T_F$  and  $T_H$  frequency histograms of fluid inclusions in quartz.

minerals (later identified as hematite), fibrous birefringent mineral, and NaCl (?)

#### Microthermometry

Persistence of metastable liquid phase at temperatures below  $-150^{\circ}\text{C}$ , nucleation of cubic salt crystals, formation of salt hydrate which presented phase changes and incongruent melting were observed in a few inclusions. Only in one case a cubic salt crystal have resisted temperatures as high as  $108^{\circ}\text{C}$ . The majority of inclusions presented ice melting between  $-10^{\circ}\text{C}$  and  $-50^{\circ}\text{C}$  with major frequency around  $-20^{\circ}$  and  $-40^{\circ}\text{C}$  (Figure 55). These low temperatures indicate the presence of  $\text{Ca}^{++}$  and explain the melting behaviour of the salt hydrates of some inclusions mentioned before. Temperatures of  $-20^{\circ}$  and  $-40^{\circ}\text{C}$  point to salinities of 21.5 wt% and 28.5 wt% of  $\text{CaCl}_2$  equivalent. The temperature of dissolution of NaCl (?) at  $108^{\circ}\text{C}$  in one fluid inclusion may indicate a salinity of 28 wt%  $\text{CaCl}_2$  equivalent in a solution of 3 wt% NaCl.

$T_H$  measurements were greatly hindered by darkness of the crystal upon heating. The few determinations made indicated temperatures in the range of  $105^{\circ}$  to  $175^{\circ}\text{C}$  but the higher values seems to be the consequence of "necking down" process (Figure 55).

#### Crushing and S.E.M.

The crushing test indicated a "very strong" gas release which presented a high solubility in kerosene. Only a few bubbles formed  $\text{BaCO}_3$  in  $\text{Ba}(\text{OH})_2$  solution. These results and the absence of large amount of liquid  $\text{CO}_2$  even during the cooling process confirm the presence larger amount of hydrocarbons in the gas phase.

The scanning electron microscopy showed numerous inclusion cavities with micaceous minerals. The EDAX detected Fe in platy, hexagonal-shaped minerals (plate XVI, photo 1 and corresponding EDAX image), which is probably hematite. This supports the interpretation of hexagonal orange flake minerals seen in inclusions as hematite.

Sample A-495-5

(D.H.143: 110.5m)

This drill-core sample represents a slightly radioactive quartz-chlorite-schists of upper contact of Main Mine Series with a quartz veinlet. The quartz veinlet presents quartz with evidences of post-crystallization metamorphic effects: fracturing, recrystallization, undulose extinction. The inclusions were similar to those occurring in sample A-495-11, i.e., multiphase and liquid-rich to vapour-rich inclusions.

Apart from solid phases similar to those of sample A-495-11, some multiphase inclusions presented fibrous birefringent minerals which could be muscovite, because they did not show the characteristic radial aggregates of dawsonites (Coveney and Kelly, 1971).

Inclusions of major interest in this sample were those with high liquid  $\text{CO}_2$  content. In three larger inclusions the solid  $\text{CO}_2$  melted at  $-62.5^\circ\text{C}$ ,  $-63.2^\circ\text{C}$ , and  $-65.0^\circ\text{C}$ , pointing out the presence of methane in the fluid phase. According to Hollister and Burruss (1976) these temperatures are indicative of 30 to 45 mole% of  $\text{CH}_4$  in  $\text{CO}_2$ - $\text{CH}_4$  system. The melting temperature of clathrates, which was between  $+7^\circ\text{C}$  and  $+7.5^\circ\text{C}$ , is meaningless for the confirmation of  $\text{CH}_4$  content because the salinity of the solution is unknown. (The salt

content in the system  $\text{CO}_2\text{-CH}_4\text{-H}_2\text{O}$  would decrease the chemical potential of water, lowering the temperature of formation of the clathrates (Holliester and Burruss, 1976)).

The critical temperatures of  $\text{CO}_2$  in four inclusions fell between  $+25.3^\circ\text{C}$  and  $+26.6^\circ\text{C}$  (homogenization into liquid phase). These phenomena indicate inclusions with high  $\text{CO}_2$  density ( $\sim 0.70\text{g/cc.}$ ). According to the estimated minimum  $T_H$  of the inclusions ( $350^\circ\text{C}$ ) this density will point to a pressure far above 1 Kbar. This value agrees with metamorphic conditions originating the present sample and its inclusions and is in the range of values found for sample A-495-179 from Nabarlek.

The crushing test always indicated inclusions with high internal pressure showing "very strong" gas release. This is in agreement with the high frequency of gas-rich inclusions. Like in sample A-495-11, the crushing in  $\text{Ba(OH)}_2$  solution and kerosene pointed to the presence of  $\text{CO}_2$  and  $\text{CH}_4$ , which reinforces the interpretation for depression of  $\text{CO}_2$  triple point. Although this depression still indicates content of  $\text{CO}_2 > \text{CH}_4$  the crushing in kerosene seems to favour the opposite:  $\text{CH}_4$  content larger than  $\text{CO}_2$ .

#### Sample A-495-11

(D.H.169: 200.40m)

This core-sample is a uraniferous chlorite-mica-quartz-schist with a quartz-vein along the schistosity of the rock. The sample is from lower Main Mine Series. The quartz from the vein presented polycrystalline texture indicating recrystallization since its formation. Many of gas-rich negative crystal shaped inclusions were clearly secondary especially the strings of gas-rich inclusions cross-cutting the boundaries between two grains. Although secondary in origin

they are most probably related to at least part of uranium mineralization. The large inclusions and the small ones of irregular shape and aqueous phase may be primary with post-formational changes. The inclusions are remarkably numerous and occur in a great variety of size, shape and composition:

1. Scattered in the vein-quartz there were few large inclusions (~50 $\mu$ ) with unusually numerous solid phases. One kind presented a large cubic NaCl crystal and numerous elongated - sometimes prismatic - birefringent minerals which were probably Ca + Mg chloride hydrates (Plate XVII, photos 2 and 3). This type of inclusions were more frequent in smaller sizes (~10 $\mu$ ) but the NaCl crystal is not always present (figure 56B). Three other inclusions of different kinds presented a large amount of unidentified, amorphous, granular, birefringent daughter minerals.

The large volume of solid phases and the low frequency may be indicative of inhomogeneous entrapment or disruption after nucleation of daughter minerals.

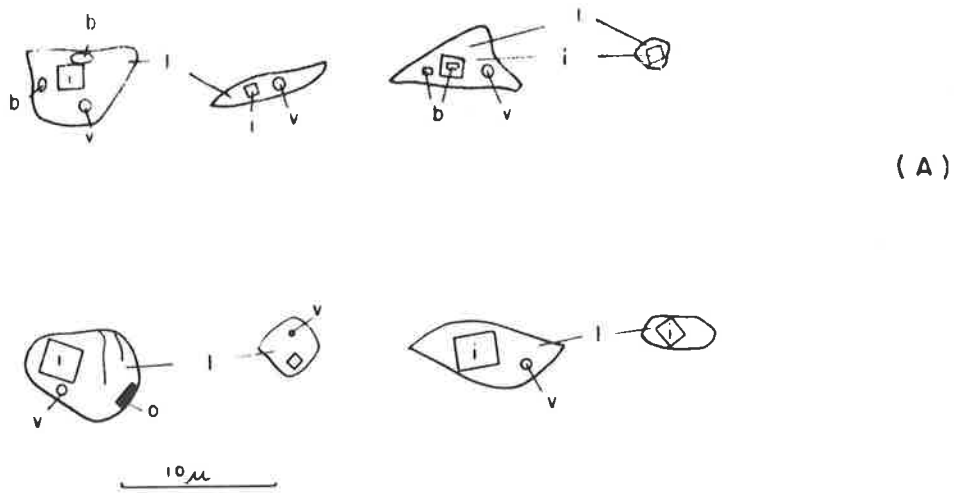
2. Apart from these inclusions the majority were of fluid rich inclusions. They could present only liquid, liquid + solid(s), liquid + vapour, or liquid + vapour + solid(s) phases. The solid and/or vapour phases generally represented less than 20 vol. % of the inclusion (Plate XVI, photo 3 and Plate XVII, photo 1). The liquid/vapour ratio was highly variable. In many inclusions the vapour phase was larger than 20 vol. %, and in few of them it could reach more than 80 vol. % (Plate XVII, photo 2).

With such a variety of inclusions, in an attempt to obtain a comprehensive understanding of the fluid composition, several clusters of inclusions were studied. Many inclusions presented very

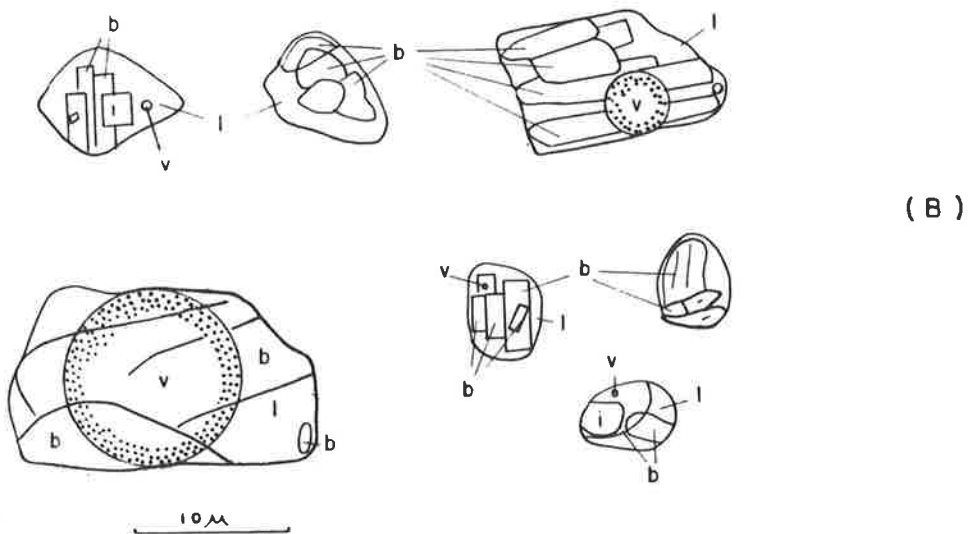


Figure 56

Multiphase inclusions in quartz from sample A-495-11



(A) fluid inclusions in quartz grain from chlorite-mica-quartz schist.



(B) fluid inclusions in quartz from a recrystallized quartz-vein. They contain larger number of minerals than the inclusions from previous group. Especially the amount of elongated birefringent minerals are self-evident. They are probably multicompositional chlorides (also see plate XVIII, photos 1, 3, and 4).

b: birefringent minerals; i: isotropic minerals, probably NaCl; l: liquid phase; o: opaque; and v: vapour phase.

unusual phase changes. For this reason, detailed description of the phenomena will be given.

Fluid inclusions in quartz from chlorite-mica-quartz schist was also examined. Inclusions with solid phases exhibited clear difference compared to similar inclusions in vein-quartz. In the latter there were more birefringent daughter minerals than in inclusions from the schist. Furthermore, inclusions in quartz from schist presented higher frequency of NaCl cubic crystals (in figure 56 compare the inclusions of group (A) to those of group (B)). The small size of inclusions in quartz from schist precluded the microthermometric study.

a) Cluster A

This cluster presented several types of inclusions. During microthermometry about a dozen inclusions could be studied.

Type A.1

A single, irregular, large inclusion (42 $\mu$ ) presented solid, liquid and vapour phases. The vapour and liquid phases represent together about 30 area % of the inclusion. The remaining space is filled by a granular, birefringent solid phase. This substance presented a refraction index lower than quartz but higher than the liquid phase. The inclusion did not freeze although the temperature was lowered down to -170°C in two different occasions. During the heating process the vapour phase decreased in size but the solid phase did not show any noticeable solution. At 362°C the inclusion leaked even before the homogenization of the fluid phase. An attempt to study the solid phase of this inclusion by S.E.M. was not successful.

Other two similar inclusions with different solid phases presented the same behaviour during microthermometry. They contained at least five different crystals and did not present vapour phase. Upon heating one of them nucleated a bubble at +283°C (leaking?) and the other decrepitated at +350°C.

Type A.2

These inclusions were smaller ( $<20\mu$ ) and presented only liquid phase. In few cases they also contained a solid phase: isotropic cubic, birefringent elongated or birefringent fibrous minerals. The freezing test presented first melting at around  $-65^{\circ}\text{C}$ . In inclusions with only aqueous phase the last ice melted between  $-10.0^{\circ}\text{C}$  and  $-11.2^{\circ}\text{C}$ . In only one case this temperature was as high as  $-5.5^{\circ}\text{C}$ . These lower values indicate salinity equivalent to  $\sim 15$  wt. %  $\text{CaCl}_2$ . Upon heating, the inclusions with solid phases decrepitated at about  $350^{\circ}\text{C}$ , well before the homogenization had occurred.

Type A.3

This group of inclusions were located along a plane and presented the following general characteristics:

- negative crystal shape.
- fairly constant liquid/vapour ratio (vapour =  $\sim 10$  vol. %).
- fairly common presence of isotropic daughter minerals.
- few inclusions with only liquid phase.
- upon freezing, formation of gas hydrates around the vapour phase. These hydrates melted before  $-32.2^{\circ}\text{C}$ .
- after freezing almost all inclusions formed isotropic, high relief, prismatic or polygonal daughter minerals which probably were salt hydrates.
- in only one liquid + vapour phase inclusion the  $T_F$  could be measured:  $-16.3^{\circ}\text{C}$ , which points to a salinity of 18.5 wt. %  $\text{CaCl}_2$  equivalent.
- the majority of inclusions became dark upon heating. In only one inclusion, with better transparency a near complete homogenization could be observed at  $+330^{\circ}\text{C}$ . The others started decrepitating at around  $+350^{\circ}\text{C}$  before homogenization.

### Interpretation and conclusions

The compositional variety of inclusions types A.1 and A.2 are indicative of inclusions disrupted after their entrapment or formed by an inhomogeneous entrapment. Effectively, the amount of solid phases in inclusions like type A.1 cannot be nucleated from the fluid of that inclusion. Reinforcing these hypothesis, the A.1 type inclusions decrepitated at  $\sim 360^{\circ}\text{C}$  without significant dissolution of the solid phase. Evidences of "necking down" seem to favor the idea of post-formational changes more than inhomogeneous entrapment. Although of characteristically secondary origin, the type A.3 inclusions may be the disrupted product from other inclusions, especially due to higher mobility of gas phases.

In these circumstances the true salinity of the fluid cannot be accurately determined. The estimated salinities for A.2 and A.3 type inclusions indicated only the lower limit. The original solution might have had higher salinity. The resistance to freeze the aqueous solution of A.1 type inclusions, the low first melting temperature for A.2 type inclusions and the formation of birefringent elongated daughter minerals upon freezing points to the presence of  $\text{Ca}^{++}$  as effectively was later confirmed by S.E.M. The melting temperatures of ice from aqueous A.2 and A.3 inclusions is in figure 57, Cluster A.

The decrepitation at relatively low temperatures for quartz ( $\sim 360^{\circ}\text{C}$ ) is supposed to be the consequence of high internal pressure of inclusions (later confirmed by crushing test) and weakness caused by metamorphic recrystallization (polycrystalline texture).

#### b) Cluster B

The main purpose for the selection of these inclusions was to study the composition of their liquid phase. The selected inclusions were monophasic (liquid) or biphasic (liquid + vapour). Only

SAMPLE A - 495 - II - Melting Temperatures

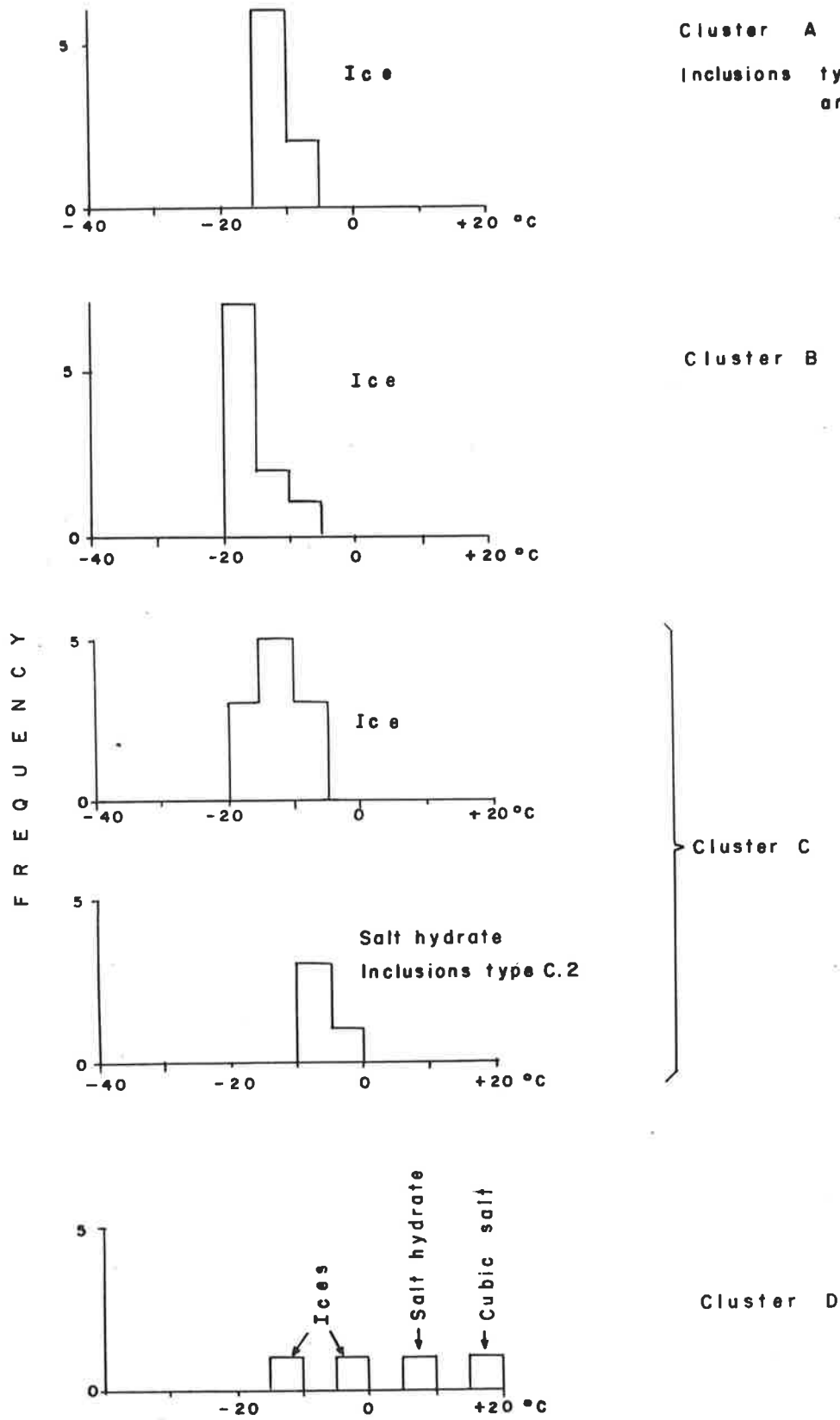


Figure 57:  $T_F$  frequency histograms of four clusters of fluid inclusions (A, B, C, and D) in quartz.

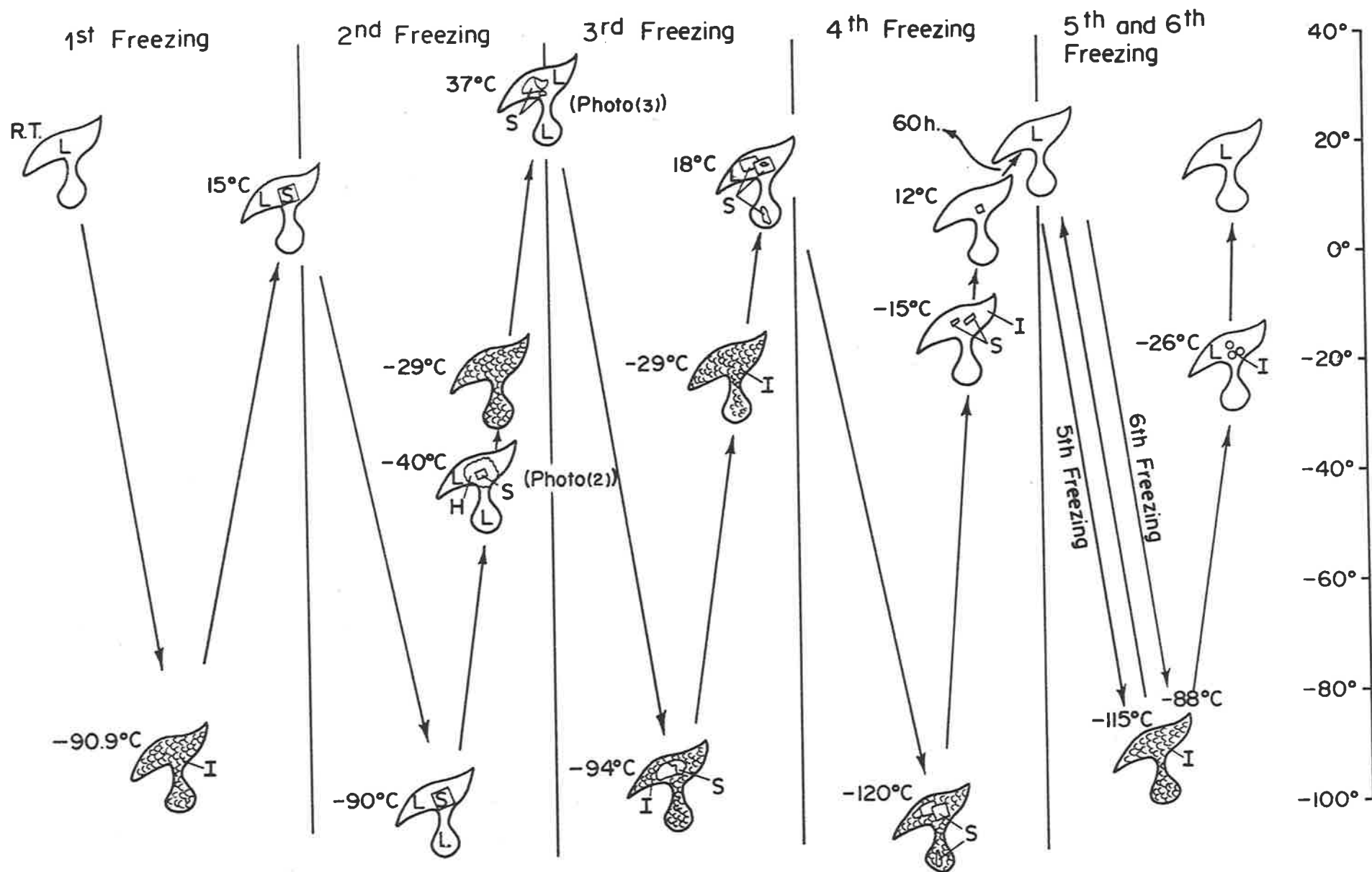


Figure 58: Sample A-495-11. Unusual phase changes in inclusion no. 2, cluster B, during the freezing tests. Also see Plate XVI, photos 2 and 3. (RT: room temperature; L: liquid; I: ice; S: solid; H: salt hydrate).

one contained an isotropic amorphous substance. The liquid/vapour ratio was variable. Five monophasic inclusions showed the most unusual phase changes during the freezing test. Because of this peculiarity the process was repeated six times until the inclusions presented again the same initial phases. For reference purposes the inclusions were numbered 1 to 5. In figure 58 the phase changes observed for inclusion No. 2 is schematically illustrated.

#### b.1. First freezing

The sample was cooled down to  $-151^{\circ}\text{C}$ . The liquid started solidifying upon warming at  $-80^{\circ}\text{C}$ . The first melting started at  $-27^{\circ}\text{C}$  forming round shaped ice crystals. In five liquid + vapour phase inclusions the ice melted between  $-10^{\circ}\text{C}$  and  $-18^{\circ}\text{C}$ . In monophasic (liquid) inclusions the instant of formation of salt hydrates (light green crystals) and the melting of last ice could not be observed. Upon slow warming in inclusions 1, 2, and 3, the salt hydrates melted incongruently at  $+25.4^{\circ}\text{C}$ ,  $+15.0^{\circ}\text{C}$ , and  $+26.3^{\circ}\text{C}$  respectively, nucleating a large isotropic, greenish, cubic crystal of NaCl (?). In inclusion No. 2, this crystal occupied an estimated surface of 15 area % (figure 58, 1st. freezing). Considering that at the beginning these inclusions were filled only with aqueous phase, the nucleation of such large daughter minerals were a surprising phenomenon.

#### b.2. Second freezing (Figure 58, 2nd. freezing)

The second freezing was performed on the following day. The liquid phase solidified at  $-120^{\circ}\text{C}$  and the NaCl crystal remained unaltered. Upon warming, at  $-44^{\circ}\text{C}$  the NaCl started reacting with the water from the melting ice to form  $\text{NaCl}\cdot 2\text{H}_2\text{O}$  (Plate XVI, photo 2). The reaction progressed continuously until the whole NaCl had been consumed.

At that point ( $-26^{\circ}\text{C}$ ) the entire inclusion acquired an homogeneous aspect (the ice and the salt hydrates became indistinguishable). At  $-19^{\circ}\text{C}$  the commencement of new melting could be noticed. The continuous melting left an amorphous isotropic substance which became slightly birefringent at  $+27^{\circ}\text{C}$  (Plate XVI, photo 3). Although these phase changes were described specifically for inclusion No. 2, they were also observed in inclusions Nos. 1, 3, and 4.

### b.3. Third freezing

The sample was frozen a third time. At  $-94^{\circ}\text{C}$  the inclusions Nos. 1, 2, 3, and 4 were frozen presenting two solid phases: ice and NaCl. At  $-39.5^{\circ}\text{C}$ , the melting ice reacted with NaCl, producing NaCl dihydrate as in the second freezing, and at the same temperature of  $-26^{\circ}\text{C}$  all NaCl had reacted. A different aspect noticed at that point was the change of solid phase into a much coarser substance, different from previously formed salt hydrates.

The temperature was dropped again down to  $-48^{\circ}\text{C}$  and the first melting was measured at  $-33.5^{\circ}\text{C}$ . In inclusion No. 1 the last solid melted at  $+5.9^{\circ}\text{C}$ . Just before, at  $+5.5^{\circ}\text{C}$  a cubic crystal had been nucleated. In inclusion No. 2 the last solid melted at  $+1.0^{\circ}\text{C}$  nucleating, this time, at least four crystals. Two of them presented cubic form and the others were elongated. In inclusion No. 4 the melting of last solid was at  $+0.7^{\circ}\text{C}$  and also nucleated a cubic crystal. The crystals nucleated in the three inclusions showed a light green colour and were probably NaCl.

### b.4. Fourth freezing

After two days the sample was submitted to a new freezing test, when it was cooled down to  $-120^{\circ}\text{C}$ . The inclusions presented



similar phase changes until the formation of a homogeneous solid substance ( $-26^{\circ}\text{C}$ ). From that point, a very slow warming was performed and at the end the sample was kept for one hour between  $-1.7^{\circ}\text{C}$  and  $+0.6^{\circ}\text{C}$ . During this period of time the inclusions Nos. 5, 1, and 3, in this sequence, had the salt hydrates melted incongruently forming cubic or prismatic NaCl crystals. After this period of time, in inclusion No. 4, the salt hydrate had not yet melted. Then, the sample was cooled again down to  $-24^{\circ}\text{C}$  and kept for seventy minutes at that temperature. The growth of salt hydrate could then be observed. This hydrate finally melted while the temperature was kept between  $-2.9^{\circ}\text{C}$  and  $-0.7^{\circ}\text{C}$ , but it did not nucleate any crystal like in previous freezings or like other inclusions during this freezing test. The inclusion No. 2 presented again a different phase change: warming up after being frozen, at around  $-15.0^{\circ}\text{C}$ , it became completely transparent. The solid phase was hardly visible. Only two tiny crystals presented higher relief. After the first cooling ( $-120.0^{\circ}\text{C}$ ), when the temperature was kept between  $-1.7^{\circ}\text{C}$  and  $+0.6^{\circ}\text{C}$  for one hour the last salt hydrate presented strong birefringence and a small prismatic crystal in the centre. After the second cooling (cooling down to  $-24.0^{\circ}\text{C}$ , warming up, and keeping the temperature between  $-2.9^{\circ}\text{C}$  and  $-0.7^{\circ}\text{C}$  as described for inclusion No. 4) the very slow melting of the salt hydrates could be observed. From that range of temperature, the sample was cooled again down to  $-7.5^{\circ}\text{C}$  and an increase of salt hydrates could be noticed. Subsequently keeping the temperature between  $-4.9^{\circ}\text{C}$  and  $-2.5^{\circ}\text{C}$  for 30 minutes no change in the size of hydrate was noticed. The last hydrate melted incongruently forming on tiny cubic crystal after keeping the temperature between  $-2.5^{\circ}\text{C}$  and  $0.0^{\circ}\text{C}$  for one hour. At  $+12^{\circ}\text{C}$  this incongruently formed cubic crystal still presented the same aspect. After all these cooling processes, in inclusion No. 3, the NaCl crystal amazingly had increased

more than twenty times in size. More surprising was the dissolution of these daughter minerals in all inclusions during the week-end (~60 hours) when the temperature did not exceed +20°C. The inclusions were again filled only with aqueous phase, the same aspect they presented before the first microthermometric study.

#### b.5. Fifth freezing

The sample was frozen once more down to -115.0°C and the inclusions presented a very fine grained texture. The first melting was observed at around -28.5°C. The ice in inclusion No. 3 melted at -19.0°C forming numerous tiny NaCl crystals. Similar phase changes were observed in all other inclusions at higher temperatures. At -1.0°C the formation of NaCl dihydrates and in a few other inclusions of tiny birefringent salt hydrates were visible. At room temperature the former had melted but the latter were still present.

#### b.6. Sixth freezing

During this last cooling the inclusions were all frozen at -80.0°C. The first melting occurred at -33.0°C. At -24.8°C all inclusions suddenly became clear forming large rounded ice platelets. The inclusions No. 1 to 5 had their last ice melted between -16.1°C and -18.5°C. The melting temperature in seven other inclusions was just below -20.0°C (Figure 57, Cluster B). The temperatures indicate salinities of 20.6 to 22.2 wt. % NaCl equivalent. At the end the inclusions showed the same aspect and composition they presented before the first freezing test.

### Interpretation and conclusions

A definitive explanation for these unusual phase changes (always in the same solution!) cannot be easily found. One can see that the aqueous solution was a concentrated multi-component brine. The nucleation of solid phases indicated NaCl and CaCl<sub>2</sub> hydrates. The salt content seems to be very close to the eutectic concentration of the system, and metastable phases were formed according to different rates of temperature changes.

#### c) Cluster C

This cluster was represented by a dozen inclusions which could be separated into two groups:

##### Type C.1

Two large inclusions (>50 $\mu$ ) were similar to the inclusion described in A.1, but the present inclusions showed apart from granular solid phase a elongated octogonal birefringent mineral. The solid phases occupied more than 50 area % of the surface of inclusions. No microthermometric measurements were made.

##### Type C.2

The other inclusions presented regular shape (many negative crystals) and liquid + gas phases. An interesting feature in some of these inclusions was the possibility of measuring separately the melting temperatures of ice and of salt hydrates in the same inclusion (Figure 57, Cluster C). The ice was characteristically rounded, presented index lower than solution and melted at higher rate than the salt hydrates. These hydrates presented polygonal form, index higher than solution and very low melting rate.

The melting temperatures of salt hydrates ( $-10.0^{\circ}\text{C}$ ) indicate salinities of 36wt. %  $\text{CaCl}_2$  or 24 wt. %  $\text{NaCl}$  equivalents.

Solutions of such different salinities point to mixing of different fluids or, in the present case, disruption after entrapment probably as a consequence of metamorphic processes.

d) Cluster D

Inclusions from this cluster were either one phase (liquid) or two phases (liquid + vapour). The first melting occurred between  $-54^{\circ}\text{C}$  and  $-76^{\circ}\text{C}$  but the  $T_F$  of the ice was possible to be measured in only two cases (Figure 57, cluster D). During the freezing process many inclusions nucleated a tiny near cubic daughter mineral which did not form  $\text{NaCl}$  dihydrate. They were probably other chloride hydrates. In two inclusions the melting temperature of these hydrates was  $+8.1^{\circ}\text{C}$  and  $+19.3^{\circ}\text{C}$ . These values and the low first melting are indicative of very saline brines (38.0 to 42 wt. %  $\text{CaCl}_2$  or 27 wt.%  $\text{NaCl}$  equivalents for the temperature of dissolution of the salts).

The heating test showed only one inclusion homogenizing at  $+273^{\circ}\text{C}$ . The majority decrepitated between  $+330^{\circ}\text{C}$  and  $+340^{\circ}\text{C}$  before homogenization had occurred. These decrepitations (at such low temperatures) seem to be caused by inclusions with high internal pressures and/or weakness in quartz structure similar to the phenomena observed in inclusions from Cluster A. In many inclusions the bubble size increased after  $100.0^{\circ}\text{C}$  without visible leakage. This may simply be the consequence of thermal expansion of quartz leading to an increase of volume of the inclusion, the same phenomena will be described in Cluster G.

e) Cluster E

Inclusions from this cluster were present in a large variety of size, shape, and composition (Plate XVII, photos 2 and 3). The composition of the inclusions varied from single-phase (only liquid or only vapour) to multi-phase. Among the latter the most characteristic were inclusions with several daughter minerals like those of above mentioned photos. In many inclusions the solid phases covered more than 20% of their surface. These solid phases were formed by one large cubic crystal and many elongated - sometimes prismatic - minerals. Less frequently hexagonal platelets were present. The elongated minerals were strongly birefringent with angle of extinction between  $9^{\circ}$  -  $12^{\circ}$ . The S.E.M.-E.D.A.X. analyses indicated the presence of Ca, Mg, Na, K, and Cl in similar minerals from inclusion cavities which suggest chloride hydrates of these alkaline and alkaline earth elements (Plate XVIII, photos 1, 3, and 4). Upon freezing, the cubic crystal formed hydrate which melted just before  $0^{\circ}\text{C}$  (compare photos 3 and 4 in Plate XVII), indicating that this crystal was NaCl. No change in other daughter minerals were observed. Upon heating no dissolution of these daughter minerals could be observed. The vapour bubble when present disappeared at around  $+74^{\circ}\text{C}$ . Above  $+168^{\circ}\text{C}$  inclusions of all types presented an increase in bubble size. The cause may be the same as given for clusters A and D. Above  $+225^{\circ}\text{C}$  these inclusions started decrepitating.

Liquid-phase or liquid + vapour phase inclusions presented melting of last ice mainly between  $-5^{\circ}\text{C}$  and  $-15.0^{\circ}\text{C}$  (Figure 59), Cluster E) which indicate salinity of 10 to 16 wt %  $\text{CaCl}_2$  equivalent. The  $T_{\text{H}}$  was not considered because of highly variable liquid/vapour ratio.

SAMPLE A-495-II Melting Temperatures

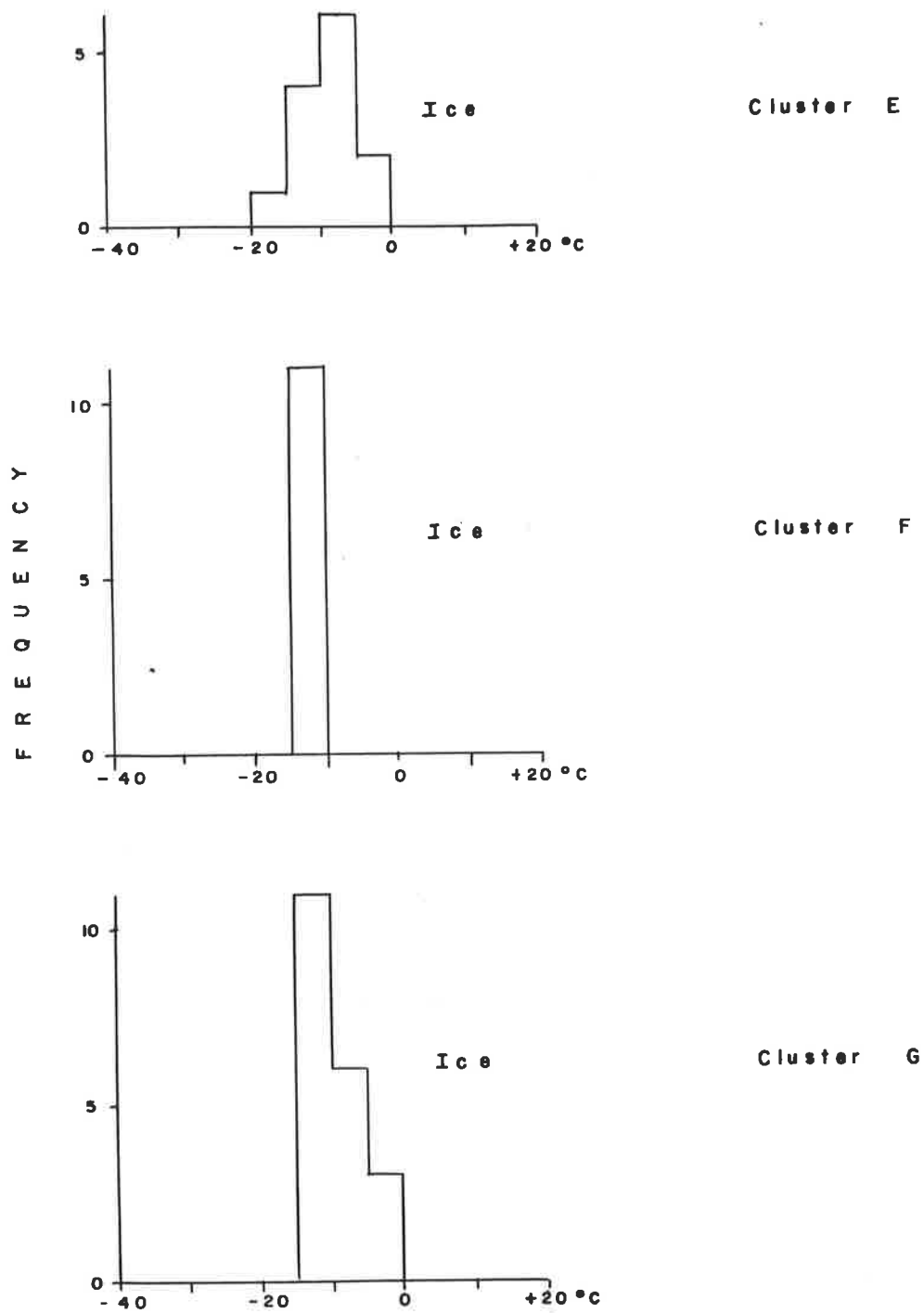


Figure 59:  $T_F$  frequency histograms of clusters E, F, and G of fluid inclusions in quartz.

Few nearly pure vapour-phase inclusions were also present. They presented no phase changes during microthermometry.

The coexistence of inclusions with supersaturated and others with insaturated brines can again be explained only by independent origin, inhomogeneous entrapment, or post-entrapment changes. Furthermore the heating test suggested the multi-phase inclusions would decrepitate before homogenization could possibly occur indicating the solid phases were not nucleated after the formation of inclusions.

f) Cluster F

This cluster presented mainly inclusions filled only with liquid-phase. Few of them presented small vapour-phase or cubic daughter minerals. The last ice in 11 inclusions melted between  $-12.4^{\circ}\text{C}$  and  $-13.4^{\circ}\text{C}$  corresponding to a salinity or  $\sim 16$  wt. % of  $\text{CaCl}_2$  equivalent (Figure 59, Cluster F).

g) Cluster G

This cluster was formed by inclusions containing only liquid or liquid + vapour phases. In the latter the liquid/vapour ratio was fairly constant: the vapour phase had 5% to 10% of the volume of the inclusion. During microthermometry many inclusions presented again unusual phase changes.

During the first freezing almost all inclusions were frozen at  $-80^{\circ}\text{C}$ . The last ice melted between  $-3.5^{\circ}\text{C}$  and  $-15.0^{\circ}\text{C}$ , indicating salinities in the range of 5 to 18 wt. %  $\text{CaCl}_2$  equivalent (Figure 59, Cluster G). Afterwards the sample was submitted to a stepwise heating up to  $250^{\circ}\text{C}$ . Only three two-phase inclusions homogenized into liquid phase between  $210^{\circ}\text{C}$   $230^{\circ}\text{C}$ . The vapour phase after becoming just a dot remained in brownian movement for an interval

of more than  $50^{\circ}\text{C}$ . This is quite an unusual resistance to homogenization. Subsequently the cooling from  $250^{\circ}\text{C}$  down to  $+70^{\circ}\text{C}$  caused the nucleation of a vapour-phase in some inclusions that were monophasic before heating. In these inclusions, no sign of leakage had been observed during the first heating process. From  $+70^{\circ}\text{C}$ , the sample was heated again to  $+245^{\circ}\text{C}$ , left overnight at that temperature (for 11 hours), and cooled down to room temperature. After this treatment a new freezing was performed.

For better illustration three different sequences of phase changes during the whole microthermometric process above described will be given in detail.

One inclusion (No. 1) with  $55\mu$  and tetra-hedrical shape presented vapour-phase of 5 vol.% before the heating test. The bubble after becoming just a point before  $+200^{\circ}\text{C}$  disappeared only between  $+220^{\circ}\text{C}$  and  $230^{\circ}\text{C}$ . Upon cooling the vapour-phase did not reappear even when the sample was frozen to  $-80^{\circ}\text{C}$ .

Another inclusion (No. 2) with  $25\mu$  and trapezoidal shape was monophasic before the heating process. During the cooling process, after being heated to  $+250^{\circ}\text{C}$ , it nucleated a bubble and an amorphous dark daughter mineral. At  $+70^{\circ}\text{C}$  the vapour-phase occupied an area of 5% of the inclusion. The new heating to  $+245^{\circ}\text{C}$  was able to homogenize the fluid phases only after being left overnight (11 hours). During the next cooling process, at  $+150^{\circ}\text{C}$ , two bubbles were suddenly nucleated simultaneously. One of them dissolved again almost immediately. With further cooling the second bubble increased in size and at  $+80^{\circ}\text{C}$  it was nearly covering the entire surface of the inclusion. From that point the bubble started shrinking again and at  $+50^{\circ}\text{C}$  covered approximately 60% of the surface of the inclusion. Finally at  $+25^{\circ}\text{C}$  this vapour-phase represented only 10% of the same surface.



A third (No. 3) inclusion was also monophasic before the microthermometry. During the second freezing it nucleated a bubble at  $-10^{\circ}\text{C}$  which disappeared again at  $-90^{\circ}\text{C}$ . The last solid phase melted incongruently at  $-11.8^{\circ}\text{C}$  forming a vapour phase. This bubble did not disappear anymore and had at room temperature a volume of 5% of the inclusion.

The majority of inclusions from the present cluster presented phase-changes similar to those just described.

#### Interpretation and conclusions

These unusual phase-changes are probably the consequence of different thermal expansion and internal atomic rearrangement of the recrystallized and stressed host quartz. These processes during the heating test caused an increase in the volume of inclusions larger than the expansion of the liquid phase resulting in nucleation or increase of bubble. During the cooling process the shrinking of the volume of inclusions may not be as instantaneous as the thermal contraction of the liquid phase. This would cause at first the spreading of the vapour-phase and later, its contraction when the internal crystal arrangement had again been equilibrated (e.g. - inclusion No. 2). Another plausible explanation may be a possible reversal in solubility of gases ( $\text{CO}_2 + \text{CH}_4$ ) in chloride rich brines with temperature changes as it was confirmed by Duffy et al. (1961) within the range of the experiment.

The formation of a daughter mineral upon heating as in inclusion No. 2 may be a consequence of pH change of the solution during the heating test in a process similar to the one that caused the change in the daughter minerals of inclusion No. 1 in the sample A-495-172B.

Scanning Electron Microscopy (Plate XVIII)

The S.E.M. of freshly broken surfaces of quartz from the vein displayed the best cluster of inclusion cavities and salt content. The photo 6 is an example of these surfaces. Apart from a group of NaCl crystals on the surface (Photo 2), probably formed by evaporation of the brine, a variable cluster of solid phases could be studied and the composition determined.. Elongated platy, prismatic, hexagonal platy, and micaceous morphology can be seen on the photos 1, 3, 4, and 5. These habits correspond to the same morphology of solid phases found under optical microscope in:

- a) solid phase rich inclusions (Cluster E, Plate XVIII, photos 2 and 3),
- b) inclusions of group B in Figure 56, and
- c) daughter minerals (salt hydrates) nucleated during microthermometry study.

So, a good correspondence could be established between the solid phases studied by S.E.M. and ordinary microscopy. The E.D.A.X. determination of minerals from nearly 50 inclusion cavities allowed to draw a more precise knowledge on the nature of the solid and liquid phases studied by microthermometry. Many minerals from Plate XVIII presented Ca, K, Cl, Mg, and Na but their proportion in each mineral seems to be highly variable. In photo 1, for instance, the mineral a presented the strongest peak for Ca. The mineral b presented the strongest peak for Mg and the second strongest for K, and the mineral c presented the strongest peak for K and the second strongest for Mg. The same elements were detected in minerals of photos 3 and 4. In photo 5, the Ca and Mg were not present but Fe became present. In other cavities the presence of Al with Cl was also detected. These elements indicated that the majority of solid phases were multiple chlorides which seem to be able

to form isomorphous mixture at least to a certain extent. These data show the complex multicomponent system we are dealing with and the inherent difficulties in interpreting correctly the phase changes occurred during the microthermometry.

Apart from chlorides, minerals giving only the peak for Ca was sometimes detected (e.g.-Photo 1). The mineral was probably  $\text{CaCO}_3$ . Micaceous minerals showing component elements of sericite and chlorite were also frequently present.

#### Crushing Test

The crushing test always presented a "very strong" gas release, indicating inclusions with high internal pressure.

The crushing in  $\text{Ba(OH)}_2$  solution indicated two types of bubbles. About 20% of the bubbles disappeared fairly rapidly forming a tangle of  $\text{BaCO}_3$  crystals. The remaining bubbles dissolved very slowly in the solution leaving no trace of reaction products.

The crushing in kerosene indicated a majority of bubbles dissolving completely in this solvent. Bubbles of  $30\mu$  of diameter dissolved in less than 10 seconds. Others with  $150\mu$  of diameter took nearly five minutes to dissolve completely. These values are in agreement with each other considering that the volume of the larger bubble is 125 times larger than the volume of the smaller bubble, and at the same time, the surface becomes only 5 times larger.

These solubility tests indicated that there were at least two different gases in the vapour phase of the inclusions:  $\text{CO}_2$  and hydrocarbons where the former were subordinate to the latter. The smaller amount of  $\text{CO}_2$  also is in agreement with the complete absence of liquid  $\text{CO}_2$  at room temperature or during freezing tests.

Conclusions for sample A-495-11

1. After examining more than 200 inclusions, microthermometric measurements in more than 80 and S.E.M.-E.D.A.X. determinations in nearly 50 inclusions were performed. Ordinary microscopy of other inclusions and crushing tests in glycerine, barium hydroxide solution and kerosene completed the study of the present sample.
2. The determination of a complete chronology of formation of inclusions were not possible but the inclusions located along a plane (healed fracture?) crosscutting the boundaries of quartz grains were of secondary origin and formed at the latest stage. These inclusions were generally richer in vapour phase and frequently presented negative crystal forms. The latter inclusions were sometimes almost completely filled with vapour-phase.
3. The salinity of these secondary inclusions would not be differentiated from other inclusions. They ranged from oversaturated to near 8 wt.% of salt ( $\text{CaCl}_2$  or NaCl equivalents). The  $T_F$  of ice in saturated or insaturated solutions were mainly between  $-5^\circ\text{C}$  to  $-15^\circ\text{C}$  (Figure 57 and 59).
4. The variable liquid/vapour ratio in secondary inclusions were the main difference from other inclusions. This range varied from only aqueous to almost pure gas inclusions. The hydrocarbons and subordinate  $\text{CO}_2$  detected by the crushing test were certainly gases liberated mostly from these gas-rich inclusions.
5. Many irregular shaped aqueous inclusions, especially from Cluster B and G, presented phase changes that were different at each freezing and heating test. This non-uniformity of phase changes are probably the result of different warming or cooling rates during the test associated to the different thermal expansion or contraction of recrystallized quartz.

6. Few  $T_H$ , between 200°C and 300°C, in liquid + vapour inclusions have no significance to the temperature of entrapment of inclusions. The value of 300°C, the same temperature determined from the mineral assemblage by Binns et al. (1979) may be just coincidental. The number of  $T_H$  determinations are too small to be statistically valid. The majority started decrepitating between 330°C and 360°C well before the homogenization had been attained. The decrepitation at relatively low temperatures for quartz is considered to be the sum of high internal pressure in inclusions and weakness in crystal structure due to high recrystallization.

The S.E.M. and microthermometry defined the solid phases as NaCl plus other multicompositional chlorides.

8. Although no straightforward relation between chloride-rich solutions and uranium mineralization had been found, the close physical relationship between both elements suggests the possible influence of these brines in the uranium mineralization.

#### General Conclusions

With the exception of sample A-495-3, the fluid inclusions for Jabiluka samples were very similar to those studied in sample A-495-179 of Nabarlek. Few type (a) inclusions (liquid-rich) presented exceptionally high content of solid phases like in sample A-495-179 from Nabarlek. But in the Jabiluka samples the SEM indicates major frequency of chlorides of Ca, K, Mg and Na with large amount of Ca (compare: Plate XVIII and Plates XI to XIV; figure 36 with Figure 56 and Plate XVII, photos 2 and 3). The SEM findings are in agreements with microthermometric data.

Unusual phase changes in inclusions from sample A-495-11 was interpreted as consequences of highly saline solutions, different

rates of heating or cooling, and changes in the volume of inclusions due to the differential thermal expansion and contraction of quartz and fluid. Those observations may be of some significance in the fluid inclusion study.

In type (b) inclusions the vapour phase very frequently presented more conspicuous fringe of liquid  $\text{CO}_2$ . The density ( $0.7 \text{ g CO}_2/\text{cc}$ ) and pressure ( $>1 \text{ Kbar}$ ) of carbon dioxide is in the same range determined for sample A-495-179. In opposition to the data of this Nabarlek sample, the crushing and freezing tests in the Jabiluka sample indicated larger amounts of hydrocarbon than  $\text{CO}_2$ .

Results from idiomorphic quartz of sample A-495-3 are in the same range of many hydrothermal quartz from the Nabarlek deposit.

Indication of large amount of hydrocarbons - probably methane - in all samples seems to be of major significance for uranium mineralization.

REFERENCES

- ADDY, S.K. (1973) - The problem of ore genesis at Ducktown, Tennessee: interpretation of stable isotopes ( $O^{18}/O^{16}$ ,  $C^{13}/C^{12}$ , and D/H), microprobe and textural data. Columbia University, Fac. of Pure Science, Ph.D. thesis (unpublished).
- ANTHONY, P.J. (1976) - Nabarlek uranium deposit. In Economic Geology of Australia and Papua New Guinea: v.1 - Metals (ed. C.L.Knight), pp. 304-308 (the Australasian Institute of Mining and Metallurgy: Melbourne).
- AYRES, D.E. and EADINGTON, P.T. (1975) - Uranium mineralization in the South Alligator River Valley. Mineralium Deposita, v. 10, pp. 27-41.
- BARANOV, V.I., LE-TIEN TU, and KOROBKOV, V.I. (1962) - Geochemistry of uranium and thorium in the granitic rocks of the Kyzyltau Massif (Central Kazakhstan). Part 2: Modes of occurrence of radioactive elements in granitic rocks. Geochemistry, no. 5, pp. 469-483.
- BARANOV, V.I. and TLEUBERGHENOVA, G. (1956) - Application of the micro-radiographic method utilizing liquid emulsions to a study of the content and distribution of radioactive elements in rocks. Geochemistry, no. 2, pp. 184-191.
- BAZAROV, L.Sh. (1966) - A device for freezing inclusions in minerals. (Abstr.). Fluid inclusion Research - Proceedings of COFFI, v.2, p.28, 1969.
- BECK, L.S. (1969) - Uranium deposits of the Athabasca region, Saskatchewan. Saskatchewan Department of Mineral Resources, Report no. 126.
- (1977) - Changing ideas on metallogenesis of Saskatchewan's uranium deposits. Can. Mining Journal, April 1977, pp. 49-52.
- BIGEISEN, J. and MAYER, M. (1947) - Calculation of equilibrium constants for isotopic exchange reactions. Jour. Chem. Phys., v. 15, pp.261-267.
- BINNS, R.A., McANDREW, J., and SUN, S-S. (1979) - Origin of uranium mineralization at Jabiluka. In International Uranium Symposium on the Pine Creek Geosyncline, Extended Abstracts, pp. 20-25.
- BLATTNER, P. (1972) - N.A.A. formulae. Unpublished leaflet.
- (1975) - Oxygen isotopic composition of fissure grown quartz, adularia, and calcite from Broadlands Geothermal Field, N.Z. Am. Jour. Sci., v. 275, pp. 785-800.
- BLATTNER, P. and BIRD, G.W. (1974) - Oxygen isotope fractionation between quartz and K-feldspar at 600°C. Earth Planet. Sci. Letters, v. 23, pp. 21-27.

- 
- (1976) - Corrected and consistent oxygen isotope geothermometers. Stable Isotope Conference, Lower Hutt, N.Z., August 1976, 4p. (unpublished).
- BLATTNER, P. and HULSTON, J.R. (1975) - A pair of solid reference samples to trace drift and proportional errors of  $^{18}\text{O}$  scale. Institute of Nuclear Sciences, D.S.I.R., Contribution no. 691, INS-LN-41, 4p. (unpublished).
- 
- (1977) - Proportional variations of geochemical  $^{18}\text{O}$  scales - an interlaboratory comparison (in press).
- BONEV, I.K. (1977) - Primary fluid inclusions in galena crystals. I- Morphology and origin. Mineralium Deposita, v. 12, pp. 64-76.
- BOTTINGA, Y, and JAVOY, M. (1973) - Comments on oxygen isotope geothermometry. Earth and Planet. Sci. Letters, v. 20, pp. 250-265.
- BOWIE, S.H.U. (1951) - Autoradiographic techniques in geological research. Bull. Geol. Survey Great Britain, v. 3, pp. 58-79.
- BOYARSKAYA, R.V. (1973) - Advantages of electron microscopy in studying fluid inclusions in minerals. Fluid Inclusion Research - Proceedings of COFFI, v. 6, p. 26, 1973.
- BOZZO, A.T., CHEN, H-S., KASS, J.R., and BARDUHN, A.J. (1973) - The properties of the hydrates of chloride and carbon dioxide. 4th International Symposium on Fresh Water from the Sea, v. 3, pp.437-451.
- CHAIXMECA (1973) - Platine à écrasement sous microscope (Licence ANVAR-C.N.R.S.). Explanatory leaflet.
- CLAYTON, R.N. and MAYEDA, T.K. (1963) - The use of bromine pentafluoride in the extraction of oxygen from oxides and silicates for isotopic analysis. Geoch. Cosmoch. Acta, v. 27, pp. 43-52.
- CLOCCHIATI, R. (1975) - Les inclusions vitreuses des cristaux de quartz. Fluid Inclusion Research - Proceedings of COFFI, v.8, pp. 41-42, 1975.
- COPPENS, R. (1950) - Étude de la radioactivité de quelques roches par l'émulsion photographique. Bull. Soc. Fr. Min. Cristall., Paris, v.73, n° 4-6, pp. 217-321.
- CORNELIUS, K.D. (1976) - Preliminary rock type and genetic classification of uranium deposits. Econ. Geology, v. 71, pp. 941-942.
- COVENEY, R.H. and KELLY, W.C. (1971) - Dawsonite as a daughter mineral in hydrothermal fluid inclusions. Contrib. Min. Petrol., v.32, pp.334-342.
- CRICK, I.H. and MUIR, M.D. (1979) - Evaporites and uranium mineralization in the Pine Creek Geosyncline. In International Uranium Symposium on the Pine Creek Geosyncline, Extended Abstracts, pp. 30-33.
- CUNEY, M. (1974) - Le gisement uranifère de Bois-Noirs - Limouzat (Massif Central - France): Relations entre minéraux et fluides. Thèse, Univ. Nancy, France.



- DAHLKAMP, F.J. (1979) - Uranium occurrences in Northern Saskatchewan, Canada, and their mode of origin. In *Theoretical and Practical Aspects of Uranium Geology*, The Royal Society of Lond, pp. 115-130.
- DEICHA, G. (1950) - Essais par écrasement de fragments minéraux pour la mise en évidence d'inclusions de gaz sous pression. *Bull. Soc. Fr. Miner. Crist.*, v. 73, pp. 439-445.
- (1973) - (Scanning electron microscopy of cavities in gangue and rock minerals). (Abstr.). *Bull. Soc. Fr. Miner. Crist.*, v. 96, n° 4-5, p. XIX (in French).
- DEVEREUX, I. (1968) - Oxygen isotope ratios of minerals from the regionally metamorphosed schists of Otago, New Zealand. *New Zealand Sci.*, v. 11, n° 3, pp. 526-548.
- DOBROVOL'SKAYA, M.G., BOYARSKAYA, R.V., and VASIL'EVA, G.L. (1973)- On the fluid inclusions in highly ferruginous sphalerite from the Savinskoe no. 5 deposit, East Transbaikal. (Abstr.). *Fluid Inclusion Research - Proceedings of COFFI*, v.6, p. 34, 1973.
- DUFY, J.R., SMITH, N.O., and NAGY, B. (1961) - Solubility of natural gases in aqueous salt solutions. I - Liquidus surfaces in the system  $\text{CH}_4$ - $\text{H}_2\text{O}$ - $\text{NaCl}$ - $\text{CaCl}_2$  at room temperatures and at pressures below 1000 psia. *Geochem. Cosmoch. Acta*, v. 24, pp. 23-31.
- ERMAKOV, N.P. (1965) - Studies of mineral-forming solutions. In *Research on the Nature of Mineral-forming Solutions*. Editor: D.E. Ingerson, International Series of Monographs in Earth Sciences, v. 22, Part I, pp. 1-348, Pergamon Press.
- ERMAKOV, N.P., KALYUZHNYI, V.A., and MYAZ', N.I. (1957) - Results of mineral thermometric investigations of some smoky quartz crystals from the Volynia district. In *Research on the Nature of Mineral-forming Solutions*. Editor: D.E. Ingerson, International Series of Monographs in Earth Sciences, v. 22, Part II, pp. 490-503, 1965, Pergamon Press.
- FERGUSON, J. (1979) - Metamorphism in the Pine Creek Geosyncline and its bearing on stratigraphic correlations. In *International Uranium Symposium on the Pine Creek Geosyncline*, Extended Abstracts, pp.71-74.
- FERGUSON, J., EWERS, G.R., and DONNELLY, T.H. (1979) - Model for the development of economic uranium mineralization in the Alligator Rivers uranium field. In *International Uranium Symposium on the Pine Creek Geosyncline*, Extended Abstracts, pp. 79-82.
- FORD, J.H. and GREEN, D.C. (1977) - An oxygen and hydrogen isotope study of the Panguna porphyry-copper deposit, Bougainville. *Jour. Geol. Soc. Australia*, v. 24, part 2, pp. 63-80.

- FRENCH, B.M. (1966) - Some geological implications of equilibrium between graphite and a C-H-O gas phase at high temperatures and pressures. *Rev. Geoph.*, v. 4, no. 2, pp. 233-253.
- FRIEDMAN, I. and O'NEIL, J.R. (1977) - Compilation of stable isotope fractionation factors of geochemical interest. *Data of Geochemistry*, M. Fleischer edition, U.S.G.S. Professional Paper 440-KK.
- GALUP, A.L., GREENWOOD, B., and WILSON, J.F. (1975) - A microscope cold stage. (Abstr.). *Fluid Inclusion Research - Proceedings of COFFI*, v. 8, p. 59, 1975.
- GARLICK, G.D. (1969) - Oxygen. In *Handbook of Geochemistry*, v. II/I, sec. 8B, ed. K.H. Wedepohl, Springer-Verlag, Berlin.
- GARLICK, G.D. and EPSTEIN, S. (1966) - The isotopic composition of oxygen and carbon in hydrothermal minerals at Butte, Montana. *Econ. Geol.*, v. 61, pp. 1325-1335.
- GRANT, J.M., WILKINSON, N., and HALLS, C. (1976) - Analysis of fluid inclusion daughter salts using a scanning electron microscope. *Current research on fluid inclusions and on mineral deposits*, A.M. Evans, (Conference report), *Jour. Geol. Soc. Lond.*, v. 134, p. 390, 1977.
- GRITTI-BAUDRACCO, C. (1975) - Fluid inclusions in some gangue minerals from deposits in southern France, (Abstr.). *Fluid Inclusion Research - Proceedings of COFFI*, v. 8, p. 66, 1975.
- HALL, W. (1969) - Oxygen and carbon isotopic composition of ore and host rock of selected Mississippi Valley deposits. U.S.G.S. Professional Paper 650-C, pp. C140-C148.
- HAYAKAWA, N., NAMBU, M., and AOSHIMA, T. (1969) - Trial manufacture of a heating stage for use under high pressure, (Abstr.). *Fluid Inclusion Research - Proceedings of COFFI*, v. 2, p. 45, 1969.
- HEGGE, M.R. (1977) - Geologic setting and relevant exploration features of the Jabiluka uranium deposit. *Proc. Australas. Inst. Min. Metall.*, no. 264, pp. 19-32.
- HILLS, J.H. and RICHARDS, J.R. (1976) - Pitchblende and galena ages in the Alligator Rivers region, N.T., Australia. *Mineralium Deposita*, v. 11, pp. 133-154.
- HOEVE, J. and SIBBALD, T.I.I. (1978) - Mineralogy and geological setting of unconformity-type uranium deposits in northern Saskatchewan. *Min. Assoc. Canada, Short course handbook on "Uranium deposits their mineralogy and origin"*, M.M. Kimberley ed., v. 3, Sec. B, pp. 457-484.

- HOLLISTER, L.S. and BURRUSS, R.C. (1976) - Phase equilibria in fluid inclusions from the Khtada Lake metamorphic complex. *Geochem. Cosmoch. Acta.* v. 40, pp. 163-175.
- HOPWOOD, T.P. (1971) - A study of structural ore controls at Nabarlek, Northern Territory. Report Newaim Pty. Ltd. (unpublished).
- HUDSON, J.D. (1977) - Stable isotopes and limestone lithification. *The Jour. Geol. Soc. London*, v. 133, pp. 637-660.
- IKORSKIY, S.V. (1964) - Hydrocarbon gases and bitumens in rock-forming minerals of the Khibiny stock. *Acad. Sci. U.S.S.R. Doklady, Earth Sci. Sec.*, v. 157, pp. 90-93. (English translation).
- \_\_\_\_\_ (1970) - The inclusions of hydrocarbon gases and bitumens in the minerals of some igneous rocks (after an example of the Khibiny alkali massif) (Abstr.). *Fluid Inclusion Research - Proceedings of COFFI*, v. 3, p. 27, 1970.
- I.A.E.A. (1974) - Formation of uranium ore deposits. *Proceedings of a Symposium, Athens, International Atomic Energy Agency, Vienna*, 750 p.
- JEHL, V. (1974) - Standardization and calibration in microthermometry apparatus ( $-180^{\circ}$  /  $+600^{\circ}$  C range), unpublished manual, pp. 21-27.
- KALYUZHNYI, V.A. (1958a) - Homogenization curves in mineralogical thermometry and their plotting. In *Research on the nature of mineral-forming solutions*, Editor: D.E. Ingerson, *International Series of Monographs in Earth Sciences*, v. 22, pp. 565-577, 1965, Pergamon Press.
- \_\_\_\_\_ (1958b) - The study of the composition of captive minerals in poliphase inclusions. *Intern. Geol. Rev.*, v. 4, no. 2, pp. 127-138, 1962.
- \_\_\_\_\_ (1960) - Methods of study of multiphase inclusions in minerals. Kiev, Izdatel. Akad. Nauk Ukrainskoy RSR, 169 p. (in Ukrainian).
- \_\_\_\_\_ (1961) - Mineral forming solutions from inclusions in minerals. *Referativnyi Khim., Khim., Abs.* (15G70 (in Russian), 1962.
- \_\_\_\_\_ (1973) - New instruments for studies of inclusions of mineral-forming fluids and principles of their use. *Fluid Inclusion Research - Proceedings of COFFI*, v. 7, pp. 90-91, 1974.
- KELLY, W.C. and GODDARD, E.N. (1969) - Telluride ores of Boulder County, Colorado. *Fluid Inclusion Research - Proceedings of COFFI*, v. 3, p. 30, 1970.
- KHARMALOV, Ye.S. (1973) - Construction of an apparatus for fine control of the speed of freezing of preparations in a cryostage by the use of liquid nitrogen. *Fluid Inclusion Research - Proceedings of COFFI*, v. 7, p. 99, 1974.

- KHETAGUROV, G.V. (1971) - Technique of studying gas liquid inclusions in a microthermo-chamber. Fluid Inclusion Research - Proceedings of COFFI, v. 4, p. 38, 1971.
- KLEVTSOV, P.V. and LEMMLEIN, G.G. (1960) - Pressure correction for the homogenization temperatures of aqueous NaCl solutions. Acad. Sci. U.S.S.R., Earth Sci. Sec., v. 128, pp. 995-997.
- KNIPPING, H.D. (1974) - The concepts of supergene versus hypogene emplacement of uranium at Rabbit Lake, Saskatchewan, Canada. In Symposium on the Formation of Uranium Ore Deposits - I.A.E.A. - Athens, 750 p.
- LANDIS, G.P. and RYE, R.O. (1974) - Geologic, fluid inclusion, and stable isotope studies of the Pasto Buena tungsten-base metal ore deposit, Northern Peru. Econ. Geology, v. 69, pp. 1025-1059.
- LANGFORD, F.F. (1974) - A supergene origin for vein-type uranium ores in the light of the Western Australia calcrete-carnotite deposits. Econ. Geology, v. 69, pp. 516-526.
- \_\_\_\_\_ (1978) - Origin of unconformity-type pitchblende deposits in the Athabasca basin of Saskatchewan. Min. Assoc. Canada - Short course handbook on "Uranium deposits, their mineralogy and origin", M.M. Kimberley ed., v. 3, sec. B, pp. 485-499.
- LANGMUIR, D. (1978) - Uranium solution-mineral equilibria at low temperatures with applications to sedimentary ore deposits. Geochem. Cosmoch. Acta, v. 42, pp. 547-569.
- LARSON, L.T., MILLER, J.D., NADEAU, J.E., and ROEDDER, E. (1973) - Two sources of error in low temperature inclusion homogenization determination, and corrections on published temperatures for the East Tennessee and Laisvall deposits. Econ. Geology, v. 68, pp. 113-116.
- LE BEL, L. (1976) - Fluid inclusion study of the porphyry copper deposit of Cerro Verde-Santa Rosa, South Peru, Part I: the quartz sericite alteration. Current research on fluid inclusions and on mineral deposits, A.M. Evans (Conference report), Jour. Geol. Soc. Lond., v. 134, p. 392, 1977.
- LEROY, J. (1971) - Les épisienites non minéralisées dans le massif de granite à deux micas de Saint-Sylvestre (Limousin-France). Equilibres entre minéraux et solutions. Thèse, Univ. Nancy, I, (unpublished).
- LINKE, W.F. (1965) - Solubilities of inorganic and metal organic compounds (4th. ed.): Am. Chem. Soc., 1914 p.
- LITTLE, H.W. (1974) - Uranium in Canada. Geol. Surv. Canada, Paper 74-1, Part A, Report of activities, pp. 137-139.

- MATHEWS, G.W. (1978) - Uranium occurrences of uncertain genesis. In Geologic characteristics of environments favorable for uranium Deposits, D.G. Mickle and G.W. Mathews (editors), U.S. Depart. of Energy Rep. GJBX-67(78), pp. 221-250.
- METZGER, F.W., KELLY, W.C., NESBITT, B.E., and ESSENE, E.J. (1977) - Scanning electron microscopy of daughter minerals in fluid inclusions. *Econ. Geology*, v. 72, pp. 141-151.
- METZGER, F.W., NESBITT, B.E., and KELLY, W.C. (1975) - Scanning electron microscopy of daughter minerals in fluid inclusions (Abstr.). *Geol. Soc. Am., Abstr. with Progr.*, v. 7, p. 1199.
- MILLER, S.L. (1974) - The nature and occurrence of clathrate hydrates. In *Natural Gases in Marine Sediments*, I.R. Kaplan ed., New York, Plenum Press, pp. 151-177.
- McCREA, J.M. (1950) - On the isotopic chemistry of carbonates and a paleotemperature scale. *J. Chem. Phys.*, v. 18, pp. 849-857.
- McKINNEY, C.R., McCREA, J.M., EPSTEIN, S., ALLEN, H.A., and UREY, H.C. (1950) - Improvements in mass spectrometers for the measurement of small differences in isotopic abundance ratio. *Rev. Sci. Intr.*, v.21, p. 724.
- NEEDHAM, R.S. and STUART-SMITH, P.G. (1976) - The Cahill Formation - host to uranium deposits in the Alligator Rivers uranium field, Australia. *BMR Jour, Austr. Geol. and Geoph.*, v. 1, pp. 321-333.
- \_\_\_\_\_ (1979) - Geology of the Alligator Rivers uranium field. In *International Uranium Symposium on the Pine Creek Geosyncline, Extended Abstracts*, pp. 143-146.
- NESBITT, B.E. and KELLY, W.C. (1975) - Fluid and magmatic inclusions in the carbonatite at Magnet Cove, Arkansas (Abstr.). *Geol. Soc. Am., Abstr. Programs*, v.7, p. 1212.
- \_\_\_\_\_ (1977) - Magmatic and hydrothermal inclusions in carbonatite of the Magnet Cove complex, Arkansas. *Contrib. Min. Petr.*, v. 63, no. 3, pp. 271-294.
- NIER, A.O. (1947) - A mass spectrometre for isotope and gas analysis. *Rev. Sci. Intr.*, v. 18, p. 398.
- \_\_\_\_\_ (1950) - A redetermination of the relative abundances of the isotopes of carbon, nitrogen, oxygen, argon, and potassium. *Phys. Rev.*, v. 77, pp. 789-793,
- OHMOTO, H. and RYE, R.O. (1970) - The Bluebell Mine, British Columbia: I. Mineralogy, paragenesis, fluid inclusions and the isotopes of hydrogen, oxygen, and carbon. *Econ. Geology*, v. 65, pp. 417-437.

- O'NEIL, J.R., CLAYTON, R.N., and MAYEDA, T.K. (1969) - Oxygen isotope fractionation in divalent metal carbonates. *Jour. Chem. Phys.*, v. 51, no. 12, pp. 5547-5558.
- O'NEIL, J.R. and TAYLOR, H.P., Jr. (1969) - Oxygen isotope equilibrium between muscovite and water. *Jour. Geoph. Res.*, v. 74, no. 25, pp. 6012-6022.
- PAGE, R.W., COMPSTON W., and NEEDHAM, R.S. (1979) - Geochronology and evolution of the late Archaean basement and Proterozoic rocks in the Alligator Rivers uranium field, Northern Territory, Australia. In *International Uranium Symposium on the Pine Creek Geosyncline, Extended Abstracts*, pp. 151-154.
- PARÉ, X. and DUCROS, P. (1964) - Étude par résonance magnétique nucléaire de l'eau dans le beryl. *Bull. Soc. Fr. Min. Cristall.*, LXXXVII, pp. 429-433.
- PICCIOTTO, E.E. (1952) - Utilization des émulsion liquides dans l'étude de la radioactivité des roches. *Bull. Centre Phys. Nucl., Univ. Libre Bruxelles*, no. 33.
- POTY, B., LEROY, J., and JACHIMOWICZ, L. (1976) - Un nouvel appareil pour la mesure des températures sous le microscope: l'installation de microthermometrie Chaixmeca. *Bul. Soc. Fr. Min. Cristall.*, v. 99, no. 2-3, pp. 182-186.
- POTY, B. and STALDER, H.A. (1970) - Kryometrische Bestimmungen der Salz und Gasgehalte eingeschlossener Lösungen in Quarzkristallen aus Zerrklüften der Schweizer Alpen. *Schweiz. Mineral. Petrogr. Mitt.*, vol. 50, pp. 141-150.
- PROCEEDINGS of COFFI (1969) - Notice of new instruments. *Fluid inclusion Research - Proceedings of COFFI*, v. 2, pp. 4-7.
- RASUMNY, J. (1957) - Analyse microchimique des gaz contenus dans le minéraux: formation du précipité baritique. *Compte-Rendu Sommaire, Soc., Géol. Fr.*, pp. 378-380.
- (1960) - Essais microchimiques par écrasement: réaction avec l'acide chlorhydrique. *Compte-Rendu Sommaire, Soc. Géol. Fr.*, pp. 68-69.
- RICH, R.A., HOLLAND, H.D., and PETERSEN, U. (1977) - Hydrothermal uranium deposits. In *Developments in Economic Geology* 6, Elsevier, 264 p.
- RIESE, W.C., LEE, M.J., and BROOKINS, D.G. (1978) - Scanning electron microscopy of uranium ores, Grants mineral belt, New Mexico: application to U: C: pyrite distribution. *Econ. Geology*, v. 73, p. 314.

- ROBINSON, B.W. and BADHAM, J.P.N. (1974) - Stable isotope geochemistry and the origin of the Great Bear Lake silver deposits, N.W.T., Canada. *Can. Jour. Earth Sci.*, v. 11, pp. 698-711.
- ROBINSON, B.W. and OHMOTO, H. (1973) - Mineralogy, fluid inclusions, and stable isotope of the Echo Bay U-Ni-Ag-Cu deposits, N.W.T., Canada. *Econ. Geology*, v. 68, pp. 635-656.
- ROEDDER, E. (1962) - Studies of fluid inclusions I: low temperature and application of a dual purpose freezing and heating stage. *Econ. Geology*, v. 57, pp. 1045-1061.
- (1963) - Studies of fluid inclusions II: freezing data and their interpretations. *Econ. Geology*, v. 58, pp. 167-211.
- (1967) - Fluid inclusions as samples of ore fluids. In *Geochemistry of hydrothermal ore deposits*, H.L. Barnes ed., Holt, Rinehart and Winston, Inc., Chapter 12, pp. 515-566.
- (1970) - Application of an improved crushing microscope stage to studies of the gases in fluid inclusions. *Schweiz. Mineralog. Petr. Mitt.*, v. 50, pp. 41-58.
- (1972) - Composition of fluid inclusions. *Data of Geochemistry*, U.S.G.S., Professional Paper 440-JJ, Sixth ed., 164 p.
- ROEDDER, E. and COOMBS, D.S. (1967) - Immiscibility in granitic melts, indicated by fluid inclusions in ejected granitic blocks from Ascension Island. *Fluid Inclusion Research - Proceedings of COFFI*, v. 2, pp. 65-66, 1969.
- ROSASCO, G.J. and ROEDDER, E. (1976) - Application of new laser-excited Raman spectrometer to nondestructive analysis of sulfate in individual phases in fluid inclusions in minerals. *International Geol. Congress*, 25 th., Sydney, Abstracts of Papers, v. 3, pp. 812-813.
- ROSASCO, G.J., ROEDDER, E., and SIMMONS, J.H. (1975) - Laser-excited Raman spectroscopy for nondestructive partial analysis of individual phases in fluid inclusions in minerals. *Science*, v. 190, pp. 557-560.
- RYAN, G.R. (1979) - The genesis of Proterozoic uranium deposits in Australia. In *Theoretical and Practical Aspects of Uranium Geology*, The R.S.L., pp. 85-99.
- RYE, R.O. (1966) - The carbon, hydrogen, and oxygen isotope composition of the hydrothermal fluids responsible for the lead-zinc deposits at Providencia, Zacatecas, Mexico. *Econ. Geology*, v. 61, pp. 1399-1427.
- RYE, R.O. and O'NEIL, J.R. (1968) - The  $O^{18}$  content of water in primary fluid inclusions from Providencia, North-Central Mexico. *Econ. Geology*, v. 63, pp. 232-238.

- RYE, R.O. and SAWKINS; F.J. (1974) - Fluid inclusions and stable isotope studies on the Casapalca Ag-Pb-Zn-Cu deposit, Central Andes, Peru. *Econ. Geology*, v. 69, pp. 181-205.
- SAINTIVES, J.P. (1976) - Quelques aspects des inclusions solides révélés par le microscope électronique à balayage sur l'exemple d'un quartz pegmatitique. *Bull. Soc. Fr. Min. Cristall.*, v. 99, pp. 178-181.
- SAMOYLOVICH, L.A. and KHETCHIKOV, L.N. (1968) - Pressure correction to the homogenization temperatures of aqueous salt solutions. *Geochemistry Intern.*, v. 5, pp. 1184-1189.
- SASSANO, G.P., FRITZ, P. and MORTON, R.D. (1972) - Paragenesis and isotopic composition of some gangue minerals from the uranium deposits of Eldorado, Saskatchewan. *Can. Jour. Earth Sci.*, v. 9, pp. 141-157.
- SCHWARTZKOPFF, J., SANDRIN, L., BARABAS, A., and LEROY, J. (1974) - Preparation of doubly polished thick sections for fluid inclusion studies at the Centre de Recherches Petrographiques e Geochimiques, Nancy. Unpublished Chaixmeca booklet, pp. 28-31.
- SELLA, C. and DEICHA, G. (1970) - Fractographie électronique sur un échantillon de calcite de Vaduz (Principauté du Liechtenstein). *Schweiz. Mineralog. Petr. Mitt.*, v. 50, pp. 155-158.
- SHARMA, T. and CLAYTON, R.N. (1965) - Measurement of  $^{18}\text{O}/^{16}\text{O}$  ratios of total oxygen of carbonates. *Geochem. Cosmoch. Acta*, v. 29, pp. 1347-1353.
- SHEPPARD, S.M.F. and GUSTAFSON, L.B. (1976) - Oxygen and Hydrogen isotopes in the porphyry-copper deposit at El Salvador, Chile. *Econ. Geology*, v. 71, pp. 1549-1559.
- SHIEH, Y.N. and TAYLOR, H.P., Jr. (1969) - Oxygen and hydrogen isotope studies of contact metamorphism in the Santa Rosa Range, Nevada, and other areas. *Contr. Mineral. Petrol.*, v. 20, pp. 306-356.
- SMART, P.G., WILKES, P.G., NEEDHAM, R.S., and WATCHMAN, A.L. (1976) - Geology and Geophysics of the Alligator Rivers region. In *Economic Geology of Australia and Papua New Guinea*, v. 1 - Metals, pp. 285-301 (The Australasian Inst. of Min. and Metall., Melbourne).
- SMITH, F.W. (1973) - A simple microscope freezing stage. *Miner. Magazine*, v. 39, pp. 366-367.
- SOFER, Z. and GAT, J.R. (1972) - Activities and concentrations of oxygen  $^{18}\text{O}$  in concentrated aqueous salt solutions: analytical and geophysical implications. *Earth and Plan. Sci. Letters*, v. 15, pp. 232-238.
- SOURIRAJAN, S. and KENNEDY, G.C. (1962) - The system  $\text{H}_2\text{O}-\text{NaCl}$  at elevated temperatures and pressures. *Am. Jour. Sci.*, v. 260, pp. 115-141.



- SPRY, A. (1976) - Metamorphic Textures. Pergamon Press, 350 p.
- TAKENOUCHI, S. and KENNEDY, G.C. (1965) - Dissociation pressures at the phase  $\text{CO}_2 \cdot 5\frac{3}{4}\text{H}_2\text{O}$ . Jour. Geol., v. 73, pp. 383-390.
- TAUBE, H. (1954) - Use of oxygen isotope effects in the study of hydration of ions. Jour. Phys. Chem., v. 58, pp. 523-528.
- TAYLOR, H.P., Jr. (1967) - Oxygen isotope studies of hydrothermal mineral deposits. In Geochemistry of Hydrothermal Ore Deposits, H.L. Barnes ed., Holt, Rinehart, and Winston, Inc., Chapter 4, pp. 109-142.
- \_\_\_\_\_ (1974) - The application of oxygen and hydrogen isotope studies to problems of hydrothermal alteration and ore deposition. Econ. Geology, v. 69, pp. 843-883.
- \_\_\_\_\_ (1977) - Water/rock interactions and the origin of  $\text{H}_2\text{O}$  in granitic batholiths. The Jour. Geol. Soc. Lond., v. 133, part 6, pp. 509-558.
- TAYLOR, H.P., Jr. and FORESTER, R.W. (1971) - Low  $\text{O}^{18}$  igneous rocks from the intrusive complexes of Skye, Mull, and Ardnamurchan, Western Scotland. Jour. Petrol., v. 12, part 3, pp. 465-497.
- TRUEDELL, A.H. (1974) - Oxygen isotope activities and concentrations in aqueous salt solutions at elevated temperatures - consequences for isotope geochemistry. Earth and Plan. Sci. Letters, v. 23, pp. 387-396.
- UREY, H.C. (1947) - The thermodynamic properties of isotopic substances. Jour. Chem. Soc. (London), pp. 562-581.
- VASIL'EV, V.I., DOLOMANOVA, E.I., KOSTYLEVA, E.E., and PETROVSKAYA, N.V. (1971) - Some morphological features of gas-liquid inclusions in ore-bearing quartz (from electron microscope data). Fluid Inclusion Research - Proceedings of COFFI, v. 4, p. 89, 1971.
- WAHLER, W. (1956) - Über die in Kristallen eingeschlossenen Flüssigkeiten und Gase. Geochem. Cosmoch. Acta, v. 9, pp. 105-135.
- WALPOLE, B.P., DUNN, P.R., CROHN, P.W., and RANDAL, M.A. (1968) - Geology of Katherine-Darwin region, N.T. BMR Bulletin 82 (2 vol.).
- WEISBROD, A., POTY, B., and TOURET, J. (1976) - Les inclusions fluides en géochimie-pétrologie: tendances actuelles. Bull. Soc. Fr. Miner. Cristall., v. 99, pp. 140-152.
- WENNER, D.B. and TAYLOR, H.P., Jr. (1971) - Temperatures of serpentinization of ultramafic rocks based on  $\text{O}^{18}/\text{O}^{16}$  fractionation between coexisting serpentine and magnetite. Contr. Mineral. Petrol., v. 32, pp. 165-185.

- YANATIEVA, O.K. (1946) - (Solubility polytherms in the systems  $\text{CaCl}_2$ - $\text{MgCl}_2$ - $\text{H}_2\text{O}$  and  $\text{CaCl}_2$ - $\text{NaCl}$ - $\text{H}_2\text{O}$ ) (in Russian). Zhurnal Prikladnoi Khimii, v. 19, pp. 709-722.
- YPMA, P.J.M. (1963) - Rejuvenation of ore deposits as exemplified by the Belledonne Metalliferous Province. Leiden, Netherlands, Leiden Univ. dissert., 212 p.
- (1965) - An instrument for geobarometry of fluid inclusions (Abstr.). Geol. Soc. Am. Spec. Paper 87, p. 190 (published in 1966).
- YPMA, P.J.M. and FUZIKAWA, K. (1979) - Fluid inclusion studies as a guide to the composition of uranium ore forming solutions of the Nabarlek and Jabiluka deposits, Northern Territory, Australia. In International Uranium Symposium on the Pine Creek Geosyncline. Extended Abstracts, pp. 212-215.

PLATES I to XVIII

PLATE I

Sample A-495-162

Scale: Bar = 100 $\mu$

Photo 1 - Emulsion autoradiography on quartz indicating numerous pitchblende inclusions. Vertical parallel lines are from emulsion coating.

Photo 2 - Elongated liquid (L) inclusion in quartz with botryoidal black daughter mineral (probably pitchblende (P)).

Photo 3 - Single, large, two-phased liquid (L) + vapour (V) primary inclusion. Calculations indicated that the bubble represents 20% of the volume of inclusion. Melting temperature of ice =  $-3.8^{\circ}\text{C}$ . Upon heating the liquid started to leak at  $+265^{\circ}\text{C}$ , before the homogenization had occurred indicating high pressure possibly due to the presence of  $\text{CO}_2$  and  $\text{CH}_4$ .

Photo 4 - Type (b) (gas-rich) inclusions. Ice from the largest inclusion melted at  $-19^{\circ}\text{C}$ .



PLATE II

Sample A-495-168

Photo 1 - Fluid inclusions and pitchblende trapped at the zone of growth (also see photo 4) of quartz (arrow).

Scale: bar = 100 $\mu$ .

Photo 2 - Type (a) (liquid (L)-rich) and type (b) (vapour-rich) inclusions trapped at the zone of growth of quartz. Arrows indicate directions of growth. Scale: bar = 10 $\mu$ .

Photo 3 - Emulsion autoradiography indicating pitchblende insider (a) and on the surface (b) of quartz. Parallel, near-horizontal lines are caused by emulsion coating.

Scale: bar = 100 $\mu$ .

Photo 4 - Emulsion autoradiography indicates pitchblende in zone of growth of quartz (g). Arrow indicates direction of growth.

Parallel, near-vertical lines are caused by emulsion coating. Scale: bar = 100 $\mu$ .

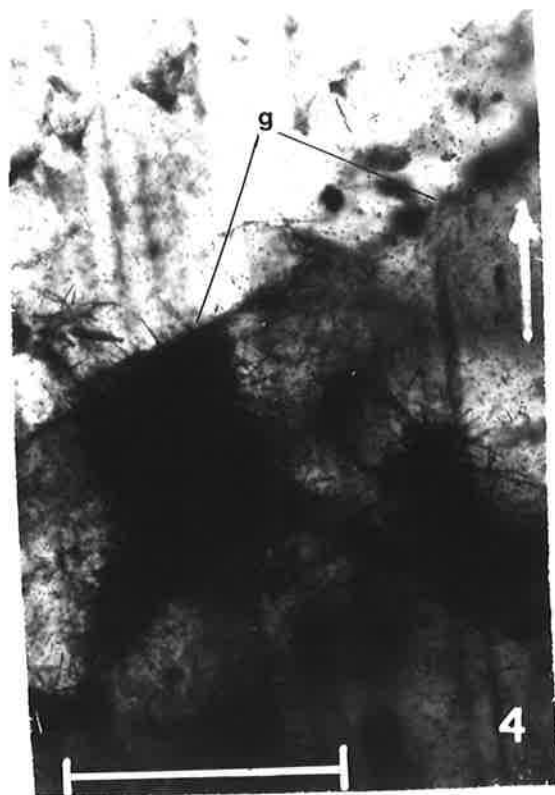
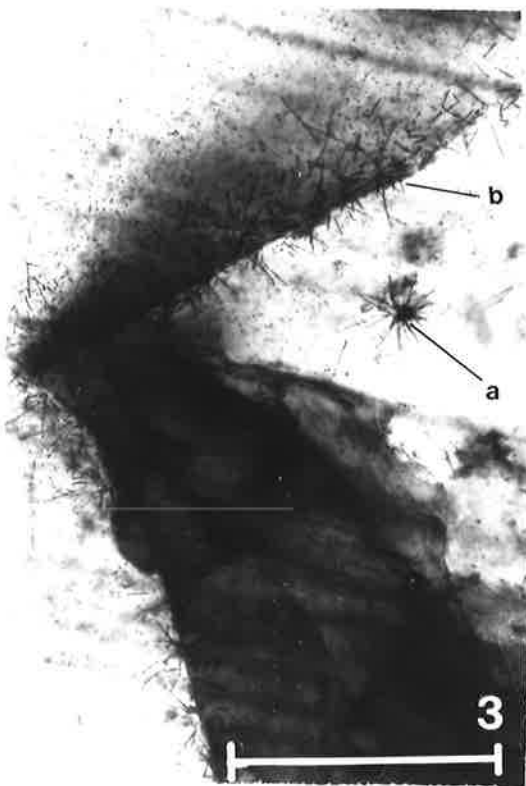
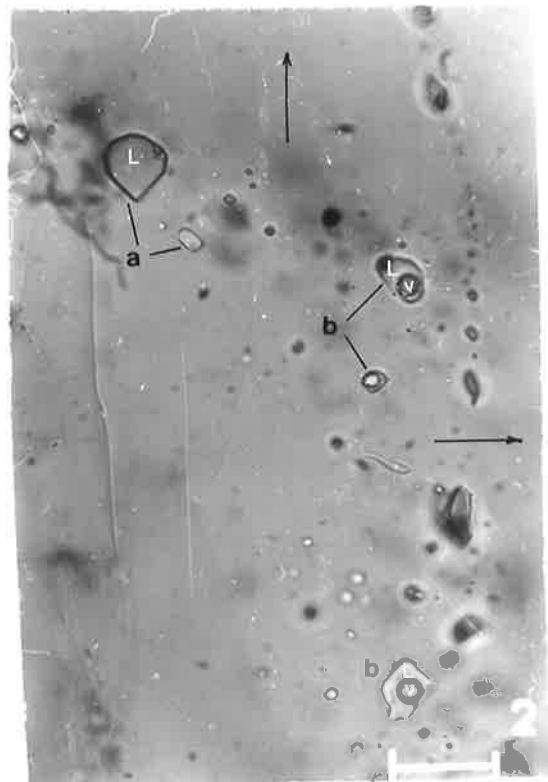


PLATE III

Sample A-495-172

Photo 1 - Idiomorphic quartz crystal with pitchblende among other opaque minerals. Scale: bar = 100 $\mu$ . Photographic emulsion coated thin section.

Photo 2 - Detail of photo 1 showing  $\alpha$ -tracks from pitchblende. Scale: bar = 100 $\mu$ .

Photo 3 - Fluid inclusions from idiomorphic quartz crystal. The larger inclusions present dark solid minerals which may be of pitchblende. Scale: bar = 10 $\mu$ .

Photo 4 - Photographic emulsion coated thin section. The source of one  $\alpha$ -tracks is a fluid inclusion (see arrow). Scale: bar = 100 $\mu$ .



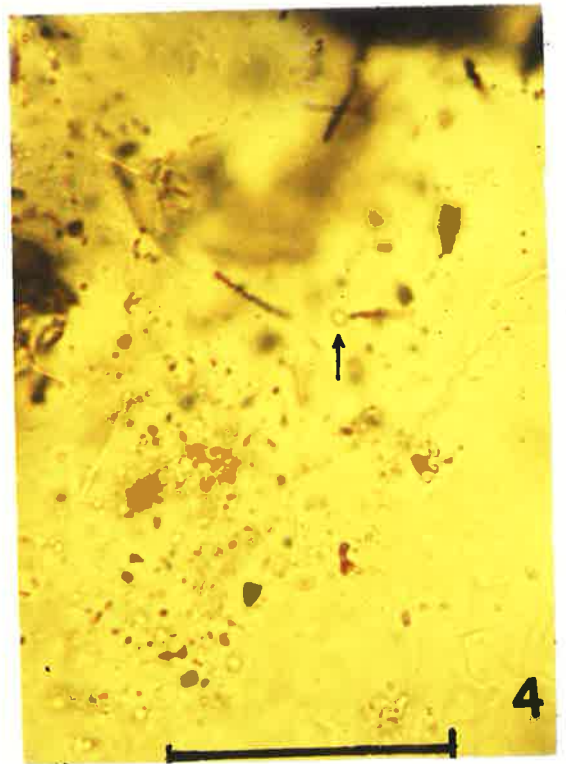
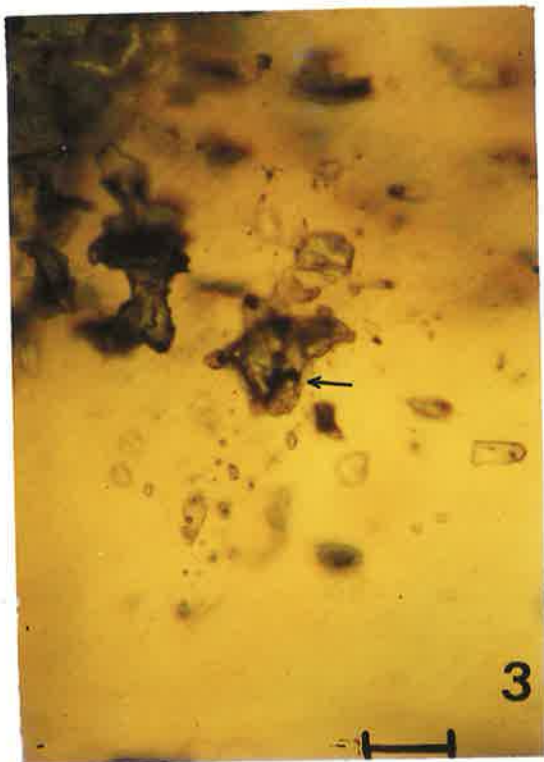
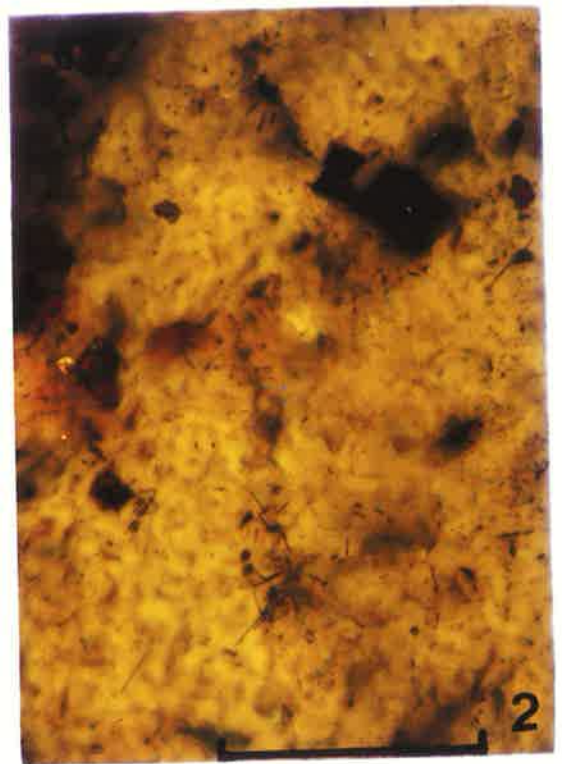
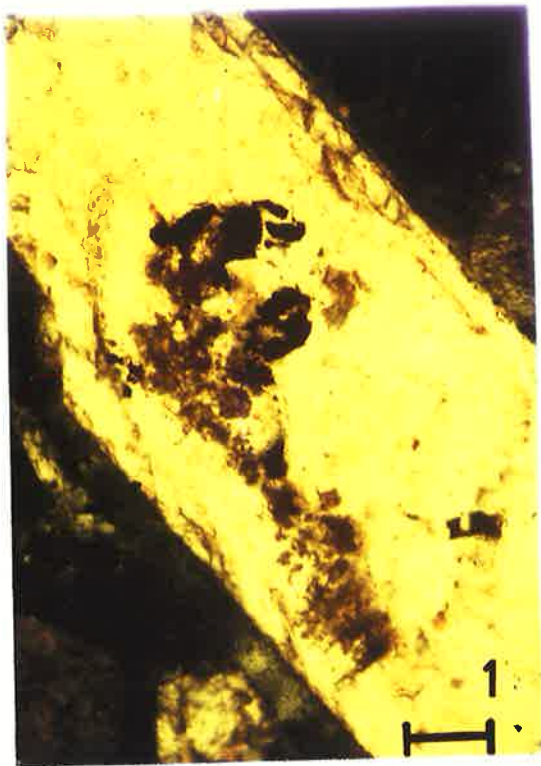


PLATE IV

Photo 1 - Sample A-495-110.

Massive pitchblende with fibrous calcite veins. Scale in mm.

Photo 2 - Sample A-495-172.

Idiomorphic quartz crystal coated with photographic emulsion. The pitchblende grain is on the surface of quartz and is the source of numerous  $\alpha$ -tracks. Scale: bar = 100 $\mu$ .

Photo 3 - Sample A-495-176.

Early-stage quartz with type (a) (liquid-rich) and few type (b) (gas-rich) inclusions. Analyser partially crossed. Scale: bar = 100 $\mu$ .

Photo 4 - Sample A-495-176.

Early-stage quartz with a type (a) fluid inclusion partially frozen after 30 minutes at  $-80^{\circ}\text{C}$  (larger inclusion at the centre of the photo). See the large solid phase (darker) and the spherical vapour-phase. At the right end of the inclusion a daughter mineral can be observed. Scale: bar = 100 $\mu$ .

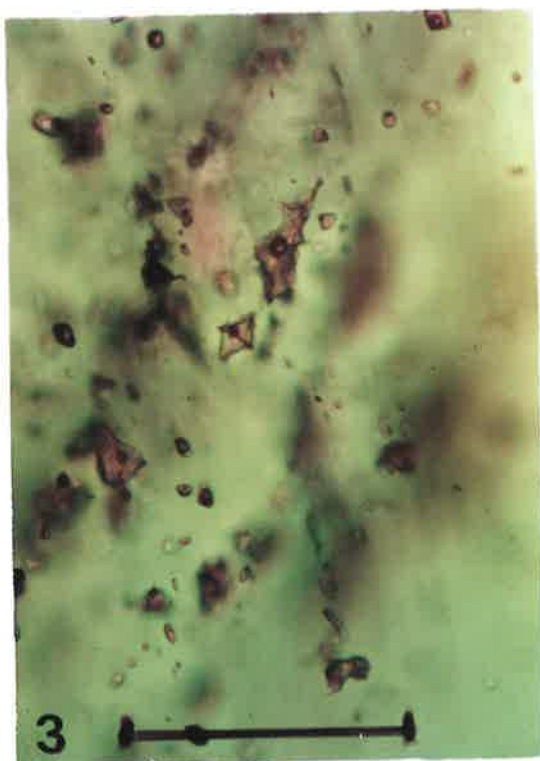


PLATE V

Photo 1 - Sample A-495-172.

A large, 3 phase fluid inclusion from quartz crystal. The radial cluster of acicular daughter minerals in the right lower corner of the inclusion was probably dawsonite ( $\text{NaAlCO}_3(\text{OH})_2$ ). They were birefringent. Scale: bar = 100 $\mu$ .

Photo 2 - Sample A-495-144.

A typical 2 phase fluid inclusion in calcite. The photo was taken at  $-37.5^\circ\text{C}$ . The rounded crystal at the center of the inclusion is ice which melted at  $-36.2^\circ\text{C}$ , and formed salt hydrate. When cooled again down to  $-155^\circ\text{C}$  the hydrate did not increase in size nor the liquid freeze. The hydrate melted at between  $-2^\circ$  and  $-3^\circ\text{C}$ . Scale: bar = 100 $\mu$ .

Photo 3 - Sample A-495-176.

A vug in quartz-chlorite breccia. Quartz of early-stage (a) and of late stage (b) are well characterized.

Scale: bar = 1 cm.

Photo 4 - Sample A-495-176.

Fluid inclusion thin section showing the levels from which the fluid inclusions from early-stage quartz - A-495-176A, A-495-176B + A-495-176C, and A-495-176D - were taken.

Scale: bar = 1 cm.

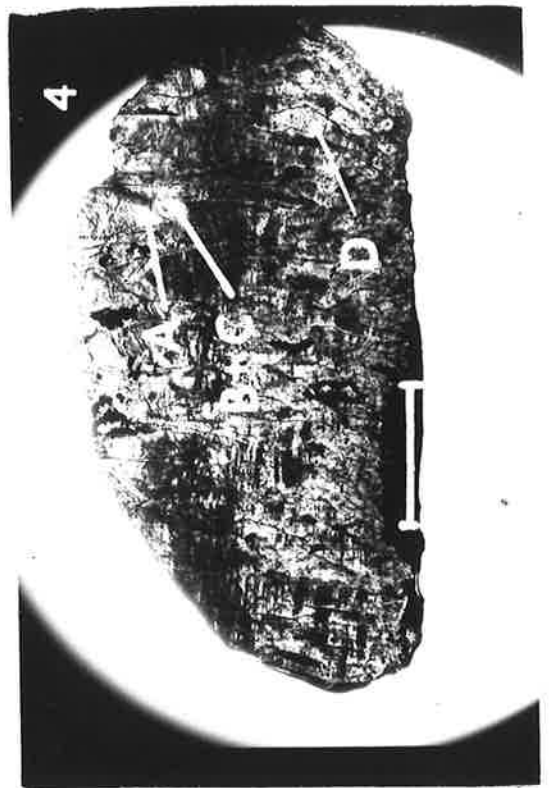
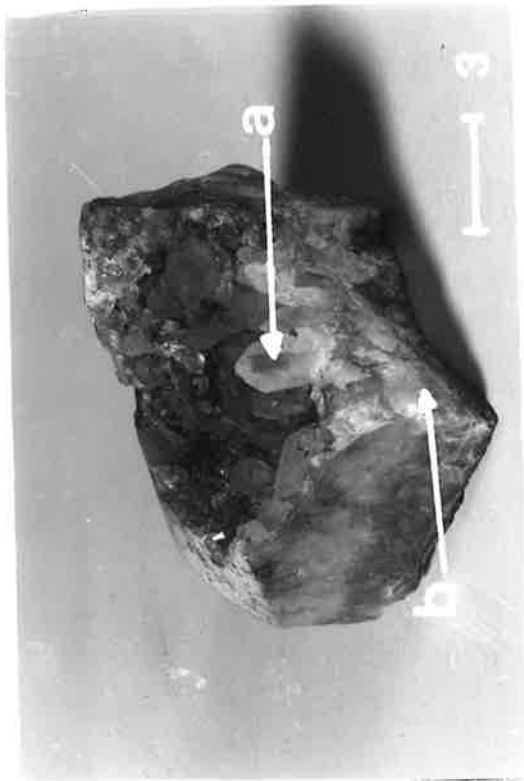
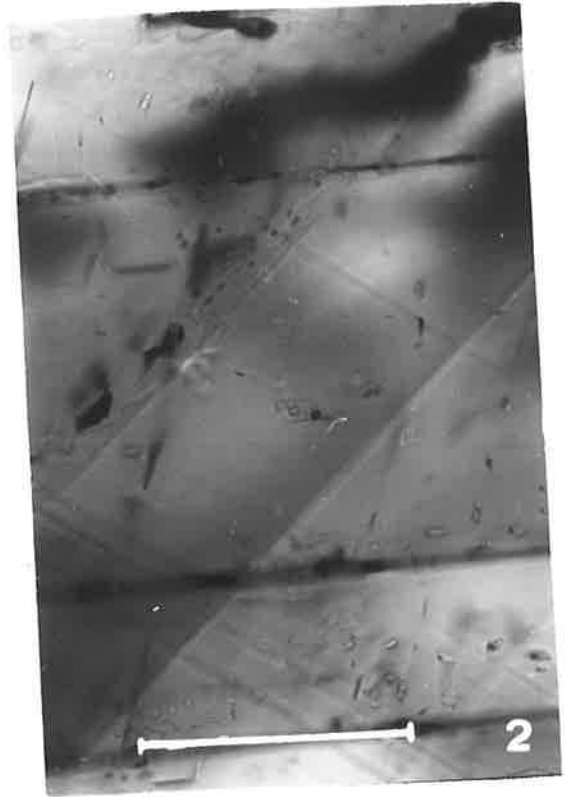


PLATE VI

Fluid inclusion open cavities with daughter mineral in quartz A-495-162.

Photos 1, 2, and 3 - Kaolinites. Photo 2 is of higher magnification showing the exceptionally well-crystallized daughter kaolinite from photo 1. The mineral of photo 3 may have been trapped as solid phase. The mineral outside the cavity in photo 3 is quartz.

Photo 4 -  $\text{CaCl}_2$  - hydrate.

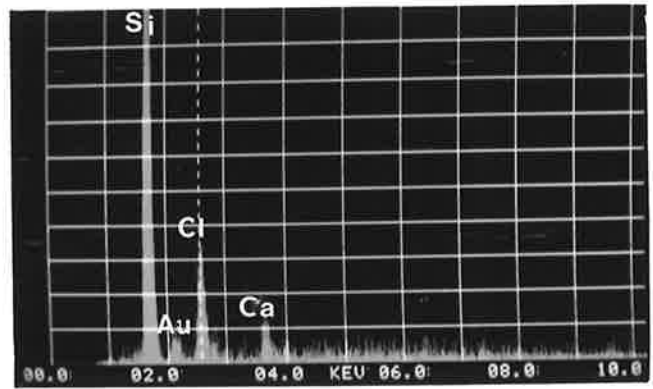
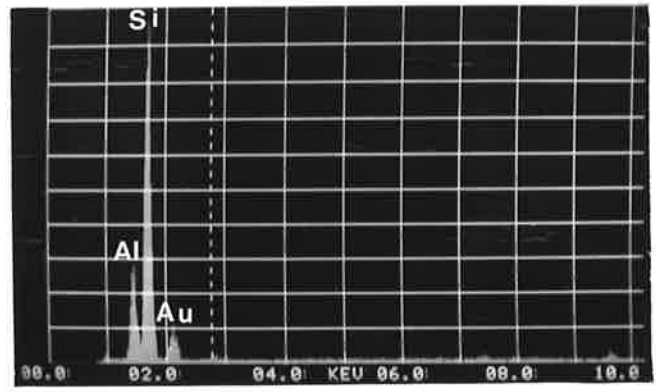
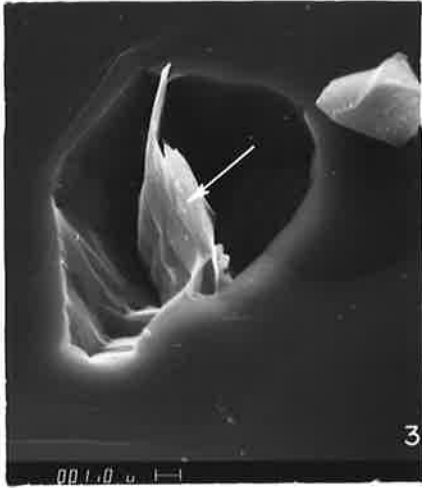
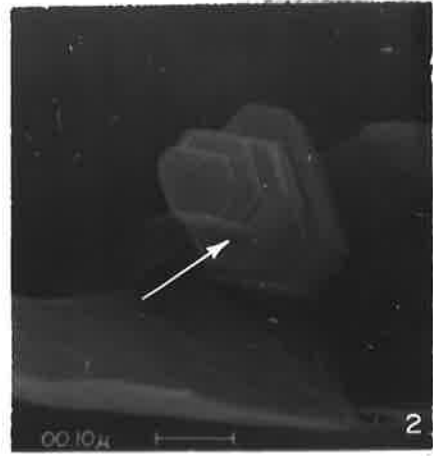
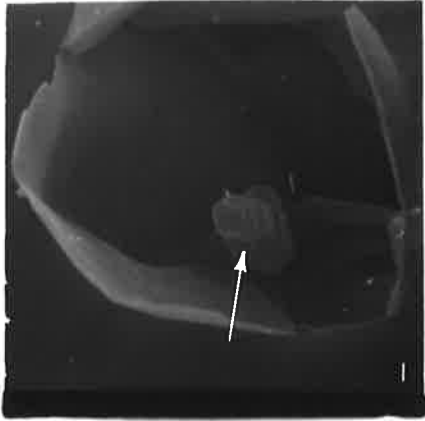


PLATE VII

Photo 1 - Sample A-495-162.

Fluid inclusion open cavity with NaCl (a) and sericite (?) (b). The sericite is probably covered by a film of NaCl and perhaps KCl which are residues of evaporation of the brine.

Photo 2 - Sample A-495-162.

Sericite (?) probably trapped as solid phase.

Photo 3 - Sample A-495-220 (calcite).

Empty fluid inclusion cavities and residues of evaporation. Mineral (a) may be  $\text{CaKCl}_3$  or KCl where the Ca peak is the influence of  $\text{CaCO}_3$  (mineral (b)).



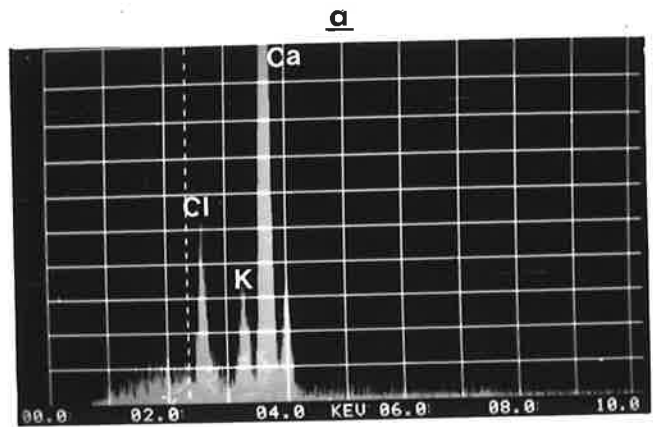
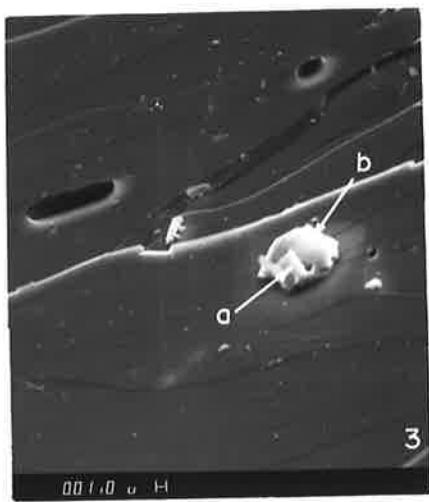
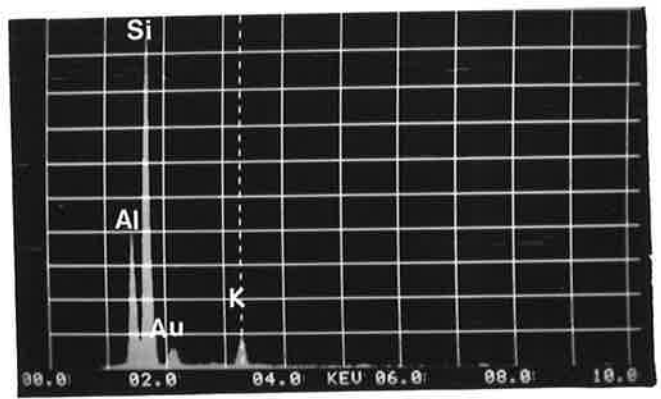
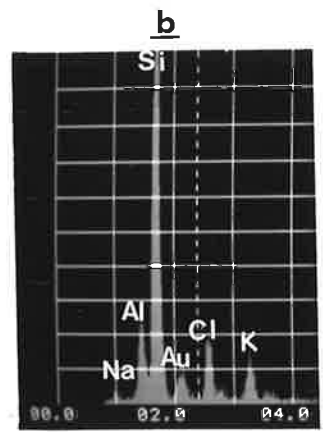
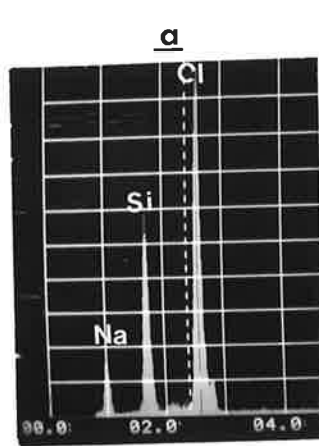
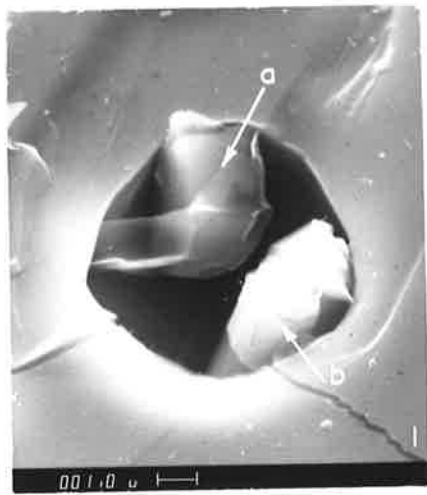


PLATE VIII

Late-stage quartz from sample A-495-172

Photo 1 - Fluid inclusion cavity with micaceous mineral (chlorite?) impregnated with Ca and K chlorides. Fragments outside the cavity are quartz.

Photo 2 - Fluid inclusion cavity with sericite.

Photo 3 - Fluid inclusion cavity with NaCl daughter mineral.

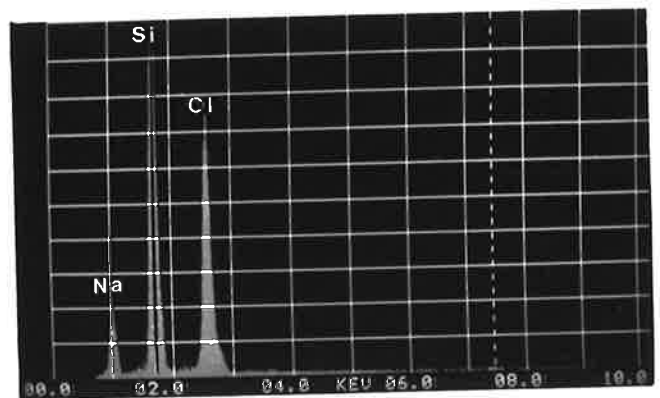
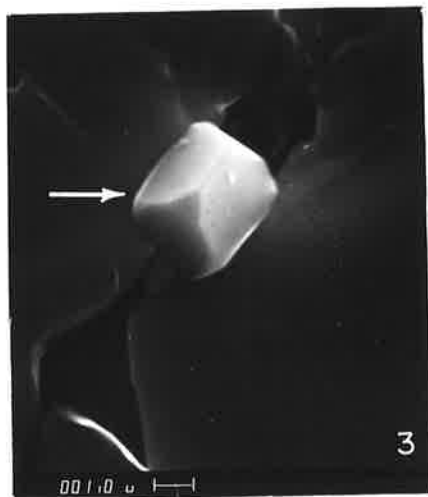
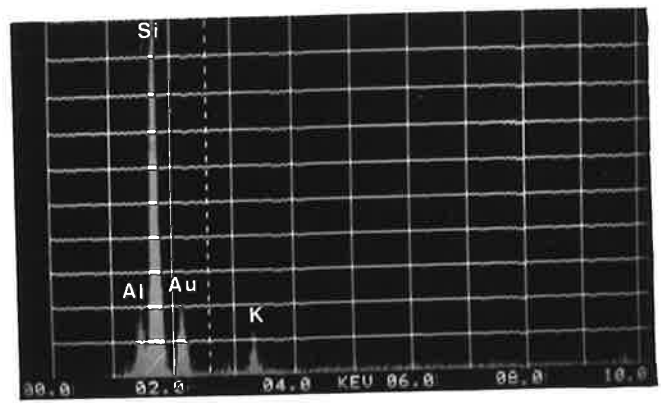
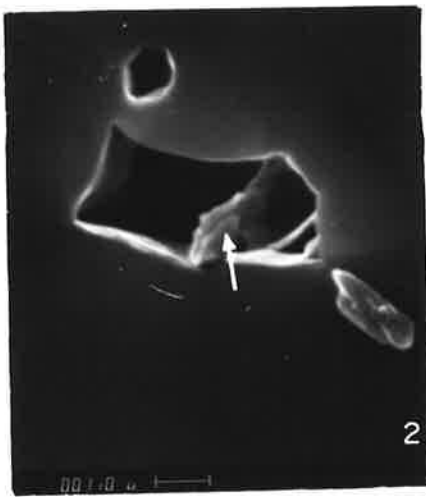
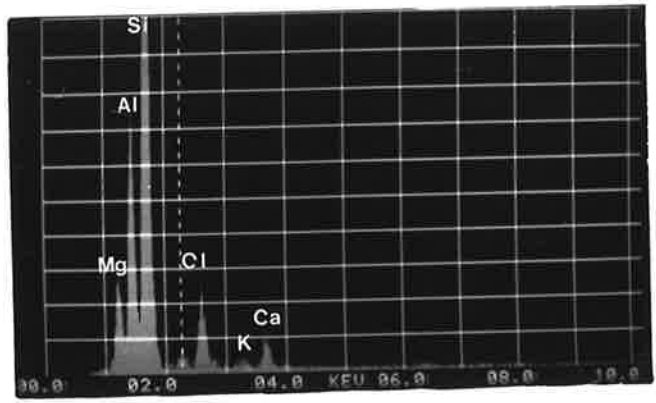


PLATE IX

Open cavities of fluid inclusions from quartz A-495-176

Photo 1 - Early-stage quartz with kaolinite.

Photo 2 - Late-stage quartz with (a) NaCl, and (b) an unidentified mineral containing Al, Si, Cl and K. If the quartz is causing Si peak, the daughter mineral may be a solid solution of  $\text{AlCl}_3 \cdot 6\text{H}_2\text{O}$  and KCl.

Photo 3 - Late-stage quartz with a "mush" of micaceous minerals and chlorides. X-rays indicate the presence of possibly as many as seven elements in the solution.

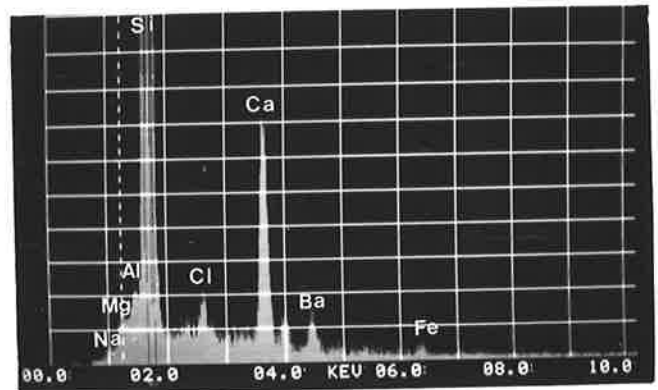
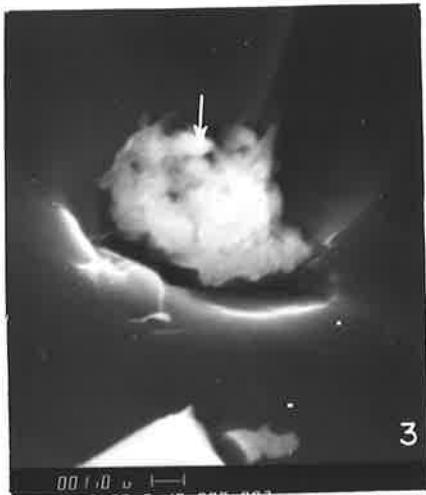
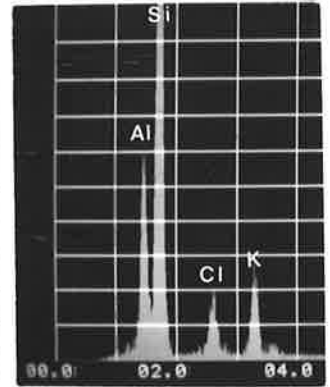
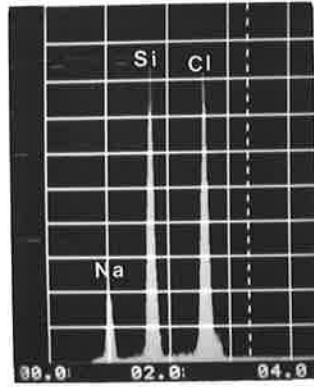
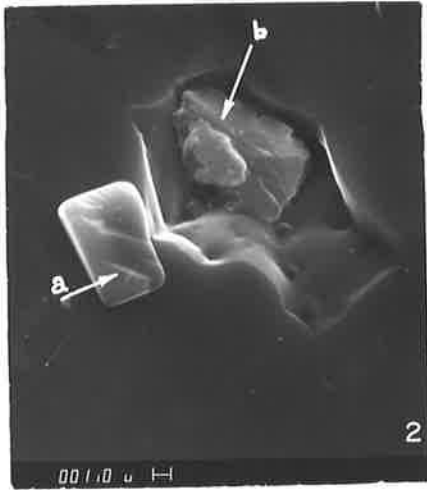
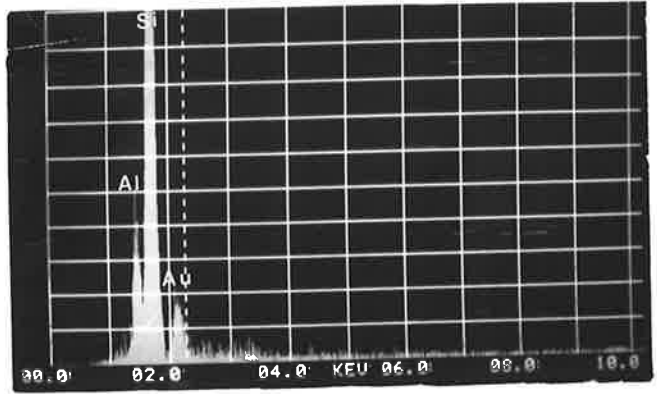
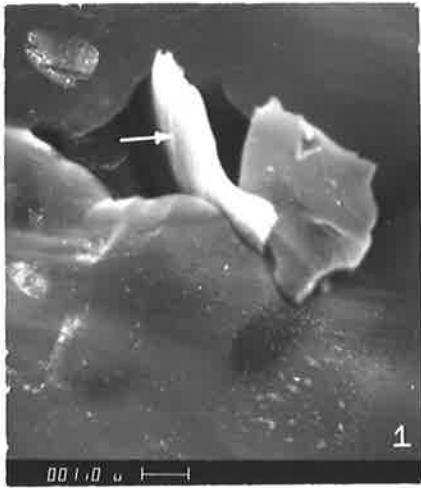


PLATE X

Sample A-495-176, late-stage quartz

Photo 1 - Fluid inclusion cavity with  $\text{FeSO}_4 \cdot \text{H}_2\text{O}$  (?)

Photo 2 - Empty fluid inclusions cavities. The cubic crystal is KCl precipitated as residue of evaporation.

Photo 3 - Fluid inclusion cavity with unidentified fibrous mineral composed with Al, Si (?) and Fe.

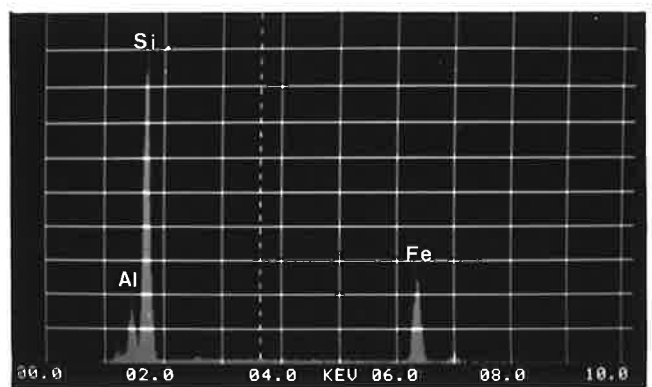
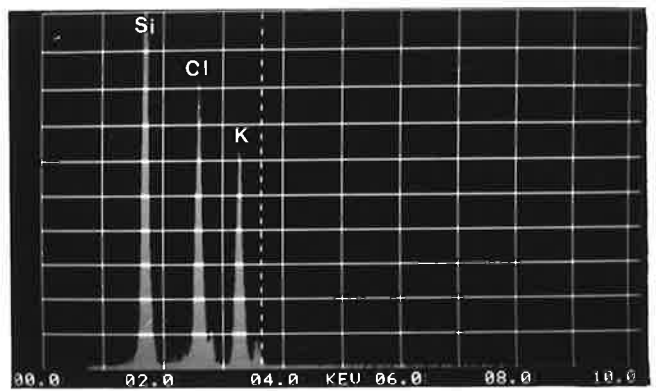
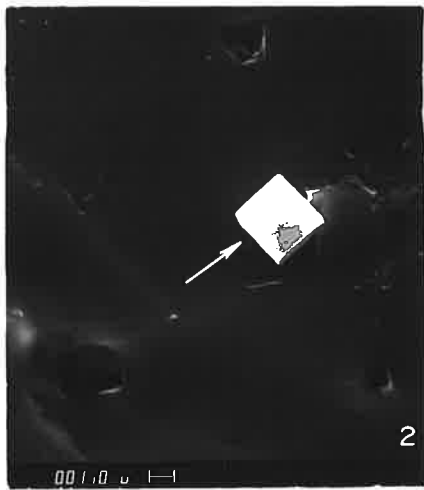
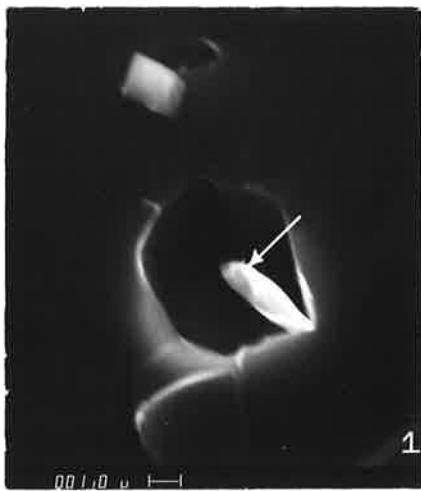


PLATE XI

Photo 1 - Sample A-495-176.

Fluid inclusion cavity in early-stage quartz with calcite daughter mineral (?).

Photo 2 - Sample A-495-176.

Dolomite in fluid inclusion cavity from late-stage quartz.

Photo 3 - Sample A-495-179.

Feldspar (anorthite?) in fluid inclusion cavity in quartz.



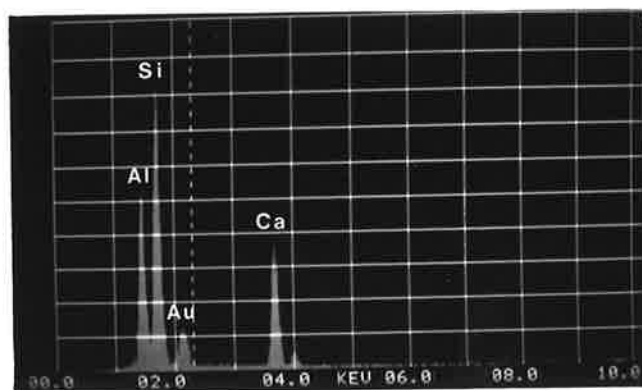
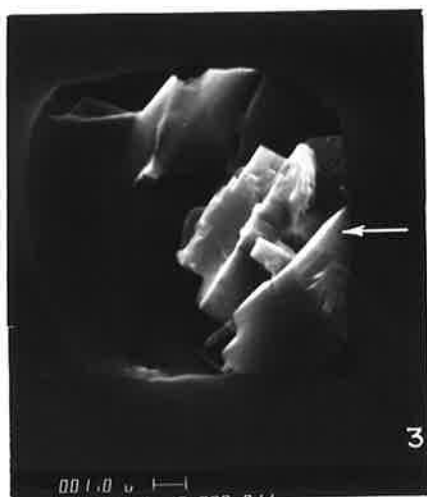
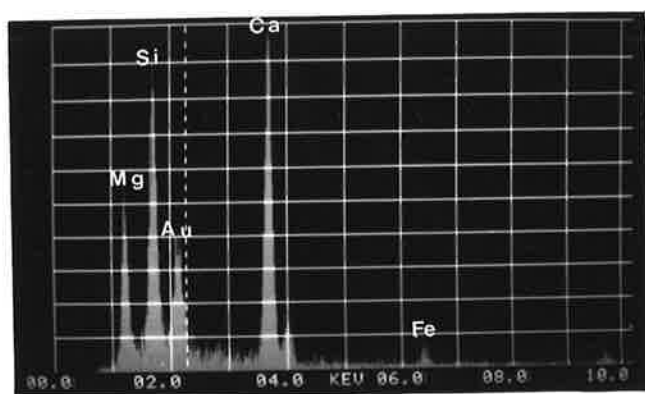
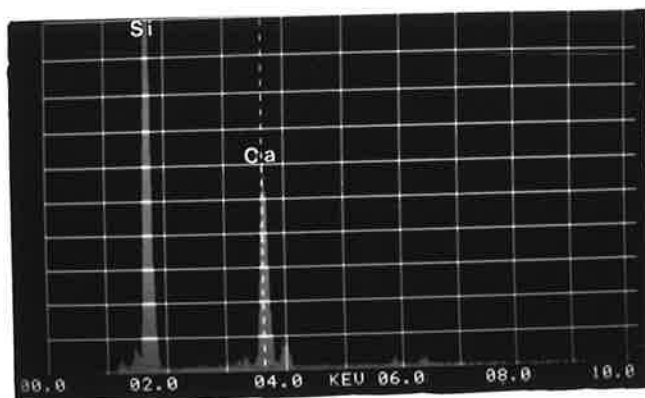
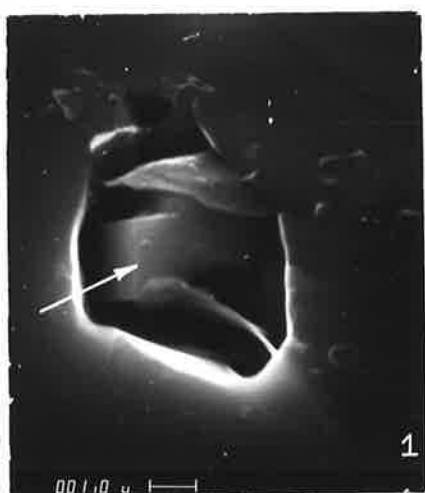


PLATE XII

Sample A-495-179

Fluid inclusion cavities in quartz containing daughter minerals

Photo 1 - (a) A complex of sulphides or sulphates of Na, Fe, Cu,  
and Zn.

(b)  $\text{CaCl}_2$  hydrate.

(c) A sulphate (?) of Na and Zn.

Photo 2 - Well crystallized  $\text{FeCl}_2 \cdot 2\text{H}_2\text{O}$ .

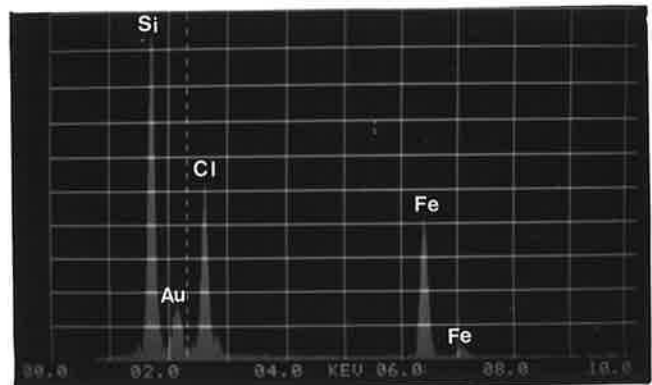
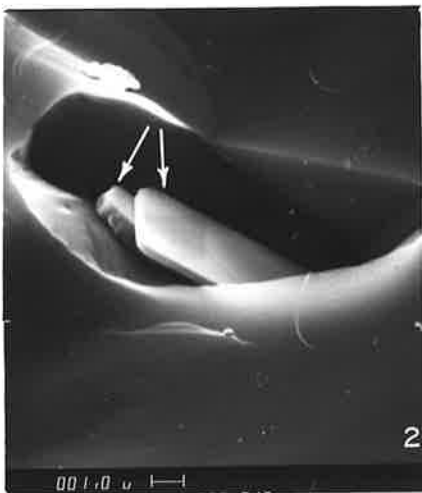
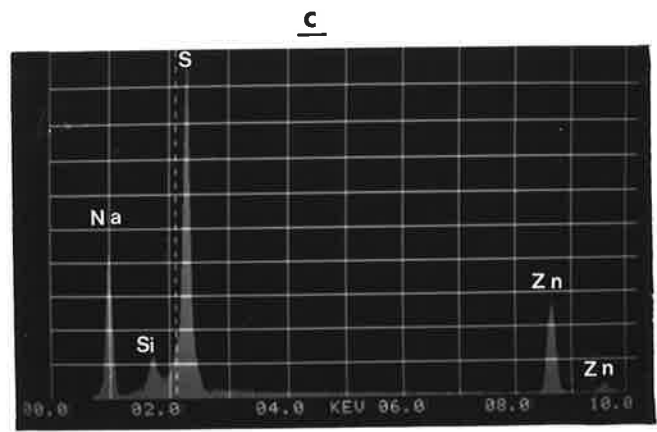
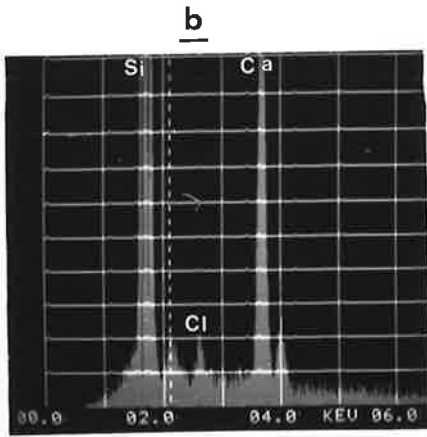
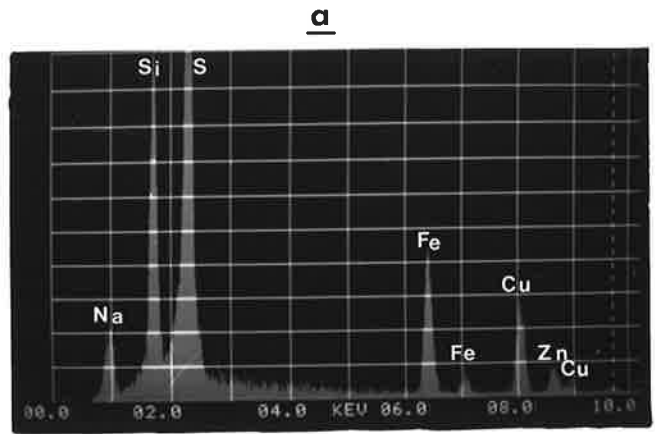
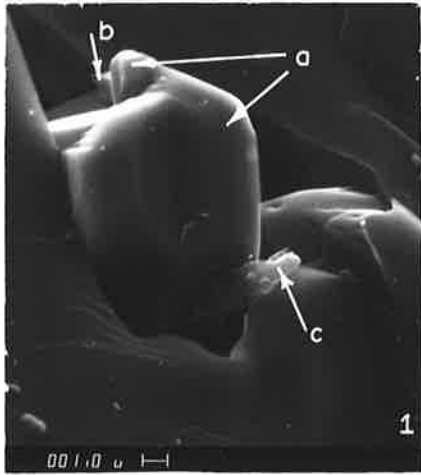


PLATE XIII

Sample A-495-179

Fluid inclusion cavities in quartz, containing daughter minerals

Photo 1 - (a)  $\text{CaCl}_2$  hydrate and  
(b) NaCl daughter minerals.

Photo 2 - Three daughter minerals:  
(a) Probably muscovite with chlorides (mainly Fe and Ca).  
(b) Ankerite (?)  
(c) Hydrated calcium silicate.

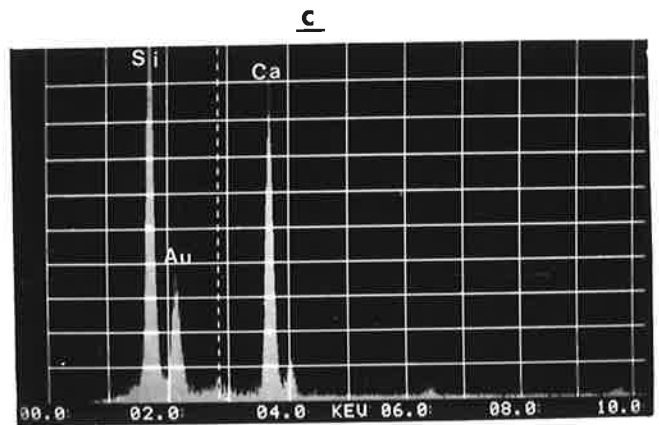
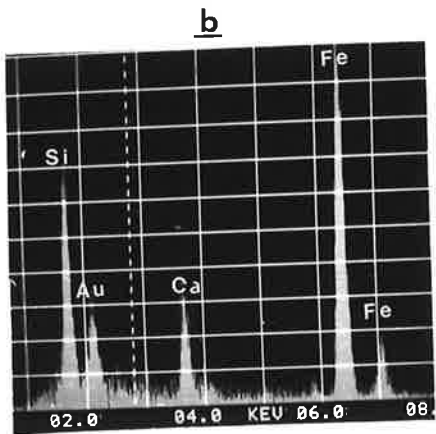
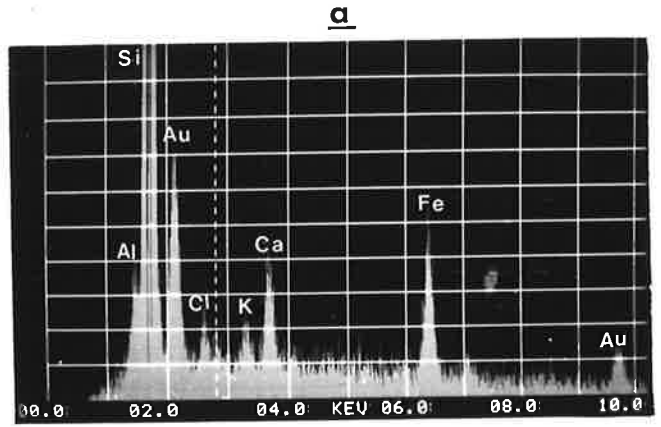
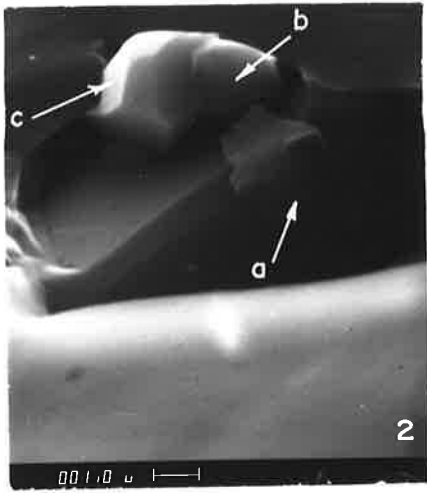
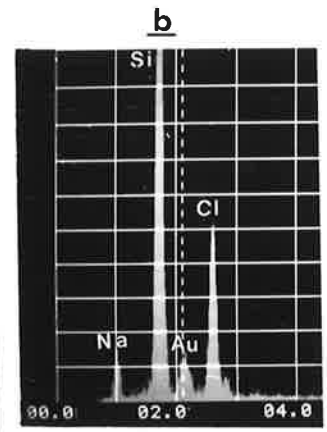
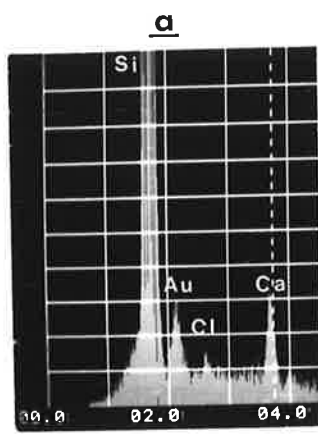
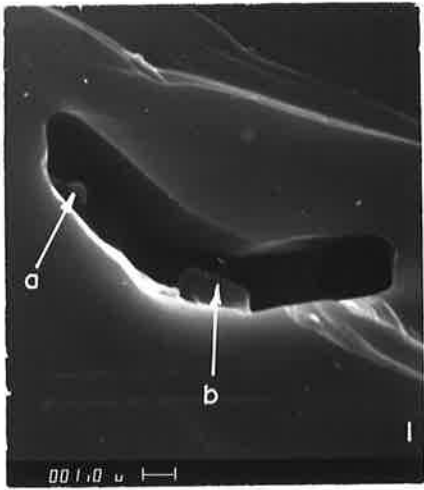


PLATE XIV

Sample A-495-179

Fluid inclusions cavities with daughter minerals

Photo 1 - (a) Ca silicate  $\text{CaSi}_2\text{O}_5 \cdot 2\text{H}_2\text{O}$  (Okenite) (?)  
(b) Zeolite (?). This mineral may be an extraneous fragment attached to mineral (a) when the inclusion was opened.

Photo 2 - Well-crystallized  $\text{CaCO}_3$ .  $\text{CaCO}_3$

Photo 3 - Dolomite.

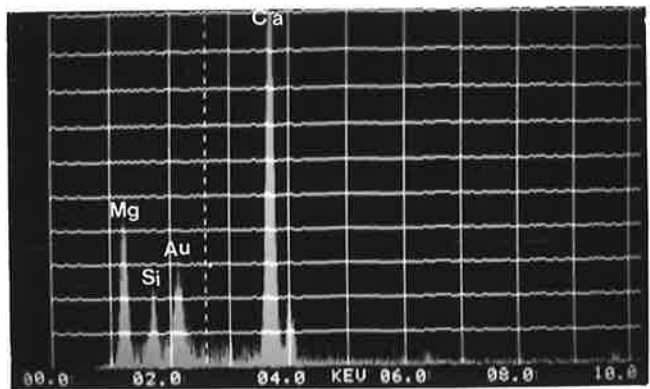
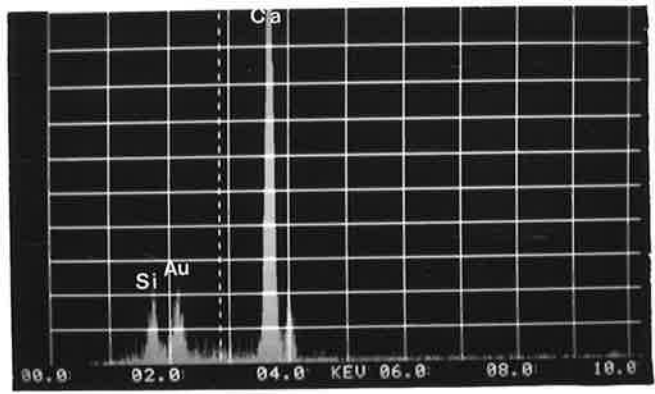
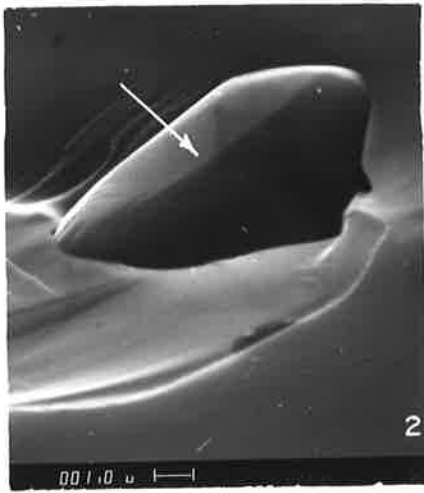
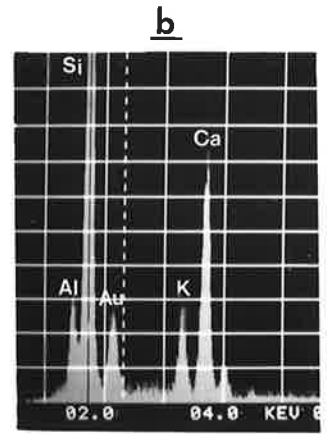
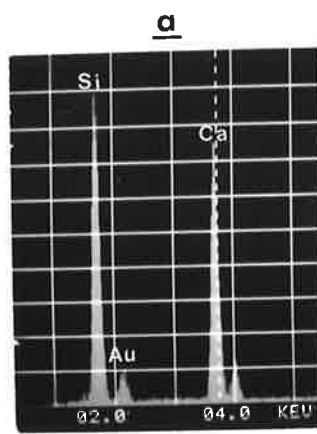
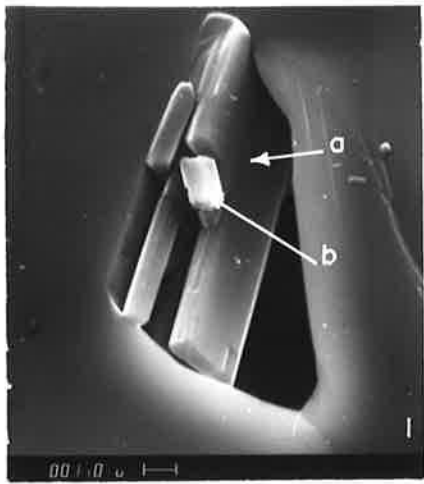


PLATE XV

Photo 1 - Sample A-495-110.

Well crystallized calcites in open cavity of a possible fluid inclusion.

Photo 2 - Sample A-495-111.

*- no record of this sample.*

Fluid (?) inclusions cavities with dolomite. Al and Si peaks are probably from sericite or kaolinite.

Photo 3 - Sample A-495-116.

Many empty fluid inclusions cavities. The needle-like minerals (arrow) are probably gypsum.



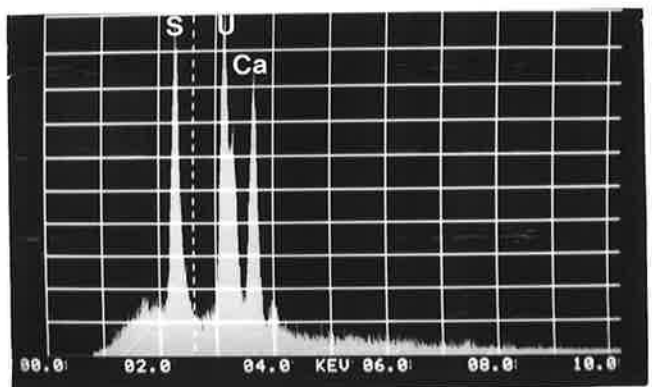
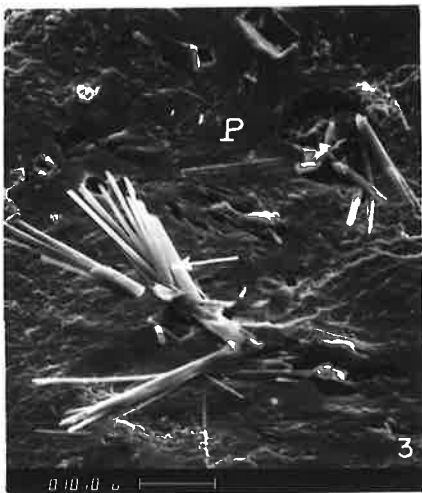
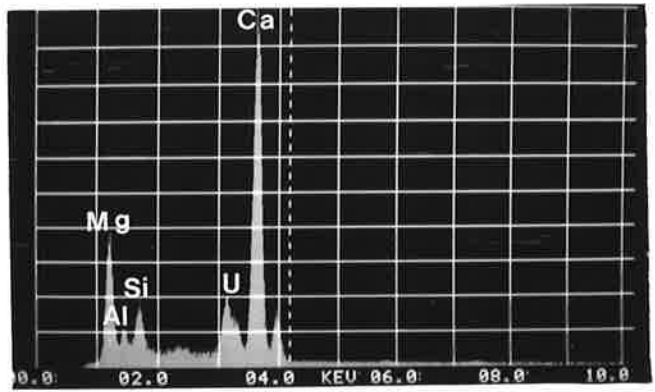
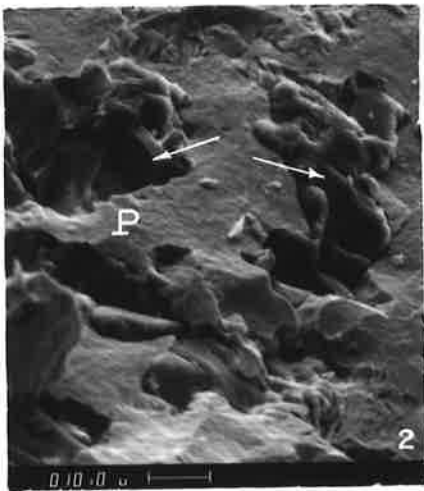
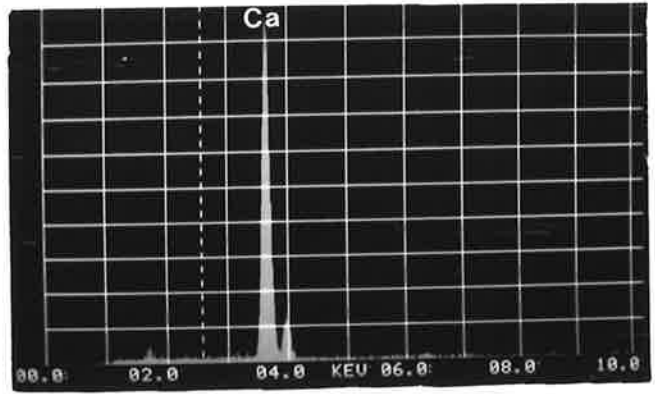
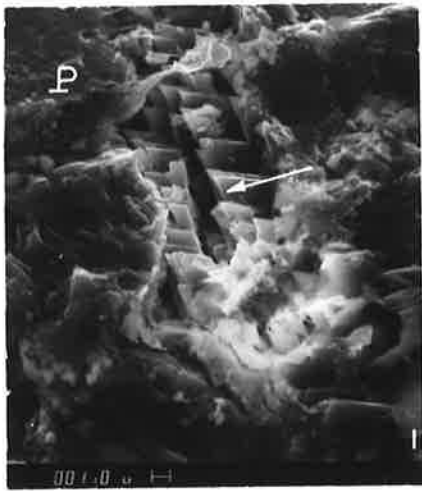


PLATE XVI

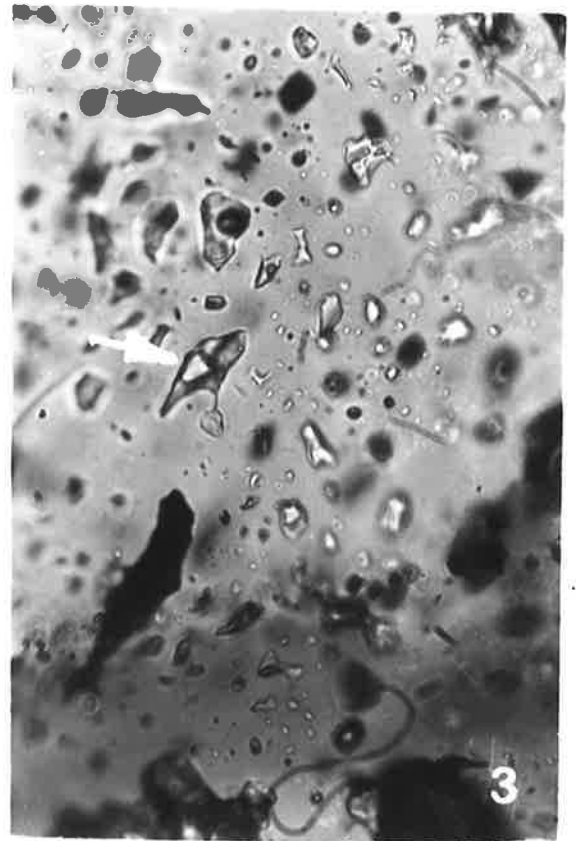
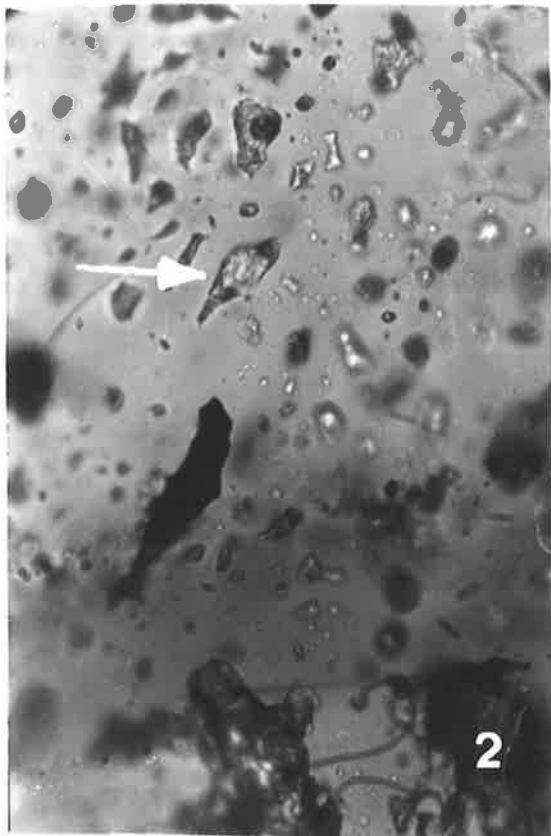
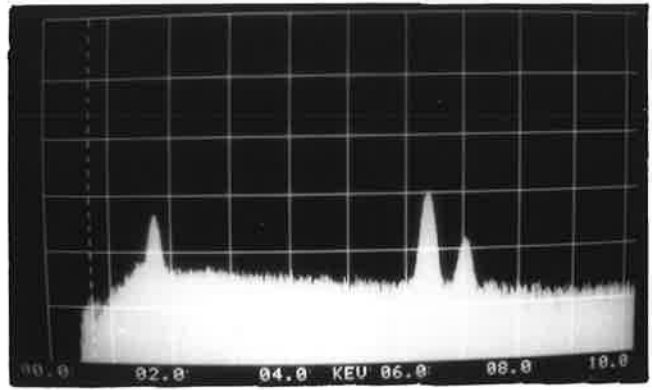
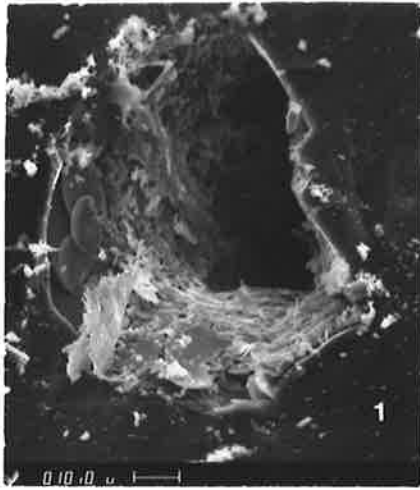
(Jabiluka)

Photo 1 - Sample A-495-3. Scale: Bar = 10 $\mu$ .

S.E.M. image of a large inclusion cavity. The rounded platelets at the bottom and left side wall are hematite. The E.D.A.X. image is from one of these platelets and clearly shows peaks of Fe (6.40 and 7.05 KEV). The peak at 1.72 KEV is from Si from quartz which is the host mineral.

Photos 2 and 3 - Sample A-495-11. Scale: Bar = 100 $\mu$ .

The arrow indicates inclusion No. 2 from Cluster B during (Photo 2) and after (Photo 3) the second freezing. Photo 2 shows the formation of NaCl.2H<sub>2</sub>O by corrosion of NaCl crystal. Photo 3 shows the newly nucleated NaCl after the melting of the hydrate.



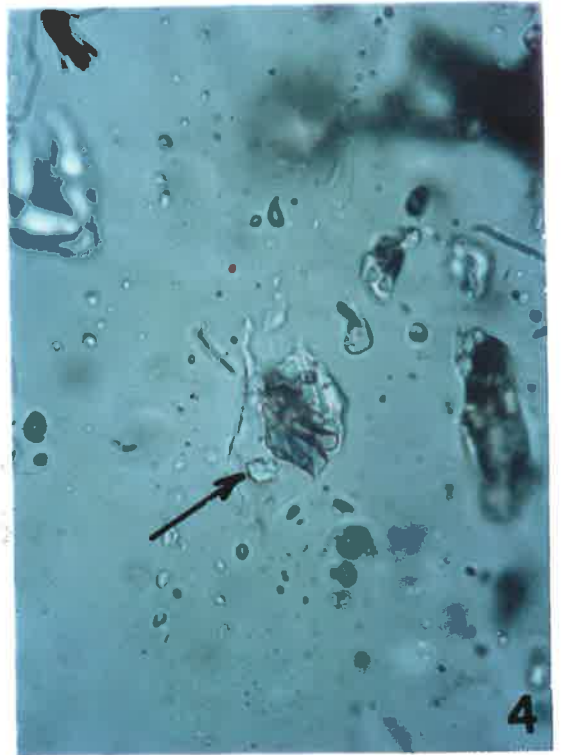
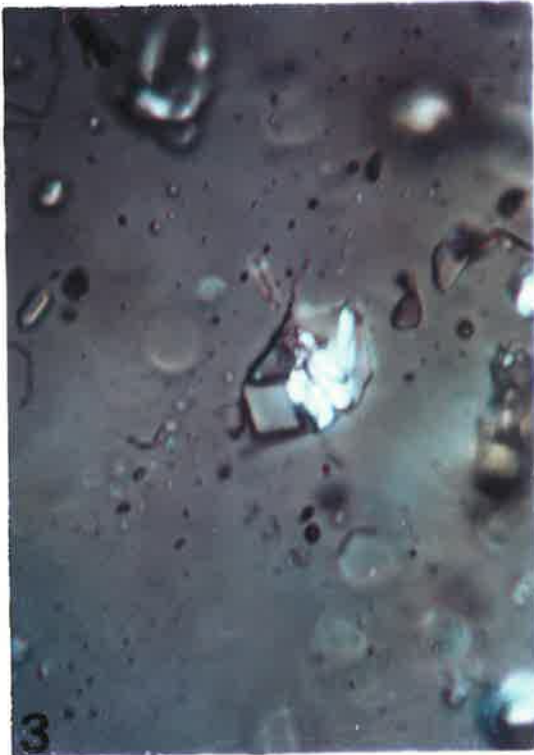
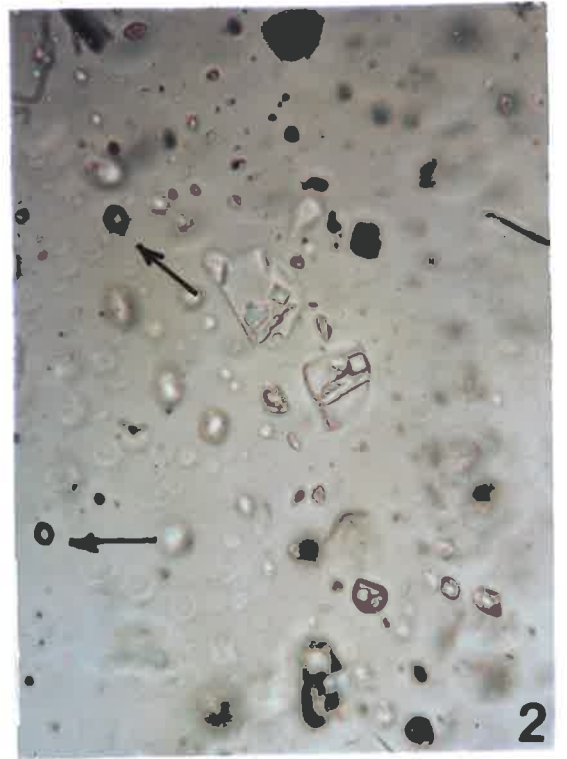


PLATE XVIII

(Jabiluka)

S.E.M. images of fluid inclusion cavities and their solid phases.

NOTE: 1. Underlined elements are those with stronger peaks.

2. Scale in micron.

Photo 1 - Inclusion cavity with numerous elongated platy and prismatic solid phases. They are all chlorides of alkaline and alkaline earth elements. The E.D.A.X. detected the following elements for each mineral pointed out in the photo:

mineral a: Ca, K, Cl, Mg, Na

mineral b: Ca, K, Cl, Mg, Na

mineral c: Ca, K, Cl, Mg, Na

mineral d: Ca (CaCO<sub>3</sub>?)

Photo 2 - NaCl crystals probably formed by evaporation of fluids from inclusions.

Photo 3 - Inclusion cavity with numerous solid phases similar to those of Photo 1. The elements are:

mineral a: Ca, Cl, Na, Mg, K

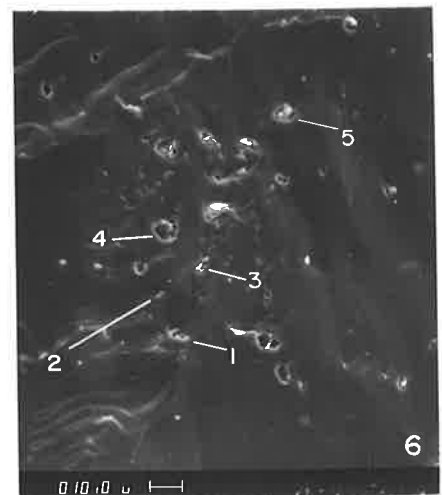
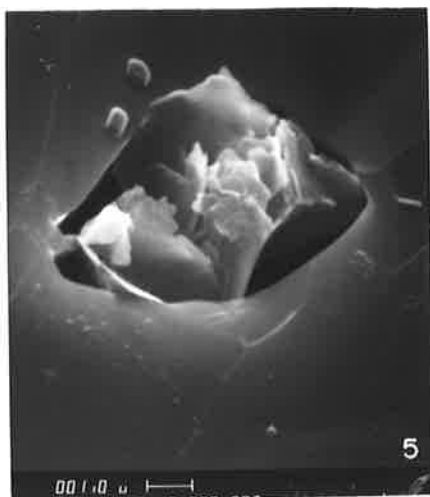
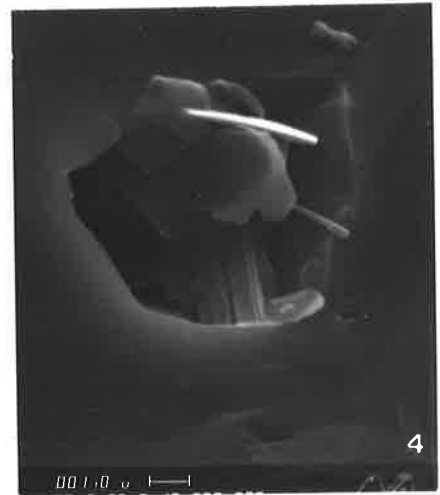
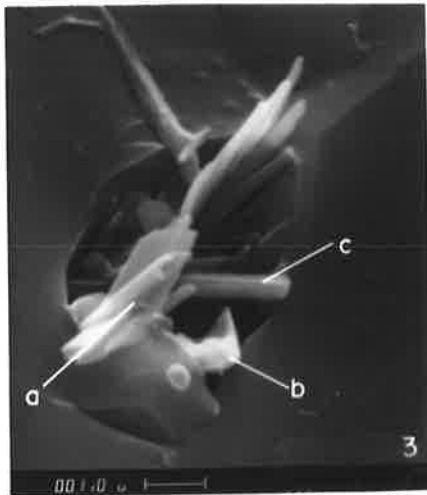
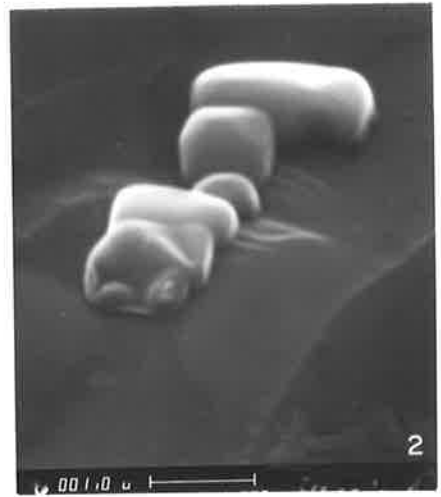
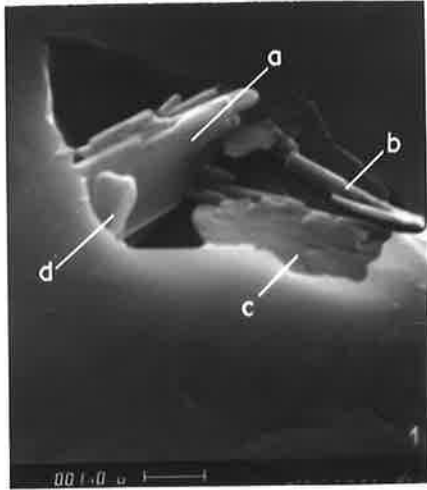
mineral b: Ca, Cl, Na, Mg, K

mineral c: Ca, Cl, Na

Photo 4 - Inclusion cavity with several hexagonal platy minerals. They all presented the same composition: Ca, Cl, Na, and K, where Ca and Cl present the strongest peaks.

Photo 5 - Inclusion cavity with many platy minerals (micaceous). The composition of Na, Cl, K, Fe suggests mixed chloride of these elements.

Photo 6 - Broken surface of vein-quartz showing many open inclusion cavities. Among them the cavities of Photos 1, 3, 4, and 5 and the situation of NaCl crystals of Photo 2 are indicated.



## ERRATA

PAGE	LINE	CORRECTIONS
iii	16	page 148 <i>read</i> page.149
iv/v	-	page viii should be inserted between pages iv and v
viii	9	(Fig. 5): Borehold <i>read</i> Borehole
6	7	Pate et al. <i>read</i> Page et al.
9	2	assimetrical <i>read</i> assymetrical
10	16	All stock types <i>read</i> All rock types
13	17	(19790) <i>read</i> (1979)
21	2	Kalyuzhni <i>read</i> Kalyuzhnyi
23	24	MCl - H <sub>2</sub> O <i>read</i> KCl - H <sub>2</sub> O
31	11	...Lemlein, 1959 <i>read</i> ...Lemlein, 1960
33	18	Kalyuzhnyi, 1958 <i>read</i> Kalyuzhnyi, 1958a
37	23	Kalyuzhnyi, 1958 <i>read</i> Kalyuzhnyi, 1958a
37	24	methodoloty <i>read</i> methodology
44	2	Nesbitt and Keyy <i>read</i> Nesbitt and Kelly
74	5	(Plate VI,...) <i>read</i> (Plate XV,...)
75	-	Line missing: "11.2.2.5.2.-sample A-495-164 (drill hole Na74)" between 11.2.2.5.1. and 11.2.2.6.1.
81	29	(=13.4°C) <i>read</i> (= -13.4°C)
120	6	Ferguson, 1980 <i>read</i> Ferguson, 1979
134	1	111.2.2.4. <i>read</i> 111.2.2.5
144	15	on page 105 <i>read</i> on page 134
146	19	(see 111.2.2.9) <i>read</i> (see 111.2.2.10)
151	8	Shiek and Taylor <i>read</i> Shieh and Taylor
156	last	Smart et al., 1975 <i>read</i> Smart et al., 1976
157	22	A-495-172D (p.42) <i>read</i> A-495-172D (p.58)
157	24	A-495-133 <i>read</i> A-495-113
157	24	A-495-133 <i>read</i> A-495-113
162	13	Rich et al., 1976 <i>read</i> Rich et al., 1977
191	3	Hollister and Burruss <i>read</i> Hollister and Burruss
191	24	Main Mine Serires <i>read</i> Main Mine Series